ulm university universität uulm

Development of enhanced analytical methods for ultratrace determination of mercury in natural water

- Dissertation -

zur Erlangung des Doktorgrades Dr. rer. nat.

der Fakultät für Naturwissenschaften der Universität Ulm

vorgelegt von

Jessica Huber

aus München

Ulm, 2017

Amtierender Dekan: Prof. Dr. Peter Dürre

Erstgutachter: Prof. Dr. Kerstin Leopold

Zweitgutachter: Prof. Dr. Mika Lindén

Tag der Promotion: 03.07.2017

Für meine Eltern

Contents

List of Abbreviations

AAS	Atomic absorption spectrometry
AES	Atomic emission spectrometry
AFM	Atomic force microscopy
AFS	Atomic fluorescence spectrometry
ASGM	Artisanal and small-scale gold mining
AT	Amalgamation technique
AuNP	Gold nanoparticle
AuNP@qt	Gold nanoparticle-coated quartz glass tubes
AuNP@SiO$_2$	Gold nanoparticle-coated silica monolith
BSE	Backscattered electron
CRM	Certified reference material
CV	Cold vapor
DGT	Diffusive gradient thin film
DMeHg	Dimethylmercury
DOC	Dissolved organic carbon
DOM	Dissolved organic matter
EDXRF	Energy-dispersive X-ray fluorescence spectrometry
EPA	Environmental Protection Agency
ERM	European reference materials
ETA	Electrothermal atomizers
FA	Fulvic acid
FDA	Food and Drug Administration
FEP	Fluorinated ethylene propylene
FI	Flow injection
FI	fluorescence intensity
FIAS	Flow injection analysis system
GLS	Gas-liquid separator
HA	Humic acid
HDPE	High-density polyethylene
HS	Humic substance
ICP-MS	Inductively coupled plasma mass spectrometry
ISO	International Organization for Standardization
IHSS	International Humic Substances Society
ID	Inner diameter
IR	Infrared

L	Length
LOD	Limit of detection
LOQ	Limit of quantification
MFA	Modified fluoralkoxy
MIO	Mediterranean Institute of Oceanography
MMeHg	Monomethylmercury
MV	Magnetic valve
NanoAu	Nanogold-based collector
NHS	Non-humic substance
NIST	National Institute of Standards and Technology
NOM	Natural organic matter
OD	Outer diameter
OSHA	Occupational Safety and Health Administration
PC	Peltier cooling
PDI	Polydispersity index
PEL	Permissible exposure limit
PES	Polyethersulfone
PET	Polyethylene terephthalate
PFA	Perfluoroalkoxy
RSD	Residual standard deviation
SE	Secondary electron
SEM	Scanning electron microscopy
SGD	Submarine groundwater discharge
SiO_2	Silica
SL	Sample loop
SPE	Solid-phase extraction
TOC	Total organic carbon
TXRF	Total X-ray reflection fluorescence
UPW	Ultrapure water
UV	Ultraviolet
UV-Vis	Ultraviolet-visible spectroscopy
V	Volume
W	Width
WHO	World Health Organization
WWTP	Wastewater treatment plant

Zusammenfassung

Quecksilber (Hg) ist ein ubiquitär vorkommender Umweltschadstoff, der von anthropogenen und natürlichen Quellen an die Atmosphäre abgegeben und schließlich in die aquatische Umwelt sowie in das Erdreich eingetragen wird. Aufgrund der hohen Bioakkumulation in der aquatischen Nahrungskette tritt eine Exposition des Menschen heutzutage meist durch den Verzehr von kontaminiertem Fisch auf. Daher ist die Überwachung der Hg-Konzentration in natürlichen Gewässern für eine effiziente Risikobewertung und für die Einhaltung von Richtlinien und Grenzwerten zwingend erforderlich. Als Alternative zu den etablierten Standardverfahren wurden im Rahmen dieser Arbeit neue analytische Methoden zur Quantifizierung von Hg in Gewässern im Ultraspurenbereich entwickelt.

Im ersten Teil dieser Arbeit wurde ein vollautomatisierter Prototyp für die reagenzienfreie Bestimmung von gelöstem Hg in wässrigen Proben entwickelt. Das Fließinjektionsanalysensystem (FIAS) beruht auf der direkten Anreicherung von Hg auf Goldnanopartikeln (AuNP), die als selektive Adsorber eingesetzt werden. Durch Kopplung mit einem Atomfluoreszenzspektrometer (AFS) wird die Detektion nach thermischer Freisetzung von elementarem Hg ermöglicht. Mit Hilfe des entwickelten Prototyps wurde die Gesamtkonzentration an gelöstem Hg in Proben eines Tiefenprofils des Schwarzen Meeres, einer Reihe von Flusswasserproben, sowie behandelter als auch unbehandelter Klärwerksproben bestimmt. Die ermittelten Werte wurden mit den Ergebnissen von Referenzmethoden (z.B. U.S. EPA Methode 1631) verglichen und somit die Genauigkeit der neuen Methode evaluiert. Diese Methode ermöglicht, im Gegensatz zu anderen, anerkannten Methoden, das Kontaminationsrisiko während der Messung zu verringern, da für die Probenvorbereitung, die Anreicherung und Desorption des Analyten keine Reagenzien eingesetzt werden. Dies führt zu einer niedrigen Nachweisgrenze von $13\,\mathrm{pg\,L^{-1}}$ und einem linearen Arbeitsbereich von 5 Größenordnungen. Zudem kann mit dieser Methode eine gute Reproduzierbarkeit erzielt werden, welche sich in einer relativen Standardabweichung von 3.26% wiedergespiegelt.

Frühere Studien haben gezeigt, dass gelöstes organisches Material in natürlichen Gewässern die Anreicherung von Hg auf AuNP-basierenden Kollektoren beeinflussen und die Wiederfindungen stark beeinträchtigen kann. Daher wurde als Teil dieser Arbeit der Einfluss von Hg-komplexierenden Substanzen, wie z. B. Humin (HS)- und Fulvinsäuren (FS) sowie von verschiedenen organischen Liganden, auf die Adsorption von Hg an AuNP systematisch untersucht. Spike Experimente in einer HS-Matrix mit einer Konzentration von gelöstem organischen Kohlenstoff (*dissolved organic carbon*, DOC) von 2,5 bis 10 mg C L^{-1} zeigten eine hohe Wiederfindung für 1 ng L^{-1} zugesetztes Hg. Die Untersuchung organischer Modelllösungen bestätigt, dass thiolhaltige Liganden einen stärkeren Einfluss auf die Anreicherung von Hg an AuNP haben als andere Liganden. Um Minderbefunde durch Hg-Komplexierung organischer Verbindungen in derartigen Gewässerproben zu vermeiden, wurde eine vollautomatisierte online UV-Bestrahlungsmethode entwickelt. Dafür wurde eine entsprechende Bestrahlungseinheit (UV-Lampe) in das optimierte FIAS-AFS integriert, um die Zersetzung organischer Materialien vor der Hg-Anreicherung am Nanogoldkollektor zu erreichen. Mit diesem modifizierten Aufbau wurden anschließend HS-Modelllösungen mit einem DOC-Gehalt von bis zu 15 mg L^{-1} untersucht. Die Quantifizierung von Hg in den Probelösungen konnte jedoch nur durch den Zusatz von Wasserstoffperoxid und 6-minütiger UV-Bestrahlung erzielt werden. Als weitere Möglichkeit eines online UV-Aufschlusses wurde die photokatalytische Zersetzung von organischen Molekülen auf Titandioxid getestet. Der Abbauvorgang der komplexierenden Liganden wird bei einer Bestrahlungsdauer von 1 min deutlich verbessert, was zu einer Wiederfindung zwischen 71 und 99% führt.

Der zweite Teil dieser Studie beschäftigt sich mit der Entwicklung eines nanogold-beschichteten *Dipsticks* für die passive Probenahme. Durch Eintauchen des neuen Samplers in das entsprechende Gewässer wird eine vor-Ort Anreicherung des Analyten ermöglicht. Dies vereinfacht die Probenahme und verringert das Kontaminationsrisiko, da der Transport und die Lagerung von flüssigen Proben entfällt. In einem ersten Ansatz wurden Quarzglasrohre als Substratmaterial für die Abscheidung von *in situ* gebildeten AuNP verwendet. Die Leistung dieser *Dipsticks* verschlechtert sich aufgrund der begrenzten mechanischen Stabilität bereits nach kurzer Zeit. Daher wurden AuNP an

einem Silicamonolithen mit hierarchischem Porensystem immobilisiert und dieses Material für die Hg-Extraktion in wässrigen Lösungen angewendet. Während der Methodenentwicklung wurde der Einfluss des Blindwerts der Lösungen, der Goldbeladung, der Expositionsdauer und des Probenvolumens untersucht. Außerdem wurde die Anreicherung von Hg auf dem Sampler unter turbulenten und statischen Bedingungen untersucht. Die poröse Struktur des goldbeladenen Silicamonolithen wurde mittels Rasterelektronenmikroskopie (REM) charakterisiert. Die Eignung des neuen Samplers zur Hg-Bestimmung in natürlichen Gewässern wurde durch Wiederfindungsversuche bestätigt. Die Wiederfindungsrate in einer gespikten Meerwasserprobe liegt dabei bei 101%. Parallel wurde die durch Anreicherung auf dem neuen *Dipstick* direkt ermittelte Hg-Konzentration in einer Süßwasserprobe mit dem Resultat der U.S. EPA Methode 1631 verglichen. Die entwickelte Methode hat eine Nachweisgrenze von 1.31 ng L^{-1} bei einer Anreicherungsdauer von nur 1 min. Zudem weist sie eine gute Reproduzierbarkeit auf, was durch eine Standardabweichung kleiner als 5.4% belegt wird.

In dieser Arbeit werden hoch sensitive analytische Methoden zur Bestimmung von Ultraspuren von Hg in natürlichen Gewässern vorgestellt. Der selektive Adsorber ermöglicht die Zersetzung und Anreicherung von gelösten Hg-Spezies und anschließende Fluoreszenzdetektion ohne den Zusatz von Reagenzien. Das Kontaminationsrisiko konnte dadurch deutlich gesenkt werden. Außerdem zeichnen sich die beschriebenen Methoden in ihrer einfachen Handhabung und der kurzen Analysenzeit aus, weshalb sie eine attraktive Alternative zu Standardmethoden der Hg-Analyse darstellen. Das optimierte FIAS-AFS kann an einen UV-Aufschluss gekoppelt werden, wodurch eine reagenzienfreie Hg-Quantifizierung in anspruchsvollen Matrices (z.B. Abwasser mit erhöhten DOC-Werten) ermöglicht wird. Das effiziente Fließsystem hat gegenüber einem *batch* UV-Reaktor Vorteile. Zusätzlich ermöglicht der entwickelte nanogold-beschichtete *Dipstick* eine vor-Ort Anreicherung durch kurzes Eintauchen des Teststicks. Dadurch kann der Analytverlust während der Probenahme, dem Transport und der Lagerung deutlich verringert werden. Des Weiteren ist die Dauer der Probenahme verkürzt, da die Filtration und Stabilisierung der Probe sowie das Reinigen von Probegefäßen entfällt. Zukünftige Studien werden sich auf die Optimierung des

Dipstick-Materials konzentrieren, um die Lebensdauer des Samplers zu erhöhen. Außerdem könnte eine Prozessoptimierung zu einer niedrigeren Nachweisgrenze führen, wodurch die Überwachung von Hg-Konzentrationen in Meerwasser möglich werden würde. Weitere Studien sollten die Robustheit der vor-Ort Anwendung des *Dipsticks* verifizieren.

Abstract

Mercury (Hg) is a ubiquitous pollutant that is emitted to the atmosphere from both anthropogenic and natural sources, transported around the globe and eventually deposited in aquatic and terrestrial environments. Human exposure to mercury occurs nowadays mainly from consumption of contaminated fish, as Hg exhibits very high bioaccumulation in the aquatic food chain. Hence, monitoring of low Hg levels in natural water is mandatory for efficient risk assessment and to meet regulations. Within this study, novel analytical methods for ultratrace Hg quantification in natural waters were developed as an alternative to the established standard procedures.

In the first part of this thesis, a fully automated prototype system for reagent-free dissolved Hg determination in aqueous samples was established. The flow injection analysis system (FIAS) is based on direct Hg preconcentration on gold nanoparticles (AuNPs) as a selective adsorbent coupled to atomic fluorescence spectrometric (AFS) detection after thermal desorption of elemental Hg. The novel prototype system was used to determine the total dissolved Hg concentration in seawater samples from a depth profile in the Black Sea, a series of river waters and untreated as well as treated municipal wastewater. Accuracy of the proposed method was confirmed by comparison of found Hg concentrations in these real water samples with those obtained by a reference method (*e.g.* U.S. EPA method 1631). The developed FIAS-AFS method offers significant advantages over established methods, because no reagents are needed for sample preparation, analyte preconcentration, and desorption which minimizes the risk of contamination. This leads to a detection limit as low as 13 pg L^{-1}. Moreover, the method provides a broad linear working range covering 5 orders of magnitude and a good reproducibility described by a relative standard deviation of 3.26%.

Earlier studies demonstrated that dissolved organic matter (DOM) in natural waters might affect Hg accumulation on the AuNP-based collector leading to minor recoveries. Hence, the influence of humic and fulvic acids (HA, FA) as well as selected organic ligands on Hg adsorption onto a AuNP-based adsorbent was systematically studied as part of this work. Spike experiments in a HA matrix with a dissolved organic carbon

(DOC) concentration between 2.5 to 10 mg C L^{-1} demonstrate a high recovery of 1 ng L^{-1} of Hg. The results obtained with organic model solutions confirm that thiol-based ligands have a stronger influence on Hg adsorption onto AuNPs than non-sulfur ligands. To overcome minor findings due to Hg complexation by organic compounds a fully automated online UV irradiation pretreatment procedure was developed. This procedure was implemented into the optimized FIAS-AFS system in order to decompose organic matter online prior to Hg accumulation onto the AuNP-collector. HA model solutions with a DOC concentration up to 15 mg C L^{-1} were investigated with the modified FIAS-AFS. Accurate Hg quantification in sample solutions was achieved by adding hydrogen peroxide to the samples prior to 6 min online UV irradiation. Alternatively, online digestion based on titanium dioxide-assisted photocatalytic decomposition of organic substances was set-up and tested. A one-minute UV radiation exposure significantly improves the degradation process, resulting in Hg recoveries between 71 to 99% for HA model solutions.

In the second part of this study, a nanogold-decorated dipstick was developed for passive sampling of Hg from water samples. The novel sampler facilitates on-site accumulation of the analyte by dipping it into the respective water body. This simplifies the sampling procedure and minimizes contamination risk due to omission of transportation and storage of liquid samples. As a first approach, quartz glass tubes were applied as substrates for the deposition of *in situ* formed AuNPs. However, the performance of the quartz glass-based dipstick deteriorated over time and its mechanical stability was proven to be limited. Hence, a mesoporous-macroporous silica monolith was applied for AuNPs immobilization and further application to Hg extraction from aqueous solution. During method development the influence of blank contribution, gold loading, exposure time and sample volume were thoroughly investigated. In addition, adsorption of Hg onto the sampler was studied under turbulent and static conditions. The porous structure of the silica monolith and the deposited AuNPs were characterized by scanning electron microscopy. The applicability of the novel sampler to natural water samples was confirmed by a recovery experiment in spiked seawater with a recovery rate of 101%. Additionally, the data received from direct determination of dissolved Hg in a freshwater sample by preconcentration onto the novel dipstick agreed with the U.S.

EPA method 1631. The developed method exhibits a limit of detection of 1.31 ng L^{-1} for an exposure time of only 1 min, featuring a good reproducibility, evidenced by a standard deviation smaller than 5.4%.

This work presents highly sensitive analytical methods for determination of ultratrace Hg in natural waters. The selective AuNP-based sorbents enable decomposition and preconcentration of dissolved Hg species followed by fluorescence detection without addition of any reagents. As a result, contamination risk and limit of quantification are significantly reduced. Moreover, the proposed methods exhibit short analysis times and easy handling providing attractive alternatives to standard methods for trace Hg analysis. The optimized FIAS-AFS can be coupled to online UV digestion enabling reagent-free Hg quantification even in demanding water matrices (*e.g.* wastewaters with elevated DOC levels). This highly efficient online procedure is advantageous over batch type UV reactors. Furthermore, the developed nanogold-decorated passive sampler allows on-site accumulation of Hg by briefly dipping it into the waters. As a result, analyte loss during sampling, transportation and storage is most efficiently minimized. Besides, sampling is shortened as filtration and stabilizing of the sample are omitted and no cleaning of sampling containers is required. Future studies will focus on optimization of the dipstick material in order to prolong its lifetime. In addition, the procedure enhancement may lead to a lower detection limit making the procedure applicable to open ocean water monitoring. Further studies will have to prove the robustness of on-site application of the dipstick in the field.

1. Introduction

Mercury is a naturally occurring element which is mainly emitted to the atmosphere as gaseous, elemental Hg (Hg^0) by both, anthropogenic and natural sources. The major fraction of anthropogenic Hg results nowadays from its use in artisanal and small-scale gold mining (ASGM) and from the combustion of fossil fuels, in particular coal. Other sources are industrial processes like metal and cement production.[1] Natural weathering of Hg-containing rocks, geothermal activities as well as episodic events, *e.g.* volcanic eruption and forest fires are some natural pathways for Hg emission.[1,2] Over the last decades industrial countries made great efforts to reduce anthropogenic Hg emissions. As an example, the European Union established an export ban for Hg and a strategy for the safe storage of metallic Hg ((EC) No 1102/2008).[3] Furthermore, strict limits regulate the Hg content in products, *e.g.* batteries, pesticides, and electronic equipment. The United States prohibited the sale, the export, the transfer and distribution of metallic Hg since January 2013 in order to reduce the availability in domestic and international markets.[4] The Minamata Convention is a global treaty that was adopted in October 2013 to protect human and environmental health from Hg and its compounds.[5] As a result of these regulations, anthropogenic Hg emissions in Europe have been reduced by approx. 40% from 1990 to 2000.[6] However, Hg emissions in developing countries in Asia, South America, and Africa have increased significantly in the last decade. The global Hg emission inventory estimates that 37% of global anthropogenic Hg emission is associated with ASGM and about 24% results from coal burning power plants due to increasing energy demand. Overall, the global anthropogenic Hg emission therefore slightly increased from 1,900 tons in 1995 to 1,960 tons in 2010.[1]

Because of the high volatility of Hg and the long-range atmospheric transport, the element is globally distributed from emission hot spots to aquatic systems, sediments and soil *via* wet and dry deposition.[7,8] This leads to an ubiquitous distribution of trace amounts of Hg in all environmental compartments. Typical Hg concentrations in pristine freshwaters and groundwater are 1 to 4 ng L^{-1}, whereas total Hg in open ocean waters is often below 1 ng L^{-1}.[9–12] Three chemical forms of Hg are naturally present in the hydrosphere: elemental Hg (Hg^0), divalent ionic Hg (Hg^{2+}) within inorganic and organic

complexes, and organic species that include both monomethylmercury (MMeHg) and its complexes and dimethylmercury (DMeHg). The organic compounds are formed from inorganic Hg through biological and abiological mechanisms and the portion of a particular species strongly depends on the water type (*e.g.* freshwater, seawater).[13,14] The most toxic species to humans and animals is MMeHg, which is produced by microorganisms, predominantly sulfate-reducing bacteria.[15] MMeHg bioaccumulates in fish and other marine organisms up to a factor of 10^6, which makes dietary intake the major exposure risk of Hg to humans. Since the worst ever case of Hg poisoning in Minamata, Japan, in the 1950s people all over the world became aware of the high toxic risks.[16] Several thousand people died after consumption of contaminated fish from Minamata Bay and hundreds of children were born handicapped. Responsible for this mass poisoning was an acetaldehyde production site (*Chisso Cooperation*), which continuously released industrial wastewater containing organic Hg species for a period of 30 years. Consequently, the European regulatory authorities allow a maximum Hg level in most fish of 0.5 mg kg^{-1}, for some larger predatory fishes the upper limit is set at 1.0 mg kg^{-1}.[17] The *World Health Organization* (WHO) and the *United States Environmental Protection Agency* (U.S. EPA) set the limit of total Hg in drinking water to 6 µg L^{-1} and 2 µg L^{-1}, respectively.[18,19]

In order to meet the regulative requirements to control low Hg levels in natural water highly sensitive and selective analytical methods are mandatory. Over the last decades various instrumental detection techniques coupled with typically cold vapor (CV) generation and amalgamation technique (AT) for analyte separation and preconcentration, respectively, have been applied for Hg trace analysis in waters.[20] However, these methods require elaborate sample pretreatment and addition of multiple reagents leading to elevated blank values that compromise analytical quality and restrict quantification limit. Consequently, the development of advanced analytical methods overcoming these restrictions and providing easy to handle, reagent-free on-site trace analysis are required. Thereby, novel nanomaterial-based strategies for Hg monitoring in environmental and drinking waters are currently in the research focus.[21] In this regard, previous studies of the research group led by *Prof. Dr. Kerstin Leopold* show that nanostructured gold collectors are perfectly suitable for direct solid-phase extraction of

dissolved Hg species from natural water.[22–24] On the basis of these findings, the aim of the present thesis was to investigate and overcome limitations of this method and to further develop the technique in order to provide a novel on-site sampling approach.

1.1. Aim of the thesis

The aim of this study was to develop a prototype system for ultratrace mercury analysis in natural water based on a reagent-free analytical method using AuNP-coated silica for direct preconcentration of dissolved Hg species from aqueous solutions. Therefore, various procedural steps of the analysis cycle as well as the collector material were optimized with the objective to present an easy to handle and compact instrument. For evaluation of the analytical method the performance characteristics (*e.g.* precision, sensitivity) were determined as part of this work. In addition, the total dissolved Hg concentration of different real water samples was analyzed within this thesis.

Dissolved organic matter strongly interacts with Hg and affects its speciation, mobility, solubility, and toxicity in the aquatic environment. The scope of the present thesis was to study possible interferences arising from dissolved organic matter on Hg preconcentration onto immobilized gold nanoparticles. Therefore, suitable organic compounds and isolates from a freshwater, *i.e.* humic and fulvic acids, were investigated to simulate real water matrices.

Previous studies demonstrated that Hg preconcentration on nanogold-based collectors is negatively affected by the DOC concentration of the sample, leading to non-quantitative Hg recovery. Hence, the aim of this study was the development of an online UV digestion unit to decompose strong Hg-DOM complexes to achieve quantitative Hg recovery.

A further goal of this scientific work was the construction of an aqueous passive sampler for Hg accumulation from natural water samples in order to overcome the disadvantages of a loosely packed particles collector and conventional bottle sampling. Therefore, different solid materials were impregnated with AuNPs and their suitability for Hg

accumulation was investigated. The influence of various parameters, *e.g.* concentration of the exposure solution and accumulation time were thoroughly investigated as part of the present work.

2. State of the art: Mercury in the aquatic environment

2.1. Natural and anthropogenic sources

Mercury is a natural element present throughout the world. It is a transition element in the group 12 with atomic number 80 and seven natural isotopes. The physical and chemical properties significantly differ from the other d^{10} elements zinc and cadmium. Hg is the only metal, which is present in its liquid state at room temperature, having a melting point of -38.84°C and a boiling point of 356.6°C. The gaseous phase consists of monoatomic Hg. The vapor pressure at 20°C is 0.0016 mbar, which results in a concentration of about 15 mg Hg per cm^3 in saturated air. Hg appears as a silvery liquid and does not react with air when it is present in a pure state. Liquid elemental Hg rarely occurs as small droplets enclosed within ores. The common oxidation states of Hg are +1 and +2, namely mercurous (Hg_2^{2+}) and mercuric ion (Hg^{2+}), respectively. Monovalent Hg(I) compounds consist of dimeric Hg_2^{2+} with covalently bound Hg atoms. Kalomel (Hg_2Cl_2) is a rarely occurring mineral and the only Hg(I) compound in the environment. Predominantly it is found in minerals like cinnabar (HgS), levingstonite ($HgS \cdot 2\,Sb_2S_3$), and montroydite (HgO). Major ore deposits are in Spain, Slovenia, Italy, Iraq and Germany.[25] Hg is also present as an impurity in non-ferrous metals and in fossil fuels such as coal. The proportion of Hg in the earth crust is $8 \cdot 10^{-6}$ weight percent.

Hg is emitted to the atmosphere through anthropogenic and natural sources. The most important natural sources are volcanic eruptions, weathering of Hg-containing rocks and geothermal activities. However, significantly higher amounts are released to the

4

environment through human activities. Suitable models have estimated the global annual Hg emissions to the atmosphere to 8,900 tonnes.[7] Thereby, anthropogenic sources account for approx. 2,000 t y^{-1}, whereas global natural emissions are estimated to 80 to 600 t y^{-1}. The remainder is contributed by re-emission of deposited Hg. This stock was emitted to the environment in the past by both anthropogenic and natural sources and was then stored in terrestrial and aquatic compartments. Forest fires are an example for re-emissions, whereby deposited Hg in vegetation is released to the atmosphere.

Most significant anthropogenic emission sources are nowadays artisanal and small-scale gold mining (ASGM) in south Asian and African countries. Thereby, liquid Hg is used to extract gold from soil and sediments through amalgamation. During thermal treatment of the obtained amalgam high quantities of gaseous Hg^0 are released to the atmosphere. In 2010 this sector accounted for 37% of the global anthropogenic Hg emissions to the air.[1] The second largest source is coal, which releases gaseous Hg during combustion within power plants. This accounts for 24% of the global anthropogenic Hg budget. Until 1990 Hg was commonly used for the production of chlorine within the chlor-alkali-electrolysis. For this purpose, Hg was used as a cathode material in the amalgamation technique. In the context of the regulation (EC) No 1102/2008, the European chlor-alkali industry started phasing out the mercury-based technology for chlorine production until 2020.[3,26] Hg was further used as a filling for thermometers and high-vacuum pumps. Today, the European Union strictly restricts and/or prohibits the use of Hg in consumer products *e.g.* batteries, electronic equipment, energy-saving lamps and pesticides. The export and import of Hg containing products is nowadays controlled and the use of Hg in industrial processes clearly diminished. Furthermore, silver amalgam is no longer used as dental filling in medical application due to the toxic inhalation of elemental Hg. Nevertheless, Hg pollution associated with the manufacturing and disposal of Hg-containing products still occurs. These may include batteries, energy saving lamps, fluorescent lamps, electrical and electronic equipment, cosmetics, paints, as well as pesticides and fungicides. Beside atmospheric emissions, Hg and its compounds are directly released into natural aquatic systems *via* contaminated effluents from Hg processing sites. Furthermore, it enters natural water by leaching from Hg-containing waste. Once emitted into the environment Hg cycles

between air, soils and water and only a small fraction is detracted by deep ocean sediments and through entrapment to mineral compounds.

2.2. Biogeochemical cycling and bioaccumulation

The lifetime of atmospheric Hg^0 was estimated to range between 8 to 24 months before it is introduced into aquatic and terrestrial systems.[8,27] Therefore, Hg is globally transported and distributed by the atmosphere and the ocean, resulting in a worldwide contamination and environmental concern.[28] More than 95% of the atmospheric Hg is present as Hg(0), which is slowly oxidized to Hg(II) in the gas phase. The most important reactants within this oxidation are O_3, $NO_3^{\bullet}$, Cl_2, H_2O_2, and $OH^{\bullet}$.[29,30] There are further processes within the liquid phase with the same oxidants.[31,32] Oxidized Hg(II) has a high solubility in water and thus readily enters the environmental compartments through precipitation. About 60% of the total atmospheric Hg is deposited to land and 40% of Hg(0) enters the marine environment and freshwaters.[33] This is somehow a contradiction to the fact that about 70% of the earth's surface is covered with water. A probable reason for this is given by *Mason et al.*[33]. The oxidation mechanism of Hg(0) to Hg(II) in aerosols occurs predominantly over land and thus the deposition rate for atmospheric Hg is higher for terrestrial than for aquatic systems. About one third of the input to terrestrial systems results from dry deposition.[33]

The major source of Hg to the oceans is atmospheric Hg, which enters the marine system through wet deposition and to a less extent through dry deposition. In addition, Hg input to open ocean result from rivers and estuaries, groundwater, benthic sediments, and hydrothermal vents. Globally, about one third of the total atmospheric Hg input to the open ocean result from Hg in river discharges. Thereby, 28% of Hg in rivers reaches the open ocean while the remaining fraction is deposited in benthic sediments at ocean margins.[34] Typical concentrations of total dissolved Hg in the ocean vary between 0.2 to 0.5 ng L^{-1}, with 2 to 15% of the total Hg present as MMeHg.[35–38] Hg concentration in freshwater systems is generally higher compared to marine environments. Several studies determined the total Hg concentration in pristine lakes and groundwater with

results between 1 to 5 ng L^{-1}. About 10% of the total Hg concentration was found as MMeHg in oxic lake water.[9,10] Other freshwater samples, *e.g.* rainwater, river water, and lake water exhibit Hg concentration between 0.2 to 90 ng L^{-1} and the MMeHg fraction is typically below 20%.[24,39–44] In general, MMeHg concentration in freshwater is strongly depending on the water properties, especially on the dissolved oxygen content. Once dissolved in natural water Hg(II) undergoes complex chemical and biochemical transformations. Most of the Hg(II) (ca. 70%) is readily reduced to elemental Hg, which is sparely soluble in water and thus evades from the water surface. Natural water are mostly supersaturated in Hg(0) compared to the air above. Only a small portion of Hg is removed from the system by gas evasion and sedimentary burial. **Figure 1** illustrates a scheme of the biogeochemical cycle of Hg including its chemical, photochemical and biochemical conversion in the atmosphere as well as in the aquatic system. In addition, Hg species and predominant complexes in anoxic and oxic waters are emphasized.
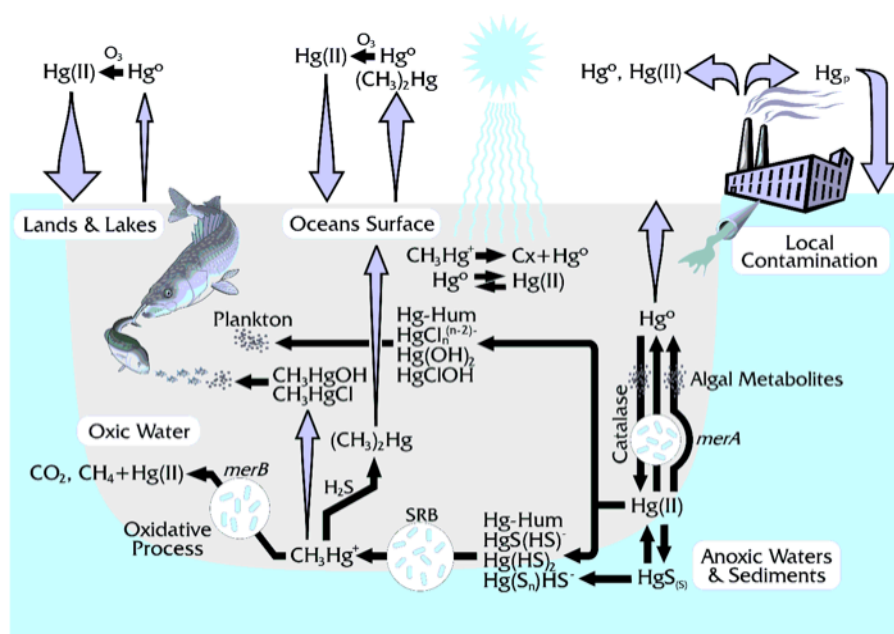
Figure 1*: The biogeochemical cycle of mercury (reprinted with permission from Schäfer et al.[45], copyright 2002 by Taylor & Francis).*

Three forms of dissolved Hg are present in the aquatic environment: elemental mercury (Hg(0)), inorganic mercury (Hg(II)) and organic mercury (MMeHg, DMeHg) species. In general Hg(0) concentration is higher near the air-water interface, whereas MMeHg and

Hg(II) concentrations are higher in deeper waters near the sediments. According to thermodynamic calculations divalent Hg is not available in the free, ionic state.[46] In oxic waters Hg(II) is rather complexed by hydroxide ($Hg(OH)^+$, $Hg(OH)_2$, $Hg(OH)_3^-$) and chloride ($HgCl^+$, $HgClOH$, $HgCl_2$, $HgCl_3^-$, $HgCl_4^-$). Among the organic mercury species, DMeHg is unreactive and highly volatile, which leads to evaporation to the atmosphere. On the other hand MMeHg is usually present as chloro (MeHgCl) and hydroxo (MeHg(OH)) complex.[47] However, the sort of complex depends strongly on the water properties, *e.g.* parameters like nutrient content, pH, temperature, dissolved oxygen and sulfide content, chloride and dissolved organic carbon (DOC) concentration. In the deep ocean (> 1,000 m) the sulfide concentration increases and thus influences Hg complexation. Due to the high affinity of Hg(II) to sulfur ligands complexes such as $Hg(SH)_2$, $Hg(SH)S^-$, HgS_2^{2-} are formed in anoxic waters and near the sediment. In addition, insoluble cinnabar (red, HgS) and metacinnabar (black, HgS) precipitate in deep water layers. Also MMeHg forms complexes with sulfide ligands (*e.g.* $MeHgS^-$) in anoxic waters. Reduction and oxidation processes of Hg within natural water are controlled by both chemical and biochemical processes. MMeHg is formed from Hg(II) through biochemical methylation processes in the anoxic water layer near the sediment from anaerobic bacteria like sulfate-reducing bacteria (SRB). MeHg is a strong neurotoxin that bioaccumulates through the food chain. Thus, controlling Hg concentration in natural water and in fish is mandatory to preserve humans from Hg intoxication.

2.3. Exposure risk and toxicological properties

All Hg compounds are toxic to humans and animals, however the extent of risk depends amongst others on Hg speciation, the duration and exposure pathway and the health status of a given individual. In general, organic mercury compounds are more toxic than inorganic species. Metallic Hg and insoluble mercury sulfide (HgS) are less toxic. However, inhalation of elemental mercury and absorption *via* the lungs is most hazardous for humans. As mentioned earlier, the use of Hg in consumer and medical products has been reduced in European and other western countries over the last decades

due to the awareness of possible health risks. However, some Hg containing products (*e.g.* energy saving lamps) are still manufactured today and thus workers are potentially exposed to Hg. The U.S. *Occupational Safety and Health Administration* (OSHA) sets the permissible exposure limit (PEL) for elemental Hg to 0.1 mg m^{-3}.[48] In Germany, the *Bundesanstalt für Arbeitsschutz und Arbeitsmedizin* restricted the Hg concentration of working atmosphere to 0.02 mg m^{-3}.[49] In everyday life humans may face toxic Hg vapor due to breakage of Hg-containing fluorescent lamps or thermometers. In developing countries there is only little awareness of the toxicological effects owing to Hg and regulations for safe working conditions are poor. Here, liquid Hg is used for the extraction of gold from sediments and soil. During the thermal treatment of the formed amalgam elemental Hg is evaporated and released into the atmosphere. Thus, workers are directly exposed to high concentrations of harmful Hg vapor. A study by *Drasch et al.*[50] demonstrated that in addition to the gold miners, residents living in the vicinity of gold mines are also exposed to critical Hg concentrations. Inhaled Hg is highly mobile and distributes to all parts of the body. Hg vapor can pass the lipid monolayers of the cell membrane, the blood-brain and placental barriers probably due to its physical properties. The first sign of an acute Hg(0) intoxication is dyspnea, followed by *e.g.* chest pain, nausea and chills. Chronic Hg exposure may exhibit a different course of disease and symptoms such as tremor and psychological disturbances occur most frequently. High exposure to gaseous Hg(0) may result in damage to the kidneys and respiratory tract or even death.[51]

The high toxicity of MMeHg was first recognized in the 1860s when two technicians died of poisoning during synthesis of these compounds. Nevertheless, methyl- and ethylmercury species were used as antifungal agent for agricultural applications till 1970. In late 1971 a mass MMeHg poisoning incident occurred in Iraq. Seed grains were treated with a MMeHg containing fungicide, imported from Mexico and the United States to Iraq. These seeds were initially not intended for human consumption but due to some factors the toxic grain was consumed by Iraqi residents. Another tragic mass intoxication occurred in Japan when between 1932 and 1968 the Hg containing effluent of an acetaldehyde manufacturing plant was introduced into the sea at Minamata Bay.[16,52] This pollution affected at least 50,000 fishermen and their families who

consumed contaminated marine organisms. It was later discovered that Hg(II) is biomethylated by microorganisms and bioaccumulated in fish, seafood and marine mammals as MMeHg. This pathway is until today the most common Hg intake source and exposure risk for humans. Accumulation factors of up to 10^6 are observed in predatory fish and marine mammals and regular consumption can be harmful. Large, long-lived marine (*e.g.* shark, swordfish, tilefish, and king mackerel) and freshwater (*e.g.* bass, trout, and pike) predators exhibit the highest MMeHg concentration. MMeHg predominantly binds to free amino acids and proteins in the muscle tissue of fish. As a consequence, law regulates the maximum permitted concentration of Hg in fish. The European Union established a limit of 0.5 mg kg^{-1} for smaller fishes and 1.0 mg kg^{-1} for predatory fish (*e.g.* monkfish, pike, tuna).[17] The US *Food and Drug Administration* (FDA) limits Hg in fish to 1 mg kg^{-1}. The major portion of about 95% of ingested MMeHg is absorbed in the gastrointestinal tract, followed by distribution to all tissues. The toxic effects of MMeHg are mainly on the central nervous system. As a first symptom numbness of limbs was reported in the literature, followed by dysarthria, loss of hearing and lack of coordination. Hg concentration in blood and urine is an indicator for inorganic Hg intoxication; total Hg in scalp hair and whole blood is determined to trace exposure to MMeHg. A detailed review on the toxicological effects of Hg and its compounds is published by *Clarkson* and *Magos*.[51]

2.4. Natural organic matter and its interaction with Hg species

Natural organic matter (NOM) is ubiquitous in our environment and influences the mobility, distribution and speciation of metal pollutants in natural water. It arises from allochthonous organic matter (*e.g.* leaves, wood) and autochthonous matter (*e.g.* algae) through physical, chemical and microbiological transformation, a process called humification. Another source for NOM is dead animal tissue. The exact formation pathways are not yet fully elucidated and still of great interest in research. Total organic carbon (TOC) is often used as a synonym to natural organic matter since the

contribution of carbon from contaminants of anthropogenic origin in natural water systems is generally insignificant. TOC is operationally classified into two size fractions. All dissolved organic compounds that pass through a filter with a pore size of 0.20 to 0.45 μm are considered as dissolved organic carbon (DOC). However, this fraction comprises not only the truly dissolved compounds but also contains colloids, a part of the humin fraction and complexes with fulvic and humic acids. The filter residue is named particulate organic carbon (POC), which accounts for approx. 10% of the total organic carbon content in natural water. Reported data for DOC concentration in natural water vary over a wide range, with the lowest values observed in seawater and groundwater ([DOC] < 2.5 mg L^{-1}).[53–56] Highest DOC concentrations are found in soil porewater and marshes ([DOC] = 15-30 mg L^{-1}) and in freshwaters influenced from wetland and peatland leaching.[57] DOC concentration is furthermore depending on the climatic zone (*i.e.* temperate, arid, tropical and subarctic zone).[58] The chemical composition of DOC is highly complex including both low-molecular-weight organic molecules and multifunctional large organic compounds. Organic acids account for a considerable proportion of DOC, along with a smaller fraction of bases and neutral compounds.[59]

Organic matter present in soil and sediment is categorized into humic substances (HS) and non-humic substances (NHS). Thereby, HS comprise of fulvic acids (FA), humic acids (HA) and insoluble humin. This classification of soil HS was adopted for dissolved organic matter in aquatic systems. Non-humic substances in natural water consist, among others, of amino acids, fatty acids, phenols, sterols, natural sugars, hydrocarbons, urea and porphyrins.[58] The categorization of HS in aquatic systems differs slightly depending on the respective extraction and separation technique. Thereby, *Thurman* and *Malcolm*[60] classified dissolved organic matter (DOM) based on the solubility in acid and alkaline solution and adsorption properties of the separated compounds. As the natural concentration of dissolved organic carbon is in the range of mg per liter, large volumes of water have to be processed to obtain milligram to gram quantities of isolated humic substances. The hydrophobic fraction of DOM preferentially adsorbs onto a XAD-8 resin. This hydrophobic fraction is further classified into humic acids (HA) and fulvic acids (FA). HA are insoluble at pH values below 2 and thus can be separated from

FA by acidification of the eluent. FAs on the other hand are soluble in alkaline and acid solution. The U.S. *International Humic Substances Society* (IHSS), founded in 1981, offers isolated HA and FA from various sources (*i.e.*, soil, water) as standard and reference material. These are extracted *via* the XAD-8 resin adsorption method. The availability of such materials allows better comparison and evaluation of scientific data.

In natural water the portion of HS within dissolved organic matter is significantly depending on the type of water. The amount of HS in stream and river water varies between 20 to 80%, the proportion of HS in lakes and swamps ranges from 60 to 80%.[61–64] Seawater and estuaries exhibit a lower HS fraction of 2 to 20% with respect to dissolved organic carbon. In general, the amount of fulvic acids in natural water is higher compared to humic acids.[65] As an example, *Harvey et al.*[66] investigated water from the Gulf of Mexico and determined a FA fraction between 62 to 98% of the total HS content. *Day et al.*[61] found a FA fraction > 80% of total humic substances in three streams and one lake sample.

HS possess a heterogeneous chemical structure. The color of HS varies from yellow to brown or black. HS occur in dissolved and solid phases and their molecular weight is given as weight-averaged molecular weight (M_w) or as number-averaged molecular weight (M_n). The ratio M_w/M_n is called the polydispersity index (PDI). *Chin et al.*[67] determined the weight-averaged molecular weights of aquatic fulvic acids and unfractioned organic matter in good agreement with other literature to range between 845 to 2,310 g mol^{-1}. An overview of the elemental composition of HA and FA was given by *Schnitzer*[68] and *Steinberg*[69] (see **Table 1**). The major functional groups in HS are carboxyl, phenolic hydroxyl, alcoholic hydroxyl, carbonyl, quinone and methoxyl groups; ether, ester and ketone groups may also be present.[58] It is clear from **Table 1** that FA exhibit a higher content of acidic groups compared to HA.

Table 1: *Elemental composition and functional groups of humic and fulvic acids (adapted from Steinberg[69], copyright 2003 by Springer, reprinted with permission).*

Element	HA [%]	FA [%]
C	53.6-58.7	40.7-50.6
H	3.2-6.2	3.8-7.0
N	0.8-5.5	0.9-3.3
O	32.8-38.8	39.7-49.8
S	0.1-1.5	0.1-3.6
Functional groups	**HA [meq g^{-1}]**	**FA [meq g^{-1}]**
Acid groups, total	5.6-8.9	6.4-14.2
Carboxylic acids	1.5-5.7	5.2-11.2
Phenolic OH	2.1-5.7	0.3-5.7
Alcoholic OH	0.2-4.9	2.6-9.5
Quinoide/keto C=O	0.1-5.6	0.3-3.1
Methoxy OCH$_3$	0.3-0.8	0.3-1.2

Malcolm et al.[70] investigated DOM deriving from streams, marine systems and soils and clearly demonstrated the differences regarding their composition by using spectroscopic techniques, isotope analysis, amino acid analysis and pyrolysis mass-spectrometry. Moreover, even within one particular environmental system (*e.g.* within a certain type of water) the characteristics of DOM can differ significantly. Further analysis methods such as UV-vis spectroscopy, infrared spectroscopy, fluorescence spectroscopy and elementary analysis are applied to characterize aquatic humic and fulvic substances.

Nowadays, the application of HS in different sectors is versatile. HS are used in agriculture as additives for fertilizers due to their characteristic properties. Furthermore, industrial processes such as concrete production and leather preparation make use of HS.[71] In addition, HS were applied to remove contaminants from natural water or wastewaters due to their high capability to complex inorganic and organic pollutants.

It is well known from the literature that mercury strongly interacts with dissolved organic matter influencing its bioavailability, solubility, mobility, speciation and

toxicity.[72] A quantitative indication for the interaction between Hg and DOM is based on the positive correlation of their concentrations.[73,74] However, not only positive but also negative correlation between DOC in natural water and Hg concentration in fish tissue was observed.[75,76] *Haines et al.*[76] investigated Russian lakes and fish and reported that HgCH₃Cl concentration and color are the two parameters which directly relate to Hg content in fish. On the other hand, *Grieb et al.*[75] found negative correlation between Hg concentration in fish and DOC concentration in water.

The transportation of Hg from contaminated soils into streams, lakes and groundwater was traced back to the strong complexation capability of organic compounds.[77,78] Spectroscopic studies performed by *Xia et al.*[79] support earlier theories that dissolved Hg is most probably attached to organic acids *via* sulfur-containing ligands. The preference of Hg for sulfur ligands, the less electronegative halides, and N-containing ligands is based on its classification as a B-type metal cation. B-type metals have a soft sphere of highly polarizable electrons in the outer shell. Stability constants for Hg(II) complexation with reduced sulfur sites (*e.g.*, sulfide, thiol) far exceed those with oxidized sulfur ligands. Sulfur is a minor element in humic and fulvic acids and ranges between 0.1 to 3.6 wt% (see **Table 1**). *Xia et al.*[80] estimated the fraction of reduced sulfur in IHSS *Suwannee River* humic and fulvic acids as 46% and 35% of the total S, respectively. Even if the elemental fraction of S is low in HA and FA the concentration of reduced sulfur within DOM far exceeds Hg concentration in pristine natural water. *Ravichandran et al.*[81] found another evidence for strong Hg-DOM interaction during investigations with insoluble red cinnabar and black metacinnabar (HgS). Thereby, organic matter, which was isolated from a natural source induced dissolution of HgS. Furthermore, the precipitation of HgS was inhibited in the presence of DOM.[82]

However, stability constants for Hg-DOM complexes are rarely reported in the literature and stated values vary by several orders of magnitude. *Ravichandran*[83] summarized stability constants of Hg-DOM complexes from recent studies. These values derive from investigations with aquatic humic substances.

14

Table 2: *Stability constants for Hg with natural dissolved organic matter deriving from different methods.*

Method	Source of organic matter	pH	Conditional stability constant (log K)	Ref.
Competitive ligand with octanol-water partitioning	Aquatic HS	variable	10.6-11.8 (for low-sulfidic site) 22.4-23.8 (for high-sulfidic site)	[84]
Adsorption to peat and model fitting	Aquatic HS released from peat during adsorption experiment	6.0	25.8-27.2 (strong binding sites) 7.3-8.7 (weak binding sites)	[85]
Competitive ligand exchange	Organic matter in stream and waste water treatment plant	-	> 30	[86]
"Reducible" titration	DOM from lakes and rivers	7.5	21-22.9	[87]

The differences may arise from several factors such as a varying composition of organic matter and the experimental conditions of the studies. In addition, the sensitivity of the analytical method to separate free Hg and Hg-DOM complexes plays a key role for stability constant calculations.

The literature presented so far is dealing with inorganic Hg(II) but complexation of MMeHg by dissolved organic matter was also observed and reported (*e.g. Miskimmin*[88] and *Hurley*[89]). *Hintelmann et al.*[90] used HA and FA isolates from lake water to investigate the interaction of these humic substances with MMeHg. HA exhibit two binding sites for MMeHg and a stability constant for the stronger one was calculated as $1.3 \cdot 10^{12}$ under pH and ionic strength conditions applied. Consequently, an absolute amount of 0.2 ng CH_3Hg^+ was bound per mg humic acid.

2.5. Mercury trace analysis in waters

2.5.1. Established and standard methods

In order to meet the regulative requirements for monitoring low Hg levels in natural water highly sensitive and selective analytical methods are mandatory. Over the last decades various instrumental detection techniques have been applied for Hg ultratrace determination in waters, *e.g.* atomic absorption spectrometry (AAS), atomic fluorescence spectrometry (AFS), inductively couple plasma-mass spectrometry (ICP-MS), and total X-ray reflection fluorescence (TXRF) analysis.[91–96] A combination of these techniques with *e.g.*, cold vapor (CV) generation and amalgamation technique (AT) for analyte separation and preconcentration, respectively, significantly enhances the sensitivity of these methods. Furthermore, coupling to chromatographic techniques allow speciation, typically after derivatization. A review article by *Leopold et al.*[20] summarizes analytical techniques for both, total Hg determination and Hg speciation, in natural water.

On the basis of these instrumental techniques global authorities have provided well-documented protocols for Hg determination in natural water samples. The *Environmental Protection Agency* (EPA) method 1631 "Mercury in Water by Oxidation, Purge and Trap, and Cold Vapor Atomic Fluorescence Spectrometry" is the most common procedure in this context.[97] A corresponding method (EN ISO 17852: 2006) published by the *International Organization for Standardization* (ISO) uses the same strategy for Hg ultratrace analysis of drinking, surface, ground and rain water.[98] These standard procedures are based on sample oxidation, purge (CV) and trap (AT) of gaseous Hg and subsequent detection by AFS. Thereby, a batch or a flow injection system may be used. The guideline includes purification procedures for all reagents and gives instrumental requirements. It names suitable materials for the applied apparatus and containers, indicates precautions regarding potential contamination and gives detailed instruction on system suitability testing in order to obtain reliable results. The method is applicable for Hg determination in a broad variety of water samples in a concentration range from 0.5 to 100 ng L^{-1}. The method detection limit was determined to be 0.2 ng L^{-1}. As the absolute amount of preconcentrated Hg can be increased with

increasing sample volume the LOD could be minimized to 0.05 ng L^{-1} applying this method with particular caution on sample and reagent handling. Since U.S. EPA method 1631 has been used as a reference method in this work a detailed description can be found in the experimental section (see section 6.6.1). However, elaborate sample preparation and addition of various reagents for *i.e.* Hg species transformation and organic matter decomposition restrict the detection limit of this method and lead to an increased risk of contamination. In order to minimize blank contribution clean working procedures have to be followed and reagent purification has to be performed prior to application. Furthermore, highly oxidizing and partly toxic reagents, *e.g.* BrCl or KMnO$_4$, are used to digest dissolved Hg species and complexes in natural water. Hg analysis by CV-AFS is a time-consuming technique, depending on the sample matrix digestion may take up to 12 hours. In addition, bulky instrumental equipment and multistep sample preparation under strict conditions complicates on-site application. The common practice comprises sampling, transportation and storage of the water samples followed by laboratory analysis. Consequently, the demand for portable, easy to handle, and rapid analytical devices for on-site analysis and monitoring purposes has increased over the last years.

Nanomaterials (NMs) appeared to be a promising tool for heavy metal trace analysis due to their outstanding sorption properties.[99,100] Since it was shown that NMs are suitable sorbents for Hg preconcentration the interest in NMs and their application to Hg trace analysis in waters has grown significantly. The recent trends in NM-based methods are covered within the next section.

2.5.2. Nanomaterials for Hg trace analysis

Nanomaterials or nanostructured materials exhibit by definition at least one dimension in the size range between 1 to 100 nm.[101] They can exist in various shapes, from zero- to three-dimensional structures, and common types of NMs are particles, tubes, prisms, rods, layers, dendrimers and quantum dots. NMs exhibit unique chemical and physical properties. The number of surface atoms increases continuously with decreasing particle

size and as the binding sites of the surface atoms are unsaturated adsorption and desorption phenomena will occur, potentially followed by surface reactions. One reason for using NMs for analytical approaches is the higher ratio of surface-to-bulk atoms. Since the surface atoms are in steady contact with the dissolved analyte a high amount of surface atoms is enhancing the preconcentration step.[102–104] The release of the analyte can be performed by elution or thermal desorption prior to measurement. In addition, NMs can be applied to enhance detection techniques due to their special optical properties. Metallic NPs exhibit surface plasmon resonance (SPR). This phenomenon is visualized by the color difference of bulk gold and gold particles in the nanometer scale. A dispersion of 13 nm spherical AuNPs exhibits a bright red color, whereas a bulk gold material appears yellow. This is explained by the free electrons in the metal which interact with an incoming light beam. As a result the light is attenuated which is visible in a red-shift of the spectrum. SPR measurements of metal NPs were performed by means of colorimetric sensing of Hg as the plasmon absorption maximum is shifted in the presence of the analyte. Therefore, nanostructures, mostly made of Ag or Au, can be applied as colloidal solution without modification or after surface functionalization with different ligands, *e.g.* oligonucleotides. Fluorescence measurement is also possible using nanomaterials. It was shown that various nanomaterials show advantageous properties for fluorescence resonance energy transfer (FRET) sensors compared to organic dye molecules. Fluorescent assays are typically based on the high quenching efficiency of AuNPs meaning that the fluorescent emission of a dye molecule (*e.g.* Rhodamine B) is dramatically decreased upon binding to NPs. NMs are furthermore applied for the modification of electrodes within electrochemical methods. For this purpose mostly AuNP are used due to their high conductivity and catalytic activity. Nanostructures offer the possibility to use surface enhanced Raman scattering (SERS) for trace metal analysis, which is usually applied to adsorbed molecules on rough metal surfaces.

The application of NMs for novel analytical approaches for the ultratrace Hg analysis is diverse and an increasing number of research articles have been reported over the last years. A recently published review article by *Huber et al.*[21] summarizes novel NM-based strategies that are feasible for ultratrace Hg determination in natural water or drinking water. These novel approaches using NMs aim to substitute elaborative sample

pretreatment by simplified procedures or try to enhance detection techniques. The objective of these new techniques is to reduce time- and reagent-consuming analytical steps and to develop easy to handle and portable instrumentation for on-site analysis. The review focusses on methods that were already applied to real water samples to proof the principle of possible matrix effects. The methods were furthermore categorized into two groups according to their established detection limits. A LOD below 2.0 µg L^{-1} is suitable for Hg monitoring in drinking water, while Hg determination in pristine natural water requires a LOD below 0.1 µg L^{-1}. This section covers the research trends in Hg ultratrace analysis using novel nanostructured materials that enhance selectivity, sensitivity and reproducibility. Novel NM-based methods for Hg analysis and their analytical parameters (*e.g.* LOD, duration) are evaluated and methods with best performance are highlighted.

Nanomaterial-assisted methods for solid phase extraction

Solid phase extraction (SPE) is a sample pretreatment step to separate the target analyte from the matrix and to preconcentrate the analyte before the instrumental measurement. This pretreatment technique can be further used for species analysis or to convert the physical and/or chemical state of the sample in a way that it is suitable for subsequent analysis. Due to their versatile benefits sorbents made of NMs were integrated to SPE methods for Hg determination in waters. One advantage of such NMs is the high amount of surface atoms that leads to a higher extraction capability and lower reagent consumption. Several examples of NMs utilized for Hg trace analysis were reported, recently. Au and Ag NPs, oxidized carbon nanotubes (OCNT) and imprinted polymeric nanoparticles (IPNPs) were applied to selectively adsorb and enrich Hg from waters.[22–24,105–108] The most important parameters of the methods described below are summarized in **Table 3**.

Table 3: Nanomaterial-based methods for solid phase extraction of dissolved mercury.

Analytical Method	Nanomaterial	LOD / EF	Working Range	Time [min]	Hg Fraction	Ref.
SPE CV-AAS	OCNTs	1.9 ng L^{-1} / 150	2-500 ng L^{-1}	3	Hg^{2+}	[105]
SPE CV-AFS	AuNP-mNP	1.5 ng L^{-1} / 80	5-200 ng L^{-1}	17	Hg^{2+}	[107]
SPE ICP-MS	SiO$_2$/AgNPs	2.0 ng L^{-1} (Hg^{2+}) 4.0 ng L^{-1} (tHg) / 100	5-200 ng L^{-1}	60	tHg	[108]
SPE GF-AAS	Ag/AuNPs@ membrane filter	0.4 ng L^{-1} / dng	4-500 ng L^{-1}	dng	Hg^{2+}	[106]
FIA-assisted SPE-AFS	Nanostructured Au collectors	0.08 ng L^{-1} / 1,000	0.08-100 ng L^{-1}	7	tHg	[24]

ndg: data not given.

Parodi et al.[105] presented an on-line flow injection system in combination with oxidized carbon nanotubes for SPE of Hg(II). The preconcentrated amount of Hg was eluted by hydrochloric acid, and the resulting solution was measured by standard CV generation combined with AAS detection. A similar approach regarding the detection technique applied AuNP-modified Fe$_3$O$_4$ magnetic core-shell particles to adsorb Hg(II).[107] The dispersion was separated by a magnet and the remaining particles were rinsed with hydrochloric acid to release Hg. This solution was subsequently analyzed by CV-AFS. *Yordanova et al.*[108] used amino-functionalized silica as supporting material for AgNPs to selectively adsorb inorganic Hg (Hg^{2+}). Quantification of Hg^{2+} was performed by ICP-MS after complete dissolution of the formed amalgam with a mixture of concentrated nitric acid and hydrogen peroxide at 90°C. Consequently, new sorbent material has to be used for each adsorption/desorption cycle. The duration for extraction and subsequent elution (60 min) is considerably higher compared to other novel SPE-based methods for Hg analysis. Within this work, an additional analysis for total Hg was performed after mineralization of the sample. The concentration of methylated Hg was derived by subtraction. *Panichev et al.*[106] used nylon membrane filters as a substrate to

immobilize Au and Ag NPs as SPE tool. Aqueous samples were then oxidized with $KMnO_4$ in order to oxidize all Hg species. Next, a reduction step was performed with $NaBH_4$ to generate Hg(0). In contrast to classical CV generation, the dissolved Hg(0) was adsorbed at the NPs deposited on the filter by direct filtration. Hg was removed from the sorbent by thermal desorption and analyzed with an AAS.

All presented examples exhibit values for the limit of detection for inorganic mercury in the same range (0.4 to 2.0 ng L^{-1}). Hence, from the sensitivity point of view all approaches are applicable for Hg determination in pristine waters. The methods were applied to real water samples (*e.g.* river water, well water, lake water, seawater) and featured good recovery rates for the tested Hg spike concentrations. However, the presented methods were not able to determine the total amount of Hg in water except for the method presented by *Yordanova et al.*[108]. However, for the determination of tHg an acid microwave digestion was necessary to transform $MeHg^+$ into Hg^{2+}. The analysis time is a critical factor for on-site sampling and high throughput analysis. Hence, this parameter was chosen to evaluate the novel NM-based SPE methods. According to this aspect the method based on OCNTs presented by *Parodi et al.*[105] shows outstanding performance with only 3 minutes per analysis.

In contrast to the methods mentioned above reagent-free SPE of total Hg in natural water was demonstrated by the research group led by *Prof. Dr. Kerstin Leopold*. Therefore, nanostructured Au collectors or AuNPs immobilized on silica particles were applied as specific Hg adsorbent.[22–24] For these studies a quartz glass microcolum, filled with the nanostructured Au material, was coupled to a FIAS-AFS. Quantitative adsorption of various Hg species (Hg^0, Hg^{2+}, $MeHg^+$, ethyl-Hg, phenyl-Hg were tested) onto a nanostructured Au surface was systematically studied and it was demonstrated that the surface morphology of the gold collector is critical regarding Hg species adsorption. The process is explained by a three step mechanism based on the catalytic activity of nanogold. Nanostructured gold provides methyl group stripping, reduction and amalgamation of the formed Hg^0 (see Figure 2).[23] Dissolved Hg^0 is directly adsorbed by the nanostructured surface *via* amalgamation. Moreover, a similar capacity was shown for the preconcentration of dissolved Hg using gold nanoparticle (AuNP) coated silica particles instead of nanostructured bulk gold. This novel methods performs

without the addition of any reagents for species transformation, preconcentration and release of Hg^0 for detection. Hence, the risk for contamination is minimized and an remarkable LOD of 0.08 ng L^{-1} was achieved.[24]
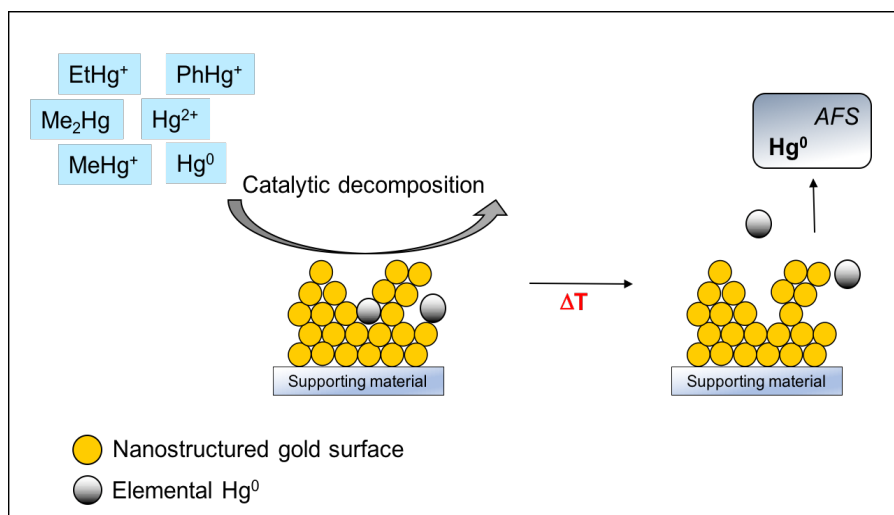
Figure 2: *Catalytic decomposition of dissolved mercury species on a nanostructured gold surface, subsequent thermal desorption and atomic fluorescence spectrometry of mercury.*

Nanomaterial-assisted methods for in-situ Hg trace analysis

The development of portable sensors is straightforward towards miniaturization of analytical techniques, which is of current interest to environmental monitoring. Recently, two articles were published giving an overview of nanostructured sensors for heavy metal detection.[109,110] In addition, advances towards lab-on-chip (LOC) analysis and microfluidic chips are presented. Sensors can be divided due to their different signal transduction mechanisms, *e.g.* electrochemical or optical. Thereby, optical sensors are based on colorimetric, fluorescent, surface-enhanced Raman scattering and surface plasmon resonance (SPR) devices. The working principle of an optical sensor is based on a shift of the absorbance maximum or a change in absorption intensity caused by the interaction of the NM with the analyte, *e.g.* the shift of the absorption maximum of the SPR of AuNPs. NMs were used in many different shapes, *e.g.* nanoparticles, nanoprisms, nanocages, nanorods mostly consisting of Au or Ag.

Fluorescence and colorimetric sensing methods are advantageous over instrumental techniques since they are simple with portable set-ups, fast, inexpensive and simple.[111–120] In some cases sample preparation steps are time-consuming, thus on-site measurement is yet hindered. The LODs of NM-assisted colorimetric Hg probes and detection techniques based on fluorescence are typically within a range from 0.1 to 2 μg L^{-1}. With the identified performance these novel analytical tests are certainly a good alternative to check drinking water for its Hg(II) content as the maximum tolerable level of inorganic Hg is 2 μg L^{-1} defined by the U.S. EPA. Analysis of natural pristine water is not possible at the current state of research. However, for the determination of tHg, further investigations on other Hg species are required and/or suitable sample pretreatment steps have to be adapted for this purpose . In addition, it is conspicuous that for most of the colorimetric and fluorescent detection methods neither reference materials were analyzed nor results were compared with an instrumental standard method. Thus, the accuracy of the method is not fully validated. The answer of the fluorescence signal is very fast, still duration of sample preparation is reported to be between one to two hours which prolongs the overall analysis time enormous.

A very low LOD of 1.7 ng L^{-1} has been achieved by a colorimetric approach based on the Hg^{2+} uptake of citrate-capped platinum nanoparticles (PtNPs) followed by amalgamation.[103] The uptake of the analyte inhibits the peroxidase-like activity of citrate-capped PtNPs to oxidize 3,3',5,5'-tetramethylbenzidine (TMB) by H$_2$O$_2$. The catalytic activity of the functionalized PtNPs is changed by the addition of Hg^{2+}. Thus, the intensity of the absorption peak of TMB decreases with increasing Hg^{2+} concentration. The reaction solution and the active PtNPs were mixed and incubated for 10 minutes at 45°C prior to absorption spectrometry. The applicability towards real water was tested by spiking tap water with Hg^{2+} within a concentration range between 1,000 to 5,000 ng L^{-1}. Unfortunately, the chosen experimental conditions in this work are not feasible to proof the applicability towards real water samples as they have a complex matrix composition and substantially lower Hg concentrations.

Electrochemical methods

Electroanalytical determination of Hg is performed over the past decades. EPA method 7472 describes anodic stripping voltammetry (ASV) for Hg(II) determination in water. Nanostructured electrodes and NM-modified electrodes are suitable for accumulation and electrochemical determination of Hg(II).[121,122] The introduction of NMs significantly enhanced the sensitivity and selectivity of traditional electrochemical methods. Due to their high electrical conductivity AuNPs are mostly utilized for the modification of electrodes within electrochemical sensors. The method is selective for labile Hg(II), whereas divalent Hg complexed with organic ligands or other strong inorganic or organic anions may not be detected by electrochemical approaches. Advantages of these methods are the fast response, low system costs and simplicity. Most of these techniques are not applicable towards ultratrace Hg levels due to their restricted limit of detection. Another drawback of electrochemical techniques is that the preparation of nanostructured electrodes or NM-modified electrodes is often complicated and sophisticated equipment is required.

Surface-enhanced Raman spectroscopy

Raman spectroscopy is a sort of vibrational spectroscopy that enables the structural identification of trace amounts of chemical compounds based on the unique vibrational characteristics, which is called the fingerprints. Surface-enhanced Raman spectroscopy (SERS) have been developed in the last ten years. SERS can be explained by the enhancement of normal Raman scattering by the excitation of localized surface plasmons (LSP) of adsorbed molecules on electrochemically roughened or nanostructured metallic surface. This advancement offers highly sensitive and selective detection of adsorbed molecules on nano-metal surfaces. Through functionalization of nanostructures with specific ligands that bind to *e.g.* Hg^{2+} SERS has also been applied towards sensitive Hg sensing. As an example a SERS chip based on functionalized plasmonic nanostructures is presented in the following section.[123] Therefore, silver-coated AuNPs were applied on a silicon wafer followed by surface modification with

4,4´-dipyridyl. Upon addition of dissolved Hg(II) solution SERS signal of the organic ligand was quenched. The signal quenching degree reaches a maximum after a period of 4 minutes and a sample volume of only 20 μL is sufficient. With regard to this small sample volume the LOD of this method is extraordinary low (2 pg L^{-1}). The applicability of the SERS chip for real samples was demonstrated by determination of Hg^{2+} in milk, orange juice and lake water. The results were in good agreement with a reference method (AFS) and recovery was in the range between 98 to 108%. The high sensitivity of SERS approaches is obviously an advantage over optical and electrochemical NM-based methods.[124,125] Consequently, determination of Hg in pristine natural water is conceivable, whereas studies of Hg content in seawater by SERS-based detection have not been reported yet.

3. Principles of applied analytical techniques

This chapter describes the instrumental techniques regularly applied within this work. Atomic fluorescence spectrometry (AFS) was applied for Hg(0) detection after thermal release from newly developed nanogold-base adsorbents. Compared to atomic absorption spectrometry (AAS) AFS exhibits a higher sensitivity towards Hg. Furthermore, the herein developed analytical procedure uses flow injection analysis technique, which was first reported in the 1970s. The history of flow injection analysis as well as the advantages of this method are therefore highlighted in a following chapter. For the quantitative determination of gold that was deposited onto the Hg sensitive adsorbents total reflection X-ray fluorescence (TXRF) was chosen as sensitive analytical detection method with limits of detection in the lower μg per liter range.

3.1. Atomic fluorescence spectrometry for Hg analysis

Bunsen and *Kirchhoff* first discovered the physical principle of atomic fluorescence in the 1800s. Atomic fluorescence is based on the excitation of an atom by absorption of a

photon with a specific wavelength. Thereby an outer shell electron is transferred to a higher energy level (excited state). The excited electron returns to a lower energy level within a few nanoseconds. During this process energy is emitted in the form of fluorescence radiation, which can be measured with a suitable detector. The main types of atomic fluorescence transitions are depicted in **Figure 3**. [126]
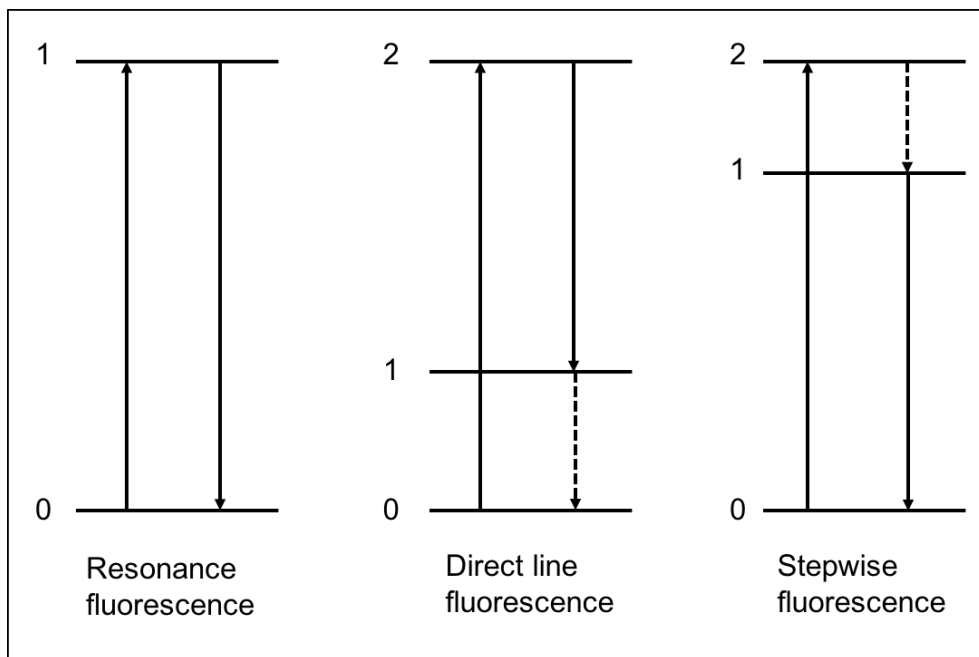
Figure 3: *Basic types of atomic fluorescence transitions.*[126]

Resonance fluorescence is observed when the excitation wavelength is equal to the emission wavelength ($\lambda_A = \lambda_F$). This kind of fluorescence is mostly used for analytical approaches. Direct line fluorescence occurs if the excited electron returns to a higher energy level. Stepwise fluorescence arises if different upper energy levels are involved in the excitation and fluorescence process. If the photon energy of fluorescence is less than the photon energy of absorption ($\lambda_F > \lambda_A$) the process is called Stokes-type fluorescence. The reverse process is termed anti-Stokes-type fluorescence ($\lambda_F < \lambda_A$). For Hg determination, the resonance transition line at 253.7 nm from the 6^3P_1 excited state to the 6^1S_1 ground state is employed (see **Figure 4**). Therefore, a line source with an emission wavelength of 253.7 nm is typically used for excitation. The fluorescence intensity obviously depends on the excitation power, which allows direct increase of detection sensitivity by increasing the power of the source radiation. The fluorescence

intensity in atomic fluorescence spectrometry is directly proportional to the concentration of the analyte at low concentrations. The parameters influencing the fluorescence intensity B_F are given in equation 3.1.[128]

Equation 3.1:
$$B_F = \left(\frac{l}{4\pi}\right) Y_{21} E_{v12} \int_0^\infty k_v dv$$

l	Path length in the direction of the detection system
Y_{21}	Fluorescence (quantum) efficiency
E_{v12}	Spectral irradiance of exciting radiation at absorption line ($v12$)
$\int_0^\infty k_v dv$	Integrated absorption coefficient over absorption line
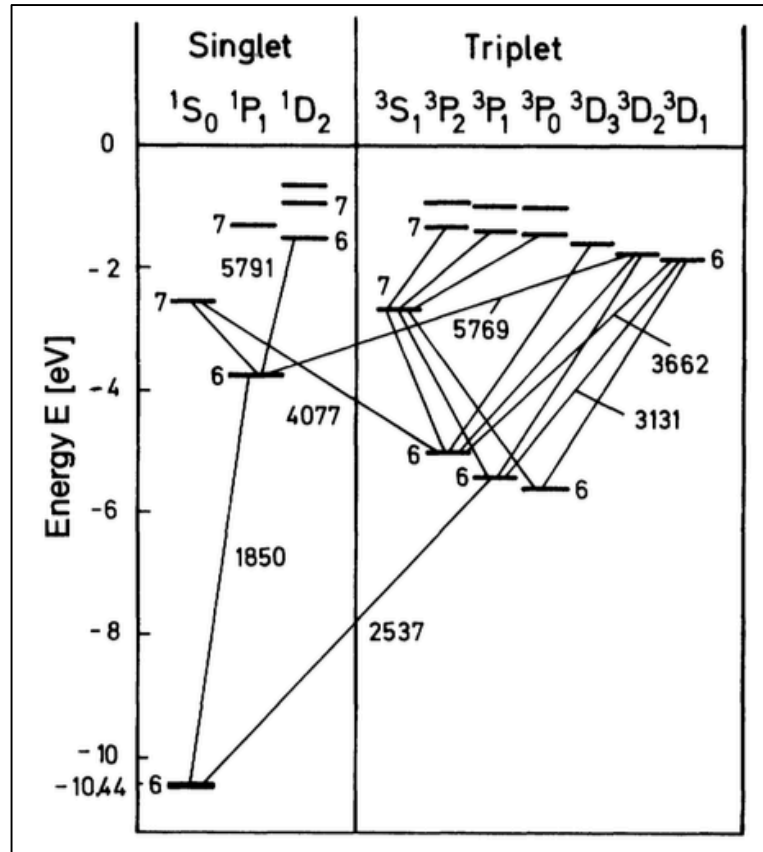
Figure 4*: Simplified energy diagram of the mercury atom (reprinted with permission from Haken and Wolf[127], copyright 2005 by Springer).*

Deactivation of excited atoms by collision with other compounds may occur in the fluorescence cell, a process called quenching. Argon (Ar) is a poor quencher with a low quenching cross-section for the 253.7 nm Hg resonance line and is thus mostly used as inert carrier gas within AFS analysis. It has been shown that the fluorescence intensity increases by a factor of 100 using Ar instead of air.[129]

Winefordner and *Vickers*[130] first utilized AFS as analytical method in the early 1960s. The instrumental set-up of an atomic fluorescence spectrometer is similar to that for AAS and atomic emission spectrometry (AES). In the case of AFS the emitted fluorescence radiation is measured perpendicular to the excitation source. **Figure 5** shows the schematic set-up of an atomic fluorescence spectrometer, which was applied throughout this work for Hg detection. Common radiation sources used for AFS are hollow-cathode-lamps, electrodeless discharge lamps, vapor discharge lamps and laser sources. They can be categorized into spectral line sources and continuum sources. Since the intensity of the fluorescence radiation is proportional to the excitation energy a high-energy source is desirable in order to achieve high sensitivity and a broad linear range. In addition, the source should provide a good short- and long-time stability.
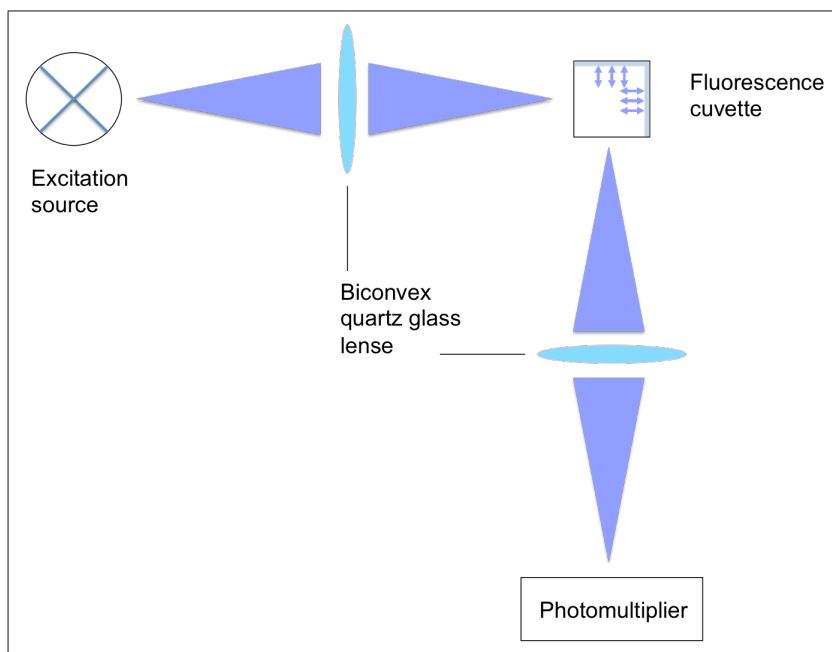
Figure 5: *Schematic set-up of a non-dispersive atomic fluorescence spectrometer.*

For more detailed information refer to *Winefordner* and *Elser*[131] who described the importance of radiation source for AFS measurements. Depending on the radiation source dispersive and non-dispersive systems can be applied for AFS. For wavelength selection in dispersive systems monochromators and filters are used. Simpler and less expensive are non-dispersive systems which can be operated without a wavelength selection if the emitting source is free of lines from interfering elements and exhibits a low background emission. This is the case for Hg vapor lamps. As a result, the optical transmission is good for non-dispersive systems.

Cold vapor generation

A basic requirement for observation of atomic fluorescence is obviously that the investigated analyte has to be present in its atomic state. Therefore, atomization by spectroscopic flames or electrothermal atomizers (ETA), *i.e.* graphite furnace, is commonly performed in AAS and AFS. Regarding the determination of Hg by flame atomization coupled to AFS, nebulizer-burner systems were used in early studies.[132] However, due to the high background signal, the detection limit for Hg analysis in *e.g.* natural water was insufficient. On the other hand, Hg exhibits an appreciable vapor pressure of 0.0016 mbar (approx. 14 mg m^{-3}) at room temperature and makes thermal or electrothermal treatment unnecessary if Hg is directly reduced to its elemental form in solution.[133] Regarding this, *Hatch* and *Ott*[134] applied tin(II) chloride ($SnCl_2$) as a reducing agent to generate elemental Hg^0, which was aerated from solution in a closed system for subsequent non-flame AAS detection. Interferences are significantly minimized as the analyte is separated from the matrix before the measurement. This technique can also be coupled to AFS and is nowadays called cold vapor (CV) generation. Commercial instrumentation for Hg determination *via* CV-AFS is available since the beginning of the 1990s.[135,136] Since $SnCl_2$ reduces only inorganic Hg(II) species, organo-mercury compounds (*e.g.* MMeHg) have to be decomposed prior to CV generation for total Hg determination. Thereby, bromine chloride (BrCl) showed good performance with respect to suitable digestion times and high Hg recovery.[137] The

method was further improved by coupling a flow injection (FI) system for CV generation to AFS.

Amalgamation technique

In order to achieve lower detection limits for Hg determination in the nano- to picomolar level preconcentration of the analyte is required prior to detection. In connection with CV generation the so-called amalgamation technique (AT) is most commonly used. Here, the aerated elemental Hg(0) vapor is preconcentrated on metals such as gold and silver.[138–141] This process is very specific for elemental Hg. Various forms and collector types filled with the respective metal, *e.g.* gauzes, films, wires and beads have been applied for Hg preconcentration. However, coated materials with a large surface area are preferred over bulk materials as Hg tends to diffuse into the solid and thus increases the possibility for memory effects.[128] A significant advantage of the AT is the separation of gaseous by-products from the analyte stream prior to fluorescence measurement. Moreover, when CV-AFS is performed directly, *i.e.* Hg reduction in solution is followed by slow release of Hg(0) and direct transport to the measurement cell by an inert gas stream, broad fluorescence peaks occur. A higher signal-to-noise ratio is achieved when Hg(0) is trapped on an adsorber and rapidly released upon heating to 500 to 700°C. It was shown that a temperature of 500°C is sufficient to release Hg from gold-coated glass beads.[142] The possibility of thermal desorption is another great advantage of preconcentration by AT, since no reagent is required for elution and desorption, which leads to minimizing reagent-consumption and contamination risk.

Further optimization was carried out using a two-stage gold amalgamation process for atmospheric Hg analysis by AFS, total Hg determination in water by AAS and dissolved, elemental Hg analysis in water by AFS detection.[143]

3.2. Flow injection analysis

The development of automated analytical methods offers a great advantage for investigations of large sample series, as in environmental monitoring of substances in air, water and soil. Manual operations and costs are minimized, sample throughput and precision of measurement increase due to less analysis time and procedural steps. In the 1970s first automated flow injection systems (FIS) were described by *Ruzicka* and *Hansen*[144] and *Stewart et al.*[145]. These methods are based on the principle of the earlier developed air-segmented flow injection system by *Skeggs*[146] in 1957. However, it was shown that non-segmented, continuous FIS in the absence of air bubbles exhibits some advantages.[147]

- Higher sample throughput
- Better response times
- Significantly higher switch on and off times
- More simple and versatile set-up

The separation of an analyte from the sample matrix by *e.g.* dialysis, extraction, and distillation can be conducted within FIS. Thereby, quantitative separation is not mandatory as the reproducibility of automated systems is very high compared to manual operation.[147] In addition, the stream can be automatically heated, filtered and/or decanted within a continuous flow analyzer.[144]

De Andrade et al.[148] first coupled the FI technique to CV-AAS for the determination of inorganic Hg in aqueous samples. The approach showed similar analytical performances compared to conventional batch CV-AAS methods with a sampling rate of 110 samples per hour. At the same time *Morita et al.* published a FI-CV-AFS system for inorganic Hg determination from standard solutions. Further development towards total Hg analysis was performed by the implementation of an online UV digestion unit.[149] In a more recent study by *Leopold et al.*[150] the applicability of automated, reagent-based digestion in FI-CV-AFS towards total Hg analysis in natural water was demonstrated.

3.3. Total reflection X-ray fluorescence analysis

Total reflection X-ray fluorescence spectrometry (TXRF) is a type of energy-dispersive X-ray fluorescence spectrometry using a specific instrumental set-up. It is applied as a non-destructive, multi-elemental method for the quantitative and qualitative analysis of trace elements in a variety of samples. Quantitative analysis is mostly performed with liquid samples that are deposited as thin layer onto a highly reflective carrier and subsequently the solvent is vaporized. For solid samples either a thin layer of a homogenous fine powder is applied on the sample carrier or the powder is prepared as suspension. TXRF is commonly applied in environmental and food analysis as well as in clinical applications and for quality control.

X-rays are situated between ultraviolet radiation and gamma radiation in the electromagnetic spectrum. Photons with an energy in the range between 0.1 to 25 keV (100 to 0.5 Å) are typically used as excitation source for analytical approaches.[151] The principle of X-ray fluorescence (XRF) is based on the interaction of an atom with X-ray photons. The excitation energy is transferred to an innermost electron, which leads to the ejection of this electron. Therefore, the atom remains in an excited state. A higher-energy level electron immediately (10^{-16} s) fills this vacancy and the energy difference between the emitted electron and the electron filling the vacancy is emitted as X-ray fluorescence. This radiation is specific for each element and various transitions result in characteristic lines, independent on the excitation source. According to the energy level, *i.e.* electron shell, to which the electron relaxes, the resulting line series are called *e.g.* K- or L- lines. A notation (α, β, γ) introduced by *Siegbahn* in the 1920s further specifies the transition within the upper energy level and the final state as can be seen in **Figure 6**.

A second process predominates for elements with an atomic number below 5 (boron). Excess energy is transferred to an outer shell electron, which results in ejection of a second, so-called Auger electron, and the atom is left in a double-ionized state. Thus, reliable results from X-ray fluorescence spectrometry are only obtained for elements from boron to uranium (Z = 5-92).
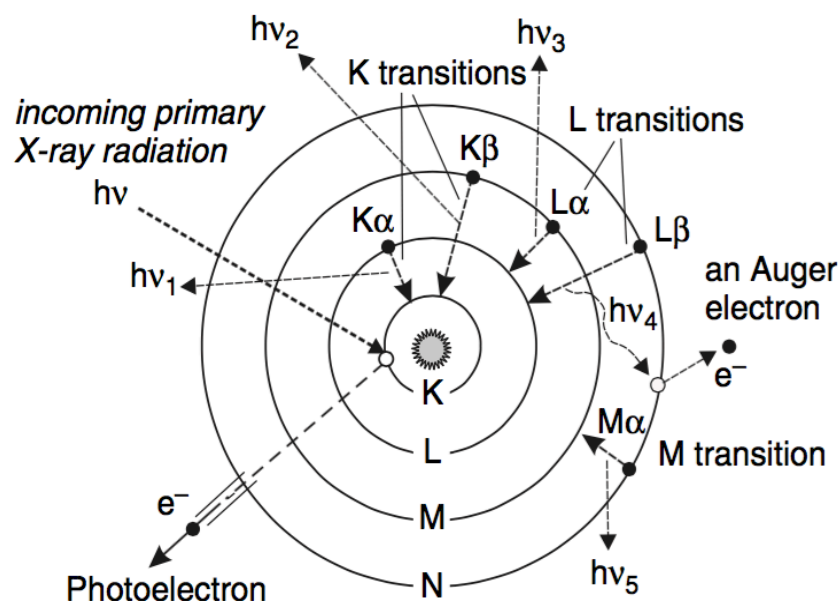
Figure 6: Schematic of the X-ray fluorescence process (reprinted with permission from F. and A. Rouessac[152], copyright 2007 by John Wiley & Sons).

X-ray radiation as excitation source for analytical (laboratory) instruments are generated *via* three different processes[147]:

1. Acceleration of electrons towards a target anode (X-ray tube)
2. Irradiation of a material with a primary X-ray to produce secondary X-ray radiation
3. Decay of radioactive substance under release of X-rays

The most common excitation source for TXRF is an X-ray tube. Thereby, electrons are generated at a heated filament and accelerated towards an anode, typically consisting of W, Cr, Cu, Mo, Rh, Ag, Fe and Co. Two different types of X-ray radiation have to be considered. A continuous spectrum named *Bremsstrahlung* is generated due to the deceleration of highly energetic electrons at the atomic core of the anode material. Thereby, the energetic state of the electron beam is lowered and the resulting energy difference is emitted as X-ray continuum spectrum. In a second process inner shell electrons of the anode are removed, subsequently replaced by an electron from an upper shell and characteristic lines are emitted similar to the process described above (see **Figure 6**). A typical set-up of a TXRF spectrometer is depicted in **Figure 7**.

The sample is prepared as a thin film deposited on a polished carrier made of quartz, silicone, germanium, glassy carbon or Perspex acrylic plastic.[154] The collimated X-ray beam hits the sample below the critical angle and is totally reflected from the support. The critical angle depends on the photon energy and the properties of the sample carrier. Using a quartz carrier and a 17.5 keV Mo-Kα line as excitation source the critical angle is below 0.1°. The atoms within the sample are thus excited and emit X-ray fluorescence radiation that is recorded by the detector placed perpendicular to the sample carrier. The energy-dispersive detector counts the emitted photons at each specific fluorescence energy within a given spectral range providing both, qualitative and quantitative, analytical information.
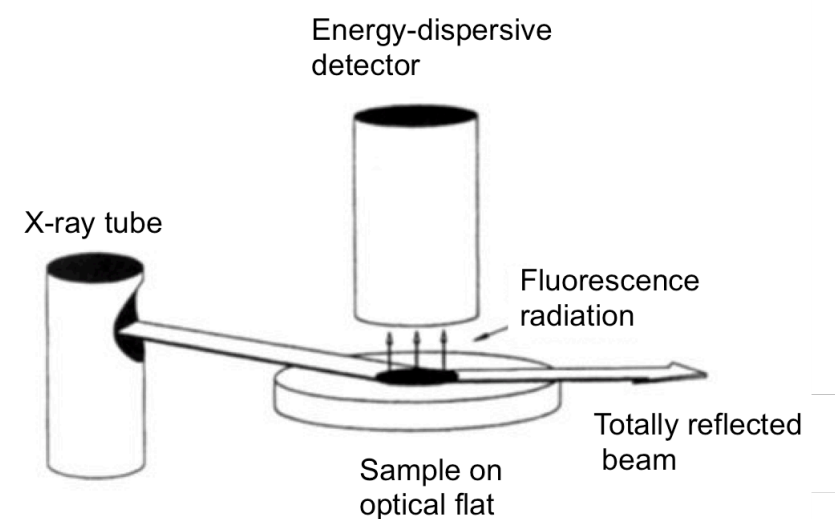
Figure 7: Schematic set-up of a total reflection X-ray fluorescence spectrometer (reprinted with permission from Klockenkämper[153], copyright 1997 by John Wiley & Sons).

The advantage of TXRF over conventional XRF is the low penetration depth of the primary X-ray radiation, which results in less absorption and scattering processes within the sample matrix. Thus, a much better signal-to-noise ratio is obtained and detection limits are improved. First TXRF instrumentation was introduced in the end of 1970.[155,156] Within this work TXRF was applied to determine the total amount of gold loaded onto the developed mercury adsorber materials.

34

4. Fully automated reagent-free flow injection analysis system for dissolved mercury analysis

Leopold et al.[22] developed a novel analytical method for ultra-trace determination of total dissolved Hg in natural water, which was first published in 2009. The method is based on the preconcentration and separation of naturally occurring dissolved Hg species, *i.e.* Hg(0), Hg(II), MMeHg and its complexes, onto a nanogold-based solid-phase collector. Dissolved mercury is defined as the fraction that passes a 0.45-μm pore-size filter while sample preparation. Hence, suspended particulate matter (> 0.45 μm) is included when talking about the total Hg concentration in *e.g.* water. Earlier studies depict the adsorption mechanism of gaseous metallic Hg on gold and silver substrates under varying conditions but this has not yet been known for Hg species in aqueous media.[157,158] *Zierhut et al.*[23] first described species selective adsorption of dissolved elemental Hg onto a gold surface. This collector, made of high purity gold gauze or beadlet, exhibits a smooth surface and quantitatively traps dissolved Hg(0) (98.2 ± 1.5%) *via* an amalgamation process. Other species *e.g.* Hg(II) and MMeHg pass the gold surface almost without chemical or physical interaction revealing less than 5% retention. Furthermore, it was shown that dissolved Hg species, *i.e.* Hg(0), Hg(II) and MMeHg, adsorb quantitatively (82 to 96%) onto a nanostructured gold surface.[23] The nanostructured surface was derived by a conditioning process, in which repeated amalgamation of dissolved Hg(0) and subsequent thermal desorption were performed. Quantitative adsorption rates for Hg species were observed for gold nanoparticle (AuNP) coated silica.[22] The adsorption process of Hg(II) and MMeHg was interpreted by the catalytic activity of nanogold *via* a three-step mechanism (see also **Figure 2**, p. 22).[23] Thereby, a nanogold-structured surface or AuNPs promote alkyl group stripping, in the case of organomercury compounds, and reduction to Hg(0), followed by amalgamation. Due to the fact that a nanostructured gold surface is thermodynamically unstable, AuNP-coated silica is preferred for analytical application.[23,159] After preconcentration of dissolved Hg species, elemental Hg(0) is thermally released from the nanogold-based collector and atomic fluorescence is measured at 253.7 nm. Thus, no liquid eluent is needed to release Hg after preconcentration. Moreover, no reagents are

required for species conversion and preconcentration, which reduces the risk of contamination and minimizes blank values. As a result, a limit of detection in the picogram per liter level for total dissolved Hg was achieved. In addition, the novel analytical method features a broad linear working range and high reproducibility. The described method was set-up as a flow injection analysis system (FIAS) coupled to an atomic fluorescence spectrometer (AFS) for Hg detection for automated analysis.

The aim of this study is to further optimize the flow injection system with the objective to develop a prototype for Hg ultratrace analysis of natural water samples. Therefore, the analytical steps and the components of the initial FIAS-AFS have been improved. Furthermore, the influence of natural occurring organic compounds towards Hg preconcentration onto the nanogold collector was investigated. Organic ligands and model solutions were used for the preliminary scientific approach. In order to digest organic matter within a water sample a reagent-free online UV digestion was implemented to the novel FIAS-AFS. Hg recovery in spiked model solutions was determined after online UV pretreatment. The effect of oxidant addition and the presence of a titanium dioxide layer in combination with sample UV irradiation were systematically studied. In addition, demanding real water samples having particularly high dissolved organic matter concentrations and/or extremely low Hg concentrations were analyzed in order to evaluate limitations and extent the applicability of this method for Hg ultratrace analysis.

4.1. Development of a prototype for Hg ultratrace analysis

The following chapter describes the optimization of various components and procedural steps of the FIAS with the aim of presenting a prototype for reagent-free ultratrace Hg determination. In cooperation with Analytik Jena AG (Jena, Germany) a fully automated and computer-controlled instrument was developed within this work. A simplified scheme of the FIAS is presented in **Figure 8** and the general steps of the analysis cycle are explained in the following.

The sample loop of predefined volume is first filled with the aqueous sample. The sample is subsequently transported by a carrier solution (0.06 M HCl) towards the nanogold collector for direct preconcentration of dissolved Hg. In a subsequent step the nanogold collector is rinsed with carrier solution and ultrapure water (UPW). After this water is removed from the collector by passing argon through the collector tube. Next, elemental Hg^0 is released from the nanogold surface by thermal desorption and transported by argon towards the AFS cuvette for detection. During the heating process remaining moisture is evaporated and subsequently condensed within a Peltier cooling
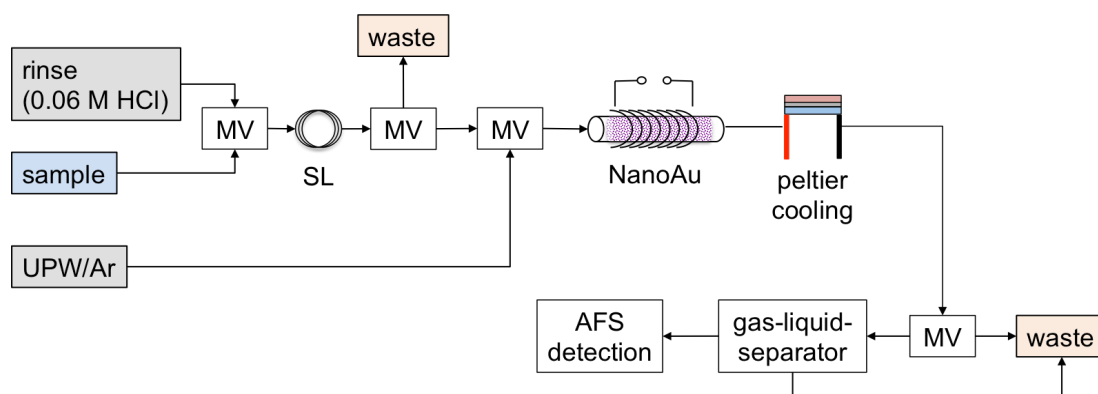
Figure 8: Schematic illustration of the flow injection analysis system coupled to an atomic fluorescence spectrometer for reagent-free Hg determination in aqueous solution (abbreviations: UPW ultrapure water; Ar argon, i.e. carrier gas; MV magnetic valve; SL sample loop; NanoAu nanogold-based collector, AuNP-coated silica).

device for separation from the gaseous analyte stream using a gas-liquid-separator. Rapid cooling of the nanogold material is achieved from the outside by a ventilator and by UPW flowing through the collector before the next sample is preconcentrated onto the nanogold collector. The FIAS was coupled to an AFS and was set up in a special laboratory for ultratrace metal analysis. A schematic illustration and a photograph of the initial set-up are depicted below (**Figure 9**).
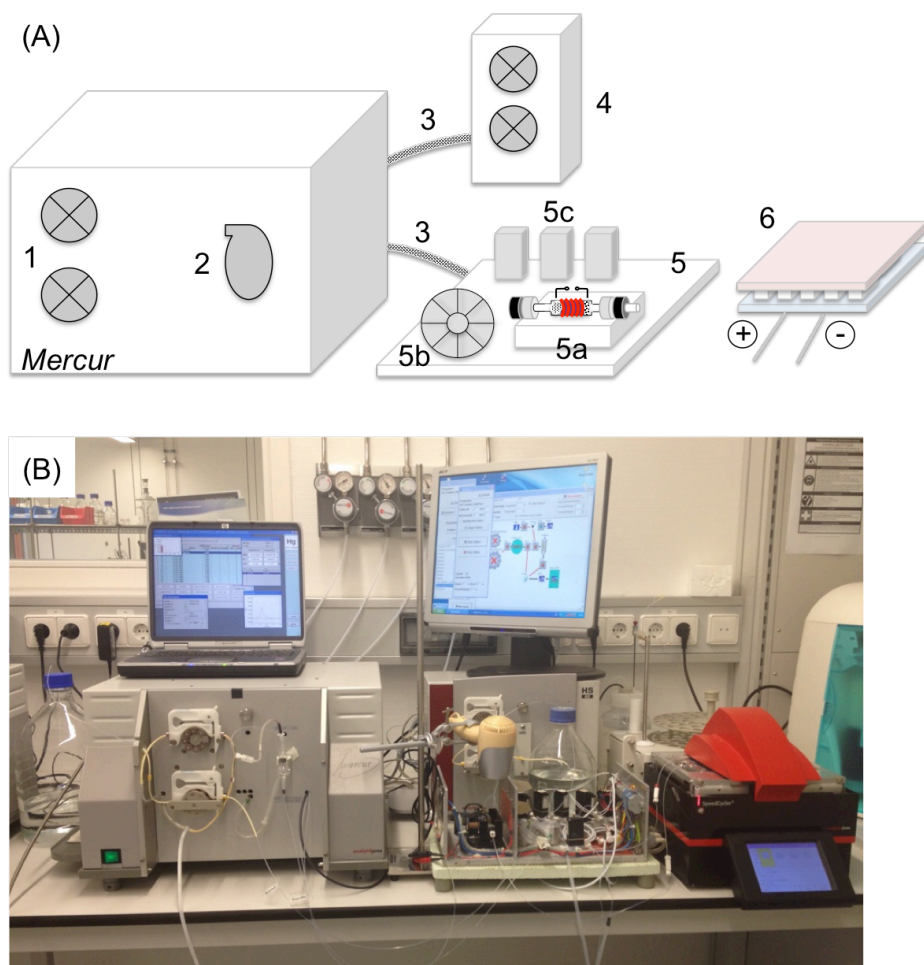
Figure 9: (A) Schematic illustration and (B) photograph of the initial flow injection analysis system coupled to an atomic fluorescence spectrometer (1 peristaltic pump, 2 gas-liquid-separator, 3 interface between Mercur AFS and FIAS/external peristaltic pump, 4 external peristaltic pump, 5 FIAS: 5a nanogold collector, 5b ventilator, 5c magnetic valves, 6 Peltier cooling device).

4.1.1. Nanogold-based collector for Hg preconcentration

Optimization of the synthesis of nanogold-coated silica

Gold nanoparticles were deposited on silica (SiO_2) particles in an analog procedure to that described first by *Leopold et al.*[22]. AuNP formation and deposition is conducted *in situ* by the reduction of gold from chloroauric acid. The pH of the gold solution was adjusted to 6.5 to 7.0 with sodium hydroxide prior to reduction. SiO_2 particles with a

size range of 63 to 200 μm and 200 to 500 μm, respectively, were applied as substrate and chloroauric acid solutions purchased from two manufacturers were investigated as a precursor. One chloroauric acid solution contains platinum (Pt) impurity in the form of a chloro complex ($[PtCl_6]^{2-}$). This is stated on the container by the producer and was not further quantified in this study. **Table 4** summarizes the results of four different batches, where the size of SiO_2 particles and the type of chloroauric acid solution was varied. The color of the derived material after drying was evaluated. In addition, the amount of gold deposited on the SiO_2 particles was determined by extracting it into *aqua regia* followed by quantitative determination by TXRF analysis.

Table 4: *Color and gold load of different batches of nanogold-coated silica.*

Batch No.	Gold source [a]	SiO₂ particle size range [μm]	Appearance after deposition (dried material)	Gold load [mg Au/g SiO₂]
1	Au	200-500	Grey	0.57 ± 0.0017 [b]
2	Au	63-200	Dark grey to purple	1.35 ± 0.0027 [b]
3	Au/Pt	200-500	Bright grey	0.74 ± 0.0015 [b]
4	Au/Pt	63-200	Dark purple	3.50 ± 0.0070 [b]

[a] Chloroauric acid from two different manufacturers without (Au) and with platinum impurity (Au/Pt),
[b] Error given as standard deviation derived from TXRF measurement.

The results show that the overall Au load is higher if smaller silica particles are used. This is explained by a higher surface-to-volume ratio of smaller particles indicating at the same time that *in situ* formed AuNPs are deposited at the surface of the silica particles rather than inside their pores, which exhibit an average pore diameter of 6 nm. The highest load of 3.50 mg Au per g SiO_2 was achieved using a Pt-containing chloroauric acid and SiO_2 particles with a size ranging from 63 to 200 μm (batch No. 4). Thereby, Pt most probably acts as a catalyst during Au^{III} reduction and immobilization of AuNPs onto the silica surface. All further investigations and characterization were therefore performed with nanogold-coated SiO_2 as derived from batch No. 4.

Characterization of nanogold-coated silica

The surface of AuNP-coated SiO$_2$ was studied by scanning electron microscopy (SEM). An exemplary secondary electron (SE) image with a magnification of 25,000x is shown in **Figure 10A**. The corresponding backscattered electron (BSE) image is shown in **Figure 10B**, in which the light spots represent the AuNPs that have regular outlines and clear inter-particle distances. Only few agglomerates of AuNPs are deposited at the silica surface. Three individual BSE images were processed using *ImageJ* software to characterize the particles in more detail. Therefore, the threshold and the contrast of the raw images were adjusted. Subsequent automatic particle identification resulted in a total number of 253 AuNPs. 79% of these particles have a roundness factor of ≥ 0.7 and were thus considered for the calculation of the average particle size and particle size distribution (see **Figure 11**). The average size of the AuNPs, evaluated from three individual images, is 23 ± 9 nm ($n_c = 199$).
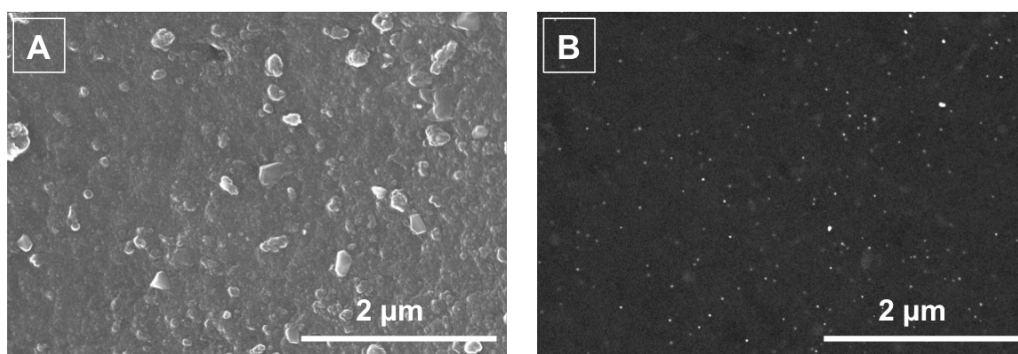
Figure 10: *Scanning electron microscopy (SEM) images of gold nanoparticle-coated silica with (A) secondary electron and (B) backscattered electron detection.*
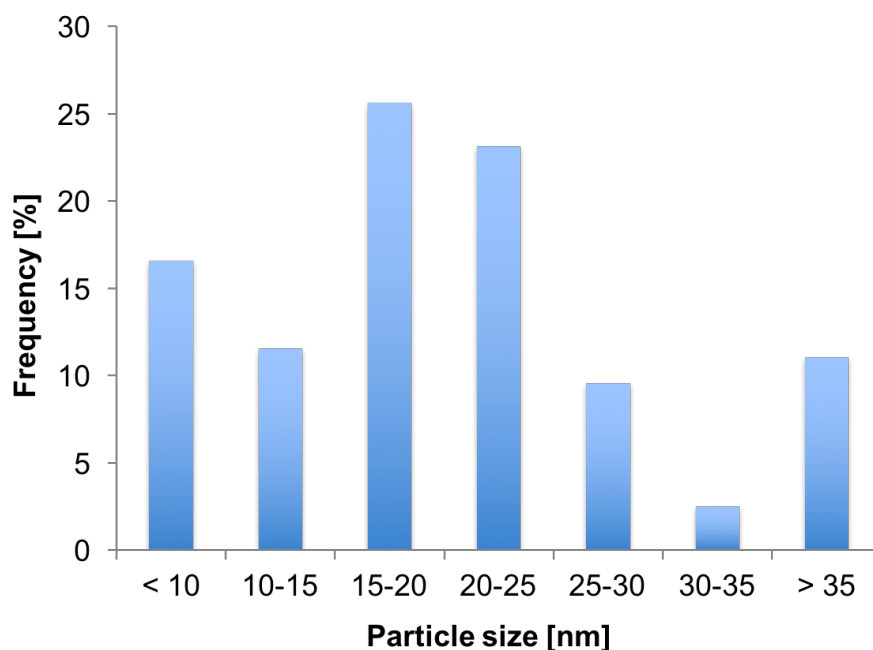
Figure 11*: Particle size distribution of gold nanoparticles on silica surface (n_c = 199, particle size given as major length, roundness factor ≥ 0.7).*

Collector design

Gold nanoparticle-coated silica particles were applied for solid-phase extraction of dissolved Hg species using a packed column that was integrated into the FIAS for automated Hg preconcentration and separation from the liquid sample. The geometry of the column and the corresponding connectors were optimized within this work for easy to handle exchange and integration of the collector into the FIAS (**Figure 12**).

The in-house made collector consists of a quartz glass tube, which exhibits a higher softening temperature than conventional soda-lime glass and is thus more robust against heat exposure. A quartz glass frit was mounted inside one end of the tube so that the loose nanogold-coated silica can be filled into the tube and fixed with a quartz wool wad at the other end of the tube. In this way, the material can easily be replaced while at the same time migration of the AuNP-coated silica particles into the linked tubing is efficiently prevented by the frit. As can be seen from **Figure 12A** the diameter of the column is reduced to 5 mm on each end of the collector tube. Both ends of the quartz glass tube were plugged into a threaded coupler (see **Figure 12C**) where the modified

fluoralkoxy (MFA) tubing was connected *via* suitable fittings. An electronically controlled heating coil surrounds the quartz glass tube.
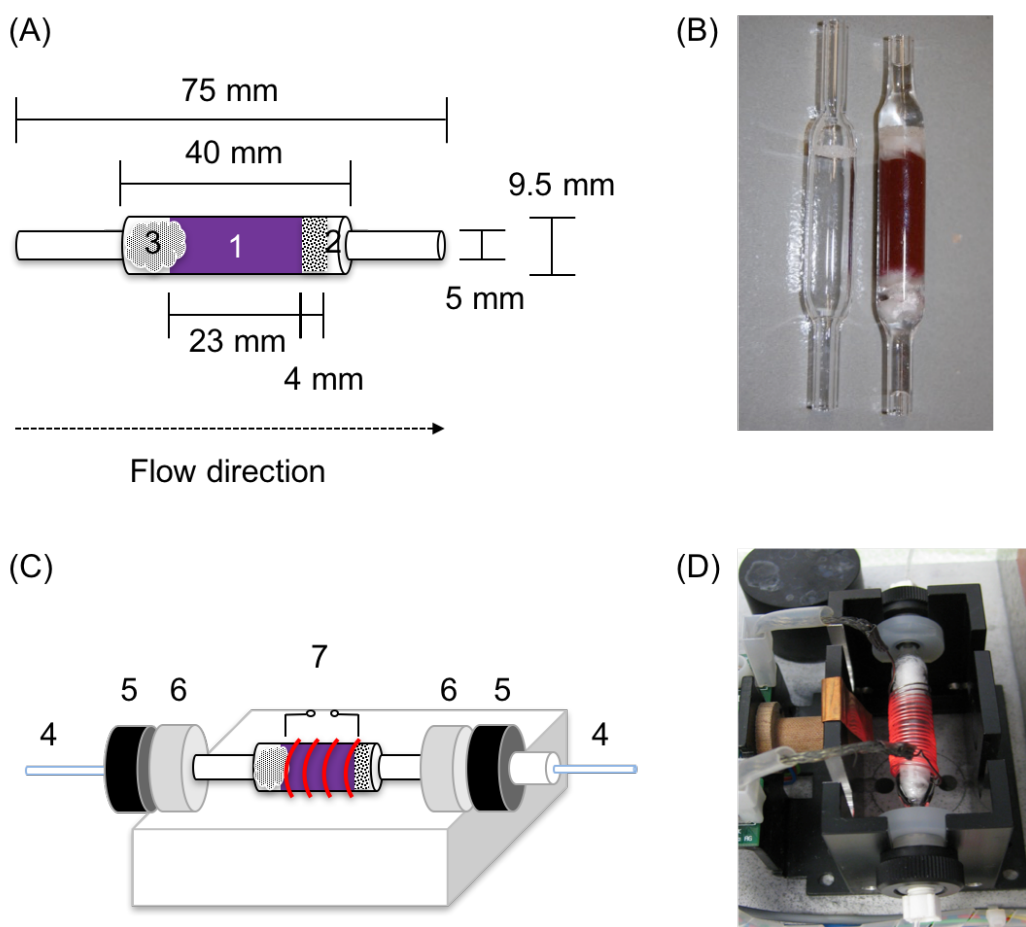
Figure 12: *(A) Schematic illustration and (B) photograph of the optimized nanogold collector, (C) Schematic illustration and (D) photograph of the holding device and integrated heating wire (remarks: diameters are given as outer diameter, wall thickness: 1 mm; 1 500 mg of nanogold-coated silica, 2 quartz glass frit, 3 quartz wool, 4 tubing connected to the FIAS, 5/6 threaded coupler, 7 heating wire).*

4.1.2. Adjustment of the cooling temperature

After preconcentration of dissolved Hg traces onto the collector, the column is rinsed with diluted HCl and water and then flushed with argon to dry the material. However, remaining moisture is evaporated when the heating step for thermal release of Hg starts. A clear time-/temperature-controlled separation of water and Hg vapor is due to the gradual heating process of the collector from the outside to the center not possible.

Water boiling temperature (100°C) and first release of Hg from the amalgam (350°C) may to some extent occur at the same time at different depth of the filling material. Hence, to avoid quenching of AFS signals due to water vapor reaching the measurement cuvette, residual water has to be removed during the complete thermal desorption step. For this purpose, a Peltier cooling (PC) device was set behind the collector in order to condense water vapor (see **Figure 13A**). Formed water droplets can then be separated from the gaseous stream *via* a gas-liquid-separator (GLS). An MFA tubing was integrated between the two semiconductor plates of the device in a meander shaped form. With the purpose of evaluating the influence of the cooling temperature on the efficiency of the water removal and/or possible re-dissolution of Hg in the water droplets the pre-set temperature of the Peltier device was varied from 4 to 15°C. As can be seen from **Table 5** the water temperature measured at the outlet of the Peltier cooling increased slightly from 10 to 17°C with increasing pre-set temperature.
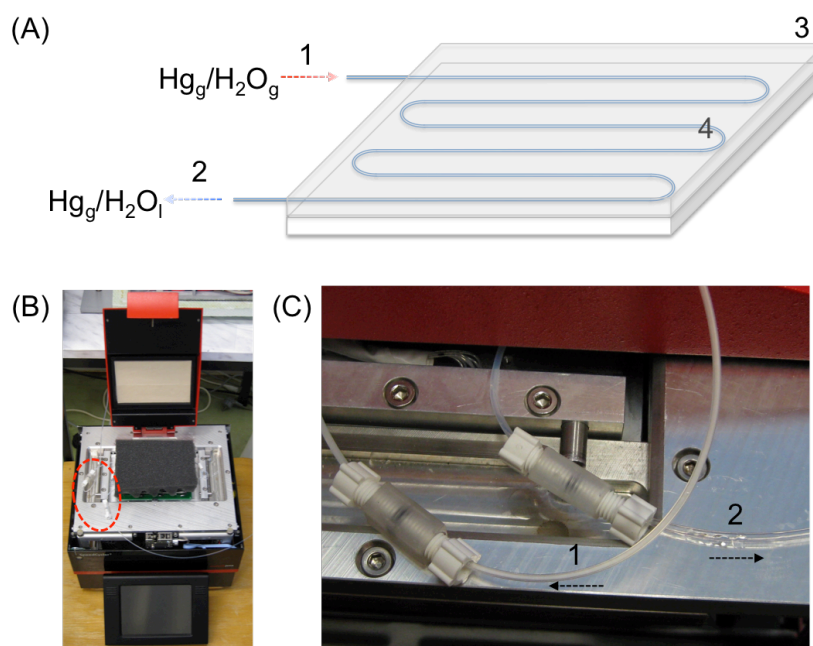
Figure 13: *(A) Schematic illustration of the Hg(0)/water pathway, (B) photo of the Peltier cooling device and (C) magnification of the area marked in (B) (remarks: 1 Peltier cooling inlet for Hg(0) and water vapor, 2 Peltier cooling outlet for Hg(0) and water, 3 cooling plate, 4 meander-formed tubing).*

Table 5: *Variation of pre-set cooling temperature and measured temperature at the outlet of the Peltier cooling device (inlet temperature was measured to be constant 94°C).*

Pre-set cooling temperature [°C]	Temperature measured at the outlet [°C]
4	10
8	13
10	14
15	17

However, to investigate possible quenching effects during AFS measurement fluorescence intensities obtained for each pre-set cooling temperature were measured and are presented in **Figure 14**.

The fluorescence intensity obtained after preconcentration of a 5 ng L^{-1} Hg(II) standard solution was constant over the investigated pre-set cooling temperature range meaning that Hg fluorescence measurement is not affected. The PC device is advantageous over a previously used ice-bath for cooling purpose as the temperature can be kept constant.[22] Moreover, it can easily be integrated to an automated prototype system and manual exchange of the cooling media is omitted.
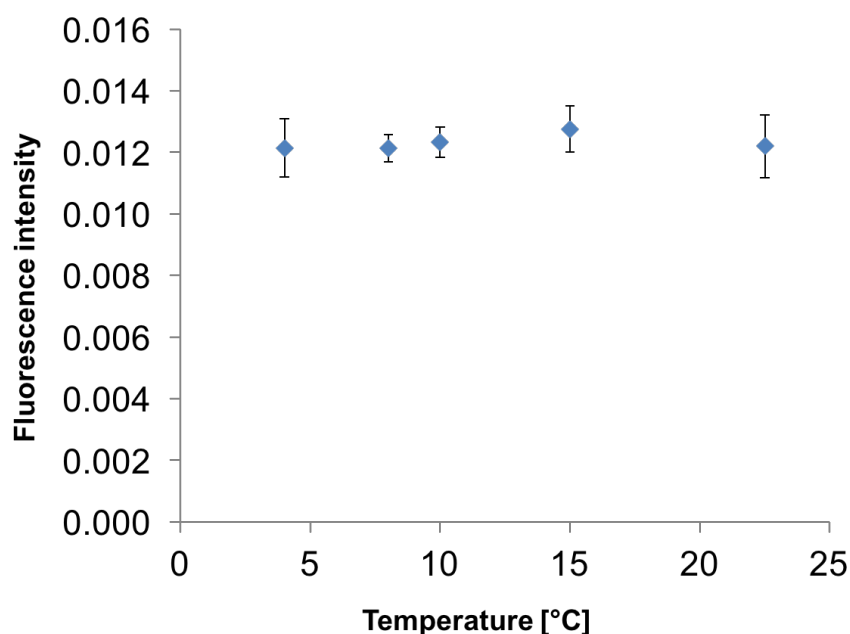
Figure 14: *Fluorescence intensity obtained after preconcentration of a 5 ng L^{-1} Hg(II) standard solution with pre-set cooling temperature of 4, 8, 10, 15 and 22.5°C (error bars represent standard deviation, n_s = 5).*

4.1.3. Optimization of thermal desorption

In order to obtain best reproducibility of Hg measurements quantitative release of Hg from the collector is required. It was shown by *Leopold et al.*[22] that release of Hg(0) from the amalgam starts at a temperature of approximately 350°C, which can be ensured within the glass tube by bringing the heating wire to glow. However, the geometry of the applied nanogold collector slightly differs in this study and therefore the duration of the heating step was evaluated using the present set-up. The heating period, which was varied from 20 to 140 seconds, and the temperature of the heating coil were controlled by *Hg-Speciation* software provided by Analytik Jena AG (Jena, Germany).

As presented in **Figure 15** the fluorescence intensity increases with increasing heating time and reaches a maximum at about 120 s. This indicates quantitative release of Hg(0) from the nanogold collector within 120 s. However, the temperature of the coil and the heat transfer depend to some extent on the number of windings of the heating wire around the quartz glass column. Since the coil is prepared manually the symmetry of the coil varies slightly from one to another. Thus, the described experiment was repeated to
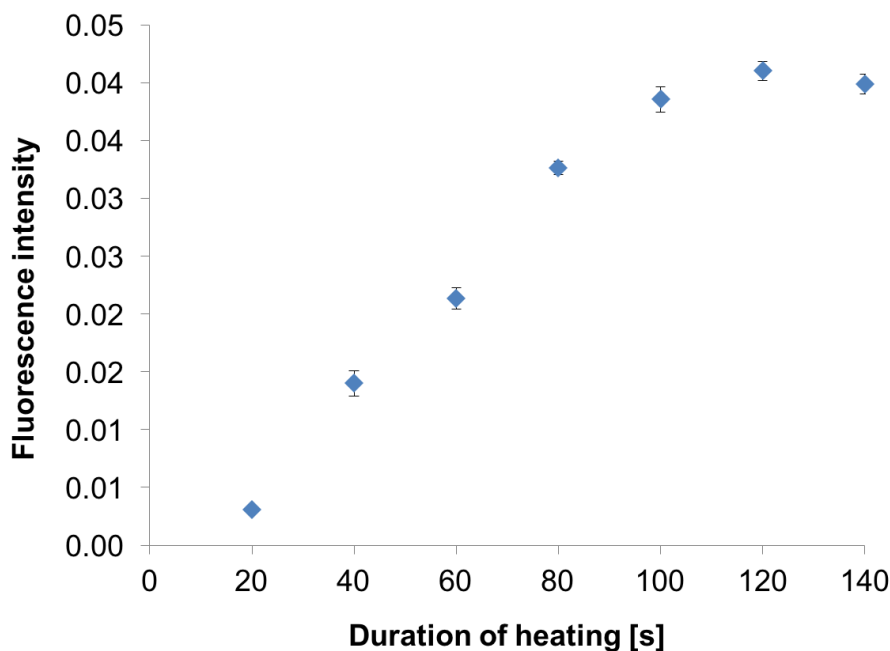
Figure 15: *Effect of heating duration on fluorescence signal intensity obtained after preconcentration of a 10 ng L^{-1} Hg(II) standard solution (error bars represent the standard deviation, n_s = 3-4).*

find the optimum heating duration after the heating coil was exchanged (lifetime of the wire approx. 500 analytical cycles). Typical heating times for quantitative thermal desorption were in the range of 80 to 120 s throughout this work.

In order to further prove the quantitative release of Hg(0) after thermal desorption for 120 s, the collector was once loaded with Hg standard solution and then heated for 120 s four times in a row. Released Hg(0) was measured by AFS after every heating cycle. Hence, any measurable fluorescence signal obtained from the 2nd, 3rd and 4th desorption step must result from residual Hg traces. **Figure 16** depicts the fluorescence intensities for the described experiment, which was repeated 3 times.

From the obtained results, it is evident that mercury is quantitatively released from the nanogold-based collector during the first thermal desorption for 120 s. Moreover, the experiment proves that there is no carry over effect in the FIA system from the collector to the AFS measurement cell.
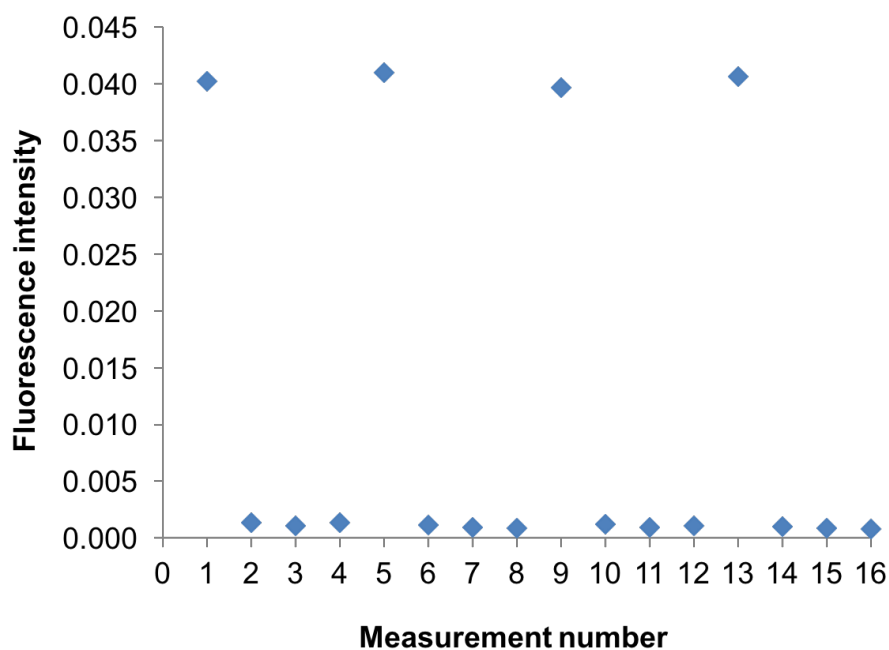
Figure 16: *Fluorescence intensity obtained after preconcentration of a 10 ng L^{-1} Hg(II) standard solution and four successive heating steps.*

4.1.4. Investigation of memory effects

With the aim of obtaining high performance of the optimized flow injection analysis system memory effects have to be excluded. Adsorption of the analyte to the tubing wall or other components within the flow system can reduce the signal intensity of the actual measured sample. On the other hand, false results are generated when the retained analyte desorbs within a subsequent analysis cycle. In particular, a sample having a very low concentration can be contaminated if it is measured directly after a high-concentrated sample. Consequently, memory effects may lead to false results and thus compromise the accuracy of the method.

Within this study, memory effects were investigated by alternating measurements of a blank solution (0.06 M HCl) and Hg(II) standard solutions of up to 200 ng L^{-1}. The sequence of measurements and the corresponding fluorescence intensities are presented in **Figure 17**. No carryover was observed for Hg concentrations up to 50 ng L^{-1} as the blank level was obtained after the first measurement of the blank solution. Even at a Hg concentration as high as 200 ng L^{-1} only very low memory effect was observed. However, in this case the blank level was obtained after three measurements of blank. Consequently, when investigating real samples, sufficient blank (0.06 M HCl) measurements were performed after calibration and in-between samples. Moreover, within a calibration experiment the lowest concentration was measured first to guarantee minimized carryover.
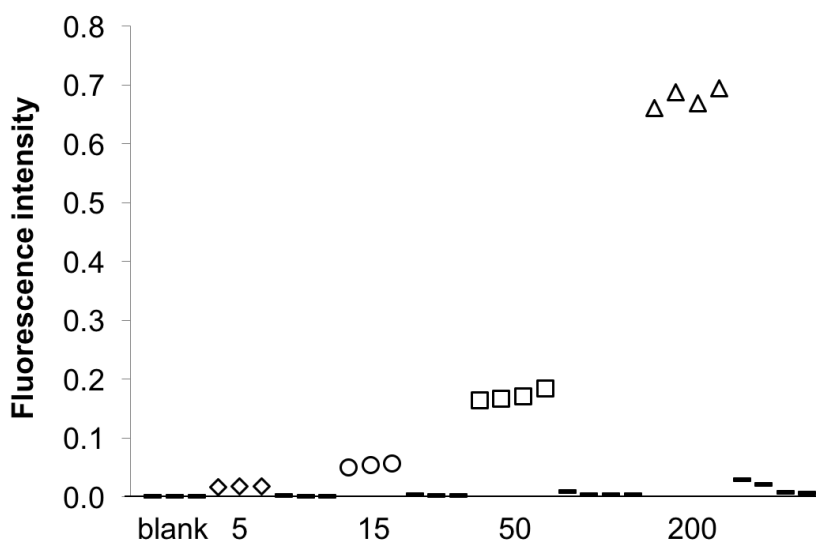
Figure 17*: Investigation of memory effects: alternating measurements of blank solution (0.06 M HCl) and Hg(II) standard solution (diamond: [Hg]=5 ng L^{-1}, circle: [Hg]=15 ng L^{-1}, square: [Hg]=50 ng L^{-1}, triangle: [Hg]=200 ng L^{-1}, dash: blank).*

4.1.5. Sensitivity enhancement

As a next step, sensitivity enhancement of the FIAS-AFS was investigated with increasing sample volumes. Therefore, sample loops with a total volume of 1.5, 3.5, 5.0, 7.0 and 12.0 mL were implemented into the flow system and calibration in adequate concentration range was performed. In general, the slope of a linear regression describes the sensitivity of an analytical method. As expected, the slope of the calibration function increases with the applied sample volume as the absolute amount of Hg within the sample increases with increasing volume (see **Figure 18**). Compared to the sensitivity derived from CV-AFS measurement an enrichment factor of up to 8 was obtained applying the optimized FIAS-AFS and a sample volume of 12 mL. As a matter of fact, the limit of detection decreases with increasing sensitivity of the method (see **Table 6**). However, using a higher sample volume increases the overall analysis time. Hence, the applied sample volume was varied throughout this work depending on the required method performance. In addition, this experiment demonstrates that quantitative adsorption was reached regardless the applied samples volume. Hence, the column capacity is at least as high as 0.24 ng Hg per gram nanogold adsorbent (as derives from
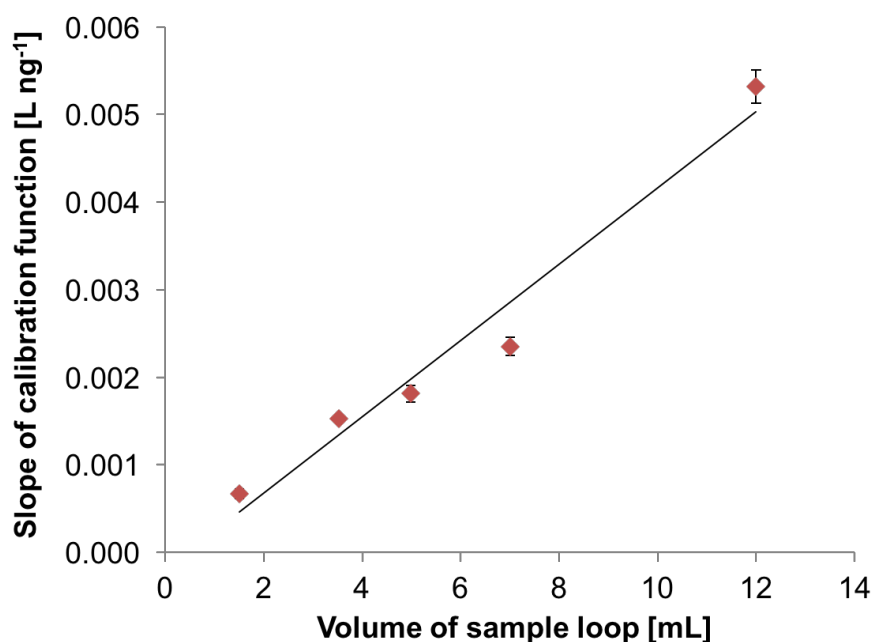
Figure 18: *Linear correlation between the methods sensitivity and the sample volume (error bars represent the uncertainty of the slope Δb, R²=0.9649).*

12.0mL · 10ngL⁻¹Hg and 500 mg of adsorbent). The capacity of the nanogold column has been investigated in more detail in a previous study by *Leopold et al.*[22]. Thereby, no breakthrough was observed for Hg concentration up to 200 ng L⁻¹ using a sample volume of 7 mL and 1 g of adsorbing material. This corresponds to quantitative adsorption of up to 1.4 ng Hg per gram nanogold adsorbent.

Table 6: *Limit of detection of the optimized FIAS-AFS achieved for different sample volumes.*

Sample volume [mL]	Limit of detection [ng L⁻¹] [a]	Relative coefficient of variation of the procedure (V_{x0}) [%] [b]
1.5	1.40	7.04
3.5	0.60	2.59
5.0	0.90	4.66
7.0	0.80	3.87
12.0	0.01	0.03

[a] As derived by *Funk et al.* [160], [b] Mathematical description of V_{x0} see chapter 7.

4.1.6. Investigation of suitability for ultratrace analysis

The optimized prototype system for reagent-free determination of dissolved Hg in natural water was set up in a new ultratrace clean laboratory (*Ulm University*). This laboratory is equipped with an air exchange system providing the room with filtered air. As a result, the laboratory is subjected to a slight overpressure (24 Pa). In addition, a lock chamber under excess pressure (12 Pa) separates the ultratrace laboratory from the corridor in order to reduce air and particle inflow. This arrangement offers best conditions for a constantly low atmospheric Hg level and facilitates analytical measurements in the ultratrace range. Still, due to the ubiquitous occurrence of Hg, blank values have to be carefully evaluated and controlled, especially when implementing a new system. Here, the blank contribution arises from instrumental components *e.g.* tubing, magnetic valves and from materials and reagents used during sample preparation. Argon as a carrier gas is decontaminated by passing a column filled with a gold gauze before entering the FIAS. Another blank contribution comes from hydrochloric acid, which is used as a stabilizing, carrier and rinsing agent to minimize adsorption effects to vessel and/or tubing walls. Hence, before each calibration experiment a blank solution was measured until stable fluorescence intensity was achieved. It was demonstrated earlier that the fluorescence intensity increases with the applied sample volume. Thus, for better comparison of a large dataset, where different sample volumes were used, the fluorescence intensity was normalized with respect to the sample volume. **Figure 19** presents the fluorescence intensity from 17 blank measurements performed on different days over a period of 31 months. The total number of analysis cycles to reach constant blank fluorescence intensity depends on various parameters like the frequency of operation and conditioning of the system. In the following only the last 6 blank values for each set of measurements are presented for a better overview. In addition, the data is illustrated in chronological order, starting with the set-up of the system in the new ultratrace clean laboratory. The blank fluorescence intensities vary between 0.0002 to 0.0006, which corresponds to approximately 0.5 ng Hg L^{-1}. Values higher than 0.0006 can be regarded as outliers. The different signal intensities may be explained by different batches of the nanogold material used for the experiments. Furthermore, little deviations in the weight of AuNP-coated SiO$_2$
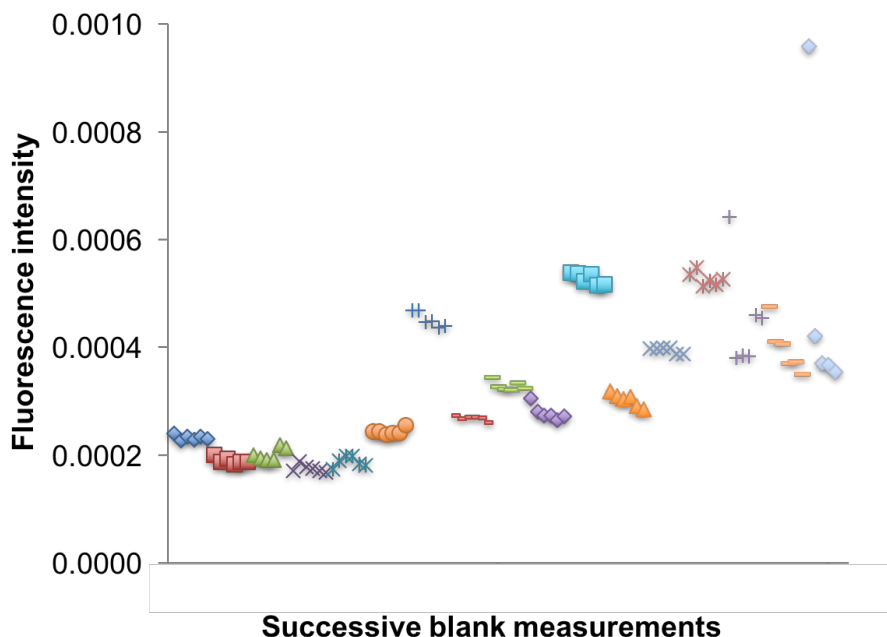
Figure 19*: Development of blank (0.6 M HCl) fluorescence intensity over a period of 31 months (same color/symbol indicates one measurement day, 17 days in total).*

results in different blank values. In addition, blank contribution from individually purified batches of hydrochloric acid play an important role. Anyway, as can be seen, the first values obtained after setting up the new FIAS-AFS system in the ultratrace clean laboratory are generally lower than those obtained towards the end of the investigated period of 31 months. Probably, as seems reasonable, continuous use of the system and the clean room for Hg analysis leads to generally higher input of Hg. Nevertheless, when the blank value is stable over the complete analysis (before and after sample measurement) the correctness of the data can be ensured.

4.1.7. Analytical figures of merit

Finally, the analytical figures of merit were determined with the optimized set-up. A typical calibration function in the concentration range from 0.1 to 0.4 ng Hg L^{-1} obtained by direct preconcentration of dissolved Hg(II) onto the nanogold-based collector is depicted in **Figure 20**. The analytical figures of merit, which describe the performance of the optimized method, are calculated from this calibration function (see **Table 7**). The

applied mathematical formulae are described in more detail in chapter 7. The optimized FIAS coupled to AFS is highly sensitive towards mercury with a detection limit as low
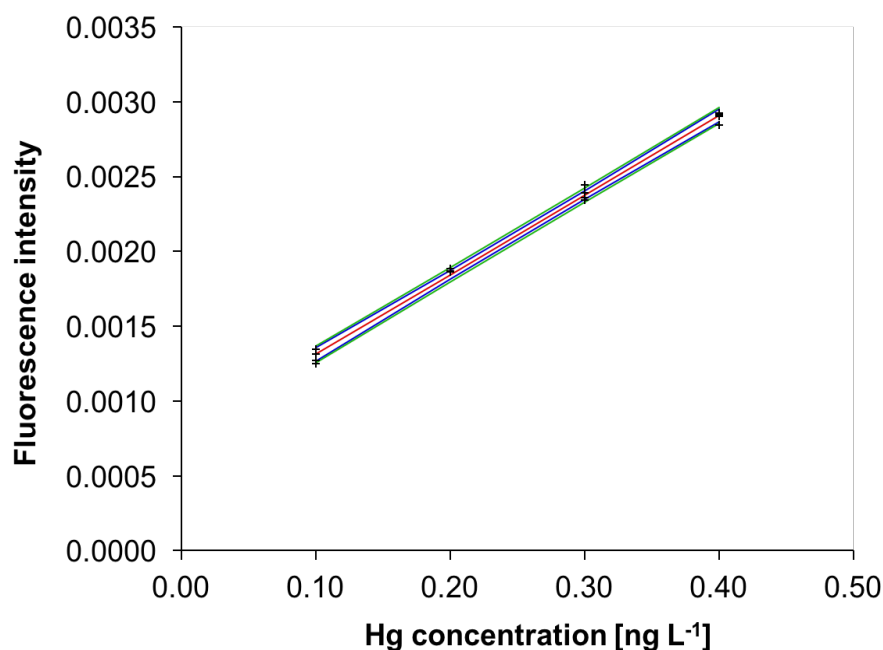
Figure 20: *Linear calibration function for Hg quantification by the nanogold-based FIAS-AFS (sample volume 12 mL; (+) calibration data, red: linear trend,* $FI = 5.32 \cdot 10^{-3} \cdot c(Hg) + 7.80 \cdot 10^{-4}$, $R^2=0.9965$, $n_c=15$, *blue: confidence interval with P=95%, green: prognosis interval).*

as 13 pg Hg L^{-1} corresponding to an absolute detection limit of 160 fg Hg. The complete analysis cycle takes approximately 10 minutes using a sample volume of 12 mL. The high precision of this method is reflected by the relative coefficient of variation of the procedure (V_{x0}) of 2.87%. Linear correlation between fluorescence intensity and Hg concentration was confirmed in a concentration range from 0.013 to 200 ng L^{-1}. Higher concentrations were not investigated to prevent the flow system from contamination, even though a linear trend is most probable for Hg concentrations higher than 200 ng L^{-1}.

It is clearly demonstrated that the optimized method is feasible for Hg ultratrace analysis. A more detailed discussion on real water application is given in chapter 7.4. The linear range over 4 orders of magnitude allows Hg analysis of pristine natural water ([Hg] < 1 ng L^{-1}) and drinking water as well as highly contaminated samples, *e.g.* wastewaters and water from industrial sites, which often exceed total dissolved Hg

concentration (tHg) of 100 ng L^{-1}. Total dissolved Hg concentration in open ocean water is usually below 0.5 ng L^{-1}, whereas tHg in *e.g.* the Adriatic Sea reaches values up to 1.6 ng L^{-1}.[11,161] Highest values of 2.4 ng L^{-1} were found in the Black Sea.[162] tHg in pristine freshwater samples varies over a broader range from less than 1 ng L^{-1} to up to 15 ng L^{-1} in humic-rich systems, *e.g.* moorland water.[24,39,42,163] In addition, the proposed method provides high reproducibility with relative standard deviations below 4% for blank solution (0.06 M HCl) and Hg(II) standard solutions. Hg preconcentration onto a nanogold column proceeds without the addition of any (toxic) reagents, *e.g.* BrCl, KMnO$_4$, HNO$_3$, and is thus advantageous over other analytical methods. The risk of contamination is minimized and at the same time elaborate sample pretreatment can be omitted.

Table 7: *Analytical figures of merit achieved by direct Hg preconcentration onto a nanogold-coated silica collector and atomic fluorescence spectrometric detection (sample volume 12 mL, n_c = 15).*

Parameters	Achieved values
Linear working range	0.013 - 200 ng L^{-1}
Calibration range	0.1 - 0.4 ng L^{-1}
Slope of the linear regression	$7.80 \cdot 10^{-4} \pm 6.69 \cdot 10^{-5}$
Limit of detection	13 pg L^{-1}
Limit of quantification	26 pg L^{-1}
Regression coefficient (R^2)	0.9965
Method standard deviation	2.87%
Sample volume (threefold measurement)	$\approx$ 40 mL
Analysis time (threefold measurement)	$\approx$ 30 min
Lifetime of the nanogold collector	> 350 cycles
Relative standard deviation (precision)	
For blank solution (0.6 M HCl), n_s = 5	3.78%
For Hg(II) standard solution ([Hg]=0.4 ng L^{-1}), n_s = 4	1.22%
For Hg(II) standard solution ([Hg]=2.5 ng L^{-1}), n_s = 40	3.26%
Residual standard deviation	$3.87 \cdot 10^{-5}$
Coefficient of variation of the procedure	$7.27 \cdot 10^{-3}$ ng L^{-1}

A comparison to other methods is given below (**Table 8**). The analysis time is reduced to approx. 10 minutes, depending on the sample volume, due to direct preconcentration of Hg from the aqueous sample. A minimum of 350 analysis cycles, with respect to standard and blank solution measurement, can be performed with one nanogold column without loss of precision or sensitivity. The preparation of the nanogold material and the packed collector column is not labor-intensive and affordable as standard chemicals are used. This is one more advantage over other solid-phase extraction procedures, which

Table 8: Approaches for mercury determination in natural water.

Analytical Method	LOD	Working range	Time [min]	Precision (RSD) [a]	Hg fraction	Ref.
Standard Methods						
EPA 1631: CV-AT-AFS	0.05 ng L^{-1}	0.05-100 ng L^{-1}	30	21% [b]	Reducible Hg	[97]
EPA 245.1: CV-AAS	0.2 µg L^{-1}	0.2-10 µg L^{-1}	5	dng	tHg	[164]
EPA 7472: ASV	0.1 µg L^{-1}	0.1-10,000 µg L^{-1}	10	3.8%	Hg(II)	[165]
Instrumental Techniques						
CV-ICP-MS	0.7 ng L^{-1}	0.7-100 ng L^{-1}	4	2.6% (n=6)	tHg	[94]
TXRF	0.7 µg L^{-1}	10-1,000 µg L^{-1}	17	7.0%	tHg	[166]
Nanomaterial-based Methods						
FIAS-AFS	0.013 ng L^{-1}	0.013-200 ng L^{-1}	10	3.26% (n=40)	tHg	This method
Colorimetry [c]	1.7 ng L^{-1}	2-800 ng L^{-1}	10	2.9%	Hg(II)	[103]
SERS [d]	0.002 ng L^{-1}	0.002-20 ng L^{-1}	4	dng	Hg(II)	[123]

[a] RSD: residual standard deviation; [b] Quality Control Acceptance Criteria for initial precision; [c] Nanomaterial: Citrate-capped platinum nanoparticles; [d] Nanomaterial: Silver nanoparticle-coated gold nanoparticles / 4,4´-dipyridyl, ndg: data not given.

are often based on highly complex and expensive adsorbents. The analytical performance of the presented reagent-free FIAS for dissolved mercury analysis is compared to standard methods (*e.g.* U.S. EPA), examples of established instrumental techniques and recently developed nano material-based (NM) approaches (see **Table 8**).

In order to achieve high sensitivity, instrumental techniques as well as standard methods (see EPA method 1631 and 245.1 in **Table 8**) for ultra-trace mercury determination are typically based on CV generation and/or AT for separation and preconcentration of the analyte, respectively. Today, the U.S. EPA method 1631 and modifications of this method are most frequently applied towards Hg monitoring of different aquatic systems.[12,97,167,168] Strong oxidizing agents are used to decompose organic matter within the sample, followed by CV generation, *i.e.* Hg(0) formation and amalgamation prior to AFS detection. Hence, these sample pretreatments have some draw backs namely a high number of applied procedural steps and input of (toxic) chemicals for matrix decomposition and analyte transformation. The required reagents must be prepared under ultratrace conditions and/or must undergo elaborative cleaning procedures. This leads to an increased LOD and high risk of contamination. In general, on-site analysis is possible with these methods, but related to cost-intensive and elaborate preparation prior to and during sample analysis. The herein proposed method offers a cost effective and environmentally friendly alternative. Another standard method recommended by the U.S. EPA, method 7472, describes Hg determination in aqueous samples by anodic stripping voltammetry (ASV). It is a direct method without preconcentration of the analyte, which leads most probable to a high LOD of 0.1 µg L^{-1}. The method shows a good precision (RSD = 3.8% for a 5-fold measurement of 5 µg L^{-1} Hg(II) standard) and a broad linear working range but still it is not suitable for ultratrace Hg analysis.

Pyhtilä et al.[94] published a CV-ICP-MS method for total Hg determination in high DOC-containing water samples. Despite the addition of reagents for NOM oxidation and CV generation this method reaches a low LOD of 0.7 ng L^{-1}. This detection limit is sufficient for high DOC-containing real water measurements with a Hg concentration between 3.6 to 38.9 ng L^{-1}. As a disadvantage it is to mention that this method requires time- and reagent-consuming sample pretreatment procedures. ICP-MS is a bulky, cost- and maintenance-intensive instrumentation and thus not feasible for on-site analysis of

Hg traces within natural water. TXRF is a well-established analytical method for trace metal analysis within preferably liquid samples. In general sample preparation is straightforward as it is diluted with an internal standard and directly applied onto the reflective carrier. Due to the high vapor pressure of Hg at room temperature TXRF analysis is more challenging for this element. *Margui et al.*[166] found out that the addition of thiourea leads to non-volatile Hg complexes that are measurable with TXRF. However, the derived detection limit of 0.7 $\mu g\,L^{-1}$ is sufficient for some wastewater samples but considerably too high for Hg analysis in the nanogram to picogram per liter range.

With the aim to overcome the disadvantages of instrumental techniques, such as bulky and sophisticated instrumentation, time- and reagent-consuming sample preparation big efforts towards novel strategies that provide easy handling, miniaturized systems and fast Hg analysis in waters were made within the last years. Thereby, NMs as a tool to enhance separation efficiency, higher selectivity and the possibility for portable systems are in the focus of current research on Hg trace analysis. The structure, character and type of NMs that are utilized are versatile as shown in chapter 4.5.1. Nanoparticles, nanoclusters, nanofilms, nanotubes and nano dots made of *e.g.* Ag, Au, oxidized carbon, SiO_2, imprinted polymers are just some of the frequently used formats of NMs.[21] Here, two examples that are feasible for pristine water analysis are compared with the developed method. *Wu et al.*[103] presents a colorimetric mercury sensor which is based on the peroxidase-like activity of citrate-capped platinum nanoparticles (PtNPs). This activity is inhibited by the addition of Hg^{2+}, which is reduced to Hg^0 on the PtNPs surface. The LOD for Hg^{2+} was 1.7 $ng\,L^{-1}$ and is suitable for ultratrace Hg detection in waters. Still, the applicability of this method was not studied for other Hg species, like, *e.g.* methylmercury and dissolved Hg(0). In addition, tap water is not a proper example for a real matrix as it is less complex and not comparable with natural water systems. These exhibit a high level of complex natural matter which most probable diminishes the analytical performance of the colorimetric probe. As a second example a highly sensitive SERS chip is presented to evaluate the performance of the nanogold-based FIAS-AFS [123]. A silicon substrate was modified with Ag-coated AuNPs exhibiting SPR and an Hg(II) specific organic ligand. In the absence of Hg^{2+} the organic ligand interconnects

the metallic nanocomposite material followed by a strong Raman signal. The organic ligand coordinates to Hg^{2+} upon addition, thus leading to signal quenching. An advantage of this method is the extraordinary low LOD (2 pg L^{-1}) derived with a sample volume of 20 µL. However, sample and chip preparation are time-consuming and diminishes on-site application. Furthermore, sample pretreatment with nitric acid at 90°C for two hours increases the risk of contamination.

4.1.8. Conclusion

The principle of dissolved Hg preconcentration onto a nanogold-based column was utilized to set up a fully automated prototype for ultratrace Hg analysis.[22,23] The design of the nanogold column and its implementation to the FIAS-AFS were optimized within this work. In addition, nanogold-coated silica particles with a high gold load of 3.5 mg Au per gram SiO_2 were prepared and the surface was thoroughly characterized using scanning electron microscopy. A homogenous coating of the silica surface with an average AuNPs size of 23 ± 9 nm was obtained. Furthermore, the optimized thermal desorption step results in quantitative release of pre-concentrated Hg within 80 to 120 s. The integrated Peltier cooling device ensures condensation of evaporated water during thermal desorption of the analyte. Thus, Hg(0) can be fully separated from interfering moisture and fluorescence measurement is not affected by quenching effects when the cooling temperature is pre-set to 15°C. In addition, no carryover effect occurs up to Hg concentration of 50 ng L^{-1}. Furthermore, only three blank measurements are necessary to rinse the system after measurement of Hg solution as high as 200 ng L^{-1}. In order to obtain constant and low blank values the optimized prototype was set up in an ultratrace clean laboratory with overpressure and continuous air exchange. The blank fluorescence intensity fluctuated within a tolerable range over a period of 31 months and was constant within one set of measurement. The analytical performance of the prototype was demonstrated by aqueous calibration with Hg(II) standard solutions. The reagent-free method provides an extraordinary low detection limit of 13 pg Hg L^{-1} and a linear working range over 4 orders of magnitude (0.013 to 200 ng L^{-1}). Thus, the developed prototype can in general be applied towards both pristine natural water and contaminated

water samples. The novel prototype system is enhancing on-site application as sample preparation is omitted and the instrumentation is compact.

Figure 21 shows the schematic illustration and a photograph of the novel prototype for ultratrace Hg analysis. During the development process the length of the tubing, the pathway of liquid flow and gas stream (controlled *via* magnetic valves), the duration of individual analytical program steps and the duration and temperature of the thermal desorption were varied and optimized. The flow injection system and related components are combined as *NanoQuas*, which is placed on top of the *Mercur* AFS. Compared to the initial FIAS-AFS set-up (see chapter 4.1) the herein developed prototype is compact and therefore robust and easy to transport. The electronic circuit is constructed in a way that external peristaltic pumps can be omitted. A cover with built-in ventilation grate promotes heat dissipation during thermal treatment of the nanogold column.
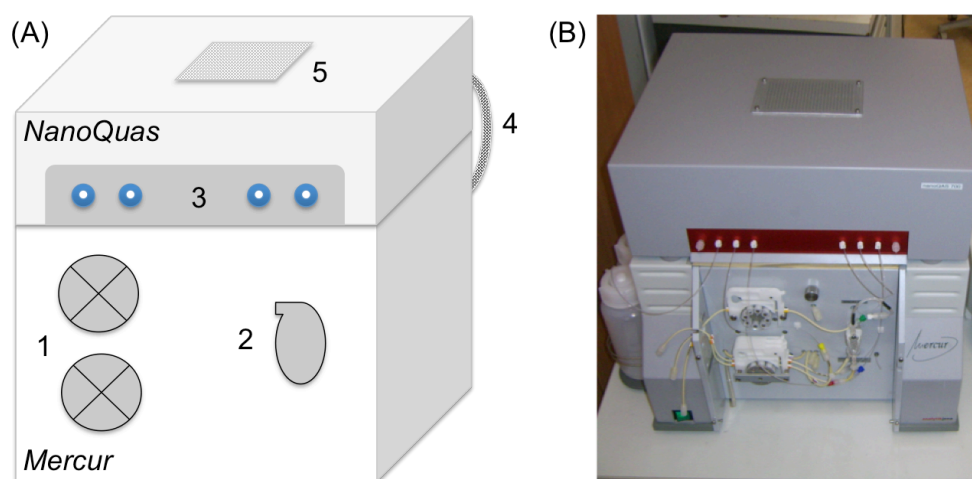
Figure 21: *(A) Schematic illustration and (B) photograph of the developed prototype for total dissolved Hg analysis by direct preconcentration onto a nanogold-based collector (1 peristaltic pumps, 2 gas-liquid-separator, 3 connections for tubing, 4 interface between Mercur and NanoQuas, 5 ventilation grate).*

4.2. Investigation of possible limitations by Hg complexing organic ligands

The preceding chapter described the development of a prototype for reagent-free determination of dissolved Hg after accumulation onto AuNP-coated silica. Since the optimization is based on the instrumental set-up and improvement of analytical steps the analytical principle did not change compared to previous work performed by *Leopold et al.*[22]. The validation of the method was accomplished earlier by investigating the reference material ORMS-4, which is a river water sample spiked with inorganic Hg.[22] The determined Hg concentration was in good agreement with the certified value, which is reflected in a recovery of 101%. Thus, the accuracy of the novel nanogold-based method was confirmed. However, ORMS-4 is prepared in 0.5% (v/v) BrCl as a stabilizing agent. According to the U.S. EPA method 1631 BrCl digests dissolved organic compounds within a natural water sample and transforms all Hg species to a reducible form, *i.e.* Hg^{2+} ions.[97] Hence, this certified reference material (CRM) contains in contrast to any real water sample only labile Hg species. Other CRMs like groundwater (*e.g.* ERM®-CA615) and seawater (*e.g.* BCR®-579) have a lower dissolved organic carbon (DOC) concentration compared to freshwater and are thus preserved in diluted nitric acid or hydrochloric acid (pH 2). The addition of nitric acid to a groundwater CRM to a pH of 2 most probably does not result in complete decomposition of dissolved organic matter. However, groundwater has a low level of DOC and is thus not suitable to study the application of the herein developed prototype towards organic rich natural water. According to the current state of knowledge none of the well-established institutes (*e.g.* NIST, ERM) produce a high DOC-containing natural water reference material with specified Hg concentration and at the same time less oxidizing conditions. Therefore, a different approach to systematically investigate the influence of dissolved organic compounds towards Hg preconcentration onto the nanogold collector within the optimized FIAS-AFS was taken within this work.

A model developed by *Lamborg et al.*[169] clearly demonstrates that under low salinity conditions (ca. 15‰, *e.g.* river, lake, estuary water) organic complexes dominate Hg speciation at even low DOC concentrations. Still, *Leopold et al.*[22] found reasonable Hg

concentrations (0.5 to 6.2 ng Hg L^{-1}) for seven natural water and a wastewater by direct preconcentration onto a nanogold column without sample pretreatment and species conversion. The salinity of these samples ranges between < 1 and 34. However, the maximum DOC concentration of these samples was 160 μM (1.9 mg C L^{-1}), which is often exceeded in freshwater. Moreover the results derived by the novel method were not compared with established methods (*e.g.* CV-AFS) or interlaboratory studies. Due to the fact that there is no high DOC containing CRM specified for its Hg content and at the same time without BrCl as a stabilizing agent it is challenging to validate the novel nanogold-based method by measurement of reference materials. Therefore, the aim of this part of the work was to study the influence of dissolved organic matter within model solutions towards Hg accumulation onto nanogold-coated SiO$_2$ particles. The following sections describe the performance of the proposed method towards spiked and non-spiked model solutions containing specific organic ligands or humic substances extracted from different sources. Thereby, the U.S. EPA method 1631 was used as a reference method to investigate the true Hg concentration in various model solutions.[97]

4.2.1. Impact of organic ligands

As mentioned earlier, divalent Hg species, *i.e.*, Hg(II), in natural water strongly bind to small inorganic and organic ligands as well as to dissolved organic matter, which is ubiquitous in the aquatic environment. This interaction is mainly attributed to the coordination of Hg to reduced sulfur sites within the organic compounds.[47,83] However, Hg also binds to oxygen and nitrogen containing functional groups. In the following section the influence of organic model substances towards Hg preconcentration onto nanogold-coated silica particles is described. For this purpose, model solutions containing different low-molecular-weight organic ligands were analyzed with the optimized FIAS-AFS. These compounds exhibit in contrast to humic and fulvic acids a distinct molecular structure with various functional groups, *i.e.* thiol, carboxyl, amino, thioketone, thioether. Possible interferences during Hg preconcentration onto the nanogold collector within the FIAS-AFS can thus be associated with particular binding sites within the organic model compounds. Disodium ethylenediaminetetraacetic acid

60

(Na₂EDTA), thiourea, cysteine, urea, glutathione and methionine were applied as organic model substances. The structural formula of the herein investigated organic model substances are shown in **Figure 22**. EDTA is a 6-fold chelating ligand and used as complexing agent mainly in detergents and preservatives as well as in industrial cleaning processes to complex *e.g.* Ca^{2+}, Mg^{2+} Cu^{2+}, Ni^{2+}, Cd^{2+} and Pb^{2+}.[170,171] As a result of these versatile applications of EDTA, discharge to natural aquatic systems through wastewater streams is likely to occur. Concentrations of EDTA in river water and lakes as well as reported concentrations of urea, thiourea, cysteine and glutathione in natural water samples and wastewaters are presented in **Table 9**. Concentration of methionine in natural water was not yet reported in the literature.
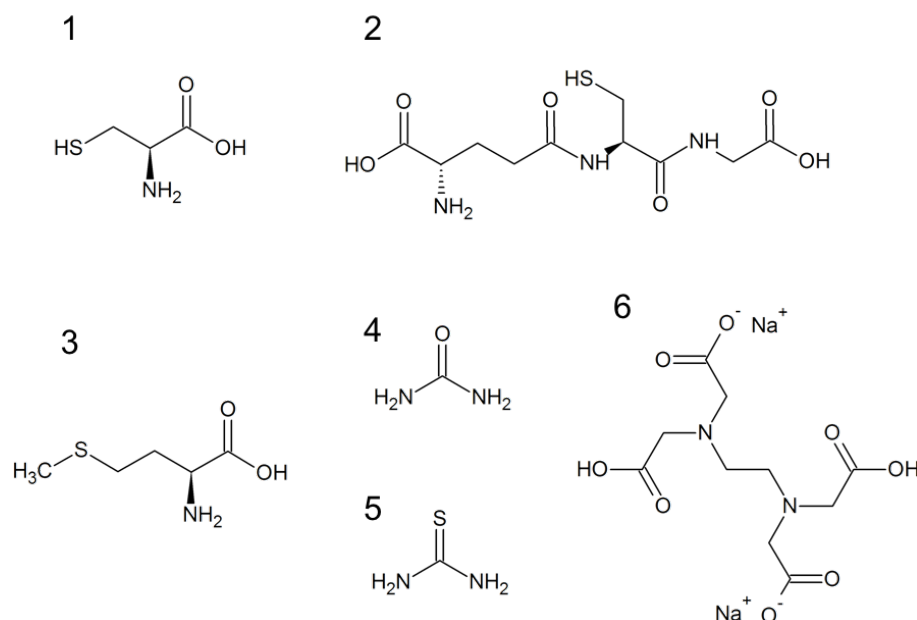
Figure 22: *Structural formula of (1) cysteine, (2) glutathione, (3) methionine, (4) urea, (5) thiourea and (6) Na₂EDTA.*

Table 9: *Concentration of organic model substances found in natural water and wastewater.*

Organic model compound	Water sample	Concentration	Ref.
EDTA	River *Ill* (France)	158 µg L^{-1}	[172]
	Lake *Saimaa* (Finland)	2-50 µg L^{-1}	[173]
	River *Main* (Germany)	5-13 µg L^{-1} [a]	[174]
Urea	Seawater (Pacific Ocean)	< 61 µg L^{-1}	[175]
Thiourea	Wastewater	2.33-2.53 mg L^{-1}	[176]
	Seawater (North Sea)	2.79 mg L^{-1}	[176]
Cysteine	Lake *Ängessjön* (Sweden)	1.45-1.70 ± 0.12 µg L^{-1}	[177]
	Wetland (stream water, Sweden)	2.79-3.51 ± 0.24 µg L^{-1}	[177]
	Wetland (soil pore water, Sweden)	3.76-18.17 µg L^{-1}	[177]
Glutathione	Wetland (soil pore water, Sweden)	3.40-27.04 ± 2.77 µg L^{-1}	[177]
	River *Mersey* estuary water (United Kingdom)	4.92-98.34 µg L^{-1}	[178]

[a] Median EDTA concentration of the river *Main* (at Bischofheim) from 1999-2014.

Mercury contamination of organic model compounds

As a preliminary investigation Hg contamination of the organic model substances was determined *via* CV-AFS. The substances were therefore digested in concentrated nitric acid prior to CV generation. Thereby, organic compounds were completely oxidized and Hg was transformed to its labile Hg^{2+} species. The digests of all model substances were diluted to a final DOC concentration of 1,000 mg L^{-1}. Blank contribution resulting from the oxidizing agent was considered for correct data evaluation. To quantify Hg contamination within the model solutions an external calibration was performed by CV-

AFS measurement of aqueous Hg(II) standard solutions. Hg concentration found by acid digestion followed by CV-AFS measurement is presented in **Figure 23**.
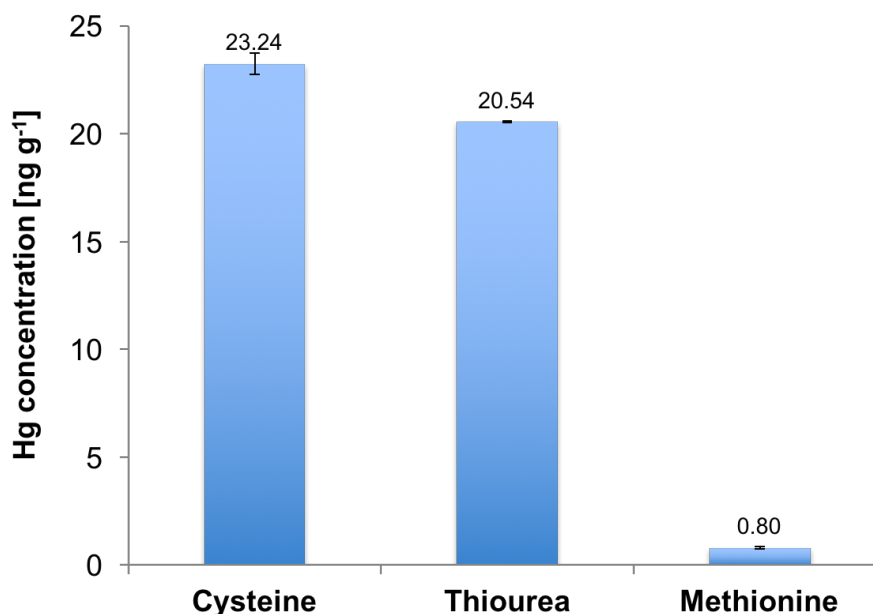
Figure 23*: Hg concentration in cysteine, thiourea and methionine derived by CV-AFS after acid digestion (error bars represent the standard deviation, n_s = 3 for thiourea, n_s = 4 for cysteine and methionine).*

As can be seen from the results in **Figure 23** total Hg contamination, given in nanogram per gram of the organic ligand, is highest for cysteine and thiourea. This might come from atmospheric Hg deposition during storage. On the other hand, Hg contamination possibly arises from contaminated reagents and/or materials involved in the production process. Methionine exhibits a significant lower Hg blank level. Hg concentration in 1,000 mg C L^{-1} Na$_2$EDTA, glutathione and urea model solution determined by CV-AFS after total acid digestion was below the limit of quantification (LOQ) of 0.73 ng L^{-1}. However, these findings are not indicative for less affinity of the respective ligands towards Hg as the contamination originates from random (external) sources. In addition, cysteine, thiourea and methionine were dissolved in 0.06 M HCl, analogous to Hg(II) standard solutions for external calibration, and labile Hg was directly determined *via* CV-AFS. Direct measurement of labile Hg in Na$_2$EDTA, glutathione and urea model solution was omitted as Hg concentration determined by total acid digestion followed by CV-AFS was below the LOQ. Here, only cysteine model solution shows a reasonable

value for labile Hg (2.07 ng g^{-1}), which corresponds to 9% of the total Hg concentration within cysteine (23.24 ng g^{-1}). The functional groups of cysteine, *i.e.* carboxyl, amino and thiol group are protonated in acidic media. This leads most probably to partial release of Hg^{2+} from its initial coordination site. The free or labile Hg fraction within thiourea and methionine model solution is below the LOQ (0.46 ng L^{-1}) for direct CV-AFS. These results indicate that Hg within thiourea and methionine is bound more strongly compared to Hg bound to functional groups within cysteine and that acidification (0.06 M HCl) leads to a partial release of Hg from cysteine, whereas the binding sites of thiourea and methionine seem not to be affected by acidification. To explain this, the pK$_B$/pK$_A$ values of cysteine and thiourea are taken into account, since total Hg within methionine is near the LOQ. These constants describe the affinity of functional groups to take up or to liberate a proton within an aqueous solution. The smaller the pK$_b$ or the pK$_a$ the higher is the tendency to take up or to liberate a proton, thus acting as a base or as an acid, respectively. Thiourea exhibits a low pK$_a$ of -1.[179] Thus, in aqueous solution the amino groups within thiourea tend to act as an acid and liberate a proton resulting in NH$^-$. However, within this study the model solution is acidified to a pH value below 2, which might hinder deprotonation of the two amino groups. A possible explanation for the low recovery using direct CV-AFS after dissolution of thiourea in 0.06 M HCl is that Hg is coordinated to one of the free electron pairs of the thioketone group. The thioketone group is not protonated under the given acidic conditions and thus Hg is not released as its labile form. The pK$_a$ value of the thiol group of cysteine (8.33) reveals a certain affinity of the thiol group to accept a proton.[180] Hg, as an electrophile, has a high affinity towards sulfur-containing functional groups as mentioned earlier. Thioketones (R$_2$-C=S) and thiolates (R-S$^-$) form a strong coordination complex with Hg(II). Thus, coordinated Hg might be released from the thiol group after protonation and thus lead to the findings within the CV-AFS measurements. The pK$_a$ value for the carboxyl and amino group within cysteine is 1.92 and 10.78, respectively.[180]

Hg contamination initially present within the investigated organic compounds was furthermore analyzed by the optimized FIAS-AFS. Therefore, model solutions of 1,000 mg L^{-1} DOC concentration (analogous to the previous section) were prepared in

0.06 M HCl and were then directly preconcentrated onto the nanogold column. External calibration was performed with aqueous Hg(II) standard solution. However, the obtained fluorescence intensity for all model solutions is in the range of the blank level. The blank in this case is represented by the fluorescence intensity resulting from the measurement of diluted hydrochloric acid as a sample. This finding indicates that initially present Hg within the organic model compounds is hindered from nanogold preconcentration under the given conditions. All further investigations using Hg(II) spiked model solutions were conducted with significant lower DOC concentration of the model solutions ranging between 10 to 50 mg L^{-1}. Thus, Hg blank contribution was not considered during data evaluation.

Mercury recovery in spiked organic model solutions by FIAS-AFS

In a next set of experiments, Hg recovery from spiked model solutions was investigated by using the optimized FIAS-AFS. Therefore, urea, Na$_2$EDTA, thiourea, cysteine, glutathione and methionine were prepared in 0.06 M HCl with a constant DOC concentration of 10 mg L^{-1}. The model solutions were spiked with Hg(II) in a range between 1 and 100 ng L^{-1} and were subsequently analyzed with the FIAS-AFS. External calibration was performed with aqueous Hg(II) standard solutions. The respective Hg recovery for each organic model compound is obtained from the slope of the recovery function (see **Table 10**). As can be seen from **Table 10** Hg recovery in spiked model solutions varies significantly between 30 to 98%. The regression coefficient ranges between 0.9588-0.9968 and reflects a high linear correlation for the investigated concentration range. A high recovery (84-98%) was found for urea, Na$_2$EDTA and thiourea model solution by direct preconcentration onto the nanogold column. These results indicate that the interaction between spiked Hg(II) and immobilized AuNPs predominates over interactions with functional groups within urea, Na$_2$EDTA and thiourea. As described earlier the chloride concentration of the investigated model solutions also affects the formation and stability of Hg complexes. A high recovery of spiked Hg might thus be a result of Hg-chloro complex formation followed by reduction of Hg(II) at the nanogold surface and amalgamation of Hg(0).

Table 10: *Recovery of spiked Hg(II) in organic model solution with DOC concentration of 10 mg L^{-1} (uncertainty is derived from confidence interval of the recovery function, nc = 22-24).*

Model substance	Recovery [%]	Uncertainty [%]	Regression coefficient
Urea	97.54	2.52	0.9968
Na$_2$EDTA	92.79	7.77	0.9654
Thiourea	83.51	2.31	0.9961
Cysteine	43.92	3.64	0.9660
Glutathione	41.20	1.32	0.9950
Methionine	30.16	2.92	0.9588

Hg(II) is a soft metal cation and tends to form stabile complexes with sulfur-containing organic and inorganic (*i.e.* S^{2-}, SCN^-, $S_2O_3^{2-}$) ligands.[83] This is in good agreement with the high recovery found for urea and Na$_2$EDTA model solutions, as both compounds do not contain any sulfur functional group. However, a high recovery (83.51%) was also obtained for Hg(II) spiked thiourea model solution. *Martell et al.*[181] reported a stability constant of log K = 22.1 for a HgL$_2$ type complex of thiourea and free Hg^{2+} ions. Still, the study by *Martell et al.*[181] was conducted under different experimental conditions, with an ionic strength of 0.5 M and without the presence of gold nanoparticles. Significantly lower recovery rates were obtained for spiked cysteine, glutathione and methionine model solutions (30 to 44%). This might be a result of strong interaction between spiked Hg(II) and the organic compounds in acidic solution (0.06 M HCl). A major fraction of added Hg(II) probably binds to the organic ligands under the given conditions. For cysteine and glutathione this may be explained by the strong interaction of Hg(II) with thiol functional groups within the organic compounds. On the other hand, methionine with a S-methyl thioether group (CH$_3$-S-R) shows also strong affinity to artificially added Hg(II) in the presence of 0.06 M chloride and the nanogold column. This hinders preconcentration onto the nanogold-based collector within the FIAS-AFS.

In a next step, concentration-dependent experiments with these model substances were performed. Therefore, urea, Na$_2$EDTA, thiourea, cysteine, glutathione and methionine were prepared in 0.06 M HCl with a DOC concentration between 2 and 50 mg L^{-1}. A

constant Hg(II) spike of 10 ng L^{-1} was added to all model solutions. External calibration was performed with aqueous Hg(II) standard solution. Found Hg concentration by the optimized FIAS-AFS with increasing DOC concentration in urea, Na$_2$EDTA and thiourea is presented in **Figure 24A**. The results obtained for cysteine, glutathione and
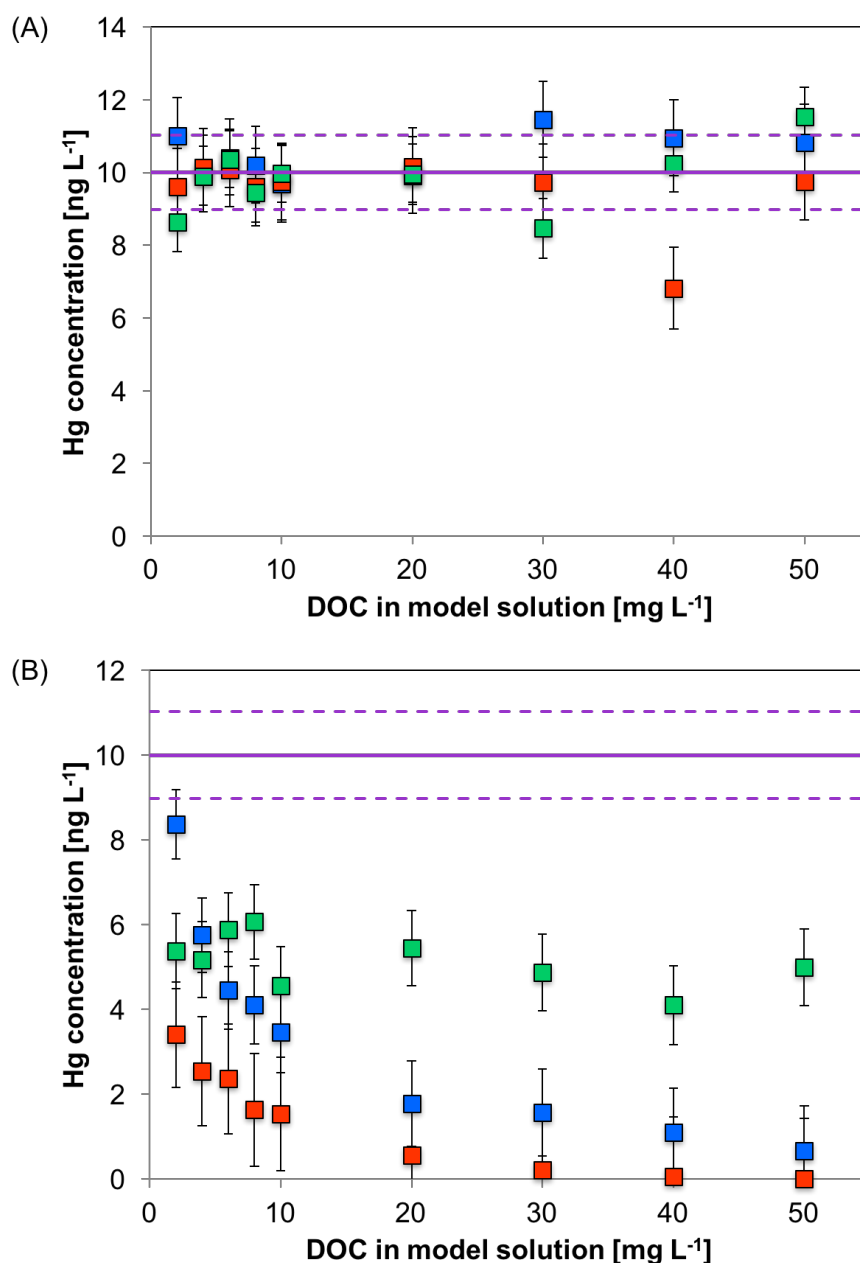
Figure 24: *(A) Hg recovery in urea (green), Na$_2$EDTA (red) and thiourea (blue) and (B) in cysteine (blue), glutathione (red) and methionine (green) model solution with DOC concentration ranging from 2-50 mg L^{-1} and [Hg] = 10 ng L^{-1} (error bars represent the uncertainty as derived from the prognosis interval of the calibration function, n$_c$ = 9).*

methionine are summarized in **Figure 24B**. The results in **Figure 24** show a similar trend to those described in the previous section. A mercury spike of 10 ng L^{-1} in urea, Na$_2$EDTA and thiourea is almost quantitatively found over the investigated DOC concentration range (see **Figure 24A**) using the optimized FIAS-AFS. The derived values for the spiked model solutions fluctuate around the value found for a 10 ng L^{-1} aqueous Hg(II) standard solution. The deviations from this reference value are tolerable for ultratrace Hg analysis. A different trend is observed in the case of cysteine and glutathione model solutions (see **Figure 24B**). Hg recovery significantly decreases with increasing DOC concentration from 2 to 50 mg C L^{-1}. This trend confirms that thiol functional groups dominate Hg complexation under the given conditions and hinders Hg from amalgamation with AuNPs. On the other hand Hg recovery from spiked glutathione model solution is even less. This might be explained by the chemical structure, the increased number of possible binding sites and influences by steric hindrance. Hg recovery in methionine model solution does not follow a clear trend (see **Figure 24B**). It is higher compared to Hg recovery in cysteine and glutathione model solution and ranges between 41 to 61% of the initially spiked Hg(II) concentration. In conclusion, Hg determination from spiked DOC-containing samples depends strongly on the nature of the occurring substances, *i.e.* their functional groups and steric structure. Hence, further investigation have to be performed in order to adept the present FIAS-AFS for the purpose of measurement of Hg in DOC-rich waters.

4.2.2. Impact of humic acid as a model substance

Humic substances influence the mobility and availability of Hg in soil and water. The DOC concentration in freshwater typically range from 1 to 60 mg L^{-1}.[182] Seawater and open ocean water usually exhibit a much lower DOC concentration below 1.5 mg L^{-1}.[183,184] The impact of dissolved HA on Hg preconcentration onto a nanogold-based collector has been systematically studied using the optimized FIAS-AFS described in section 4.1. As part of this thesis, the influence of humic acid (HA) as a model substance on the optimized FIAS-AFS was investigated. The origin of this HA is not clearly defined by the manufacturer. Still, the black and non-crystalline appearance

68

of this HA and the fact that the extraction of HA from natural water is very elaborative lead to the assumption that the herein used HA originates from soil or coal. Thus, HA model solution represents a fraction of DOM, which is leached from the landscape and subsequently drained into aquatic systems rather than produced *in situ* through microbial activity.

Characterization of humic acid as a model substance

Qualitative analysis of humic substances is challenging due to the broad variability of molecular sizes, functional groups and chemical behavior (see section 2.4). Humic substances are non-stoichiometric materials and the concept of a net formula is extremely limited. Earlier studies determined the elemental composition of humic substances in order to illustrate differences between humic and fulvic acids, and to show variation of these compounds according to their sources.[185,186] In this work, the elemental composition of HA model substance was studied by elemental analysis of the solid material (see **Table 11**). Thereby, the carbon, hydrogen, nitrogen and sulfur mass fraction was determined directly. The oxygen content was calculated by mass difference. It is known from the literature, that sulfur is a minor constituent in HAs extracted from freshwater, ranging between 0.1 to 1.5% by weight.[69] The found sulfur concentration in the herein used HA is 0.32 wt% and thus similar to those reported in the literature. Sulfur within DOM occurs as reduced (*e.g.*, thiol, sulfide) as well as oxidized (*e.g.*, sulfonate, sulfate) species. Of these only the reduced functional groups are thought to be important for Hg binding. About 20% of the total sulfur content in DOM is estimated to be in the reduced form.[83] On the other hand, *Haitzer et al.*[187] suggested that only 2% of the reduced sulfur sites are available for Hg binding. Still, the binding sites within organic matter that are considered far exceed Hg concentrations in natural water. However, a direct comparison with literature data referring to aquatic HA is not recommended as the herein used HA is derived from random organic material as stated by the manufacturer. Still, *Chaplin et al.*[188] found similar values for HA that was used within this work. The results obtained from elemental analysis of HA were used to prepare a stock model solution with regard to dissolved organic carbon. The carbon

content of 36 wt% was considered for the preparation of HA model solutions within the following chapters.

Table 11: *Elemental composition of humic acid used as a model substance (average of two measurements).*

Model compound	C [%]	H [%]	N [%]	S [%]	O [%]
Humic acid	36.19	3.48	0.81	0.32	59.20

Investigation of memory effects

Handling DOC-containing solutions within a flow system suspects to cause memory effects in Hg ultratrace analysis due to its partly hydrophobic nature and affinity to bind Hg. Thus, as a first investigation alternating measurements of Hg(II) spiked HA model solutions and a blank solution (0.06 M HCl) were carried out with the optimized FIAS-AFS (see section 4.1). Therefore, the concentration of HA model solutions was adapted to DOC concentrations in natural water. HA model solutions with a total carbon concentration of 2.5, 5.0 and 10.0 mg L^{-1} were spiked with 100 ng L^{-1} Hg(II) standard solution. The fluorescence intensity obtained after preconcentration of spiked HA model solutions and blank solution is depicted in **Figure 25**. Thereby, each HA model solution was measured 4-fold followed by 12 measurements of the blank solution. It is clear from **Figure 25** that only little carryover occurs when handling HA model solutions within the optimized FIAS-AFS. Constant fluorescence intensity for the blank solution after measuring a HA model solution is obtained after 3-4 measurement cycles. The fluorescence intensity resulting from the blank solution after measuring a 2.5 mg L^{-1} DOC containing HA model solution is slightly higher compared to the blank solution directly measured after 5.0 and 10.0 mg L^{-1} DOC model solution. This effect is explained by conditioning of the FIAS during the very first measurements of the HAmodel solution. Apart from that, memory effects were not observed for measurements utilizing higher concentrations of HA. Thus, the set-up of the optimized
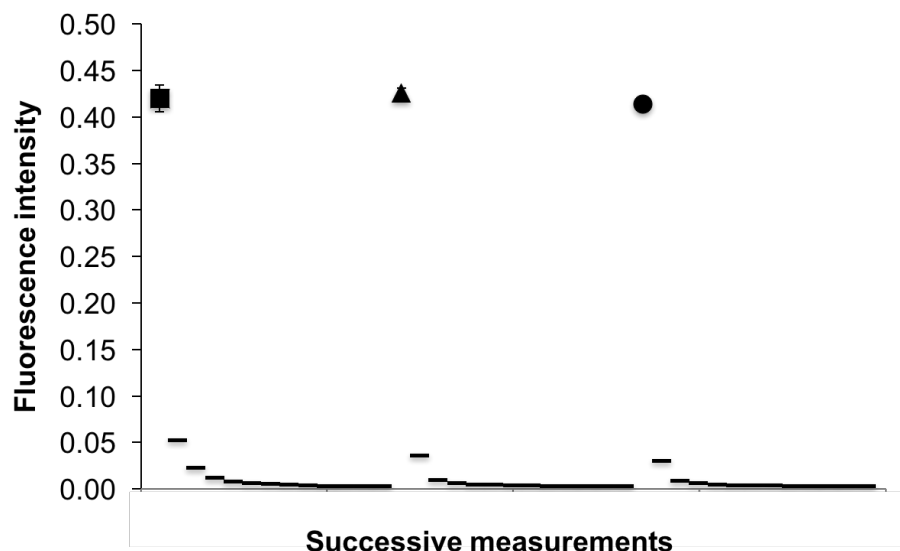
Figure 25: *Alternating fourfold measurement of HA model solution with [Hg] = 100 ng L^{-1} and [DOC] = 2.5 mg L^{-1} (square), [DOC] = 5.0 mg L^{-1} (triangle), [DOC] = 10.0 mg L^{-1} (circle) and single measurement of 0.06 M HCl blank solution (dash) (error bars represent one standard deviation, n_s = 4; reprinted with permission from Leopold et al.[42], copyright 2012 by Springer-Verlag).*

FIAS-AFS and the analytical process for Hg preconcentration onto a nanogold collector are suitable for the analysis of complex matrices such as HA model solutions.

Mercury contamination of humic acid model substance

In general, ultratrace analysis of Hg in water requires special cleaning procedures to reduce blank contribution from utilized reagents and materials. Here, HA model solutions were purposely applied without further cleaning procedures in order not to decompose the organic compounds. Hence, Hg blank contribution of the material was determined according to U.S. EPA method 1631.[97] Therefore, HA model solutions with a DOC concentration of 2.5 to 25.0 mg L^{-1} were digested with BrCl in order to completely oxidize the organic matter and to transform any possible Hg contamination to reducible Hg(II). BrCl was the reagent of choice as it is stated in the earlier literature that halogens readily cleave alkyl-mercury bonds and oxidize dissolved organic matter.[189] Consequently, also methylated Hg species are transformed to "reducible" Hg^{2+}. The total Hg concentration of the digested samples was determined *via* CV

generation followed by AFS measurement. As expected, total Hg concentration found is linearly increasing with the DOC concentration of HA model solutions (see **Figure 26**, $c(Hg) = (7.27 \cdot 10^{-1} \pm 1.63 \cdot 10^{-2}) \cdot c(DOC) + 1.69 \cdot 10^{-1} \pm 1.44 \cdot 10^{-1}$, $R^2 = 0.9905$). The average Hg contamination in HA model solutions as derived by the slope of the linear regression is 0.73 ± 0.02 ng Hg per mg DOC. Hg contamination of humic acid may occur from natural sources, which include organic and inorganic Hg species. On the other hand, Hg contamination might result from the extraction procedure or from atmospheric Hg deposition during storage. The determined Hg blank concentration of HA is used as a reference value for all further investigations.
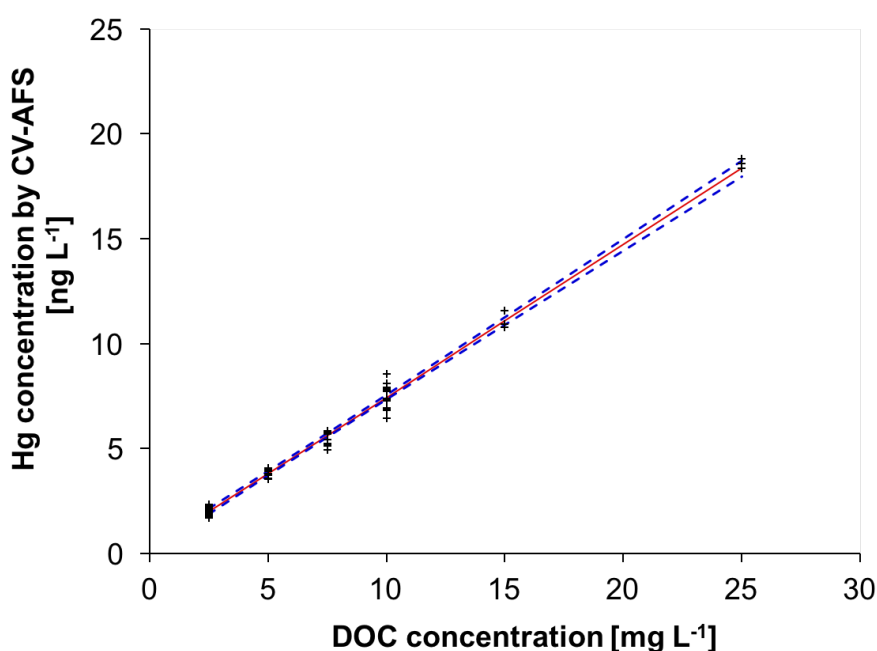
Figure 26: *Hg concentration in humic acid model solution with [DOC]=2.5-25.0 mg $^{-1}$ determined by U.S. EPA method 1631(n_c = 77, (red) linear trend, (blue) confidence interval; reprinted with permission from Leopold et al.[42], copyright 2012 by Springer-Verlag).*

Hg determination in humic acid model solution by FIAS-AFS

As a next step, HA model solutions with different DOC concentration were subjected to direct preconcentration onto the nanogold column using the optimized FIAS-AFS. This experiment was performed to investigate the binding strength between Hg and functional groups within HA in the presence of AuNPs. Thereby, AuNPs are supposed to act as a competing binding partner for Hg. The non-spiked HA model solutions with DOC concentrations of 2.5 to 10.0 mg L^{-1} were analyzed with the FIAS-AFS. External calibration was performed by measurement of aqueous Hg(II) standard solutions in 0.06 M HCl. Found Hg concentration in HA model solutions was then compared with data obtained after total oxidation CV-AFS. It can be seen from **Figure 27** that only a small fraction of Hg initially present in dissolved HA model solution could be found by direct preconcentration onto the nanogold column (recovery = 13-27%).
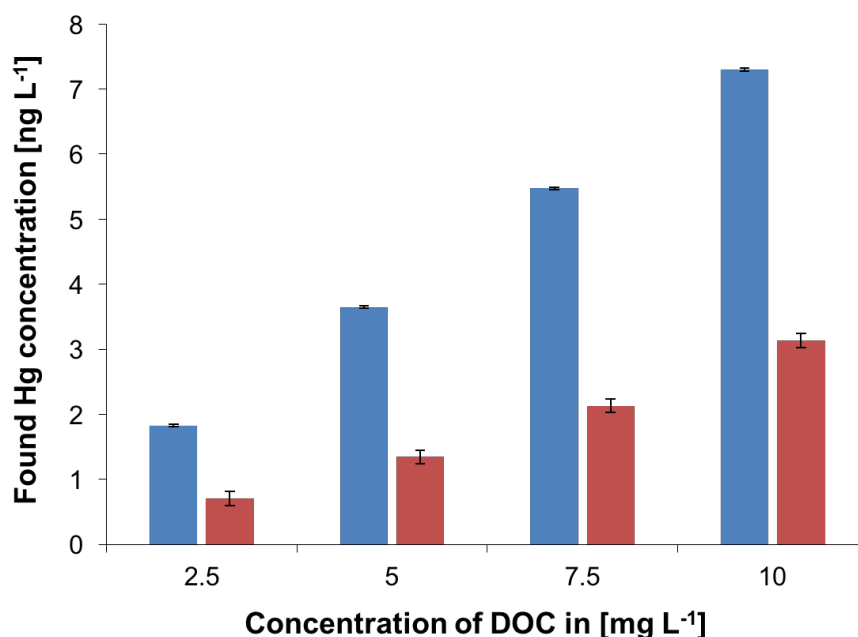
Figure 27: *Recovery of Hg in dissolved humic acid by FIAS-AFS (red) and respective data obtained by U.S. EPA method 1631 (blue) (error bars for FIAS-AFS measurements represent uncertainty derived from confidence interval of external calibration, n_s = 3-5; reprinted with permission from Leopold et al.[42], copyright 2012 by Springer-Verlag).*

The measurable amount of Hg linearly increases with the DOC concentration in HA model solution. Obviously Hg-DOM complexes are highly stabile under the given conditions. The low but measureable fraction of found Hg in HA model solutions can be

attributed to labile Hg-HA complexes that decompose under acidic conditions, *i.e.* Hg ions are replaced by hydrogen protons. Moreover, Hg complexation by chloride ions and subsequent amalgamation with AuNPs may occur. Earlier studies clearly demonstrated that AuNP-coated SiO_2 is capable of quantitative Hg preconcentration from estuary waters with a salinity of 34 and a DOC concentration of 1.8 mg L^{-1}.[22] An explanation for this is that the ligand exchange of the Hg ions is dependent on the concentration of the competing ligands. Thus, the most abundant Hg chloro complexes in saline waters strongly dominate over the Hg-DOM complexes and interact with nanogold *via* amalgamation. Quantitative recovery of Hg(II) chloro complexes in aqueous standard solutions has also been shown in the present work. It is well known from the literature that humic matter does not compete for Hg binding in seawater due to the high chloride concentration and at the same time the low amount of dissolved organic matter. The chloride concentration of seawater is approx. 19 g L^{-1} (0.55 M). *Fitzgerald et al.*[190] among others pointed out that the speciation of Hg(II) in natural water is exclusively dominated by chloride contrary to earlier studies that suggested hydroxide as another important ligand competing for Hg complexation. As a matter of fact, organic complexes are predominant under low-chloride conditions in *e.g.* lake and river water. Under oxic estuary and marine conditions (low [DOC]) a Hg-Cl complexation model (see **Figure 28**) clearly shows the tendency of Hg to form different chloro complexes in the absence of competing organic substances. The investigated HA model solutions here were prepared in diluted hydrochloric acid resulting in a molar concentration of 0.06 mol Cl L^{-1} which is equivalent to only 2.13 g Cl L^{-1}, hence almost one order of magnitude lower. Since stability constants for Hg-DOM complexes are significantly higher compared to chloro complexes, high chloride excess is required to push the equilibrium toward chloro complexes. However, *Drexel et al.*[85] differentiate between weak and strong binding sites for Hg(II) within DOM released from peat. Weak interactions were attributed to carboxyl and phenolic functional groups, whereas strong interactions were explained *via* reduced sulfur sites within DOM. The conditional binding constants ranged from log K = 7.3-8.7 M^{-1} for the weak binding sites within DOM and varied between log K = 22.8-23.2 M^{-1} for the strong DOM binding sites. From this point of view it is reasonable that strong binding sites within HA model solution retain the major fraction of initially present Hg. In summary, initial Hg content

of HA model solution is not quantitatively recovered by direct preconcentration onto the nanogold column without sample pretreatment.
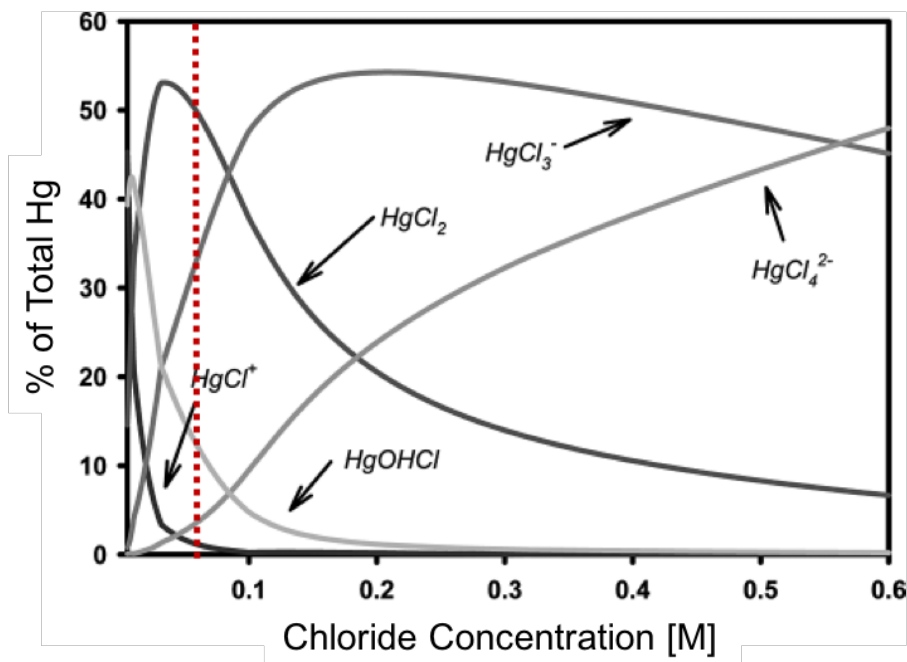
Figure 28: *Progression of Hg-Cl complexes over the range of estuarine and marine salinities (reprinted with permission from Fitzgerald et al.[190], copyright 2007 by American Chemical Society).*

Mercury recovery in spiked humic acid model solution

In another part of this work, recovery experiments were performed to investigate Hg preconcentration onto a nanogold column from HA model solutions of varying DOC concentration. Therefore, adequate volume of Hg(II) standard solution was added to HA model solutions ([DOC] = 2.5-10.0 mg L^{-1}) resulting in a final spike concentration of 1 ng Hg L^{-1}. The freshly prepared spiked HA model solutions were then analyzed with the optimized FIAS-AFS. The absolute difference between found Hg concentration in spiked and non-spiked (see previous section) HA model solution is presented in **Table 12**. Quantitative recovery of 1 ng Hg L^{-1} spike in HA model solutions with a DOC concentration of 2.5, 5.0, 7.5 and 10.0 mg L^{-1} is obtained by direct preconcentration onto the nanogold column. This indicates that, under the given conditions, artificially added

Table 12: *Mercury recovery in spiked HA model solutions (spiked [Hg] = 1 ng L^{-1} as Hg(II), error represents expanded uncertainty derived from confidence interval of external calibration, n_s = 3-4; reprinted with permission from Leopold et al.[42], copyright 2012 by Springer-Verlag).*

DOC concentration of HA [mg L^{-1}]	Recovery of spiked Hg(II) [ng L^{-1}]
2.5	1.07 ± 0.21
5.0	0.71 ± 0.21
7.5	1.36 ± 0.21
10.0	1.29 ± 0.22

Hg(II) interacts only weakly with HA functional groups or does not bind to these functional groups at all. Instead, chloro complexes are formed with spiked Hg(II) as the HA model solutions are prepared in 0.06 M HCl. These Hg-chloro complexes exchange with AuNPs and Hg is quantitatively adsorbed. The findings presented in the previous section suggest that the major fraction of Hg initially present in HA model solution is strongly bound by the organic compounds. Still, quantitative data on active binding sites within HA is difficult to evaluate and consequently information on the ratio of the binding sites within HA and Hg is limited. Still, a recent review by *Ravichandran et al.*[83] leads to the following theoretical approach. Elemental analysis of the applied HA shows that 0.32% organic matter by weight is sulfur. Assuming a reduced sulfur content of 20% (of total sulfur) within the HA results in a molar concentration of reduced sulfur (S_{red}) sites within the investigated HA ([DOC] = 2.5-10 mg L^{-1}) between $1.39 \cdot 10^{-7} - 5.56 \cdot 10^{-7}$ M. Thus, a total Hg concentration (Hg$_{tot}$) of 1 ng L^{-1} ($5.0 \cdot 10^{-12}$ M) within HA model solution leads to a molar ratio of about $2.79 \cdot 10^4 - 1.11 \cdot 10^5$ (S_{red}/Hg$_{tot}$). Hence, Hg recovery in spiked HA model solution does most probable not result from a lack of free binding sites but is most probable a kinetic effect. Regarding analytical method development, this is an important finding, since spiking any DOC-rich sample with Hg most probable will result in quantitative recovery, if the analysis is performed shortly after preparation. This means that recovery experiments using spiked DOC-rich samples do not reflect the behavior of real samples and hence are unsuitable for validation of Hg determination in such samples.

4.2.3. Impact of aquatic humic and fulvic acid

For the following investigations humic (HA) and fulvic acids (FA) extracted from river water were used as model substances to further study the interactions between Hg and naturally occurring organic compounds. HA and FA standard samples were derived from the *International Humic Substances Society* (IHSS). These samples were extracted from *Suwannee River* in Georgia (USA), a blackwater river with DOC concentrations ranging from 25 to 75 mg L^{-1} and pH values below 4.[191] The samples were isolated from river water by the XAD-8 resin adsorption method and are thus most representative for dissolved organic matter within the aquatic environment.[60] *Benoit et al.*[84] presented conditional stability constants for Hg complexes with DOM isolated from surface water. Thereby, the hydrophobic fraction of DOM, which is mostly present in the eutrophic, sulfidic site show a stability constant of log K = 11.8. A value of log K = 10.6 was found for the hydrophilic fraction of DOM representative for an oligotrophic, low-sulfide site.

Elemental composition of the aquatic humic substances

Information on the elemental composition of the herein used standard HA and FA is provided by the IHSS (see **Table 13**).[192] It is notable that O/C fraction by weight is significantly lower compared to HA derived from Alfa Aesar. This might be explained by less oxidative transformation within the IHSS HA and FA.

Table 13: *Elemental composition of humic acid and fulvic acid extracted from Suwannee River.*[192]

Humic substance (IHSS)	C [%]	H [%]	N [%]	S [%]	O [%]
Standard HA	52.63	4.28	1.17	0.54	42.04
Standard FA	52.34	4.36	0.67	0.46	42.98

Mercury contamination of aquatic humic and fulvic acid

A *Suwannee River* HA model solution ([DOC] = 100 mg L^{-1}) was digested with aqua regia and Hg concentration was subsequently determined by CV-AFS. External calibration was performed with Hg(II) standard solutions under the same conditions. Hg contamination of the 100 mg C L^{-1} HA model solutions was found to be 94.56 ± 0.46 ng L^{-1} corresponding to 0.95 ± 0.46 ng Hg per mg DOC. Hg contamination of *Suwannee River* fulvic acid model solution ([DOC] = 100 mg L^{-1}) was determined by microwave-assisted digestion in aqua regia followed by CV-AFS. Due to minor findings applying external calibration with aqueous Hg(II) solution, the standard addition method was applied for this sample. The Hg contamination for two digested samples was determined to be 0.43 ± 0.18 ng Hg per mg DOC. The obtained Hg concentrations in *Suwannee River* HA and FA *via* total oxidation CV-AFS serve as reference values for the following investigations.

Hg determination in non-spiked aquatic humic and fulvic acid solution

HA and FA model solutions of 2, 4, 8, 10, 30 and 50 mg C L^{-1} were investigated with the optimized FIAS-AFS. The results were compared with reference values obtained by CV-AFS as described above. Regarding a low DOC concentration of 2 mg L^{-1} for both, humic and fulvic acid model solutions, almost quantitative recovery was obtained by FIAS-AFS. However, higher DOC concentrations result in a decrease of Hg recovery. This effect is greater for HA (see **Figure 29A**), where Hg recovery in 4 to 50 mg L^{-1} DOC model solutions is ranging between 10 to 46%. On the other hand, Hg recovery in FA model solutions was determined between 25 to 104% for DOC concentration from 4 to 50 mg L^{-1}. The results clearly show that Hg initially present within the model substances binds more strongly to active sites/functional groups within HA over FA.
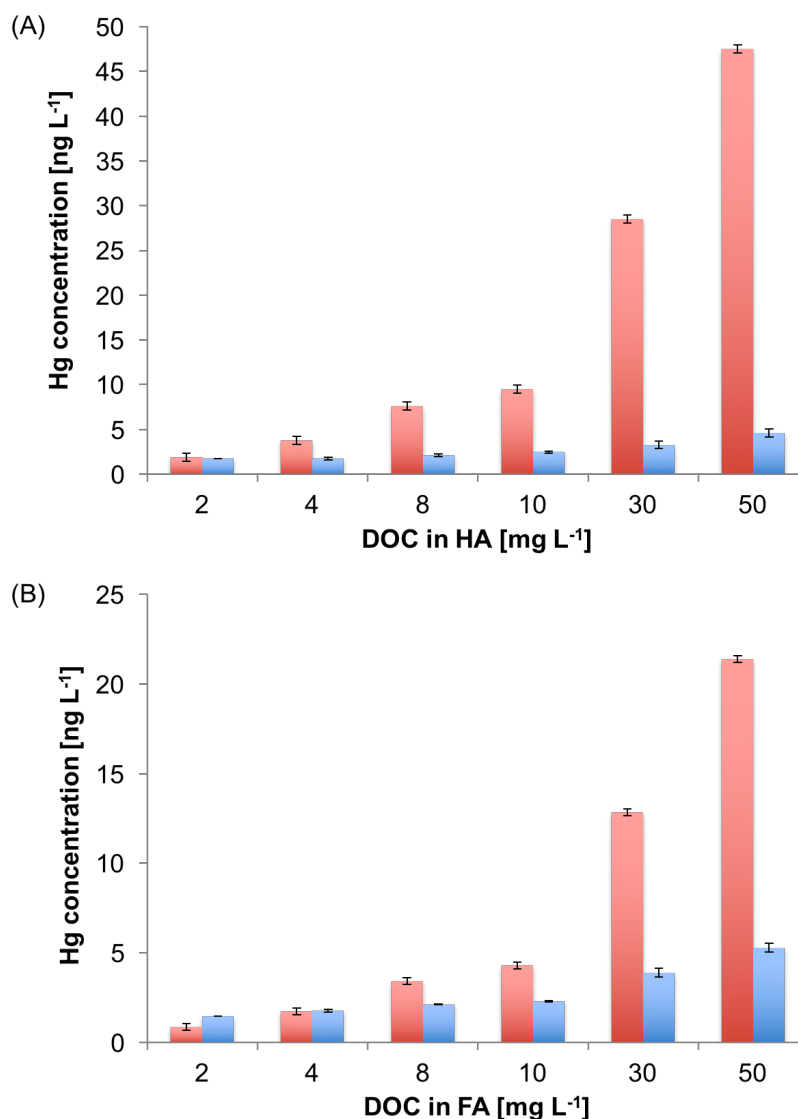
Figure 29: *Hg recovery in non-spiked HA and FA model solutions with varying DOC concentration between 2-50 mg L^{-1} (blue) and corresponding reference values (red) derived from CV-AFS measurements (error bars (blue) represent standard deviation, $n_s = 3$; error bars (red) represent uncertainty derived from external calibration, $n_c = 12$ (HA), $n_c = 17$ (FA)).*

Mercury recovery in spiked aquatic humic and fulvic acid

The following section presents the results of a recovery experiment using HA and FA solutions. Therefore, the model solutions with a constant DOC concentration of 10 mg L^{-1} were spiked with Hg(II) standard solution resulting in a spike Hg concentration of 1 to 100 ng L^{-1}. The model solutions were then passed over the

nanogold collector and found Hg concentration was calculated from the aqueous calibration. A recovery function is obtained by plotting the found Hg concentration against applied Hg concentration (see **Figure 30**). Found Hg is linearly increasing with the applied Hg(II) spike concentration for both HA and FA. The slope of the linear
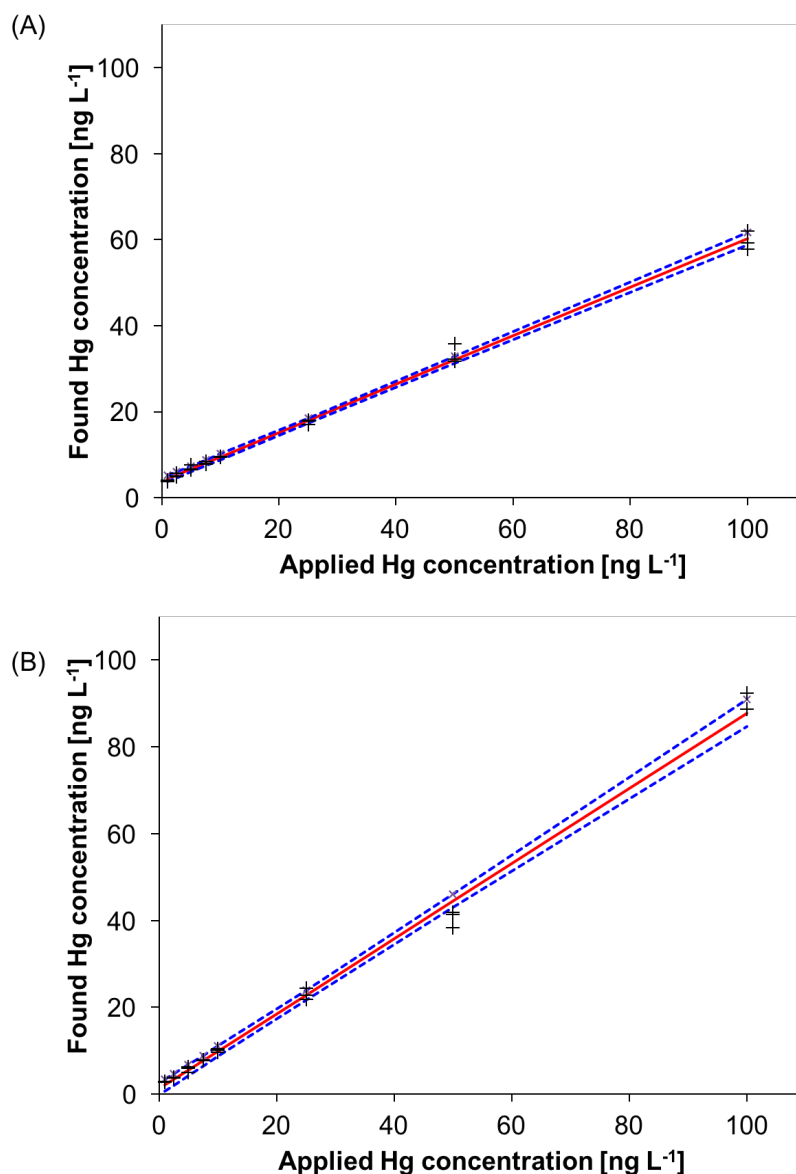
Figure 30: *Hg recovery in humic acid (A) and fulvic acid (B) model solution (n_c = 24 for HA, n_c = 23 for FA, (red) linear trend, (blue) confidence interval).*

regression corresponds to Hg recovery rate in HA and FA model solutions. The Hg recovery rate in a 10 mg C L^{-1} HA is 56.39%, in FA of same DOC concentration a recovery rate of 86.61% is obtained. Hg recovery rates, the corresponding uncertainties

and the regression coefficient (R^2) for the described recovery experiments are summarized in **Table 14**.

Table 14: Recovery rates in HA and FA model solutions ([DOC]=10 mg L^{-1}, [Hg]= 1.0-100 ng L^{-1}).

Humic substance	Recovery [%]	Uncertainty [%] [a]	Regression coefficient (R^2)
Fulvic acid	86.61	3.00	0.9942
Humic acid	56.39	1.46	0.9966

[a] The uncertainty is derived from the confidence interval of the linear regression with $n_c = 24$ for HA, $n_c = 23$ for FA and P=95%.

Xia et al.[80] determined the sum of reduced sulfur groups (RSR, HSR) in *Suwannee River* HA and FA to be about 46% and 35% of the total sulfur, respectively. This observation supports the herein presented results. The lower recovery for HA can be explained by the higher content of active binding sites (reduced sulfur) and thus higher complexation rate towards Hg-HA complexes. On the other hand, nanogold-coated silica particles readily adsorb spiked Hg(II) in FA model solution due to the lower fraction of favored binding sites (RSR, HSR). Further recovery experiments in HA and FA model solutions were conducted with varying DOC concentration. Therefore, HA and FA with a DOC concentration of 2, 4, 8, 10, 30 and 50 mg C L^{-1} were investigated. Each model solution without additional Hg(II) spike was processed in the FIAS and Hg was detected by AFS as described earlier.

A second set of model solutions was spiked with aqueous Hg(II) standard solution resulting in a concentration of 10 ng L^{-1}. The absolute difference of found Hg concentration in spiked and non-spiked HA und FA model solutions is depicted in **Table 15**. Quantitative recovery of spiked Hg was determined for a HA model solution with a DOC concentration of 2 mg L^{-1}. Increasing the DOC concentration up to 50 mg L^{-1} however leads to an overall decrease in Hg recovery. Decrease of recovery is not fully constant which might be a result of the short reaction time.

Table 15: *Results for the recovery experiments in HA and FA model solutions spiked with 10 ng Hg L^{-1}.*

DOC concentration in HA/FA [mg L^{-1}]	Recovery of spiked Hg in HA [ng L^{-1}]	Recovery of spiked Hg in FA [ng L^{-1}]
2	10.21 ± 1.10	13.18 ± 1.13
4	8.84 ± 1.10	13.57 ± 1.13
8	6.66 ± 1.09	13.82 ± 1.13
10	7.37 ± 1.08	14.20 ± 1.14
30	6.73 ± 1.08	13.51 ± 1.13
50	6.91 ± 1.07	11.65 ± 1.12

In addition, the time difference between preparation of the spiked solutions and analysis is most probably not identical for the six samples. The decreasing recovery of Hg in HA model solution is explained by an increasing number of binding sites for Hg(II) and the formation of Hg-HA complexes over coordination to AuNPs and subsequent amalgamation. On the other hand, interaction between spiked Hg(II) and dissolved FA seems to be less. Hg recovery of FA model solution with a DOC concentration between 2 to 30 mg L^{-1} is in the same range. The slight over determination might be a result of the added Hg(II) amount. Complexation reaction and the respective equilibrium might be influenced by the changing Hg concentration. The highest investigated DOC concentration of 50 mg L^{-1} shows a slightly lower Hg recovery compared to lower DOC concentrations in FA solution. A similar trend was observed in the previous experiment where the observed recovery rate for Hg at constant HA and FA concentration (10 mg L^{-1}) was significantly higher for Hg-spiked FA model solution.

4.2.4. Conclusion

The results of the recovery experiments in this chapter demonstrate the impact of organic compounds towards direct Hg preconcentration onto a nanogold-based adsorbent. Different organic ligands and humic and fulvic acids, a portion of DOM, were utilized as model solutions. The initial Hg contamination of the model solutions was determined by total digestion CV-AFS as reference method. Hg(II) spiked and non-spiked model solutions were then subjected to direct preconcentration onto the nanogold-based collector followed by AFS measurement. Urea, Na$_2$EDTA and thiourea influenced Hg accumulation onto AuNPs to a lesser extent. This was demonstrated by a high recovery of 84-98% obtained for a constant DOC concentration of 10 mg L^{-1} and Hg concentration from 1 to 100 ng L^{-1}. In contrast, cysteine, glutathione and methionine hinder Hg(II) from accumulation onto the nanogold collector, which is reflected by low recovery values (30 to 44%). A similar trend was observed for a constant Hg spike concentration and increasing DOC concentration in model solutions. These findings demonstrate that thiol-containing ligands like cysteine and glutathione compete more for Hg binding in the presence of AuNPs compared to other non-sulfur ligands (urea, Na$_2$EDTA). However, comparing these data with literature is challenging as systematic studies on stability constants for Hg with various inorganic and organic ligands are conducted under different experimental conditions. More specifically, they are not obtained in the presence of active AuNPs.

Humic acid has a very complex structure and exhibits a wide range of functional groups, thus memory effects were examined for the optimized FIAS-AFS before using HA as another model substance. As a result, only little carryover occurs when handling Hg(II) spiked HA model solutions with DOC concentration between 2.5 to 10 mg L^{-1}. This systematic study demonstrates that the novel method is feasible for high DOC-containing samples. Hg recovery in HA model solutions is between 13 to 27%, thus Hg initially present within the HA is strongly retained by active sites rather than attracted and amalgamated by AuNPs. Quantitative recovery was obtained for Hg(II) spiked HA model solutions using the FIAS-AFS, which is explained by the formation of strong chloro complexes with the spiked Hg(II).

HA and FA extracted from a real water compartment (*Suwannee River*) were investigated as model substances that reflect real water condition. Recovery experiments for spiked and non-spiked solutions were performed. Quantitative recovery of initially present Hg was found by nanogold-based FIAS-AFS for low DOC concentrations. However, interaction with AuNPs seems to be impaired as the concentration of DOC within HA/FA model solution increase up to 50 mg L^{-1}. Two spike experiments were performed to get a better understanding of the complex reactions between organic matter and Hg in the presence of competing AuNPs. A Hg(II) spike of 10 ng L^{-1} was added to HA/FA model solution of varying DOC concentration. In addition, the recovery rates for Hg(II) spike between 1 to 100 ng L^{-1} were determined for both model substances. Interestingly a difference was observed for the two model compounds. HA tends to influence Hg accumulation on AuNPs more strongly, which is reflected in a low recovery rate of $56.39 \pm 1.46\%$. The recovery rate for FA was $86.61 \pm 3.00\%$. This significant difference suggests that HAs have a higher fraction of active sites that prefer Hg binding compared to FAs. From the elemental composition it is clear that the total amount of sulfur by weight is higher for HA (0.54%) compared to FA (0.46%).[192]

The investigation of different types of model solutions clearly demonstrated that the constitution of a real water sample is crucial for the application of the nanogold-based method for Hg analysis. The complex composition of dissolved organic matter makes it difficult to predict distinct interactions with naturally occurring Hg species. Thus, the integration of a suitable digestion procedures was further investigated within this work.

4.3. Efficiency of various digestion procedures

Digestion of dissolved organic matter in water samples is a mandatory pretreatment step for trace metal analysis. As an example dissolved metal species are partially non-reactive and thus not available for electrochemical techniques when they are complexed by DOM.[193] To overcome these problems wet digestion is often applied as a sample pretreatment step prior to detection. This procedure is performed under acid conditions, mostly with the addition of oxidizing reagents, *i.e.* hydrogen peroxide, potassium

permanganate, nitric acid, sulphuric acid, sodium persulphate and bromine monochloride to destroy dissolved organic material and release the analyte in a labile form. Standard methods for total Hg determination in natural water recommend the addition of bromine monochloride to oxidize Hg forms and species found in natural water.[97] The digestion is typically carried out under high pressure and/or elevated temperature. In order to prevent analyte loss through volatilization and to minimize reagent consumption closed systems such as microwave (MW) digestion were developed for the degradation of a variety of matrices.[194,195] In addition, the digestion time could be reduced compared to conventional batch procedures. However, the integration of MW digestion to a portable system for on-site application is difficult. Another study presented the integration of wet digestion to an automated flow injection system coupled to CV-AFS for Hg determination.[150] However, a general disadvantage of wet digestion is the increased risk of contamination caused by the addition of reagents. This leads to elevated blank levels and compromise the sensitivity of the method.

In order to improve Hg preconcentration onto the nanogold collector from high DOC containing samples a UV digestion unit was developed and implemented to the automated FIAS-AFS. Photooxidation is frequently used as a sample pretreatment for metal analysis in *e.g.* natural water and body fluids. Similar processes are applied within industrial applications, *i.e.* for the decomposition of (toxic) organic compounds and for the purification of urban and industrial wastewater. The production of ultrapure water by purification of pretreated water is also based on UV photooxidation of organic compounds. The interaction of UV light with dissolved organic compounds results in the formation of various intermediate compounds, *i.e.* excited states of DOM, hydrogen peroxide, singlet oxygen ($^1O_2$), superoxide ions (O_2^-), organoperoxy radicals and hydroxyl radicals ($\cdot OH$). These species are highly reactive and act as oxidants for dissolved organic matter. The addition of reagents like H_2O_2, O_3, $K_2S_2O_8$, $K_2Cr_2O_7$ prior to UV irradiation accelerate the mineralization process. In 1939, *Kautsky*[196] proposed first an oxidation process resulting from the interaction of sunlight with natural water. Dissolved organic compounds adsorb light and its energy is subsequently transferred to molecular oxygen. The formed reactive singlet oxygen ($^1O_2$) reacts with organic matter

and water molecules resulting in different radicals and peroxides as oxidation products. Singlet oxygen is highly reactive with a lifetime of only 2 μs.[197] *Achterberg et al.*[198] clearly demonstrated that online UV digestion is more effective compared to batch-wise UV digestion, resulting in 20 to 300 times faster decomposition of organic model substances in ultrapure water.

Within the following chapter, Hg recovery from a non-spiked HA model solution was determined by online UV irradiation followed by preconcentration onto the nanogold collector within the FIAS-AFS. Thereby, the influence of the duration of the UV treatment was investigated. Furthermore, the effect of hydrogen peroxide as assisting agent during UV-photooxidation was examined in detail using HA as a model compound. In addition, two UV bulbs with different emission maxima were tested with respect to HA degradation. Moreover, tests were conducted using a photocatalytic titanium dioxide (TiO_2) layer to enhance dissolved organic matter decomposition within the FIAS-AFS.

4.3.1. Online UV digestion of humic acid

As described in section 4.2.2, only 13 to 27% of Hg was found in non-spiked HA model solutions ([DOC] = 2.5-10.0 mg L^{-1}) *via* direct accumulation onto the nanogold collector integrated to the optimized FIAS-AFS. Hence, to improve Hg recovery in samples containing high DOC an online UV digestion unit was developed and implemented into the FIAS-AFS. The general set-up of the FIAS-AFS with integrated UV digestion unit is presented in **Figure 31**. The detailed manifold is given in the experimental procedures in chapter 6.7. The sample solution is transported to the sample loop by a peristaltic pump. By means of the rinsing solution the defined sample volume is transported into the reaction tube and irradiated for a variable duration by UV light. The subsequent steps consist of Hg preconcentration on the nanogold collector, thermal release and measurement of Hg(0) by AFS. As a first experiment, a 2.5 mg C L^{-1} HA model solution was irradiated for 3, 6, 9, 12, 15, 20 or 25 min, respectively, within the UV-assisted FIAS-AFS. After irradiation the sample is transported towards the nanogold collector for
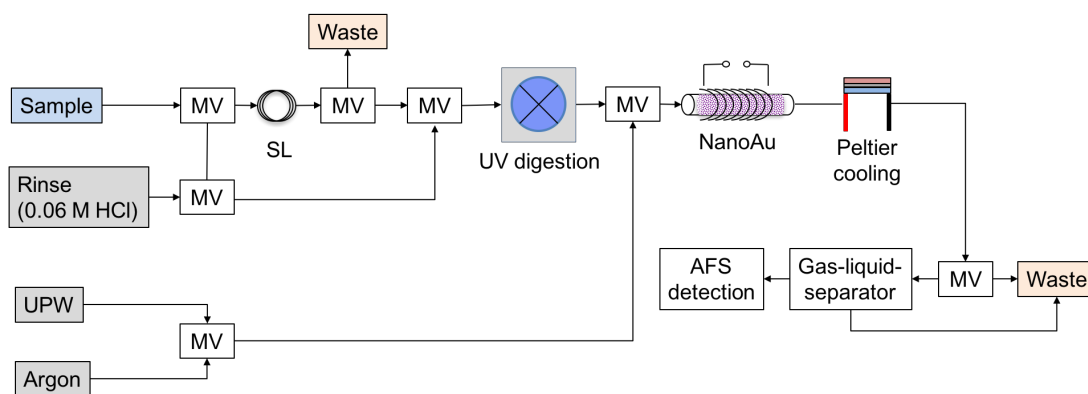
Figure 31: *Schematic illustration of the flow injection analysis system coupled to an atomic fluorescence spectrometer for online UV irradiation and Hg determination in aqueous solution (abbreviations: UPW ultrapure water; MV magnetic valve; SL sample loop; NanoAu nanogold-based collector, AuNP-coated silica).*

Hg preconcentration. The found Hg concentration was compared to reference values obtained by EPA method 1631.[97] It is clear from **Figure 32A** that online UV irradiation induces Hg release from the Hg-HA complexes as the proportion of found Hg increases with UV irradiation time. The plotted values for found Hg proportion reveal a logarithmic dependence from the irradiation time (3 to 25 min). Hg accumulation onto the nanogold co llector increases with the duration of UV irradiation until quantitative Hg recovery $(95 \pm 8\%)$ was achieved after approx. 25 minutes UV pretreatment. As these results for a $2.5 \, mg \, C \, L^{-1}$ HA model solution seem very promising analogous experiments were conducted with similar HA model solutions containing higher DOC concentration. Therefore, 5.0, 7.5 and $10.0 \, mg \, C \, L^{-1}$ HA model solutions were irradiated for 6 min or 25 min, respectively, prior to nanogold preconcentration (see **Figure 32B**). The reference values were obtained slightly higher Hg recovery values (30 to 39%, empty triangles). The maximum tested irradiation period of 25 min (empty circles) results in release of 76% of the initial Hg concentration from a 5.0 and $10.0 \, mg \, C \, L^{-1}$ HA model solution. In summary, the here tested UV digestion pretreatment does not result in quantitative Hg recovery from high DOC-containing samples (5.0; $10.0 \, mg \, C \, L^{-1}$) even after exposure to UV light for 25 min. In order to reduce the overall analysis time and to achieve reliable Hg determination in high DOC-containing samples further approaches were pursued within this work.
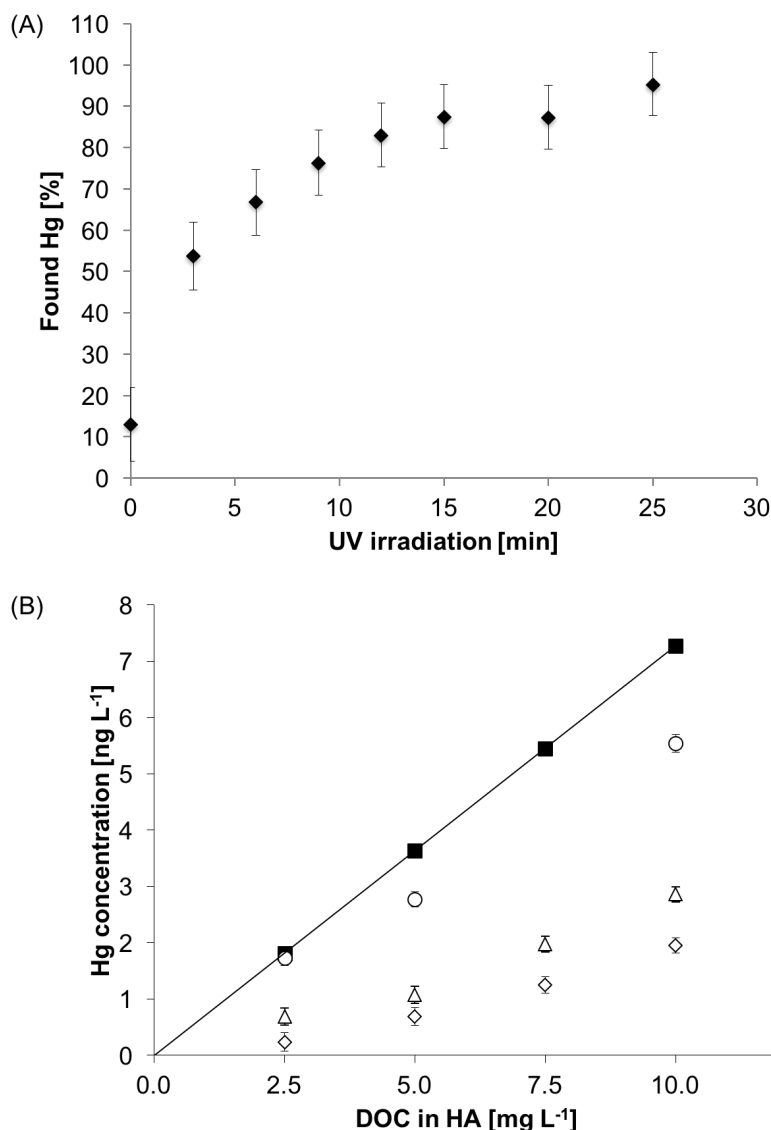
Figure 32: *Found Hg concentration (A) in 2.5 mg L^{-1} HA model solution with varying duration of UV irradiation from 3 to 25 min and (B) in HA model solutions ([DOC]=2.5, 5.0, 7.5, 10.0 mg L^{-1}) without UV pretreatment (diamond) and after 6 min (triangle) and 25 min (circle) of online UV irradiation. Reference values obtained by U.S. EPA method 1631 (filled squares) (error bars represent uncertainty derived from external calibration with Hg(II) standard solution in 0.06 M HCl, n_s=3, n_c=14; reprinted with permission from Leopold et al.[42], copyright 2012 by Springer-Verlag).*

4.3.2. Reagent-assisted online UV digestion of humic acid

As described in the previous section 25 min UV irradiation as a sample pretreatment was sufficient to quantitatively recover Hg initially present within a HA model solution with

DOC concentration $\leq$ 2.5 mg C L^{-1}. However, higher DOC concentrations hindered complete Hg recovery. In order to provide a reasonable analysis time and to apply the procedure towards high DOC-containing samples, the efficiency of a reagent-assisted online UV pretreatment was investigated. As a first attempt, hydrogen peroxide (H_2O_2) was added as an oxidizing agent. It is widely reported in the literature that H_2O_2 accelerates the mineralization of dissolved organic matter in aquatic systems.[199,200] H_2O_2 absorbs UV light and decomposes into reactive hydroxyl radicals ($\cdot$OH), which exhibit a high oxidation potential of 2.80 V.[201,202] For the following experiments the set-up described in the previous section was applied. The influence of H_2O_2 and its UV-induced decomposition products on the accumulation of Hg onto the nanogold collector was investigated first. Therefore, different levels of aqueous Hg(II) standard solutions were prepared in 0.3% and 1.0% (v/v) H_2O_2. The calibration standards were then irradiated by UV light for 6 min prior to Hg accumulation onto the nanogold collector. The performed calibration resulted in a linear function and the corresponding characteristics were compared with the data derived from calibration performed without additional H_2O_2. **Table 16** summarizes the characteristics of these calibration functions. The sensitivity of the method, derived from the slope of the linear regression, changes only slightly even after the addition of 1.0% (v/v) H_2O_2. Hence, poisoning of the catalytic active immobilized AuNPs by radical attack (*e.g.* $\cdot$OH) or other oxidizing processes can be excluded. However, higher reproducibility is obtained applying aqueous Hg(II) standard solution without H_2O_2. Still, a relative coefficient of variation of the procedure (V_{x0}) of 7.78% and 7.61% in 0.3% and 1.0% (v/v) H_2O_2 respectively, is sufficient for Hg ultratrace determination. As a conclusion, H_2O_2 is a suitable assisting agent for online UV digestion with regard to Hg accumulation onto the nanogold collector. As a next step, HA model solutions were spiked with 0.3% (v/v) H_2O_2 prior to 6 min UV pretreatment. This resulted in clearly higher Hg recovery compared to UV pretreatment without addition of an oxidizing agent. However, the first investigations show that quantitative Hg recovery could not be reached by adding 0.3% (v/v) H_2O_2. Moreover, a lower slope ($1.9 \cdot 10^{-3} \pm 0.3 \cdot 10^{-3}$ L ng^{-1} for 5 mg L^{-1} DOC; $1.5 \cdot 10^{-3} \pm 0.4 \cdot 10^{-3}$ L ng^{-1} for 10 mg L^{-1} DOC) for Hg determination in HA model solution was obtained compared to that in aqueous Hg(II) standard solutions ($3.7 \cdot 10^{-3} \pm 0.3 \cdot 10^{-3}$ L ng^{-1}). A decrease in sensitivity indicates interfering matrix effects,

which originate from dissolved HA and/or respective decomposition products. Still, a permanent poisoning of

Table 16: Characteristics of calibration functions obtained by measuring aqueous Hg(II) standard solutions (0.06 M HCl) after online UV irradiation for 6 min by FIAS-AFS with and without H_2O_2 addition ($n_c = 10$; confidence interval, P = 95%; reprinted with permission from Leopold et al.[42], copyright 2012 by Springer-Verlag).

Characteristics	Without additional reagents	With addition of 0.3% (v/v) H_2O_2	With addition of 1.0% (v/v) H_2O_2
Calibration range [ng L^{-1}]	1 – 5	1 – 8	0.4 – 32
Slope [L ng^{-1}]	$3.9 \cdot 10^{-3} \pm 0.1 \cdot 10^{-3}$	$2.3 \cdot 10^{-3} \pm 0.5 \cdot 10^{-3}$	$3.7 \cdot 10^{-3} \pm 0.3 \cdot 10^{-3}$
Intercept	$0.8 \cdot 10^{-3} \pm 0.4 \cdot 10^{-3}$	$0.3 \cdot 10^{-3} \pm 0.1 \cdot 10^{-3}$	$1.9 \cdot 10^{-3} \pm 4.3 \cdot 10^{-3}$
Regression coefficient R^2	0.9973	0.9908	0.9912
Relative coefficient of variation of the procedure (V_{x0})	3.19	7.78	7.61

the nanogold can be excluded as the adjacent measurements of aqueous Hg(II) solution showed good performance with initial slopes. To overcome these matrix effects and to achieve high sensitive analysis the calibration was performed by standard addition method. For the following experiments HA model solutions with a DOC concentration of 5.0, 10.0 and 15.0 mg C L^{-1} were prepared in 0.3% and/or 1.0% (v/v) H_2O_2. Hg concentration of the respective model solution was determined by FIAS-AFS with integrated online UV digestion for 6 min prior to Hg preconcentration onto the nanogold collector. The results and reference data derived from U.S. EPA method 1631 are presented in **Table 17**. Regarding the expanded uncertainty (UΔ) and the absolute difference (Δm) obtained from the two measurements (online UV digestion and U.S. EPA method 1631) there is no significant difference between the measurement and the reference method (see appendix **Table A6**).[203] Hence, the addition of 0.3% (v/v) H_2O_2 and 6 min online UV digestion results in quantitative Hg recovery for HA model solutions with a DOC concentration of 5.0 and 10.0 mg C L^{-1}. HA model solution with a

DOC concentration as high as 15.0 mg C L^{-1} require the addition of 1.0% (v/v) H$_2$O$_2$ for digestion of humic matter and quantitative release of Hg from complexes prior to

Table 17: *Hg recovery in humic acid (HA, Alfa Aesar) model solutions ([DOC] = 5.0, 10.0, 15.0 mg C L^{-1}) after addition of 0.3% and/or 1.0% (v/v) H$_2$O$_2$ and 6 min online UV digestion, reference value is determined by U.S. EPA method 1631 (reprinted with permission from Leopold et al.[42], copyright 2012 by Springer-Verlag).*

DOC in HA model solution [mg C L^{-1}]	Hg concentration after 6 min UV irradiation [ng L^{-1}] [a, b]	Hg concentration according to U.S. EPA method 1631 [ng L^{-1}]
5.0	4.77 ± 1.33 [c]	3.64 ± 0.02
10.0	6.55 ± 1.87 [c]	7.27 ± 0.02
15.0	8.86 ± 1.96 [c]	
	11.1 ± 2.68 [d]	10.91 ± 0.02

[a] Calibration was performed by standard addition method; [b] Uncertainties for Hg measurement derive from the confidence interval of the external calibration; P=95%; N ≥ 9; [c] Addition of 0.3% (v/v) H$_2$O$_2$ prior to 6 min online UV digestion; [d] Addition of 1.0% (v/v) H$_2$O$_2$ prior to 6 min online UV digestion.

accumulation onto the nanogold collector. In conclusion, quantitative Hg recovery in HA model solutions with a DOC concentration up to 15.0 mg C L^{-1} is achieved using standard addition method for calibration and addition of 1.0% (v/v) H$_2$O$_2$ prior to 6 min online UV irradiation within the optimized FIAS-AFS.

4.3.3. Photocatalytic decomposition of humic acid by a TiO$_2$-coated reaction tube

In the previous section, hydrogen peroxide was added to HA model solutions to enhance the formation of reactive radicals during online photooxidation. It was shown that Hg recovery significantly increased when H$_2$O$_2$ was added prior to UV irradiation of the sample probably due to the high oxidizing potential of the *in situ* formed species (*e.g.* ·OH, O$_2^-$). For the following experiments, the principle of decomposition of DOM by radical attack was transferred towards a reagent-free, photocatalytic oxidation process. A large number of studies make use of the light-induced characteristics of TiO$_2$. Thereby, TiO$_2$ is either immobilized on support materials, *e.g.* quartz sand, glass, ceramic

membrane, or the solid catalyst is suspended in aqueous medium. Many researchers focused on the effective degradation of organic pollutants in various samples by the TiO_2/UV process, *e.g.* salicylic acid, phenol, naphthalene.[204,205] A great advantage of supported TiO_2 is that a post-treatment for particle separation from the solution can be omitted. Acting as a true catalyst TiO_2 remains unchanged after the photooxidation reaction. In this work, a thin layer of TiO_2 was deposited at the inner surface of a quartz glass reaction tube. This photoreactor was then implemented to the optimized FIAS-AFS to investigate online photocatalytic degradation of HA model solutions and release of Hg prior to preconcentration onto the nanogold collector. The band gap energy, which is the energy difference between the valence band and the conduction band, of TiO_2 is $\Delta E = 3.03$ eV. Thus, an excitation wavelength less than or equal to 384 nm is needed to induce photocatalytic activation. Hence, again UV lamps were applied as excitation source within the following experiments and therefore their efficiency was tested in preliminary experiments.

Efficiency of different UV sources for humic acid decomposition

The efficiency of two different irradiation sources for decomposition of dissolved HA was investigated by UV-Vis absorption spectroscopy. In this study, a UV bulb with a maximum emission at $\lambda = 254$ nm was compared to a UV bulb, which exhibits two emission maxima at $\lambda = 254$ nm and $\lambda = 189$ nm. Thereby, a quartz glass lamp housing allows the transmission of the high energy UV radiation.

First, the influence of radicals resulting from energy-rich UV irradiation on the nanogold collector was tested. Therefore, UPW and 0.06 M HCl were irradiated for 3 min within the FIAS-AFS and the solutions were subsequently passed through the nanogold collector. The resulting fluorescence intensities for both, UPW and blank solution (0.06 M HCl), were compared before and after UV irradiation. The fluorescence intensity did not change for four consecutive measurements. Thus the radicals (*i.e.* ·OH, Cl·) formed during UV irradiation did not affect the adsorption capacity of the nanogold collector for dissolved mercury traces.

For quantitative evaluation of the photo-induced decomposition of HA a calibration experiment was performed. Therefore, the absorbance of HA model solutions of different DOC (10 to 100 mg C L^{-1}) concentration were measured between 190 to 1100 nm. The obtained UV-Vis absorption spectra do not show a clear maximum or shoulder, which is in good agreement with data presented in the literature.[206] In general, spectroscopic studies describe an exponential decrease of UV-visible light absorption by chromophoric dissolved organic matter with increasing wavelength.[207,208] This trend was also observed within this study. Consequently for calibrating the system three distinct wavelengths in the visible range (400, 450, 500 nm) were selected and the corresponding absorbance was plotted against the DOC concentration. Evaluating the DOC concentration of a sample after UV irradiation was then performed *via* the average of the calibration function at 400, 450 and 500 nm. To investigate the influence of UV radiation on the decomposition of HA model solutions, a 25 mg C L^{-1} HA model solution was irradiated with the two UV sources within a batch procedure. Thereby, the duration of UV irradiation varied between 1 and 10 min. The sample was collected after UV irradiation and directly measured by UV-Vis absorption spectroscopy. Absorbance at $\lambda = 400$, 450 and 500 nm was used to calculate the fraction of decomposed HA over the investigated irradiation time. As expected, the higher energy UV bulb causes greater HA decomposition within the investigated time range (see **Figure 33**). Up to 24% of the initial dissolved HA content was decomposed over the investigated time range when using the energy bulb that exhibits two emission maxima at 189 and 254 nm. On the other hand, the UV source with a distinct maximum at 254 nm decomposed only 2 to 11% of the dissolved HA. The aim of irradiating the HA model solution is to weaken and/or to overcome the binding energy between Hg and active binding sites within complex HA structures for subsequent adsorption of Hg onto immobilized AuNPs. Thus, quantitative oxidation of dissolved HA might not mandatory for quantitative Hg recovery. Hence, as a first attempt in the following experiments the irradiation time was kept below 10 min using the high-energy UV lamp for excitation.
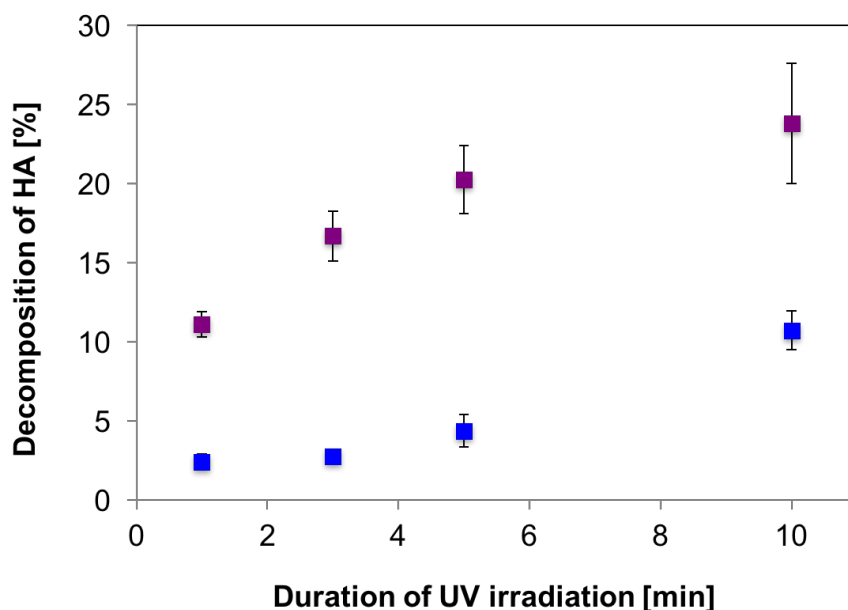
Figure 33: *Decomposition of HA model solution ([DOC] = 25 mg L^{-1}) by irradiation with a 254 nm (blue) and 254nm/185 nm (purple) light source for 1, 3, 5 and 10 min.*

Efficiency of TiO$_2$ for Hg recovery from aquatic humic acid-containing samples

A quartz glass tube was used as reaction tube due to its high UV transparency. In addition, quartz glass is more thermally stable compared to borosilicate glass, which is a key factor during TiO$_2$ coating. The immobilization of an inner photocatalytic TiO$_2$ film was achieved *via* two different synthesis routes. A straightforward procedure is based on the immobilization of TiO$_2$ particles on the quartz glass substrate. Such procedures are described in the literature and were adapted within this work.[204,209,210] Therefore, TiO$_2$ particles were suspended in UPW and subsequently pumped through the quartz glass tube. The solution was discarded and the coating was dried at 180°C. After calcination at 550°C a homogenous white layer was observed at the inner wall of the tube. Rinsing of the reaction tube with UPW and 0.06 M HCl did qualitatively not remove the TiO$_2$ coating. The described reaction tube is named "TiO$_2$_suspension" in the following. Another coating procedure follows the sol-gel process and has been suggested for instance by *Wang et al.* [211]. This approach is named "TiO$_2$_alkoxide" in the following.

94

For this coating procedure titanium (IV) isopropoxide was used as a precursor. The solution was mixed with ethanol and subsequently pipetted into the quartz glass tube. To improve the layer thickness, which was traced by visual inspection, the process was repeated two times. The tube was dried at room temperature and calcination was again performed at 550°C. The ready-made TiO_2-coated quartz glass tube and the UV bulb (254/185 nm) were implemented into the optimized FIAS-AFS as shown in **Figure 34**. In this modified FIAS the HA model solutions are transported towards the reaction tube where irradiation with UV light for 1 min takes place. The reaction tubes obtained from
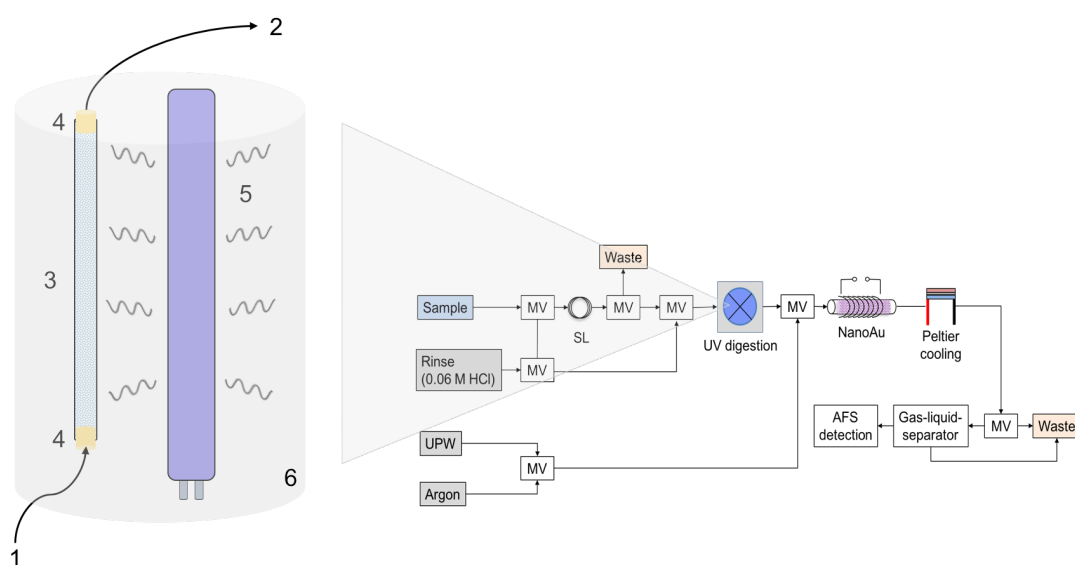
Figure 34: *Schematic illustration of the TiO_2 coated reaction tube for photocatalytic digestion (left); integration to the flow injection analysis system (right) (remarks: 1 solution coming from the sample loop, 2 solution flowing towards the nanogold collector, 3 horizontally fixed TiO_2 coated quartz glass tube, 4 silicone plugs with tubing connection, 5 horizontally fixed UV bulb, 6 aluminum foil).*

the different synthesis procedures were tested consecutively. Moreover, analogous experiments were conducted without UV irradiation of the sample for both TiO_2 coated reaction tubes. Afterwards, the sample was passed through the nanogold collector for Hg preconcentration according to the previously described optimized procedure. For these investigations HA extracted from *Suwannee River* (IHSS) was applied as a model substance. Model solutions with varying DOC concentration of 5.0, 10.0 and 15.0 mg C L^{-1} were investigated. The received results and the reference values obtained by EPA method 1631 are shown in **Figure 35**. The results clearly show that both types

of the TiO$_2$ coatings have a positive effect on Hg recovery from HA model solution. The recovery values found by direct preconcentration onto the nanogold collector are not shown in **Figure 35** for a better overview. These values were presented earlier in section 4.2.3 and found recovery values in non-spiked HA model solutions were acceptable only for lower DOC concentration of 2.0 and 4.0 mg C L^{-1}, with 93 and 46%, respectively. Whereas, for DOC concentrations up to 30 mg C L^{-1} only 12 to 25% of total Hg were recovered. Here, passing the HA-containing solution with up to 15.0 mg C L^{-1} through a
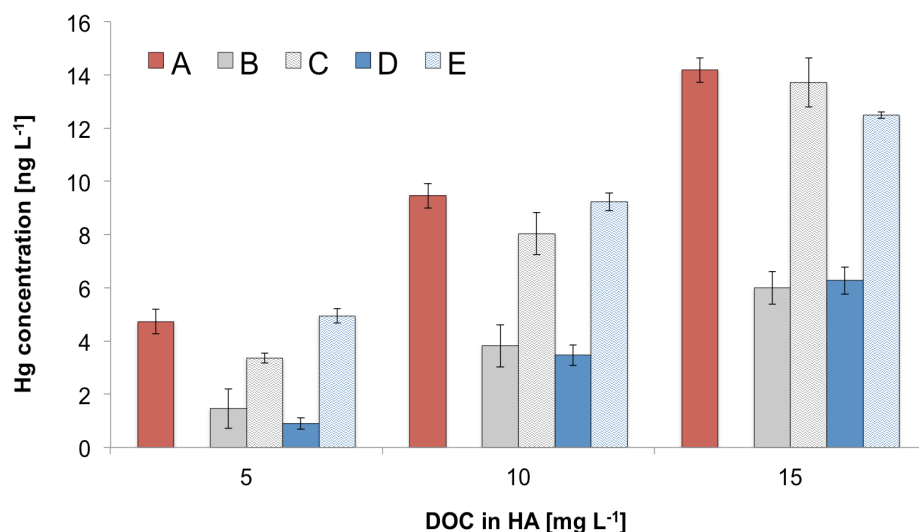
Figure 35: *Hg concentration found in HA model solution ([DOC] = 5, 10, 15 mg C L^{-1}) by (A) EPA method 1631; and by FIAS-AFS without pretreatment (B,D) and after 1 min online UV irradiation (C,E). Values (B) and (C) are obtained with TiO$_2$_alkoxide reaction tube, (D) and (E) are obtained with TiO$_2$_suspension reaction tube ((A) error bars represent uncertainty as derived from the prognosis interval of the calibration, n_c = 12; (B) error bars represent one standard deviation, n_s = 4; (C), (D), (E) error bars represent one standard deviation, n_s = 3).*

TiO$_2$_alkoxide reaction tube results in a Hg recovery of 31 to 42%, and 19 to 44% for the TiO$_2$_suspsension coated reaction tube. In the presence of the photoactive coating and under 1 min UV radiation Hg recovery increases to 71 to 97% for TiO$_2$_alkoxide, and to 83 to 99% for TiO$_2$_suspsension. Hence, a clear effect - Hg is released from HA complexes and follows amalgamation onto AuNPs - is observed when irradiating the HA model solution in the presence of both types of photocatalytic TiO$_2$ layers. For a 5 and 10 mg C L^{-1} HA model solution the recovery values are slightly higher applying the TiO$_2$_suspsension coating compared to the TiO$_2$_alkoxide reaction tube. However, this trend is reversed for the highest DOC concentration in HA model solution

(15 mg C L^{-1}), where the TiO$_2$_alkoxide tube shows higher Hg recovery. The presented experiments were performed for a proof-of-principle of the photocatalytic activity of TiO$_2$ towards HA decomposition and enhanced Hg accumulation on the AuNPs-based collector. Thus, qualitative surface analysis and quantitative measurements of the immobilized TiO$_2$ particles were not performed within this work. It is assumed that the differences in Hg recovery after irradiating the HA solution in the presence of the TiO$_2$ coating is resulting from the different particle size obtained from the two preparation procedures. This approach was not yet applied to real water samples with elevated dissolved organic carbon fraction. However, the presented experiments give a promising outlook towards quantification of dissolved Hg in demanding humic-rich waters omitting elaborative and reagent-consuming pretreatment procedures. The set-up of the digestion unit is simple and the photocatalytic TiO$_2$ reaction tube is easy to prepare using standard reagents. Furthermore, the irradiation time of only 1 min provides a high sample throughput.

4.3.4. Conclusion

This chapter describes the implementation of an online UV pretreatment to the optimized FIAS-AFS for subsequent Hg preconcentration onto a nanogold collector. As pointed out earlier, the nanogold material is not suitable to quantitatively accumulate Hg traces from humic-rich waters where strong complexation of Hg hinders the amalgamation process. In order to overcome these interactions between Hg and preferably thiol-containing functional groups within organic compounds (HA, FA, model organic ligands) and to break down dissolved organic compounds online UV pretreatment was tested within this work. For this purpose different experimental set-up and model substances were investigated. It was shown that 25 min of UV irradiation of the sample within the FIAS-AFS provides a recovery of $95 \pm 8\%$ of Hg from DOC-containing HA model solution up to 2.5 mg C L^{-1}. In order to improve analysis time and to recover Hg from samples with higher DOC content, a mild oxidant (H$_2$O$_2$) was added prior to online UV treatment within the FIAS-AFS. For this purpose, the influence of H$_2$O$_2$ decomposition products (*e.g.* ·OH) and free radicals on the nanogold collector was

investigated first revealing no permanent negative effects. Still, due to matrix effects the standard addition method was chosen for calibration to quantify Hg in HA model solutions. Thereby, quantitative Hg recovery in solutions containing up to 15.0 mg DOC L^{-1} was achieved by addition of 1.0% (v/v) H_2O_2 and 6 min UV irradiation. A further attempt was the application of TiO_2 as a photocatalytic material in order to enhance decomposition of natural HA by irradiation. For these experiments, a high energy UV bulb, that emits radiation at a wavelength of 254 nm and 185 nm, was applied. Here, irradiation duration was reduced to only 1 min in the presence of TiO_2. Two different TiO_2 coating procedures were tested, *i.e.* immobilization of TiO_2 from suspension and *via* sol-gel method. A significant increase in Hg recovery was observed for both TiO_2 layers, the recovery varied between 71 and 99%. Hence, release of Hg from humic complexes is supported by photocatalytic activity of TiO_2. This promising approach offers a reagent-free digestion procedure.

Further studies on freshwater samples with elevated DOC concentration will clarify if the photocatalytic TiO_2 layer is the best choice as sample pretreatment step integrated to the fully automated, reagent-free nanogold-based FIAS-AFS for ultratrace analysis of Hg. A characterization of the photoactive layer will probably help to better understand the decomposition mechanism and to optimize the coating parameters.

4.4. Applicability to real water samples

The applicability of the previously developed methods to demanding real water samples was evaluated within this study. Water samples were analyzed at different stages of the development process of the analytical methods. Thus, some of the samples were measured directly by the optimized FIAS-AFS without integrated sample pretreatment steps, while others passed reagent-assisted online UV digestion prior to Hg preconcentration. A broad variety of different water samples were investigated, including natural freshwater samples collected near Ulm and Munich, wastewaters and treated waters obtained from a wastewater treatment plant (WWTP) near Ulm, as well as fresh and saline waters provided by *the Geosciences Environment Toulouse* (GET,

Université Paul Sabatier). **Table 18** summarizes the investigated samples according to their origin and sampling dates. Additional information on the water samples (*e.g.* temperature, pH value) and the applied materials for sampling and sample pretreatment is summarized in **Table A1** to **A5** in the appendix.

Table 18: Real water samples investigated in this work using a nanogold-based flow injection analysis system coupled to atomic fluorescence spectrometry.

Water sample	Sample origin	Date of sampling	Appendix
Natural freshwaters			
Great Whale River	Quebec; Canada [a] (different sampling spots)	May 2011	Table A1
Isar (river water)	Dürnstein, Munich, Garching; Germany	October 2011	Table A2
Danube (river water)	Wiblingen, Ulm, Böfingen; Germany	October 2011	Table A2
Seawater samples			
Black Sea water	42°20'56''N 38°41'2''E (vertical profile)	July 2013	Table A3
Black Sea water (intercomparison study)	42°31'16''N 31°24'7''E	July 2013	Table A4
Wastewaters/treated waters			
Treated/untreated samples from WWTP [b]	*Klärwerk Steinhäule (*Ulm*)* 48°25'28''N 10°1'53''E	June 2012	Table **A5**

[a] Exact coordination of sampling spots not given (river source: 54°49'30''N 70°32'17''W, river mouth: 55°15'59''N 77°47'23''W [212]); [b] WWTP: wastewater treatment plant.

4.4.1. Determination of dissolved Hg in natural freshwater samples

Great Whale River samples

18 water samples were collected from the Great Whale River in Canada by *Lars-Eric Heimbürger* from the GET. One of the samples originates from a little branch of this river and is thus not assigned as a typical freshwater sample. Still, this sample was analyzed along with the other samples collected from this river and the specific nature is mentioned here for better data interpretation. The river water samples were measured with the optimized nanogold-based FIAS-AFS (see section 4.1) and the obtained results were compared with reference measurements at the GET. The laboratory applied the U.S. EPA method 1631 as a standard method for Hg analysis with a slight modification during reagent decontamination.[213] The DOC concentrations of the respective river samples were also determined by the GET laboratory (see **Table A1**). As evident from **Figure 36**, a good correlation between these two data sets is obtained (correlation coefficient, $R^2 = 0.9676$). The Hg concentration of 18 samples ranges between 1.3 to 6.3 ng L^{-1}, the corresponding DOC concentration of these samples ranges between 2.8 to 18.0 mg C L^{-1} (see **Figure 36**). The highest DOC value is obtained for the sample, which was collected at a small branch of the Great Whale River (18.0 mg C L^{-1}). This value is reasonable as the influence of the organic matter input is higher near the river bank. **Figure 36** points out that the error of a 3-fold measurement by the optimized nanogold-based FIAS-AFS tends to increase for water samples with a DOC concentration above 4.5 mg L^{-1} and a Hg concentration greater than 2.8 ng L^{-1}. A potent explanation for this relationship may include that the accumulation of Hg on the AuNPs-based collector is stronger affected with an increasing amount of dissolved organic matter, which thus reduces the precision of the method. Consequently, the standard deviation shows the highest value for the water sample with a DOC concentration of 18.0 mg C L^{-1}. Nevertheless, recovery of Hg could be quantitatively performed for all samples, which is also represented in the slope of the recovery function (1.05) leading to a recovery rate of $105 \pm 10\%$ for the investigated concentration range. This finding was

unexpected since our earlier studies on model substances revealed lower Hg recoveries in sample solutions with elevated DOC concentration when no sample pretreatment is performed. Further, it was demonstrated within this work that humic acids exhibit a higher tendency to bind dissolved Hg compared to fulvic acids (see section 4.2.3). However, the DOC concentration of the herein investigated river water is a sum parameter and does not provide any information on the fraction of HA and FA in the water sample. Furthermore, the amount of humic and non-humic substances in natural water systems strongly depends on the type of water (see section 2.4). In addition, it was shown that thiol functional groups within an organic model ligand may hinder Hg adsorption on the nanogold-based collector and reduce Hg recovery (see section 4.2.1). Consequently, due to the obtained results for the river water samples DOC within the matrix can be composed of either a high percentage of FA over HA or the major part of DOC consists of other organic compounds, *e.g.* amino acids, fatty acids, natural sugars
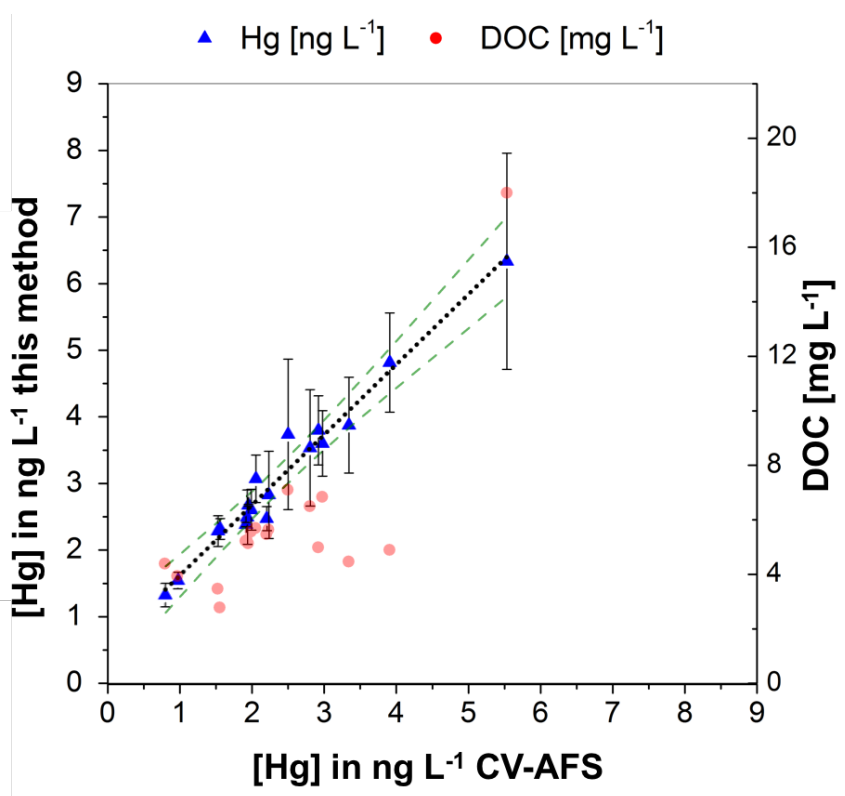
Figure 36*: Dissolved mercury concentration of 18 river water samples (Great Whale River, Canada) presented as recovery function with U.S. EPA method 1631 as reference method and corresponding DOC concentration ($y = 1.054 \cdot x + 0.574, R^2 = 0.9676$, $n_c = 54$; error bar represents standard deviation, $n_s = 3$; black dotted line: linear trend, green dashed line: confidence interval with P = 95%).*

with no specific binding tendency for dissolved Hg. Here, it seems obvious that consideration of DOC as the only parameter is not suitable to draw general conclusions.

River Isar and Danube samples

Water samples from the river Danube (Ulm) and the river Isar (Munich) were collected in October 2011. Three different sampling sites were chosen for each river, located ahead of, behind and within the city. The proposed reagent-assisted online UV digestion method as a pretreatment to dissolved Hg accumulation on the nanogold collector (see chapter 4.3.2) was applied to six river water samples. In order to evaluate the accuracy of the method toward real water analysis the samples were additionally measured according to U.S. EPA method 1631 as a reference method.[97] In addition, the DOC concentration of the river water samples was determined by the department for *Siedlungswasserwirtschaft* at the *Technical University of Munich*. The results for Hg and DOC measurement in six river water samples are summarized in **Table 19**. The obtained DOC concentrations are reasonable as DOC in most river waters is usually below 5 mg C L^{-1}. No significant differences in DOC concentration were found within the samples that were collected before, in and behind the cities Munich and Ulm. The DOC concentration varied between 2.6 to 3.9 mg C L^{-1}, with the highest value analyzed in the river Danube collected in Ulm (3.9 mg C L^{-1}).

The values found by the herein developed method are in very good agreement with the results obtained by total oxidation CV-AFS (U.S. EPA method 1631). Considering the expanded uncertainty for each sample (see **Table A6**), calculated according to *Linsinger*[203], the accuracy and the precision of the novel method were verified. Thus, the proposed reagent-assisted online UV pretreatment coupled to the optimized FIAS-AFS is feasible for ultratrace Hg determination in river water with DOC concentration between 2.6 to 3.9 mg L^{-1} and a maximum Hg concentration of 0.63 ng L^{-1}.

Table 19: *Mercury concentration of river water by FIAS-AFS integrated reagent-assisted UV digestion and U.S. EPA method 1631 and corresponding dissolved organic carbon concentration (reprinted with permission from Leopold et al.[42], copyright 2012 by Springer-Verlag).*

Sample origin	Hg concentration by reagent-assisted UV digestion [ng L^{-1}] [a]	Hg concentration by U.S. EPA method 1631 [ng L^{-1}]	DOC concentration [mg L^{-1}] [b]
River Isar in Dürnstein, before Munich	0.54 ± 0.19	0.51 ± 0.08	2.56 ± 0.26
River Isar in Munich	0.75 ± 0.19	0.63 ± 0.08	2.62 ± 0.26
River Isar in Garching, behind Munich	0.51 ± 0.16	0.58 ± 0.08	2.66 ± 0.27
River Danube in Wiblingen, before Ulm	0.61 ± 0.12	0.61 ± 0.08	2.85 ± 0.29
River Danube in Ulm	0.53 ± 0.08	0.59 ± 0.08	3.93 ± 0.39
River Danube in Böfingen, behind Ulm	0.40 ± 0.05	0.41 ± 0.08	3.02 ± 0.30

[a] Calibration for Hg measurement by reagent-assisted UV digestion method was performed by standard addition method; uncertainties for Hg measurement derive from the confidence interval of the calibration experiments with P = 95% and n_c ≥9, [b] DOC concentration determined by *S. West*, *Technical University of Munich*, using High TOC II (Elementar Analysensysteme GmbH, Hanau, Germany) with a limit of detection of 1 mg L^{-1}, uncertainty for DOC measurement expressed as 10% of the measured value.

4.4.2. Determination of dissolved Hg in seawater samples

Black Sea water samples

15 samples from the Black Sea were received in September 2013 from *Lars-Eric Heimbürger*. A vertical profile was sampled during the *2013 Dutch GEOTRACES MedBlack* cruise in July 2013 from a depth of 10 to 2040 m. For additional information (*e.g.* temperature, salinity) regarding the samples see appendix **Table A3**. In order to investigate the influence of the sampling bottle material with respect to Hg analysis in the ultratrace range, water was collected in polyethylene terephthalate (PET) bottles as well as in perfluoroalkoxy (PFA) Teflon bottles, the latter having similar properties as polytetrafluoroethylene (PTFE).[213] Many decades of experience in ultraclean working procedures demonstrate that problems can arise in sampling due to analyte loss during transport and storage or possible contamination by release of Hg from the container material.[214] Furthermore, it was shown that Hg uptake from the atmosphere can occur when porous materials like polyethylene (PE) are used for sampling.[215] Thus, guidelines often recommend using glass or PTFE bottles for efficient water sampling. On the other hand, PET bottles offer some additional advantages compared to glass or PTFE. These non-fragile, lightweight bottles are relatively inexpensive and can be discharged as recyclable plastic after use omitting time-consuming and labor-intensive cleaning steps for the reuse of sampling bottles. *Lars-Eric Heimbürger* applied CV-AFS according to U.S. EPA method 1631 to determine dissolved Hg concentration in the vertical profile of the Black Sea water samples. Two measurements were performed at each sample spot for PET sampling bottle and PFA sampling bottle. Water samples collected in PET bottles were sent to the *Ulm University*. These samples were subsequently analyzed by reagent-free preconcentration of dissolved Hg onto AuNP-coated silica (see section 4.1). The results obtained by CV-AFS using different sampling material, namely PET and PFA sampling bottles, show a similar trend for the vertical profile with slightly higher Hg concentrations for the samples that were collected in PET bottles (see **Figure 37**). The water samples that were analyzed within this work were received in PET bottles. The analysis by the nanogold-based FIAS-AFS shows a slightly different trend, but the results are still in very good agreement with the data obtained by

the reference method. A comparison of the data derived from the samples collected in PET bottles shows that the recovery ranges between 90 to 110% for 11 samples. With the exception of two samples at a depth of 145 and 175 m no significant differences between the reference measurements were observed. The results obtained were satisfactory, especially with respect to the very low dissolved Hg concentration below 1 ng L^{-1}. Hence, the herein developed optimized FIAS-AFS is a feasible method to analyze ultratraces of Hg in saline waters without any sample pretreatment or reagent-addition. This is in accordance with measurements of seawater samples presented in earlier studies.[22,24] The salinity of the investigated Black Sea water samples is lower compared to the Mediterranean Sea or seawater in the world's oceans. It ranges between 18 to 22 g L^{-1}, which is equivalent to a chloride concentration of 0.28 to 0.34 M, respectively. Assuming that the investigated seawater samples exhibit a low fraction of
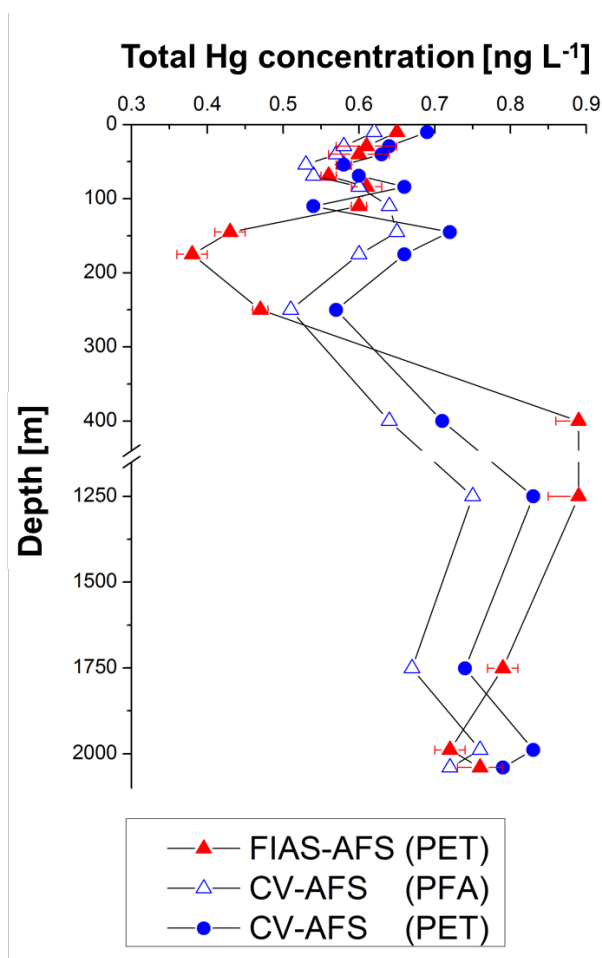
Figure 37: *Method comparison for Black Sea water depth profile (red triangle: optimized nanogold-based FIAS-AFS; blue symbols: reference method CV-AFS performed by Lars-Eric Heimbürger) (error bar represents standard deviation, n_s = 3).*

dissolved organic matter leads to the predominance of Hg-chloro complexes within this water matrix (see also **Figure 28**). Consequently, Hg from various Hg-Cl complexes is separated from the matrix through interference-free adsorption on catalytic active AuNPs used by the optimized FIAS-AFS.

In addition to the method comparison shown above an intercalibration exercise with 25 participating laboratories was organized by *Lars-Eric Heimbürger*, *Jeroen E. Sonke* and *Daniel Cossa* in 2013 within the *Dutch GEOTRACES MedBlack* cruise. Therefore, samples from the Black Sea were taken in the western gyre at 45 m depth. The samples were all stored under the same conditions until shipment in September 2013. **Figure 38** presents the data from all participating laboratories. The y-axis is depicted in logarithmic scale. As the arithmetic mean is more prone to outliers compared to the median and the geometric mean, it is a reasonable strategy to identify certain outliers within the presented set of data. The mean value of all results (including outliers) is 2.23 pM. The results of some laboratories were not taken into account for the data evaluation shown in **Figure 38**. Three values were identified as outliers (lab 6,7 and 11), two values were
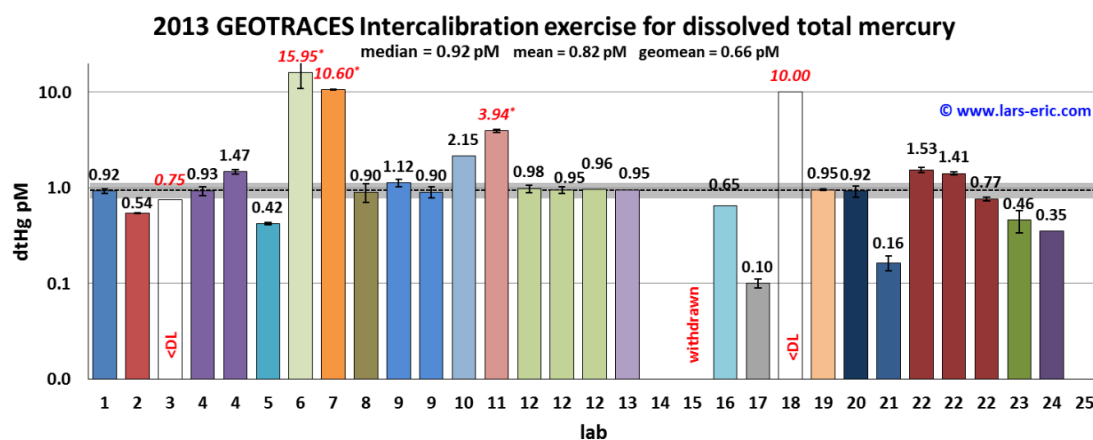
Figure 38: *Results for 2013 GEOTRACES intercalibration exercise for dissolved total mercury, dotted line: median, grey band: 20% of median, red asterisk: outliers (obtained from Lars-Eric Heimbürger, unpublished results).*

below the detection limit of the applied method (lab 3 and 18), one result has been withdrawn (lab 15) and two laboratories did not reply (lab 14 and 25). Hence, 17 values were considered for the calculation of the median (0.92 pM), the mean (0.82 pM) and the geomean (0.66 pM). Some laboratories (4, 9, 12 and 22, see x-axis in **Figure 38**) repeated the measurement after a distinctive time period. However, these results are only

gathered for informational purposes and were not considered for the evaluation. The results indicate a considerable disagreement between the participating laboratories for dissolved total Hg determination. Within this work (see lab 23 in **Figure 38**) the intercalibration sample was analyzed with the optimized FIAS-AFS by direct accumulation of dissolved Hg onto the nanogold collector without pretreatment. The precision of the herein presented method is slightly smaller compared to the submitted results by other laboratories. Obviously, the found Hg concentration of 0.46 ± 0.12 pM $(0.092 \pm 0.024$ ng Hg L$^{-1})$ is below the mean value of 0.82 pM. However, due to the very low Hg concentration of this intercomparison sample, the result obtained within this study is still acceptable for ultratrace analysis. The lower value may be explained by the applied methods within this intercalibration exercise. The majority of the laboratories uses certain chemical digestion procedures to decompose matrix constituents and to transform Hg species. These methods exhibit an increased risk of contamination, which might lead to a higher mean concentration determined in this intercomparison study.

4.4.3. Determination of dissolved Hg in wastewater and treated water samples

Wastewater treatment plant samples

Three water samples were collected at a wastewater treatment plant (WWTP, *Klärwerk Steinhäule*) near Ulm. Dissolved Hg concentration of these samples was determined by the optimized FIAS-AFS (see chapter 4.1) without online pretreatment. In addition, information on DOC concentration was provided by the laboratory of the WWTP. The filtered and acidified water samples were sent to *Heidi Pietilä*, a collaboration partner at the *University of Oulu* (Finland) for an interlaboratory comparison. The analysis at the laboratory was performed by oxidation of the organic matter prior to cold vapor inductively coupled plasma mass spectrometry (CV-ICP-MS). Hg concentration obtained from both analytical methods and the corresponding DOC values are summarized in **Table 20**.

Table 20: *Dissolved mercury concentration of wastewater treatment plant (Klärwerk Steinhäule) samples and corresponding dissolved organic carbon concentration.*

Origin	Hg concentration by optimized FIAS-AFS [ng L^{-1}] [a]	Hg concentration by CV-ICP-MS [ng L^{-1}] [c]	DOC concentration [mg L^{-1}] [e]
Input (WWTP)	2.30 ± 0.03 [b]	2.40 [d]	36.5
After physical treatment (WWTP)	2.57 ± 0.18 [b]	2.80 [d]	dng
Output (WWTP), after biological treatment	1.73 ± 0.04 [b]	2.30 [d]	5.2

[a] Measurement performed within this study, [b] Standard deviation, $n_s = 3$, [c] Measurement performed by *Heidi Pietilä, University of Oulu, Finland*, [d] no data available for uncertainty, [e] Data obtained from the laboratory *Klärwerk Steinhäule*, July 2012, no data available for uncertainty; dng: data not given.

The found Hg concentrations by the optimized FIAS-AFS are in very good agreement with the values obtained by CV-ICP-MS. As there is no data available on the uncertainty of the reference measurement significance of the differences cannot be calculated.[203] The highest Hg concentration was determined for the water sample, which was collected behind the physical treatment (*e.g.* sedimentation, filtration). Within this first cleaning step the wastewater is separated from *e.g.* sand, gravel, stones and other contaminants with a higher density compared to water. Light floating solids and lipid substances are also separated from the water surface within this cleaning step. A possible explanation for the slightly higher Hg concentration after physical treatment compared to the input sample is that the water is contaminated with Hg by the sand trap, filter or other materials used during the mechanical cleaning process. Both methods determined similar Hg concentrations for the input samples, with 2.30 and 2.40 ng L^{-1} by the FIAS-AFS and CV-ICP-MS, respectively. The lowest Hg level was found in the output sample, which is obtained after the biological treatment. Bacteria are the key players during this cleaning step, thus contaminant concentration most probably decreases through metabolic processes in the presence of oxygen. It is conceivable that this process also decreases

dissolved Hg concentration of the output. However, the differences between Hg concentrations found for the input sample and the samples collected after physical and biological treatment are small and consequently influences by other factors cannot be excluded.

The input sample exhibits a noticeable DOC concentration of 36.5 mg C L^{-1}. As the values obtained by FIAS-AFS are consistent with those obtained by total oxidation followed by CV-ICP-MS the influence of organic matter towards preconcentration onto the nanogold collector shows no significance. This may be explained by the composition of the sample matrix. DOC is used as a sum parameter in environmental analysis because the identification of millions of organic compounds is not feasible with any analytical technique within a reasonable time. Compared to natural water samples like lake water and river water, where DOC consists of a highly complex mixture of degradation products of animal and plant tissue, DOC within effluents comprises other organic compounds. These are pollutants, which result mostly from anthropogenic sources. As an example, detergents, pharmaceutical and personal care products are released into the municipal wastewater after use and excretion and thus finally reach the WWTP. It was shown within this study that some organic model ligands did not hinder dissolved Hg from accumulation onto the nanogold-based preconcentration column (see section 4.2.1). While this is in good agreement with the obtained results for the treated and untreated water samples. Consequently, a general statement on the influence of DOC concentration on accumulation on nanogold-coated silica within the FIAS-AFS cannot be given.

4.4.4. Conclusion

The developed reagent-free FIAS-AFS equipped with an integrated nanogold collector for dissolved Hg preconcentration exhibits good applicability to freshwater, saline water and untreated and treated effluent water samples. The results obtained within the previous section were compared to different reference methods and feature reasonable values for Hg recovery. Even the analysis of freshwater samples with high DOC

concentrations (Great Whale River) leads to good recovery compared to the U.S. EPA method 1631 as reference method ($105 \pm 10\%$). However, the precision of the proposed reagent-free FIAS-AFS is not consistent for a series of samples. Hence, future studies must be performed to investigate the suitability of pretreatment integrated to the FIAS-AFS in precision enhancement for analyzing these types of water samples. River water sampled from Isar and Danube with lower DOC concentration (≤ 3.9 mg L^{-1}) were successfully analyzed with the reagent-assisted UV pretreatment integrated to the FIAS-AFS. The measurements show a good precision for Hg concentrations below 1 ng L^{-1}. Hg measurements of wastewater and treated water from a municipal WWTP using the FIAS-AFS without further pretreatment were in good agreement with the results derived from a reference method. Additional analysis of these water samples revealed DOC concentrations up to 36.5 mg L^{-1}. In contrast to the analysis of river water containing a high amount of DOC, the precision of these measurements was not affected by the DOC level. The composition of the matrix of effluent water significantly differs from natural water regarding the dissolved organic substances. These compounds, mostly originating from anthropogenic sources seems to have less affinity for Hg binding. Moreover, the presented reagent-free FIAS-AFS was successfully applied to a depth profile of seawater samples and the results were compared to U.S. EPA method 1631 as a reference method. Regarding saline water samples the proposed method delivers outstanding performance for Hg concentrations below 1 ng L^{-1}. This is explained by the high concentration of Cl$^-$ (0.28 to 0.34 M) in Black Sea water samples forming $HgCl_2$, $HgCl_3^-$ or $HgCl_4^-$. In addition, the participation of an intercomparison study was part of this work. The submitted dissolved Hg concentration (0.46 ± 0.12 pM) for a seawater sample was below the calculated mean value resulting from all interlaboratory measurements (0.82 pM). However, this might be explained by the application of reagent-assisted methods used by the other participating laboratories, which increases the risk of contamination. Despite the difference from the mean value the resulting concentration determined within this thesis is still acceptable for ultratrace analysis.

A general prediction with respect to the need of an integrated pretreatment step to separate Hg-DOM complexes is difficult to realize because of the inhomogeneity of the natural water matrix. Therefore, future work should concentrate on different kinds of

real water and systematically compare the proposed pretreatment procedures presented in this thesis as well as nanogold-based FIAS-AFS without pretreatment. For a better interpretation, further parameters, *e.g.* chloride concentration, sulfide concentration, pH value and other naturally occurring dissolved metal ions, should be considered.

5. Nanogold-decorated dipstick for in situ preconcentration of dissolved mercury from natural water

The previous chapter presented the development of a prototype system for reagent-free dissolved ultratrace Hg determination. The suitability of silica-supported AuNPs for the preconcentration of naturally occurring Hg species (Hg^{2+}, Hg^0, $MeHg^+$) has been reported in earlier studies and the principle was adapted within this work.[22,23] The collector for solid-phase extraction of Hg consists of a packed column integrated to the automated FIAS-AFS. However, the applicability of the prototype for on-site analysis has not yet been successfully tested to avoid contamination from atmospheric Hg deposition or similar contamination at suitable sampling sites. In addition, on-site application would require mobile electricity and gas supply in form of a battery and a gas cylinder leading to challenges for in-field application of the prototype. Therefore, the aim of this part of the work was to develop a portable sampler for reagent-free, highly efficient solid-phase extraction of dissolved Hg from waters. Different nanogold-based adsorbents were designed and their capacity to dissolved Hg accumulation was tested by dipping the adsorbent into the sample solution. This sampling procedure offers several advantages over liquid sampling with reduced contamination of the sample by the sampling bottle and stabilizing agents, as the analyte is adsorbed strongly on a solid phase and thus contact to the surface of the sampling bottle is avoided. Furthermore, analyte loss induced by adsorption to the container wall and evaporation during transportation and storage can be minimized due to the strong interaction of the analyte to the adsorbent. As a result, special cleaning and working procedures necessary for liquid sampling are omitted using a portable sampler. Another benefit is the reduced overall sample weight and sample volume using direct accumulation of the analyte on a solid phase. Moreover, in contrast to the packed column collector presented in section 4.1.1 a single piece of solid adsorbent can be dipped into the sample solution without the need for further equipment.

The experiments presented in the following chapter were performed under laboratory conditions. Still, complete and/or partial on-site analysis is conceivable with the novel adsorbent and different sampling strategies following:

1) Bottle or grab sampling of a small volume and subsequent on-site accumulation of the analyte by immersing the adsorbent into the water sample. Analysis of accumulated Hg is performed at the laboratory.

2) *In situ* accumulation of the analyte by dipping of the adsorbent into the water body for a distinct time. Analysis of accumulated Hg is performed at the laboratory.

3) Accumulation on-site (*via* 1 or 2) followed by on-site Hg determination by miniaturized instrumentation.

5.1. Dissolved mercury preconcentration onto gold nanoparticle-coated quartz glass tube

As a first approach, a quartz glass tube was used for AuNP immobilization. The adsorbent was prepared according to a slight modification of a procedure recently developed by *Maria Schlathauer*.[216] In this study, AuNPs were prepared *in situ* by reduction of chloroauric acid and subsequent deposition onto a soda-lime glass slide. The surface of the resulting AuNP-coated glass slide was thoroughly characterized by atomic force microscopy (AFM) and scanning electron microscopy (SEM). The deposited AuNPs range from 50 to 200 nm in diameter and exhibit an average height of 76 nm. In addition, the chemical stability of immobilized AuNPs against water and hydrochloric acid (0.06 M HCl) has been demonstrated by rinsing tests and total reflection X-ray fluorescence analysis.[216] The difference to the cited study is the application of a quartz glass tube instead of a soda-lime glass slide as a substrate due to the higher thermal stability. In the following, the AuNP-coated quartz glass tubes are designated as "AuNP@qt".

5.1.1. Blank contribution in Hg quantification

The set-up of the FIAS presented earlier in chapter 4.1 was modified to detect accumulated Hg on the AuNP@qt. The principle of thermal release of Hg^0 and subsequent detection by AFS is similar as described for the packed nanogold collector. Instead of the packed collector, an empty quartz glass tube surrounded by a heating wire was connected to the FIAS-AFS *via* tubing. The AuNP@qt was then placed inside the heating cell. **Figure 39** shows a schematic set-up of the FIAS-AFS with modified heating cell. An important part of analytical method development is the control of the blank contribution resulting from *e.g.* the applied reagents, material and instrumental components. Obviously, a low and constant blank level is crucial for accurate Hg determination at ultratrace levels. Hence, as a first experiment the Hg background of the
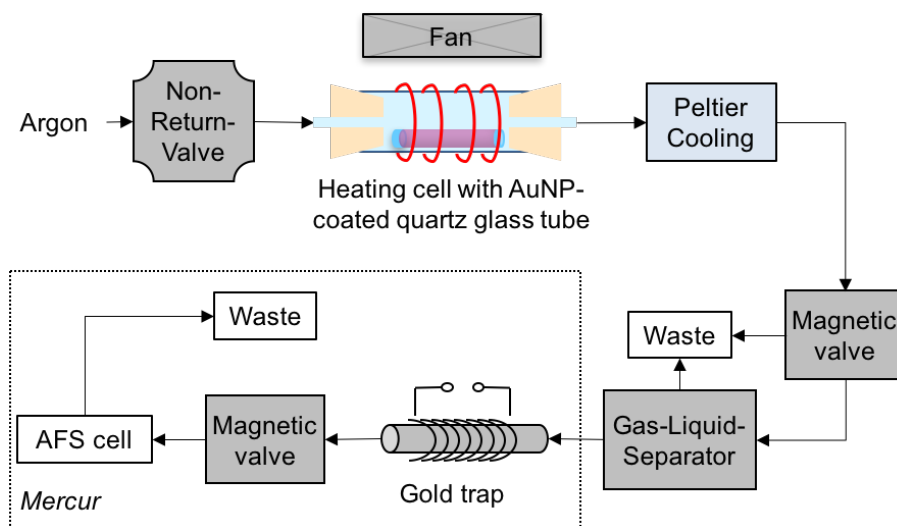
Figure 39*: Flow injection analysis system for thermal desorption of Hg(0) from nanogold-coated quartz glass tube and detection by atomic fluorescence spectrometry (modified and reprinted with permission from Huber et al.[102], copyright 2015 by American Chemical Society).*

prepared AuNP@qt was checked using the FIAS-AFS. Four freshly prepared AuNP@qt were successively inserted into the heating cell and the resulting fluorescence signal was measured during heating the quartz glass tube (see **Figure 39**). In addition, Hg contamination of AuNP@qt was investigated after storing the AuNP@qt in an empty, closed glass container overnight. The fluorescence intensity derived from freshly prepared adsorbents ranges between 0.0026 to 0.0055, which indicates an absolute Hg

amount of approx. 5 pg. The absolute amount of Hg was calculated from a calibration function using the reagent-free FIAS-AFS with a nanogold-based collector and a defined sample volume (see section 6.8). This blank contribution most probably results from reagent contamination and/or from atmospheric Hg deposition during transportation and short-time storage. The difference in Hg load between the four AuNP@qt may be explained by a slight variation in the substrate area and the amount of the *in situ* deposited AuNPs. Significant lower fluorescence intensities (0.0004 to 0.0021) were obtained after storage of the same AuNP@qt overnight. This implies that the storing conditions are suitable as only a small amount of Hg is adsorbed onto the AuNP-coated tubes overnight. Furthermore, a complete desorption of Hg from the AuNP@qt during thermal treatment is required for correct data evaluation. This has been confirmed by
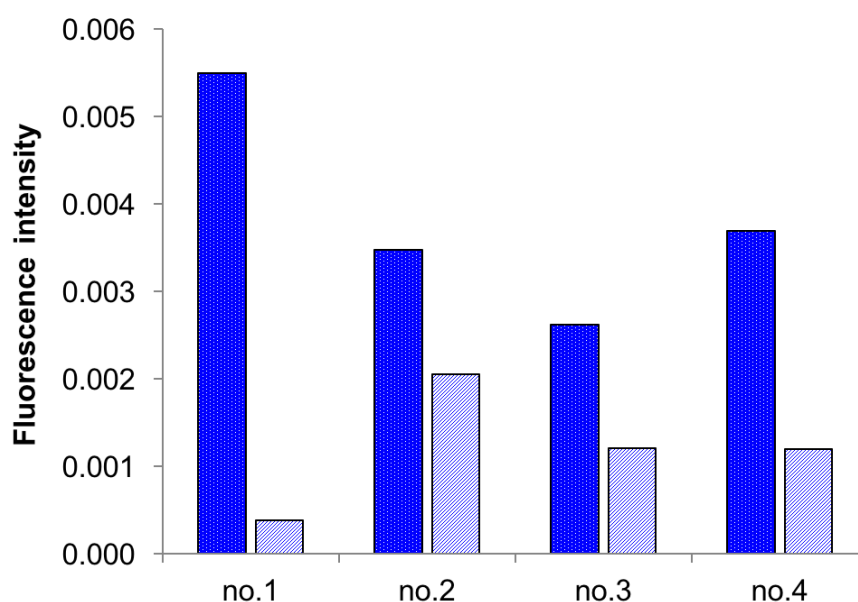
Figure 40: *Fluorescence intensity derived from thermal desorption of Hg(0) from freshly prepared gold nanoparticle-coated glass tubes (■) and after storage in closed vessels overnight (▨) (single measurements).*

successive heating of the AuNP@qt for a second and third time (data not shown in **Figure 40**). The fluorescence signal drops to 0.0001 to 0.0002, which is equal to the fluorescence intensity derived from heating the empty holding device while rinsing it with argon. Consequently, to ensure minimized Hg blank contribution during measurement, each AuNP@qt was heated and rinsed with argon within the FIAS-AFS before it was subjected to Hg accumulation from a sample solution.

5.1.2. Preconcentration of mercury at different concentrations

One individual AuNP@qt sampler was deployed in 20 mL each of 10, 50 and 100 ng L^{-1} Hg(II) standard solutions and a blank solution (0.06 M HCl) for 10 min. Afterwards, the AuNP-decorated quartz glass tube was heated three times in a row inside the FIAS-AFS. **Figure 41** depicts the fluorescence intensities resulting after the first, second and third thermal desorption step. It is clear that preconcentrated Hg quantitatively desorbs from the AuNP@qt within the first heating cycle after exposure to 10, 50 and 100 ng L^{-1} Hg(II) aqueous standard solutions. The fluorescence intensity drops to blank level after the second and remains constant after the third heating cycle for the investigated sample solution. The amount of preconcentrated Hg was calculated and plotted against Hg concentration in solution. It is shown in **Figure 42** that dissolved Hg(II) adsorbs linearly onto the AuNP@qt over the investigated concentration range ($m(Hg) = 1.22 \cdot c(Hg) + 13.44, R^2 = 0.9996$). Thus, the principle of passive sampling is followed. The found Hg mass after thermal treatment of the novel sampler within the FIAS-AFS varied between 25 to 134 pg which is equivalent to 7 to 12% of the absolute amount of Hg in solution.
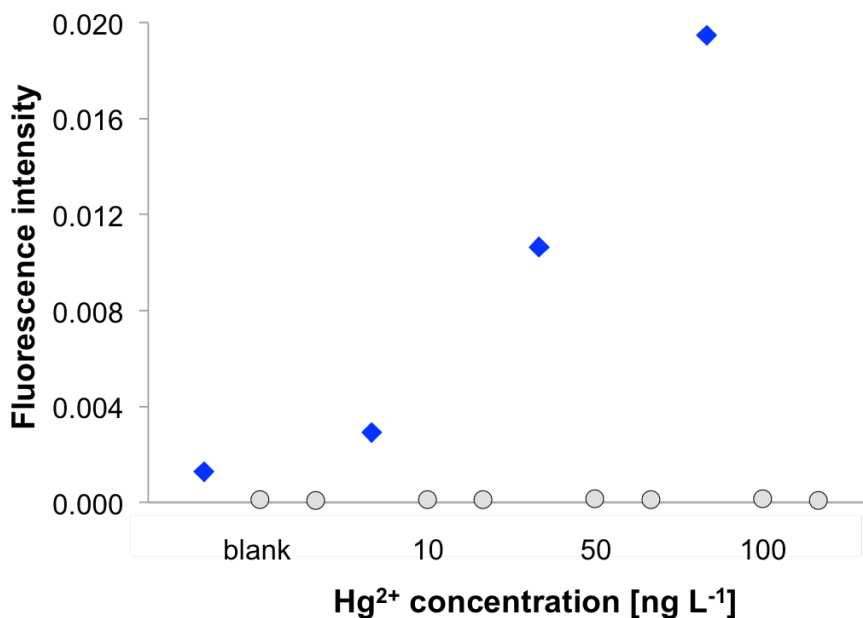
Figure 41*: Fluorescence intensity derived from thermal desorption of Hg(0) from gold nanoparticle-coated glass tube after preconcentration of blank solution (0.06 M HCl) and Hg(II) standard solutions ([Hg] = 10, 50, 100 ng L^{-1}): Fluorescence intensity after the first (◆) and after the second and third (◯) thermal desorption cycle (single measurements).*
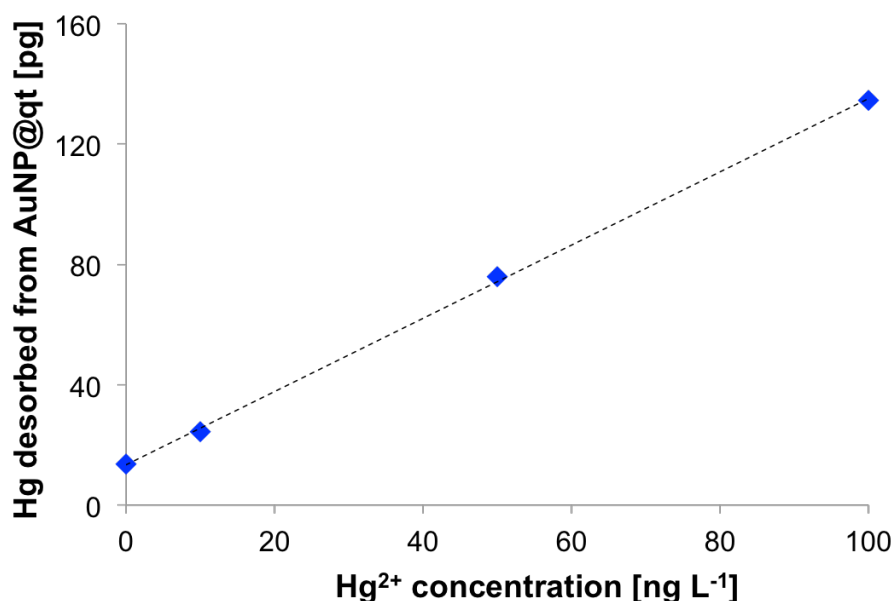
_Figure 42__: Accumulated amount of Hg on gold nanoparticle-coated glass tube from aqueous Hg(II) standard solution ([Hg]=1, 50, 100 ng L^{-1}) and from blank solution (0.06 M HCl) after 10 min (single measurements, dashed line: linear trend, $m(Hg) = 1.22 \cdot c(Hg) + 13.44, R^2 = 0.9996$)._

5.1.3. Time dependent mercury accumulation onto AuNP@qt

The influence of exposure time on Hg accumulation onto AuNP@qt was investigated and results are discussed in the following section. Therefore, a single AuNP@qt was successively exposed in 20 mL of 10 ng L^{-1} Hg(II) standard solution for 1 to 190 min. For each investigated accumulation time a freshly prepared sample solution was used. The lower concentration of 10 ng Hg(II) L^{-1} was chosen, as it better reflects naturally occurring Hg concentrations in water. The preconcentrated amount of Hg onto AuNP@qt was determined in the same manner as described earlier 5.1.1. In addition, Hg concentration of the sample solution was analyzed by the optimized FIAS-AFS (see chapter 4) after the dipstick was removed from the solution. Thus, a mass balance was obtained for the investigated time period. It is evident from **Figure 43** that the amount of Hg that binds to immobilized AuNPs increases with longer exposition time. Consistent with this finding, the Hg concentration of the corresponding solution decreases within a time interval of 190 min. The accumulated mass of Hg on the sampler increased linearly

during the first 60 min of exposure until the slope decreases at higher accumulation times. As expected, the same trend is observed for the absolute Hg amount in solution. The accumulated amount of Hg on the AuNP@qt converges to a boundary value at higher accumulation times. Here, a maximum amount of 110 pg Hg was detected after 190 min. **Figure 44** shows clearly that quantitative Hg recovery from standard solutions is not obtained for all investigated time periods regarding the sum of Hg amount found by the optimized FIAS-AFS and by preconcentration onto AuNP@qt. With respect to the exposure solution, recovery varied between 75-98%, which is still an adequate result for Hg analysis at ultratrace levels. Hg adsorption onto AuNP@qt might be influenced
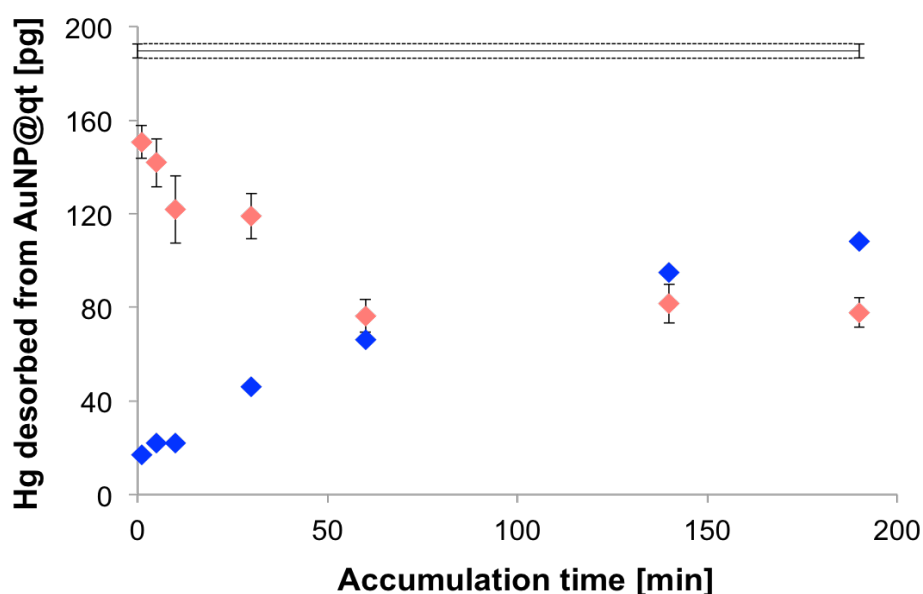
Figure 43: *Accumulated amount of Hg on gold nanoparticle-coated quartz glass tube (◆) from aqueous Hg(II) standard solution ([Hg] = 10 ng L^{-1}) and absolute Hg in solution (◆) after distinct time intervals (error bars represent the standard deviation, n_s = 3, solid line: average Hg amount in sample solution, dashed line: standard deviation, n_s = 6).*

by different parameters. First, temperature plays a key role if particles (*i.e.* ions, molecules, complexes) diffuse through a liquid phase. As the herein presented experiments were not conducted in an air-conditioned laboratory small temperature changes cannot be excluded. Furthermore, the performance of the AuNP@qt might be affected during repeated use as the AuNPs are immobilized at the outer surface of the glass tube. Consequently the risk of mechanical abrasion increases while reusing the adsorbent. In addition, repeated thermal treatment might change the morphology of the AuNPs, which probably affects the Hg adsorption process.

118
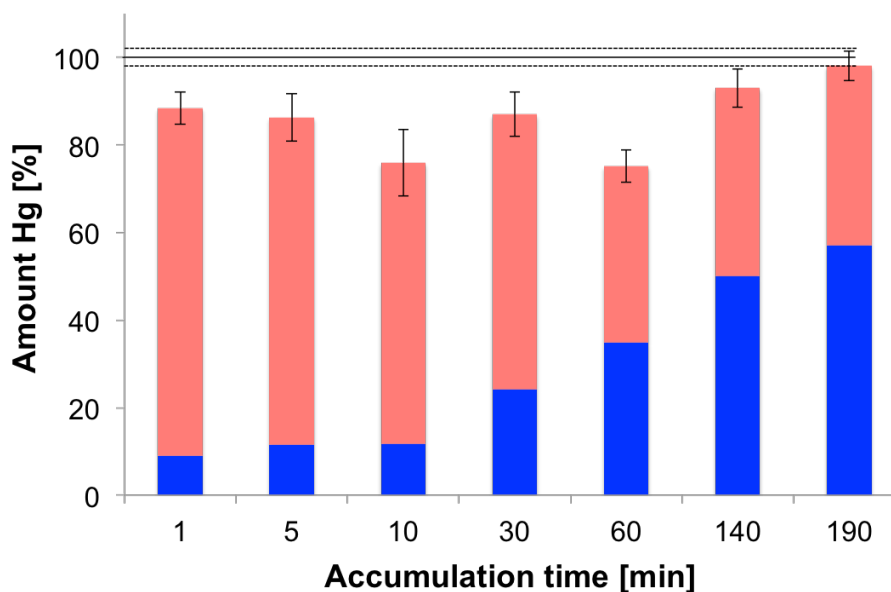
Figure 44*: Accumulated amount of Hg onto gold nanoparticle-coated quartz glass tube from 10 ng L^{-1} Hg(II) solution (■) and Hg concentration determined by flow injection analysis system coupled to atomic fluorescence spectrometry using nanogold-coated silica particles (■) given as percent of the initial Hg concentration after different exposure periods (error bars represent the standard deviation, $n_s = 3$, solid line: average Hg amount in sample solution, dashed line: standard deviation, $n_s = 6$).*

5.1.4. Reproducibility

In order to obtain information on the reproducibility of the developed AuNP@qt and their capacity on dissolved Hg adsorption, five freshly prepared AuNP@qt were deployed in 150 mL each of 0.1, 1, 3, 5, 10, 30, 50, and 70 ng L^{-1} Hg(II) standard solutions for 10 min. These experiments were performed under turbulent conditions. It is expected that the accumulation process increases while stirring the solution, which results in a higher amount of accumulated Hg on the sampler within the same time period. In addition, a non-coated quartz glass tube (blank) was simultaneously exposed to the Hg(II) standard solutions. Experimental variations are expected to be minimized as all AuNP@qt were simultaneously exposed to aqueous Hg(II) solutions. After exposure for 10 min, the AuNP@qt were successively heated within the FIAS-AFS for release and detection of Hg(0). Due to the fact that only one tube can be treated at a time, the other tubes were stored in a closed box with activated charcoal for

119

decontamination of the atmosphere. Blank contribution for a maximum storage time of one hour was investigated earlier to ensure that accumulated Hg originates from the solution rather than from the ambient air. Therefore, an AuNP@qt was heated within the FIAS-AFS until a stable fluorescence signal was obtained. After one-hour storage, the AuNP@qt was repeatedly heated and no change in fluorescence intensity was observed. Thus, contamination during storage can be excluded. The average amount of Hg adsorbed onto five equally prepared AuNP@qt under the given conditions as well as single values for the dipsticks are shown in **Figure 45**. In addition, the accumulated amount of Hg on a non-coated quartz glass tube was determined. Similar to the previous section, a linear correlation ($m(Hg) = 2.10 \cdot c(Hg) + 1.34, R^2 = 0.9972$) between Hg adsorbed onto AuNP@qt and Hg concentration of the exposure solution is obtained. In comparison to Hg accumulation presented in **Figure 42** the adsorption of Hg under turbulent condition is almost 2-times higher as the adsorption process is not limited by diffusion in this experiment. In order to demonstrate the specific affinity of AuNPs to dissolved Hg a blank quartz glass tube was exposed simultaneously to Hg(II) standard solutions of different concentration ($m(Hg) = 0.22 \cdot c(Hg) + 1.32, R^2 = 0.9510$). As expected, only a small fraction of Hg adsorbs onto a blank tube over the investigated concentration range, probably due to unspecific binding sites at the quartz glass wall. The residual standard deviation (RSD) of Hg accumulation on five individual samplers ranges between 28 to 57% for Hg concentration from 0.1 to 5.0 ng L^{-1}. For higher Hg concentration from 10 to 70 ng L^{-1} the RSD slightly decreases ranging from 11 to 21%.
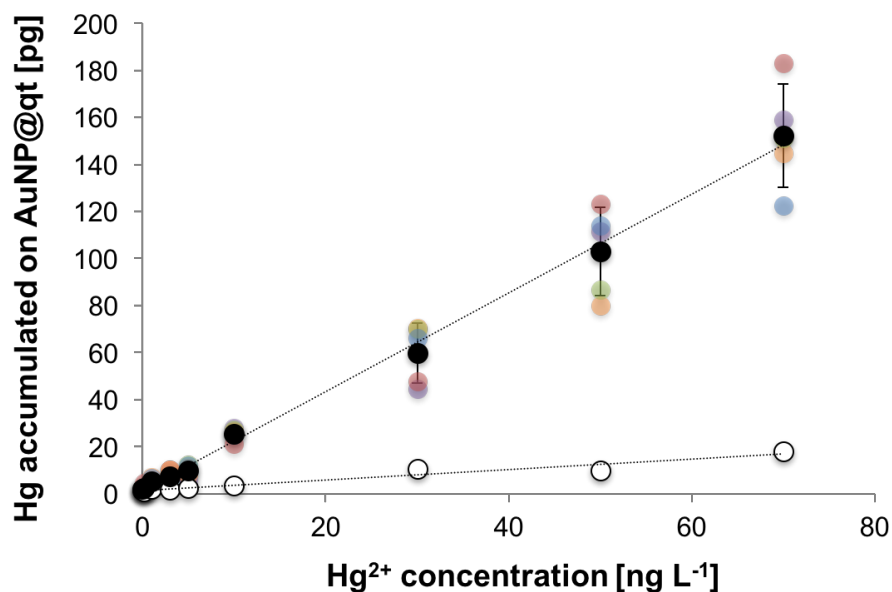
Figure 45*: Accumulated amount of Hg on five gold nanoparticle-coated quartz glass
tubes (colored circles) and on a blank tube (○) from aqueous Hg(II) standard solutions
([Hg]=0.1-70 ng L⁻¹) and from blank solution (0.6 M HCl) after 10 min (mean of
dipstick No. 1-5 (●), error bars represent the standard deviation for five adsorbents,
dashed line: linear trend for AuNP-coated adsorbent, $m(Hg) = 2.10 \cdot c(Hg) + 1.34, R^2 =
0.9972$, linear trend for blank quartz glass tube, $m(Hg) = 0.22 \cdot c(Hg) + 1.32, R^2 = 0.9510$).*

5.1.5. Application to real water samples

The AuNP-coated quartz glass tubes were dipped into a real water sample to investigate
their applicability to ultratrace Hg analysis of real waters. For this purpose, a freshwater
sample, Great Whale River in Canada, was used (detailed information on the water
sample see section 4.4). In order to exclude possible matrix interferences the water
sample was analyzed using standard addition as calibration method. Therefore, the river
water sample was spiked with Hg(II) standard solution in a concentration range between
10 to 100 ng L⁻¹. The found value ([Hg] = 4.87 ±0.12 ng L⁻¹) obtained by application of
the novel sampler agreed well with the reference value ([Hg] = 3.91 ±0.39 ng L⁻¹),
which was obtained by U.S. EPA method 1631 (see **Figure 46**). The reference
measurement was performed at the *Geosciences Environment Toulouse* (GET). A
comparison of the absolute difference (Δm = 0.96) and the extended uncertainty
(U$_\Delta$ = 0.82, coverage factor k = 2) reveals that there is no significant difference between

the measurement result and the reference value.[203] In addition, reproducibility of the external calibration was investigated with the same AuNP-coated quartz glass tubes after storage for 17 days in a closed vessel at room temperature. The performance of the adsorbents towards Hg accumulation dropped significantly after this storage period. The calibration curve did not show a linear trend. A similar effect was observed in a previous
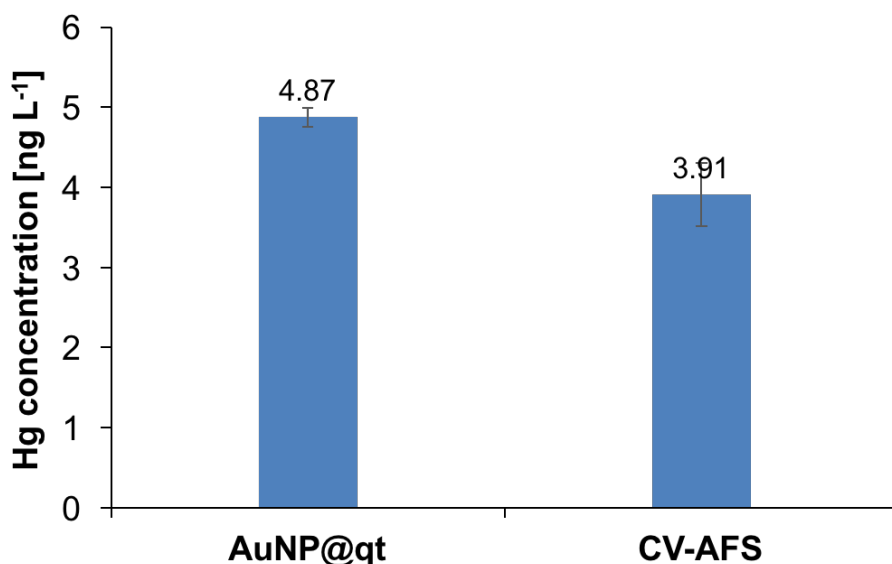
Figure 46: Dissolved mercury concentration in Great Whale River sample determined by preconcentration on the novel nanogold-based sampler and by cold vapor atomic fluorescence spectrometry as a reference method (AuNP@qt: error bar is derived from the coefficient of variation of the procedure; CV-AFS: error bar is 10% of measurement result).

study performed by *Zierhut et al.*[23]. This work gave evidence on the decreasing catalytic activity of a nanostructured gold surface over 14 days in terms of the adsorption rate of methylmercury. It was assumed that nanostructured bulk materials are thermodynamically unstable, meaning that the atoms of a nanostructure re-order and form a smooth layer, which only adsorbs Hg(0) species. Here, a reduced capacity of quartz glass-supported AuNPs for Hg(II) adsorption was observed after the storage time exceeded two weeks. This effect might be explained by agglomeration of AuNPs followed by rearrangement on the quartz glass surface resulting in a smooth gold layer. This thin gold film exhibits less adsorption capacity compared to separated AuNPs on a freshly prepared substrate. A study by *Xu et al.*[217] demonstrated that the optical properties of *in situ* deposited AuNP coatings on a glass surface can be controlled by the pH of the deposition solution. Coatings that are composed of isolated AuNPs exhibit

surface plasmon resonance at about 520 nm which results in a pink color of the glass substrate. Clusters of nanoparticles and the formation of a thin film lead to a red-shift of the absorption, thus changing the color of the substrate from pink through violet to blue. A slight color change of the herein developed AuNP@qt was observed throughout the experiments. This might also indicate morphological changes.

5.1.6. Conclusion

A novel gold nanoparticle-decorated adsorbent for Hg extraction from aqueous solution was presented in the preceding chapter. It was demonstrated that *in situ* formed AuNPs adhere to the outer surface of a quartz glass tube, which was chosen as a substrate due to its thermal resistance. Blank contamination was checked and showed satisfactory results for Hg ultratrace analysis, meaning that no elevated Hg deposition from the atmosphere within a distinct time period occurred. The absolute amount of Hg deposited on the adsorbent increased linearly over an investigated concentration range between 0.1 to 100 ng Hg L^{-1}. Another experiment clearly demonstrated that Hg sorption to AuNPs increased over time, a maximum amount of 110 pg Hg after an exposure time of 190 min was found. It was furthermore tested if the nanogold coating of the quartz glass substrate is reproducible with respect to Hg adsorption capacity between similar dipsticks. Hence, the adsorbing capacity of different AuNP@qt was compared and the results show a good reproducibility of five individual AuNP-coated adsorbents. The novel sampler was exposed to sample solutions under static and turbulent conditions. It was demonstrated that Hg adsorption onto the AuNP@qt proceeds faster for stirred sample solutions as the process is not limited by analyte diffusion in this case. The applicability of the novel sampler to natural water samples was tested using a freshwater sample. Dissolved Hg concentration of this river water sample was successfully determined by using the standard addition method for calibration. However, a significant decrease in adsorption capacity was observed after storage of the AuNP@qt for 17 days. This is most probably due to gold nanoparticle aggregation and the formation of a continuous thin film. Such particle migration may occur over time while storage of the AuNP@qt or through repeated use. Besides, mechanical abrasion of the immobilized

AuNPs may affect the performance of the dipstick. Consequently, the substrate for AuNP immobilization has to be optimized with respect to long-term stability.

5.2. Nanogold-based silica monoliths as solid-phase adsorbent for mercury analysis

The previous section clearly demonstrated that quartz glass-supported gold nanoparticles exhibit a specific affinity to dissolved Hg(II) similar to the loosely packed column presented in chapter 4. *In situ* formed AuNPs were successfully immobilized onto the non-porous surface of a quartz glass tube. However, previous results revealed that the performance for Hg accumulation is not stable. In order to overcome the mechanical stability problems of the presented AuNP@qt common support materials were taken into account as substrate for AuNP immobilization. Here, monolithic structures were chosen due to their versatile and unique properties. Monoliths are applied as support material for catalysts in *e.g.* natural gas storage, diesel particle filters, ozone abatement and automotive emission control mainly due to their high mechanical stability and the low pressure drop.[218] They commonly consist of ceramic (*e.g.* cordierite, $2MgO\ 2Al_2O_3$ $5SiO_2$) and metal materials. Metal catalysts supported on monoliths are a single entity rather than conventional fixed bed or pellet type catalysts. Monolithic silica has been in particular applied as stationary phase in high-performance liquid chromatography (HPLC) and capillary electrochromatography as an alternative to particle-based columns.[219,220] These single piece monolithic silica columns offer some advantages over conventional columns like high flow rates with low back-pressure and high specific surface area. The pore size, *e.g.* macro- and mesopores, as well as the diameter of the silica framework can be independently controlled by the reactants, synthesis conditions and postsynthesis treatment.[221] In principle, silica monoliths are prepared *via* a sol-gel process from a silica precursor (tetraalkoxysilanes) mixed with a water-soluble polymer. The sol-gel process was first reported in the early 1990s by *Nakanishi* and *Soga*[222]. The precursor is hydrolyzed by water to form silicic acid derivatives. This reaction may be catalyzed by acid or base addition, followed by a polycondensation reaction. The

124

addition of a water-soluble polymer controls the pore size and mechanical properties of the final silica network. Ageing, drying and calcination are the final steps to obtain a porous silica monolith.

In this work, two types of one piece silica monoliths were tested as substrates for *in situ* AuNPs deposition. The thermal stability and the chemical inertness of silica should diminish interferences during Hg preconcentration and thermal desorption in the analytical procedure. Furthermore, the porous structure of the silica monolith should increase the stability of immobilized AuNPs and minimize aggregation induced by thermal treatment or by long-term storage. As a first attempt, non-functionalized silica monoliths were prepared *via* a one-pot acid-base reaction as part of this work. The mechanical stability of the silica monoliths was further optimized in cooperation with the *Institute of Inorganic Chemistry II* (IC II, *Ulm University*). These solid materials were applied as a host for gold nanoparticles and the suitability of the novel adsorbents to dissolved Hg accumulation was investigated. Thereby, the influence of various parameters, *i.e.* Hg concentration of the exposure solution, the contact time, the total volume of solution, and the amount of gold loading on the silica monoliths was examined.

5.2.1. Optimization of the monolithic silica adsorbent for dissolved Hg preconcentration

Silica monoliths from acid-base reaction as substrate for gold nanoparticle immobilization

In a first attempt, silica monoliths were prepared according to a slight modification of the method described by *Zhu et al.* [223]. A block copolymer was dissolved in acid solution and mixed with tetramethyl orthosilicate (TMOS) as a silicate precursor. After ageing of the gel for several days, the final monoliths were obtained upon calcination. AuNPs were subsequently deposited onto the surface of the prepared monoliths by *in situ* reduction of chloroauric acid in a similar manner as was described earlier for silica

particles (see section 4.1.1). The prepared AuNP-coated silica monoliths (AuNP@SiO$_2$) exhibit a dark pink to purple color (see **Figure 47**, bottom) in the wet state and change to light pink after drying. This indicates the presence of isolated AuNPs with a diameter of 20 to 200 nm, which exhibit surface plasmon resonance absorption in the visible range.[224,225] The AuNP@SiO$_2$ differ in terms of shape and weight (see also **Figure 47**) which obviously leads to a different amount of gold coating. Therefore, one individual AuNP@SiO$_2$ was applied for a set of experiments throughout the following section. The influence of gold loading was systematically studied for the optimized silica monolith substrate and this is described at a later stage of this work. The novel adsorbent was exposed to 5 mL Hg(II) standard solution with a concentration of 200 to 10,000 ng L^{-1}.
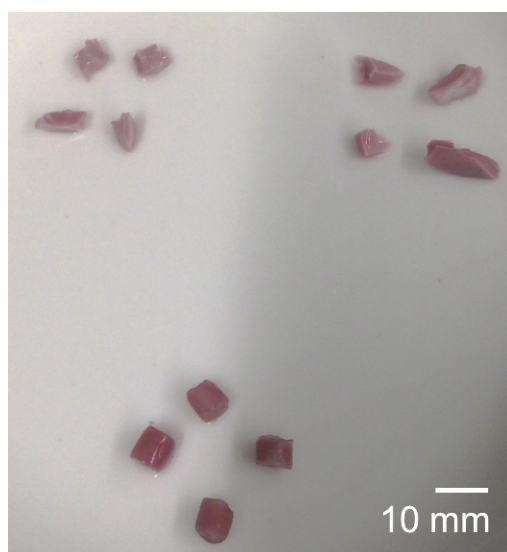
Figure 47: *Photograph of gold nanoparticle-coated silica monoliths in a wet condition (top: Silica monolith substrate obtained from the Institute of Inorganic Chemistry II, Ulm University; bottom: Silica monolith substrate prepared within this work).*

Blank contribution was checked by dipping the AuNP@SiO$_2$ into a blank solution without Hg(II) spike. Obviously, the investigated concentration range is significantly higher compared to the Hg concentration in pristine or even contaminated natural water. Still, a high concentration range was chosen for these preliminary investigations in order to overcome difficulties related to preparation and handling of Hg solutions in the ultratrace range. Hg determination was performed using the FIAS-AFS in an analogous manner as presented in section 5.1. In addition, a non-coated silica monolith (blank-SiO$_2$) was exposed to Hg standard solutions under the same experimental conditions.

Both, the AuNP-coated and blank silica monoliths were exposed to each Hg(II) standard solution for 1 min under stirring. The accumulated amount of Hg is illustrated in **Figure 48**. The accumulated amount of Hg on the novel nanogold-based adsorbent increases linearly over the investigated concentration range ($m(Hg) = 0.00004 \cdot c(Hg) + 0.01673, R^2 = 0.9972$). In contrast, a significant lower Hg fraction adsorbs to unspecific bindings sites of the blank-SiO_2. The amount of accumulated Hg increases linearly for a low Hg concentration between 200 to 1,000 ng L^{-1} ($m(Hg) = 0.00001 \cdot c(Hg) + 0.00678, R^2 = 0.9972$) but tends to reach a plateau at about 5,000 to 10,000 ng Hg L^{-1}. It is obvious that the statistical evaluation will be more precise using more data points.
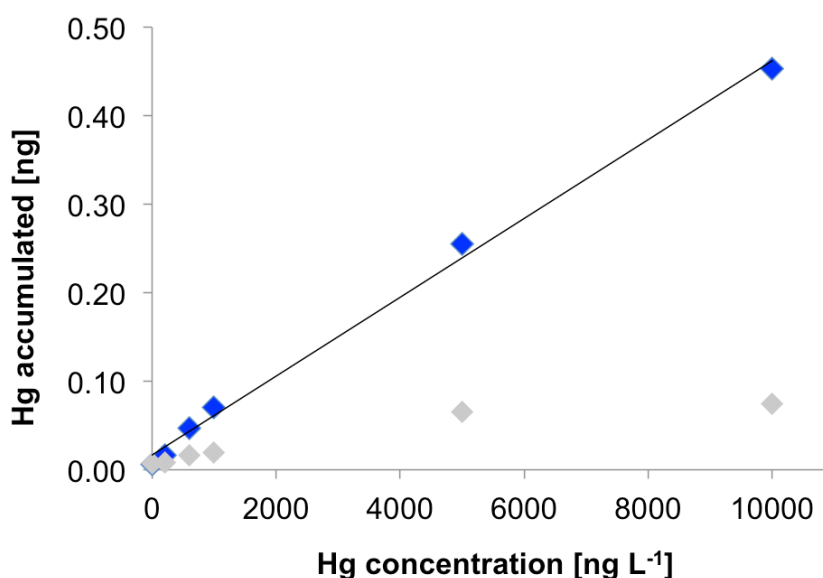
Figure 48: *Preconcentration of Hg from aqueous standard solutions ([Hg] = 200-10,000 ng L^{-1}) onto gold nanoparticle-coated silica monolith ($\blacklozenge$), $m(Hg) = 0.00004 \cdot c(Hg) + 0.01673, R^2 = 0.9972$) and onto a non-coated silica monolith ($\lozenge$).*

However, single measurements carried out here are meaningful to describe the trend of Hg adsorption onto novel AuNP@SiO_2 and for proof-of-principle. The results indicate that immobilization of AuNPs onto non-functionalized silica monoliths significantly improve Hg preconcentration from a sample solution. However, the mechanical stability of the AuNP@SiO_2 adsorbent, prepared by polycondensation of TMOS, is not very high under the given conditions. After approx. 7 analysis cycles the AuNP-coated as well as the blank-SiO_2 show a tendency to break. Thereby, one cycle consists of dipping the adsorbent into a sample solution, rinsing with UPW followed by at least two thermal treatments within the FIAS-AFS until a stable blank value is obtained. Repetitive

heating and evaporation of residual water inside the monolith pores might result in collapsing of the silica framework.

In summary, the previous section clearly demonstrated that immobilized AuNPs onto a silica monolith exhibit similar adsorbing capacities toward dissolved Hg as was shown earlier for AuNP-decorated silica particles and quartz glass tubes. However, the prepared silica monolith is not suitable for long-term application due to the low mechanical stability under the given conditions. As a consequence, detailed characterization of the prepared AuNP@SiO$_2$ was omitted within this thesis.

Mesoporous-macroporous silica monolith as substrate for gold nanoparticle immobilization

In order to overcome the disadvantages of the silica monolith substrates presented in the previous section a highly stable silica monolith was provided by the *Institute of Inorganic Chemistry II* (*Ulm University*). The preparation of this mesoporous-macroporous silica monolith is described in a recently published work by *Huber et al.*[102]. Briefly, a mixture of polyethylene glycol (PEG), tetraethyl orthosilicate (TEOS) and a surfactant was prepared. The resulting sol was left to gel, followed by a two-step aging process. Subsequent immobilization of AuNPs onto the monolithic substrate was achieved by *in situ* reduction of Au(III) to Au(0) as described in chapter 4.1.1 for silica particles. The resulting AuNP-coated silica monoliths are pink to purple in a wet condition (see **Figure 47**, top). The freshly prepared AuNP@SiO$_2$ was heated within the FIAS-AFS for decontamination according to the procedure described in chapter 5.1. Afterwards the novel dipstick was exposed to 5 mL Hg(II) standard solution ([Hg] = 200 to 10,000 ng L^{-1}) and a blank solution for 5 min. Thermal release and detection of Hg^0 was performed by the FIAS-AFS. The absolute amount of Hg, which accumulated onto the AuNP@SiO$_2$ from the respective sample solution is presented in **Figure 49**. As expected the adsorbed amount of Hg increases linearly with Hg concentration of the exposure solution ($m(Hg) = 0.0001 \cdot c(Hg) + 0.0028, R^2 = 0.9974$). In addition, the

stability of the silica monoliths (IC II) is high under the given conditions with a minimum lifetime of 23 analysis cycles.
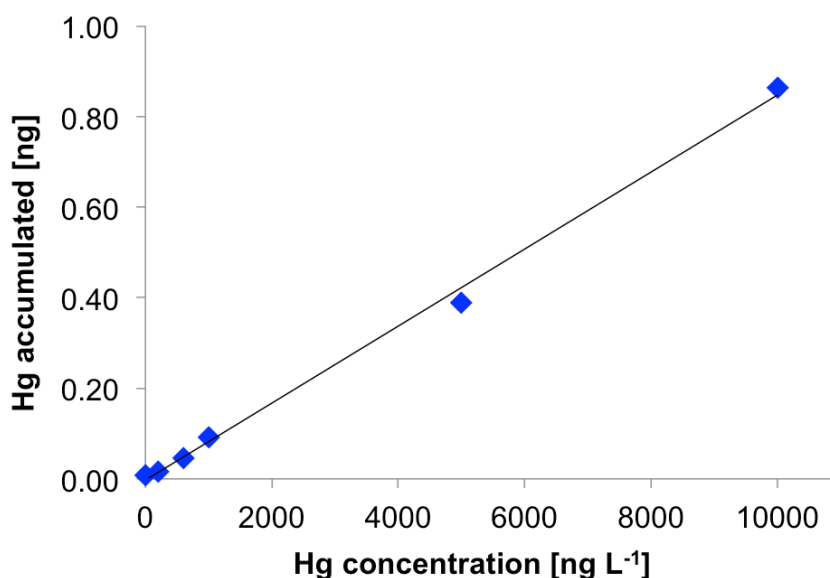
Figure 49: Preconcentration of Hg from aqueous standard solutions ([Hg] = 200-10,000 ng L^{-1}) onto gold nanoparticle-coated silica monolith ($m(Hg) = 0.0001 \cdot c(Hg) + 0.0028$, $R^2 = 0.9974$).

5.2.2. Influence of gold loading on Hg preconcentration

Another part of this work was to investigate the influence of gold loading on the silica monolith substrate on Hg adsorption onto the novel sampler. For this purpose two AuNP@SiO$_2$ fragments of different weight and shape were applied. The exact amount of deposited gold was determined by extracting gold in *aqua regia* and analyzing the supernatant by TXRF after the AuNP@SiO$_2$ were exposed to Hg(II) solution. The weight of the used AuNP@SiO$_2$ fragments and the corresponding amount of gold are summarized in **Table 21**. Hg concentration in pristine natural water is usually in the low nanogram per liter range. Thus the exposure concentration for the following tests was adapted to real conditions and varied between 5 to 50 ng L^{-1}. Both adsorbents were treated in a similar manner for best comparison of the resulting data. **Figure 50** shows a linear correlation between the accumulated amount of Hg and the concentration of the

exposure solution using two AuNP-coated samplers (AuNP@SiO$_2$_1 and AuNP@SiO$_2$_2) with different gold load.

Table 21: *Total weight of two fragments of AuNP-coated silica monolith and the gold amount determined after extraction in aqua regia.*

Adsorbent	Weight [mg]	Gold amount [µg]
AuNP@SiO$_2$_1	52	80.98 ± 0.03 [a]
AuNP@SiO$_2$_2	89	123.73 ± 0.03 [a]

[a] Standard deviation derived from TXRF measurement.

The slope of the linear regression for Hg preconcentration onto AuNP@SiO$_2$_2 with a total gold load of 124 µg ($m(\text{Hg}) = 0.00050 \cdot c(\text{Hg}) + 0.0060, R^2 = 0.9970$) differs only slightly from the slope obtained from a AuNP@SiO$_2$_1 fragment with a total gold load of 81 µg ($m(\text{Hg}) = 0.00039 \cdot c(\text{Hg}) + 0.0024, R^2 = 0.9964$). This means that the sensitivity of the proposed method, which is reflected by the slope of the linear
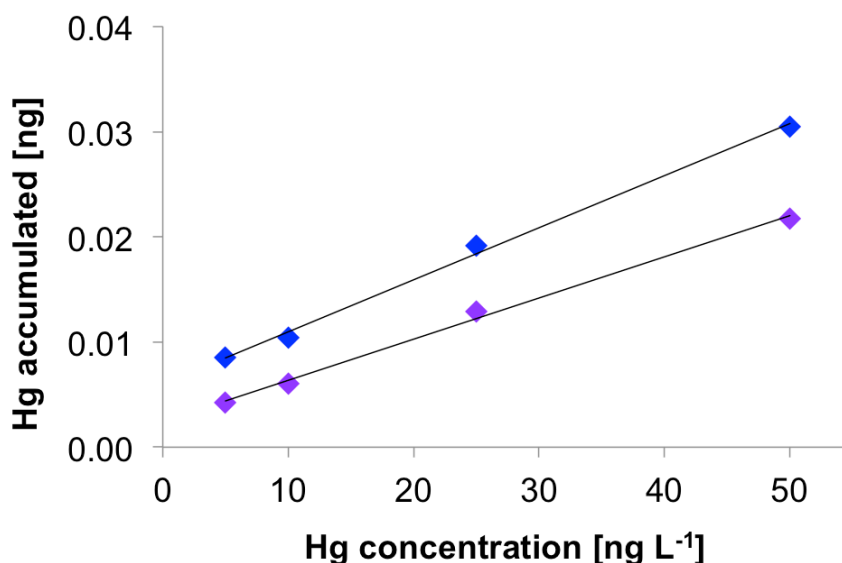
Figure 50*: Preconcentration of Hg(II) from aqueous standard solutions ([Hg] = 5-50 ng L^{-1}) on gold nanoparticle-coated silica monolith with a total gold load of 124 µg ($\blacklozenge$, $m(Hg) = 0.00050 \cdot c(Hg) + 0.0060, R^2 = 0.9970$) and 81 µg ($\blacklozenge$, $m(Hg) = 0.00039 \cdot c(Hg) + 0.0024, R^2 = 0.9964$).*

regression, is only insignificantly affected by the amount of active AuNPs. However, the difference in gold loading is small in this study and considerably higher gold loads might also lead to increased sensitivity of the method. As expected, the accumulated amount of Hg correlates with the gold loading on the monolithic substrate as the number

of bindings sites for Hg ions increases. Consequently, at this point of the method development one individual AuNP@SiO$_2$ adsorbent has to be used for external calibration and determination of an unknown Hg concentration of a sample.

5.2.3. Time-dependent Hg accumulation onto AuNP@SiO$_2$

The influence of exposure time regarding Hg preconcentration onto stable AuNP@SiO$_2$ was systematically studied and the results are presented in the following section. Therefore, the novel sampler was deployed in 5 mL Hg standard solution with a concentration of 10 and 100 ng L^{-1}, respectively. The adsorbed amount of Hg was determined after a distinctive time period, ranging from 1 min to 19 h. Due to the influence of gold loading on Hg preconcentration and the fact that the herein single piece silica monolith differ in shape and size, one individual AuNP@SiO$_2$ fragment was applied for the following experiments. The accumulated proportion of Hg given in percent of the initial concentration in solution is summarized in **Table 22**. Within the first 10 min Hg adsorbs rapidly and nearly linear onto the AuNP@SiO$_2$ for both initial Hg concentrations. Hence, calibration over time, which is mostly performed for diffusive gradient thin film (DGT) samplers, is possible within this time interval.[226–228]

Table 22: *Time-depending proportion of accumulated mercury from aqueous Hg(II) model solutions (reprinted with permission from Huber et al.[102], copyright 2015 by American Chemical Society).*

Time [min]	Proportion of accumulated Hg [%]	
	[Hg] = 10 ng L^{-1}	[Hg] = 100 ng L^{-1}
1	5	4
5	8	6
10	12	13
30	12	23
60	20	25
19 h	101	92

After 19 h the total amount of Hg in the solution adsorbed onto the sampler (92 to 101%). This indicates a minimum capacity of the applied AuNP@SiO$_2$ of 0.5 ng absolute mass of Hg. However, complete Hg adsorption is not mandatory for Hg quantification of an unknown water sample. As was described earlier in chapter 5.2.1 and 5.2.2, the Hg uptake and the concentration of the exposure solution are linearly correlated. Hence, Hg analysis *via* dipping the sampler into natural water systems is conceivable by external calibration over a defined concentration range and period of time. The results from **Table 22** indicate a fast and irreversible adsorption mechanism between AuNP-coated silica monoliths and dissolved Hg(II). Special emphasis should be placed on the high proportion of Hg that accumulated onto the novel adsorbent within only 1 min. The fluorescence intensity obtained after exposing the adsorbent to a sample solution ([Hg] = 10; 100 ng L^{-1}) for 1 min and subsequent thermal treatment significantly differs from the blank value. In this case the blank fluorescence intensity is resulting from heating a AuNP@SiO$_2$ within the FIAS-AFS without previous exposure to a Hg(II) solution. This is advantageous over other passive samplers that typically have to be deployed in the field for several hours or days before a sufficient amount of the analyte preconcentrates on the solid phase.[229,230]

5.2.4. Influence of sample volume on Hg preconcentration onto AuNP@SiO$_2$

In a proceeding set of experiments, the influence of total volume on Hg preconcentration onto the novel AuNP@SiO$_2$ was investigated in more detail. Therefore, the sample volume was increased to 4 L to simulate an infinite surrounding within a natural water body. In addition, the uptake rate of the novel adsorbent was determined in a manner that is consistent for Chemcatcher devices.[226]

For the following investigation, a custom-made set-up with a 4 L round-bottom flask was used. A detailed description on the set-up is given in section 6.8. Due to the large surface of the applied flask and the tendency of Hg^{2+} ions to adsorb onto glass surfaces the stability of a 10 ng L^{-1} Hg solution was tested by CV-AFS according to U.S. EPA

method 1631 first. Hg concentration decreases slightly within 24 h after the first filling of the precleaned 4 L flask. However, after filling the flask with Hg standard solutions for the second time the measured Hg concentration was stable over a minimum time period of 24 h. This is explained by passivation of the glass surface when the flask is filled with Hg solution for the first time. Even if the Hg solution is acidified with diluted hydrochloric acid, which enables protonation of the glass surface (Si-OH) and hinders Hg^{2+} ions from adsorbing onto the surface, few adsorption sites might be available before conditioning. After conditioning the novel set-up, AuNP@SiO$_2$ was exposed to 4 L of a 10 ng L^{-1} Hg(II) standard solution for 1 to 40 min under turbulent conditions. As can be seen from **Figure 51** Hg accumulation onto AuNP@SiO$_2$ from 4 L of a 10 ng L^{-1} standard solution follows a polynomial function ($m(\text{Hg}) = -0.00002 \cdot t^2 + 0.00149 \cdot t + 0.00817, R^2 = 0.9982$) over the investigated time period. This indicates a saturation of the adsorbent, which was already observed from the time-dependent investigations using a total sample volume of 5 mL (see section 5.2.3). Within the kinetic regime (1 to 10 min) the mass of Hg accumulated by the sampler shows a good linear relationship
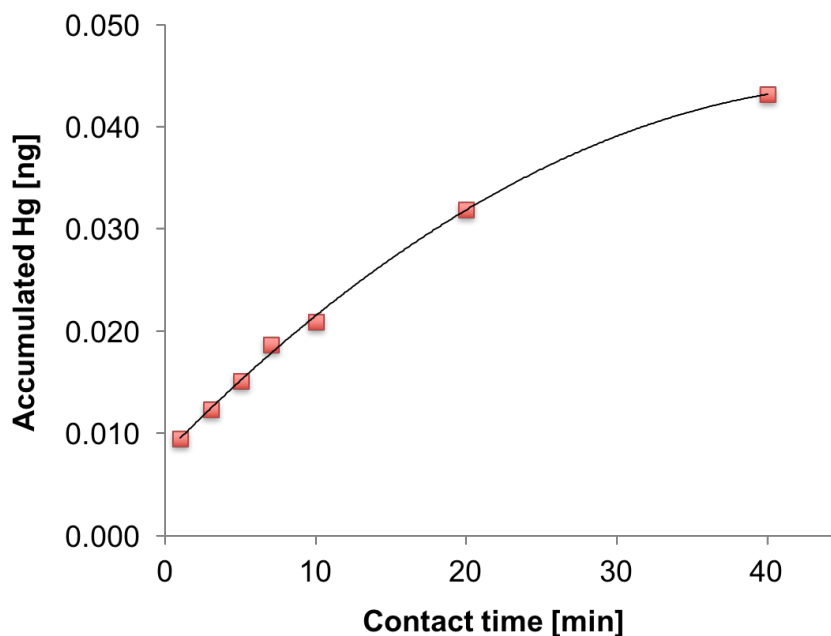
Figure 51*: Hg preconcentration onto gold nanoparticle-coated silica monolith. ($m(Hg) = -0.00002 \cdot t^2 + 0.00149 \cdot t + 0.00817, R^2 = 0.9982$; sample volume 4 L; initial [Hg] 10 ng L^{-1}, room temperature, turbulent conditions).*

with time ($m(Hg) = 0.0013 \cdot t + 0.0085, R^2 = 0.9801$). This correlation is used to determine the uptake rate of the sampler, given as mass to concentration ratio over the time range from 1 to 10 min. The slope of the linear regression (**see Figure 52**) results in an uptake rate of the novel sampler of 7.87 ± 2.06 mL h^{-1}. The obtained sampling rate was compared with values from the literature. Thereby, *Zhou et al.*[230] presented a sol-gel passive sampler for Hg monitoring in aqueous system. The adsorbent consists of a thiol-functionalized binding layer and a porous diffusive layer. A sampling rate of 8.78 mL h^{-1} was determined from the kinetic regime up to 12 h. However, for the determination of accumulated amount of Hg cracking of the sampler and acid digestion of the sol-gel was mandatory. Hence, the adsorbent is for single use only. The herein presented sampler is suitable for multiple use as reagent-free thermal desorption of Hg(0) is performed after sampling. In addition, the proposed method proceeds without additional reagents for sample pretreatment. As a consequence, the risk of contamination and the analysis time are minimized.
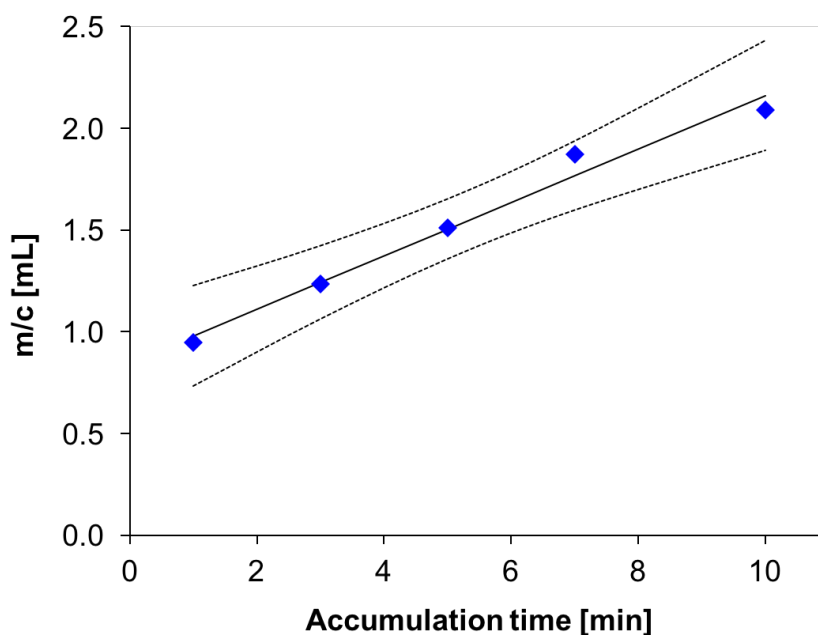
Figure 52: *Hg uptake as a function of exposure time ($\frac{m}{c} = 0.1312$ mL min$^{-1} \cdot t +$ 0.8475 mL, $R^2 = 0.9801$, solid line: linear trend, dashed line: confidence interval; sample volume 4 L, initial [Hg] 10 ng L^{-1}, room temperature, turbulent condition) (reprinted with permission from Huber et al.[102], copyright 2015 by American Chemical Society).*

5.2.5. Characterization of AuNP@SiO$_2$

The previous sections clearly demonstrated that the novel adsorbent, comprising of a silica monolith decorated with *in situ* formed gold nanoparticles, exhibits a high selectivity towards trace amounts of dissolved Hg(II). It was shown that the mesoporous-macroporous silica monoliths are more suitable as a substrate for AuNP deposition and subsequent Hg accumulation compared to former studied quartz glass substrates and silica monoliths synthetized from TMOS as a silica substrate by an acid-base reaction. As mentioned earlier the AuNP@SiO$_2$ are colored dark purple in the wet condition. This indicates embedded 20 to 200 nm in size AuNPs which exhibit surface plasmon resonance in the visible spectral range.[224,225] The appearance becomes brighter after calcination at 500°C. The structural characteristics of the non-coated monolith as well as of the AuNP@SiO$_2$ were calculated by the *Institute of Inorganic Chemistry II* (*Ulm University*) from N$_2$ sorption measurements.[102] The surface area and the pore volume decrease after AuNPs immobilization (**Table 23**).

Table 23: *Surface area, pore volume and pore size of blank and nanogold-coated silica monolith (reprinted with permission from Huber et al.[102], copyright 2015 by American Chemical Society).*

	Surface area [m^2 g^{-1}] [a]	Pore volume [cc g^{-1}] [b]	Mean mesopore diameter Dv(d) [nm]
Blank-SiO$_2$	613	0.62	5.7
AuNP@SiO$_2$	404	0.50	6.0

[a] As derived from linear isotherm approach, [b] As derived from nonlocal density function theory method.

The slight change of the mean mesopore diameter is an indication for AuNPs deposition at the silica surface rather than incorporation inside the mesopores. This is affirmed by the measurement of an adsorption-desorption hysteresis of H$_2$-type by IC II, which remained unaffected by AuNPs immobilization.[102] This is in good agreement with the average AuNP size as it greatly exceeds the mean mesopore diameter. The average size of the immobilized AuNPs was determined by scanning electron microscopy (SEM) of AuNP@SiO$_2$ after calcination at 500°C. This technique allows surface characterization of the prepared AuNP@SiO$_2$. **Figure 53A** shows an exemplary secondary electron image with a magnification of 5,000× times, the corresponding backscattered electron

image is presented in **Figure 53B**. A SEM image with a magnification of 30,000× times is depicted in **Figure 53C**. From these images the average AuNP diameter was calculated by counting particles from three different images meaning different spots on the AuNP@SiO$_2$. Thereby a total number of AuNPs of 1719 was considered for evaluation. The average AuNP size is 67 ± 51 nm. The AuNP size distribution is depicted in **Figure 53D**. Previous studies conducted in the working group of *Prof. Dr. Kerstin Leopold* demonstrated that AuNPs of this size range show adsorption of different dissolved Hg species from water samples due to their catalytic activity.[22,23]

The novel AuNP@SiO$_2$ exhibit a regular silicate framework with evenly distributed spherical gold nanoparticles separated by a clear interparticle distance. For evaluation of the particle size distribution only AuNP with a roundness factor ≥ 0.7 were taken into
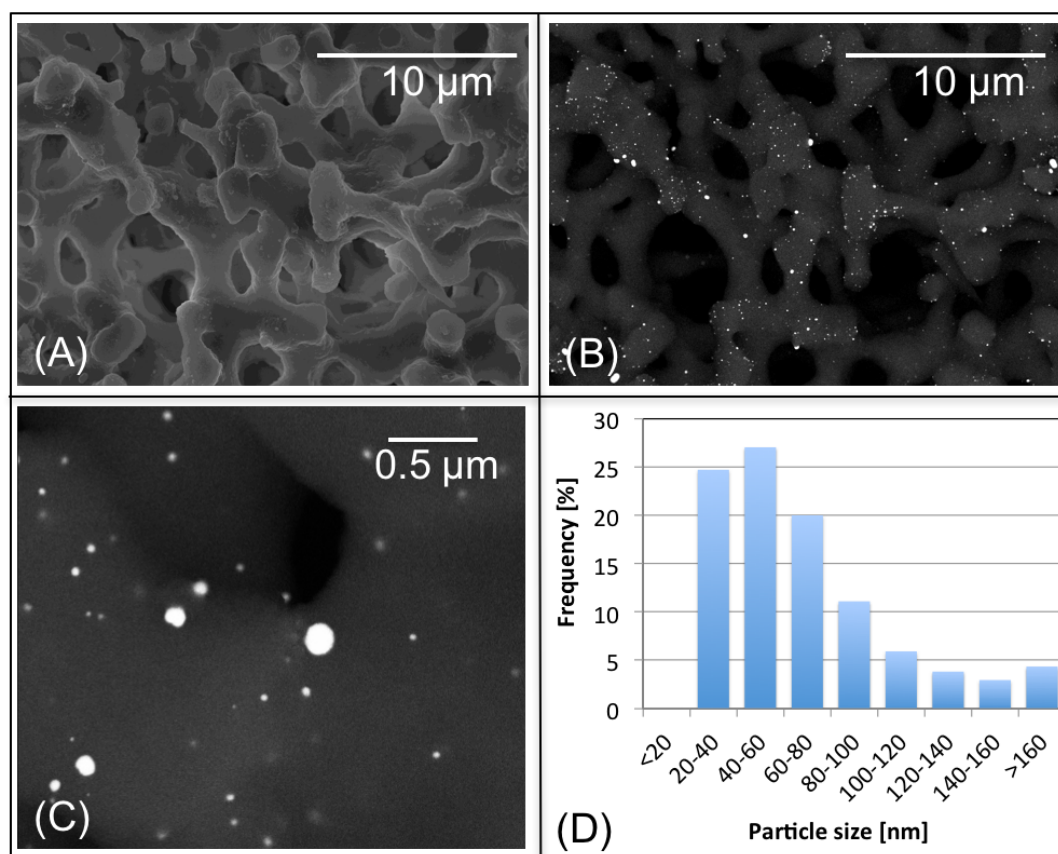
Figure 53*: Scanning electron microscopy (SEM) images of AuNP@SiO$_2$ and particle size distribution. (A) Secondary electron detection with a magnification of 5,000× times. (B) Backscattered electron detection with a magnification of 5,000× times. (C) Backscattered electron detection with a magnification of 30,000× times. (D) Gold nanoparticle size distribution on silica monolith (N = 1719; particle size is given as major particle length).*

account. Hence, the particle size is expressed as the major length rather than a defined diameter. A few AuNPs exceed a major length of 100 nm. The amount of deposited AuNPs was determined *via* TXRF after extracting the gold into aqua regia. The average Au load on the silica monoliths is 1.92 ± 0.12 µg Au per mg SiO_2. Further extracting experiments were performed in dilute HCl as the calibration standards and real water samples are stabilized by the addition of dilute HCl. Thus, the $AuNP@SiO_2$ was immersed in dilute HCl at room temperature for 10 min or 6.5 h, respectively. The Au concentration of the supernatant was determined by TXRF measurement and the results found were below the limit of detection of 0.17 µg L^{-1}. This finding certifies the stability of the novel adsorbent under these conditions.

5.2.6. Application to real water samples and validation

The nanogold-coated silica adsorbent shows good performance for Hg preconcentration from Hg(II) model solutions over a wide concentration range. The novel $AuNP@SiO_2$ adsorbent accumulates adequate amounts of dissolved Hg within a period of only one minute. For proof of principle the presented method was applied to real water samples. Recovery experiments with Hg(II) spikes were performed with a seawater sample. Determination of total dissolved Hg concentration of a submarine groundwater discharge (SGD) sample was performed to validate the proposed approach. The real water samples were provided by *Geosciences Environment Toulouse* (GET, Université Paul Sabatier) and the sample origin and the sampling date are summarized in **Table 24**.

Table 24: *Hg analysis of real water samples using the novel AuNP@SiO2 sampler.*

Water sample	Sample origin	Date of sampling
Black Sea	42°20'56''N 38°41'2''E	July 2013
Karstic spring, Font Estramar	42°51'32''N 2°57'31''E	March 2011

Hg recovery in spiked seawater samples

First, the influence of seawater on Hg preconcentration onto the novel sampler was investigated. Therefore, the seawater sample was spiked with defined volumes of Hg(II) standard solution. Natural Hg concentration of seawater is usually in the ng to pg per liter level [35,37]. Still, blank correction was performed with data derived from AuNP@SiO$_2$ accumulation in acidified, non-spiked seawater. Prior to measurement of Hg(II) spiked seawater the novel sampler was calibrated by a threefold measurement of aqueous Hg(II) standard solutions ([Hg] = 2 to 15 ng L^{-1}). Therefore, an accumulation time of one minute and a sample volume of 4 mL were chosen. The resulting calibration function is depicted in **Figure 54**. Then, AuNP@SiO$_2$ was exposed to Hg(II) spiked seawater at the same concentration level. The sampler was immersed into the sample solutions under the same conditions as the calibration experiment was performed. Due to the fact that the standard solutions and the real water samples were acidified with different hydrochloric acid as a stabilizing agent blank correction was performed for
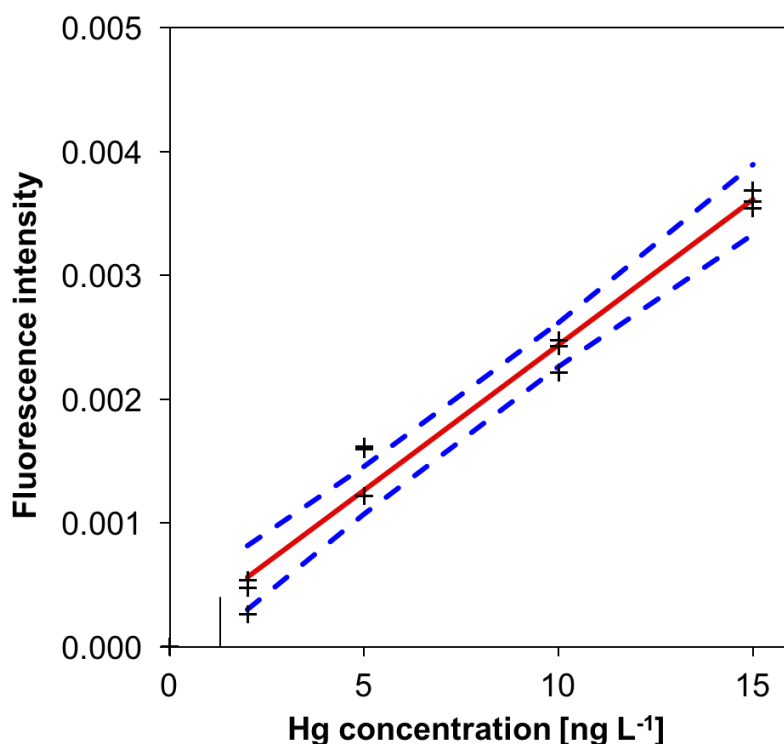
Figure 54: *Linear calibration function derived from AuNP@SiO$_2$ exposure to Hg(II) standard solution for 1 min (FI = 0.0002 · c(Hg) + 0.0001, R^2 = 0.9763; red: linear trend, nc = 12, blue: confidence interval with P = 95%, black: limit of detection; sample volume 4 mL, 150 rpm).*

138

both data sets. For the external calibration fluorescence intensity derived from accumulation in 0.06 M HCl was used for blank correction. Average fluorescence intensity obtained from AuNP@SiO$_2$ exposure to an acidified seawater sample without additional Hg(II) spike was used for blank correction of real water measurements. The recovery function obtained for replicate measurement ($n_s = 3$) of four different spike concentrations is shown **Figure 55**. As a result a recovery rate of $101.1 \pm 12.5\%$ and unbiased blank value $(0.9173 \pm 1.1756 \text{ ng L}^{-1})$ were achieved using the novel AuNP@SiO$_2$. This confirms the absence of any matrix effects. This successful recovery experiment further verifies the applicability of the novel approach for accurate and precise Hg trace determination in seawater.
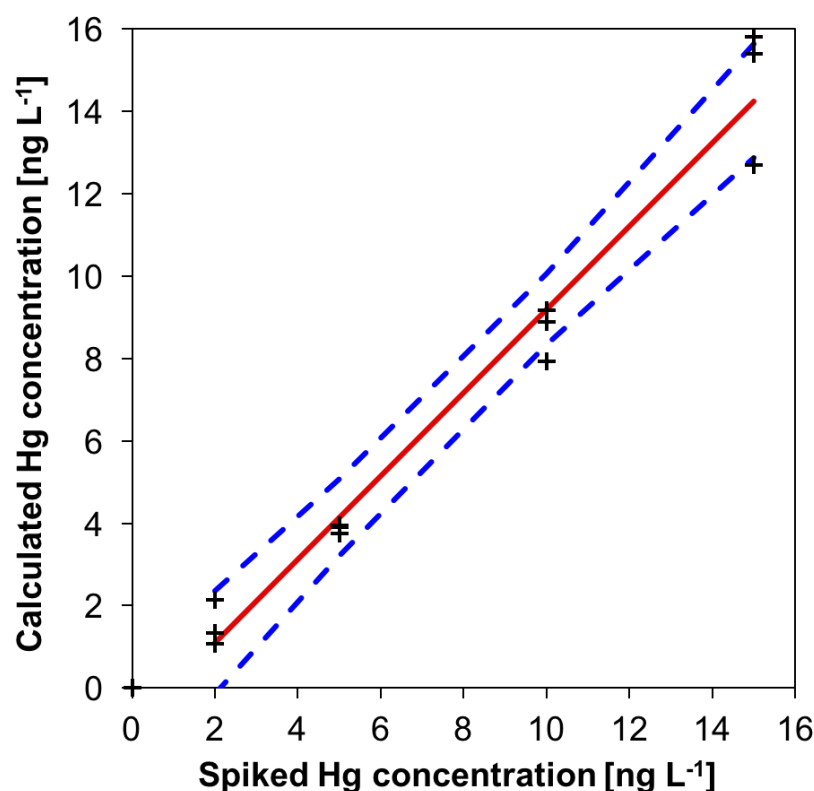
Figure 55*: Mercury recovery from a seawater sample spiked with Hg(II) standard solution (y = 1.0108 · x − 0.9173, R^2 = 0.9701, red: recovery function, n$_c$ = 12, blue: confidence interval with P = 95%; sample volume 4 mL, accumulation time 1 min, turbulent conditions).*

Determination of total dissolved Hg in natural freshwater

A non-spiked SGD sample was subjected to direct preconcentration onto the novel AuNP@SiO$_2$ sampler. Natural metal concentration in SGD waters is usually slightly higher compared to other freshwaters. Thus, SGD real water sample perfectly meets the requirements for a first application of AuNP@SiO$_2$ to direct Hg quantification. Hg concentration of SGD sample was additionally determined by U.S. EPA standard method 1631 within this work. *Heimbürger et al.* [213] analyzed the same sample according to a modification of U.S. EPA standard method 1631. The novel AuNP@SiO$_2$ was dipped into the freshwater sample for one minute. Thermal desorption of Hg(0) and AFS measurement was carried out according to general procedures described earlier. The data is evaluated *via* aqueous calibration of the AuNP@SiO$_2$. The results found by application of three different methods are summarized in **Table 25**.

Table 25: *Total dissolved Hg concentration in SGD sample found by application of the developed AuNP@SiO$_2$ sampler, standard and modified U.S. EPA method 1631 (n_s = 3, P = 95%; reprinted with permission from Huber et al.[102], copyright 2015 by American Chemical Society).*

Method	Total Hg concentration [ng L^{-1}]
Preconcentration onto AuNP@SiO$_2$	7.97 ± 0.70 [a]
Standard U.S. EPA method 1631 [97]	6.90 ± 0.33 [a]
Modified U.S. EPA method 1631 [213]	9.43 ± 0.94 [b]

[a] Measured after several month of storage, [b] Measured several days after collection.

The value found by application of the novel adsorbent (AuNP@SiO$_2$) developed within this work for preconcentration of Hg agrees well with the results obtained by using the standard method U.S. EPA method 1631. A comparison of the absolute difference (Δm = 1.07) and the extended uncertainty (U_Δ = 1.55, coverage factor k = 2) confirms that there is no significant difference between the found value and the reference method.[203] The comparison of the measurement result found by the presented method and by the modified U.S. EPA method 1631 leads to a similar result. The absolute difference of the derived Hg concentration by the two methods (Δm = 1.46) is lower than the expanded uncertainty (U_Δ = 2.34, coverage factor k = 2), thus there is no significant difference between the two results. The proposed method for Hg ultratrace

determination in a SGD sample can be compared to a reference method. However, the standard U.S. EPA method 1631 performed within this study yields in clearly lower Hg concentration compared to modified U.S. EPA method 1631 applied by the external laboratory. This difference might be explained by analyte loss through long storage time for several months. The accuracy of the proposed method was not checked by means of analysis of a reference material as there is no certified water sample available without additional oxidizing agents. As the proposed method should be applied to untreated water samples such CRMs do not fulfill the requirements.

5.2.7. Analytical figures of merit

The performance characteristics of the proposed method using a stable AuNP-decorated silica monolith as passive sampler for Hg accumulation in natural water are summarized in **Table 26**. A typical calibration function in the concentration range from 2 to 15 ng Hg L^{-1} is depicted in **Figure 56**. The novel method provides a low limit of
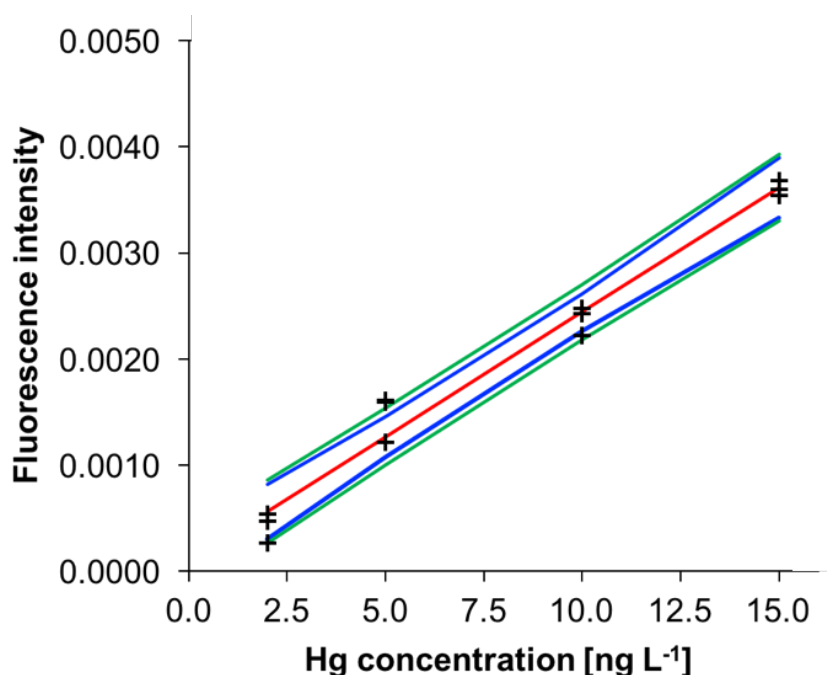
Figure 56: *Linear calibration function for Hg quantification by accumulation onto AuNP@SiO$_2$ (sample volume 4 mL; (+) calibration data, red: linear trend, $FI = 2.35 \cdot 10^{-4} \cdot c(Hg) + 9.15 \cdot 10^{-5}$, $R^2 = 0.9763$, $n_c = 12$, blue: confidence interval with P = 95%, green: prognosis interval).*

detection of 1.31. ng L^{-1}. This value was achieved by exposing the AuNP@SiO$_2$ to the sample solution for only one minute. Hence, the sensitivity of the method and consequently the LOD can be lowered by prolonging the time interval. A good reproducibility with relative standard deviations between 3.6 to 5.4% was achieved for the 3-fold measurement of a blank solution, a Hg(II) standard solution and a Hg(II) spiked real water sample. The linear working ranges covers 4 orders of magnitude which allows application to pristine waters as well as to contaminated waters. The accuracy of the method was confirmed demonstrated in the previous section by comparison of freshwater measurement to U.S. EPA method 1631 as a reference method.

Table 26: *Analytical figures of merit achieved by the novel method using AuNP@SiO$_2$ for dissolved Hg preconcentration and quantification (sample volume 4 mL, n_c = 12, accumulation time 1 min).*

Parameter	Achieved values
Linear working range	1.31 - 10,000 ng L^{-1}
Calibration range, n_c = 15	2 - 15 ng L^{-1}
Slope of the linear regression	$2.35 \cdot 10^{-4} \pm 2.58 \cdot 10^{-5}$ ng^{-1}
Intercept of the linear regression	$9.15 \cdot 10^{-5} \pm 2.43 \cdot 10^{-4}$
Limit of detection	1.31 ng L^{-1}
Limit of quantification	2.61 ng L^{-1}
Regression coefficient (R^2)	0.9763
Method standard deviation	10.56%
Accumulation rate	7.87 mL h^{-1}
relative standard deviations (precision)	
For blank solution (0.06 M HCl), n_s = 3	3.57%
For Hg(II) standard solution ([Hg] = 10 ng L^{-1}), n_s = 3	4.34%
For Hg(II) spiked seawater ([Hg] = 10 ng Hg L^{-1}), n_s = 3	5.37%
lifetime of AuNP@SiO$_2$	approx. 23 cycles
Residual standard deviation	$1.98 \cdot 10^{-4}$
Coefficient of variation of the procedure	$8.45 \cdot 10^{-1}$

5.2.8. Conclusion

The aim of this part of the work was the development of a robust dipstick for dissolved Hg preconcentration. Therefore, two types of silica monoliths were investigated as a substrate for *in situ* formed AuNPs deposition. Both AuNP-coated silica monoliths exhibit a high affinity to dissolved Hg(II) as there is a linear correlation between the absolute amount of Hg adsorbed onto the dipstick and the Hg concentration of the sample. However, it was shown that only the mesoporous-macroporous silica monolith meets the requirements regarding Hg extraction and thermal treatment as part of the analytical method. The structural characteristics were determined by our collaboration partner, the average AuNP size (67 nm) and the morphology of the novel adsorbent was analyzed by SEM as part of this thesis. Time-depending Hg(II) adsorption was demonstrated applying the mechanically more stable $AuNP@SiO_2$. The novel nanogold-based silica sampler exhibits a minimum Hg capacity of 500 pg. The kinetic adsorption regime is most probably within the first 10 min of exposure. A significant Hg load was measured after an exposure period of only one minute which is advantageous over other passive samplers for metal trace monitoring of natural water. The uptake rate (7.87 mL h^{-1}) of the novel sampler was calculated from an experiment using 4 L sample solution. An external calibration using aqueous Hg(II) standard solutions showed an impressively low detection limit of 1.31 ng Hg L^{-1} requiring a contact time of only 1 min. Separation of dissolved Hg from the water matrix and subsequent preconcentration is performed without additional reagents. The proposed method was validated by means of recovery experiments. A recovery rate of 101.1% was found for a Hg(II) spiked seawater sample. In addition, the dissolved Hg concentration of a non-spiked freshwater sample was determined by dipping the $AuNP@SiO_2$ into the sample for 1 min. In addition, the result obtained from direct measurement of a freshwater sample was in good agreement with a reference method.

The novel adsorbent offers several advantages over other passive samplers. A low risk of contamination and analyte loss is achieved due to a short contact time to the matrix solution, direct preconcentration of the analyte without sample transportation and

storage and the elimination of complicated pretreatment steps. Moreover, elaborative cleaning of sample bottles, filtration and stabilizing of the sample can be omitted.

6. Experimental procedures

The following chapter presents specific working and cleaning procedures for ultratrace analysis of mercury. Obviously, highest purity of reagents and working environment are required for most sensitive and accurate Hg detection. In this context, the physical and chemical properties of Hg play a key role. In addition, Hg is a ubiquitous element and thus present in all reagents as well as in the laboratory atmosphere. Therefore, special conditions have to be fulfilled to analyze Hg in the ng to pg per liter level. Hence, the preparation of Hg standard solutions, reagents and model solutions is described in detail in the following section. As part of this work, nearby located aquatic systems were subjected to sampling for subsequent determination of dissolved Hg concentration. The sampling procedure and the sample pretreatment are further illustrated. In addition, the preparation and characterization of different adsorbents for direct accumulation of dissolved Hg species is described. Furthermore, all procedures and applied materials regarding the development and optimization of the novel analytical methods for Hg determination in natural water are depicted within the following chapter.

6.1. General working procedures for mercury ultratrace analysis

All Hg measurements and cleaning procedures presented within this study were performed in a clean room to minimize contamination. This laboratory is equipped with an air exchange system resulting in an indoor pressure of 24 Pa to keep constantly low atmospheric Hg levels. In addition, a lock chamber under excess pressure (12 Pa) separates the ultratrace laboratory from the corridor in order to reduce particle contamination. This arrangement offers best conditions for a constantly low atmospheric Hg level and facilitates analytical measurements in the ultratrace range. The laboratory is further equipped with an atomic fluorescence spectrometer specialized for Hg analysis. Hg standard solutions with a concentration higher than 1 μg L^{-1} were handled and prepared in a neighboring laboratory. All these precautions were taken to keep Hg

blank contribution as low as possible. All reagents used throughout this work were purchased in the highest available purity, respectively. Some of these reagents, *e.g.* chemicals for Hg analysis by means of the U.S. EPA standard method 1631, were precleaned by the manufacturer with regard to mercury concentration and maximum Hg levels are stated on the container. All volumetric glass flasks and other glass vessels, which were not in use for approximately 4 months as well as new materials, were cleaned with saturated bromine chloride (BrCl) solution before use. Therefore the flask/vessel was filled up to volume with 1% (v/v) freshly prepared BrCl, closed with a suitable plug and left over night in a fume hood. After disposal of BrCl the flask/vessel was rinsed with UPW three times before use. Containers, which were not used immediately after cleaning, were filled with 0.06 M HCl, closed and stored in the ultratrace clean laboratory until use. All volumetric glass flasks frequently used for calibration experiments were labeled with the respective Hg concentration and were used for the same or similar concentration range. These flasks used for calibration experiments were rinsed once with 0.12 M HCl and then with UPW three times between successive experiments.

6.2. Reagents for mercury ultratrace analysis

Mercury standard solutions

Mercury stock standard solution (mercury (II) nitrate, $1,000 \, mg \, Hg \, L^{-1}$, Merck, Darmstadt, Germany) and diluted Hg standard solutions were stored at 4-7°C in the dark. All Hg(II) standard solutions were prepared in precleaned volumetric glass flasks by successive dilution of the stock solution in 0.06 M HCl. Hg(II) standard solutions up to $10 \, mg \, L^{-1}$ were prepared monthly, dilutions comprising a Hg concentration of $100 \, \mu g \, L^{-1}$ were prepared weekly. The preparation of high concentrated Hg(II) standard solutions was carried out in a separated laboratory under non-clean room conditions. Hg(II) standard solutions with a concentration $\leq 1 \, \mu g \, L^{-1}$ were prepared freshly on the day of the experiment and handled and stored in the clean room. All Hg(II) standard

solutions for external calibration were prepared by adequate dilution of the stock solution in 0.06 M HCl.

Reagents for standard method U.S. EPA method 1631

Bromine chloride (BrCl) was used as an oxidizing agent within U.S. EPA method 1631.[97] Therefore potassium bromide (KBr, p.a., Merck, Darmstadt, Germany) and potassium bromate (KBrO$_3$, p.a., Merck, Darmstadt, Germany) were placed in a drying oven at 260°C for Hg decontamination for at least 2 h. Afterwards, 4.32 g KBr was dissolved in 400 mL 12 M hydrochloric acid (HCl). The solution was stirred at room temperature for about 1 h until the salt was completely dissolved. Then, 6.08 g KBrO$_3$ was added slowly to the solution under continuous stirring. The colorless solution initially turned yellow and remained deep orange after dissolving the complete amount of KBrO$_3$. The resulting saturated BrCl stock solution was kept in a fume hood within the clean room and was used for a maximum of 2 weeks. Special care must be taken during dissolving the bromine containing salts in concentrated HCl due to the release of hazardous volatile halogens *i.e.* Cl$_2$, Br$_2$, BrCl. The pre-reductant for decomposition of excess BrCl was prepared freshly before use. Hydroxylammonium hydrochloride solution (NH$_2$OH·HCl, p.a., $c(Hg)_{max} = 10^{-6}$ % (m/m), Merck, Darmstadt, Germany) was prepared by dissolving 7.5 g in 25 mL UPW. Stannous chloride (SnCl$_2$·2H$_2$O, p.a., $c(Hg)_{max} = 10^{-6}$ % (m/m), Merck, Darmstadt, Germany) was used as a reducing agent and was prepared freshly on the day of the experiment by dissolving 11.9 g in 41 mL 12 M HCl. The solution was filled up to a volume of 500 mL with UPW. Due to the formation of stannous (IV) oxide (SnO$_2$, cassiterite) upon storage, the same bottle connected to the automated flow system for CV-AFS was used throughout this study. Furthermore, all tubing that is transporting SnCl$_2$·2H$_2$O during analysis were rinsed thoroughly with diluted HCl after use. Freshly prepared 0.5 M HCl was used as a carrier and rinsing solution within U.S. EPA method 1631.

Other reagents

All solutions were prepared in ultrapure water (UPW) with a resistivity of 18.2 MΩ cm. UPW was derived from a *Synergy® UV* ultrapure water system (Merck Millipore, Billerica, USA).

All acidified aqueous solutions were prepared from a high-purity 12 M HCl (p.a., $[Hg]_{max} = 0.001$ mg L^{-1}, Merck, Darmstadt, Germany). Real water samples were acidified with 0.06 M HCl after filtration.

Hydrogen peroxide (35% (v/v), Staub & Co, Nürnberg, Germany) was used as an oxidizing agent during online UV digestion of organic model solutions. The container was covered with aluminum foil and stored at 4-7°C in the dark to prevent H_2O_2 decomposition through light exposure. All dilutions were prepared freshly from the concentrated solution (35% (v/v)) in UPW.

6.3. Model solutions

Model solutions from humic acids

Humic acid (Alfa Aesar, Karlsruhe, Germany) was received as a black, crystalline powder and stored in the dark at room temperature. It is derived from random organic material as indicated by the manufacturer. A stock solution of HA was prepared by dissolving 138.2 mg in 100 mL UPW. This solution exhibits a dissolved organic carbon (DOC) concentration of 500 mg L^{-1}, which was determined by elemental analysis. The stock solution was kept in the dark at 4-7°C for a maximum of two weeks. All HA model solutions with a lower DOC concentration were freshly prepared by dilution of adequate aliquots of the stock solution (500 mg C L^{-1}) in 0.06 M HCl.

Model solutions from aquatic humic and fulvic acids

Standard humic acids (*Suwannee River* Humic Acid Standard II) and fulvic acids (*Suwannee River* Fulvic Acid Standard II) were derived from the *International Humic Substances Society* (IHSS, Denver, USA). The organic material is extracted from river water and commercially available in the form of a desalted, freeze-dried solid. A HA and FA stock solution with DOC concentration of 100 mg L^{-1} was prepared by dissolving 20.22 mg and 20.58 mg in 100 mL UPW, respectively. This stock solution was passed through a 0.45-µm pore size polyethersulfone (PES) syringe filter (Pall Corporation, Ann Arbor, USA), acidified with 0.06 M HCl and kept in the dark at 4-7°C for a maximum of two weeks. All dilutions of the HA and FA model solution were freshly prepared by diluting adequate aliquots of the stock solution (100 mg L^{-1}) in 0.06 M HCl.

Model solutions from other organic compounds

Thiourea (Sigma-Aldrich, St. Louis, USA), urea (p.a., Merck, Darmstadt, Germany), cysteine (R configuration, for synthesis, Merck Schuchardt OHG, Hohenbrunn, Germany), glutathione (reduced L configuration; BioChemica, AppliChem GmbH, Darmstadt, Germany), methionine (L configuration, for synthesis; Merck Schuchardt OHG, Hohenbrunn, Germany) and disodium ethylenediaminetetraacetic acid ($Na_2EDTA \cdot 2H_2O$, Merck, Darmstadt, Germany) were used without further purification of the commercially available product. A stock solution of cysteine was prepared by dissolving 336.25 mg in 100 mL UPW. This results in a DOC concentration of 1,000 mg L^{-1}. Elemental analysis was omitted for these organic model compounds as the carbon mass fraction is clearly defined by the molecular formula. The stock solution was kept in the dark at 4-7°C for a maximum of four weeks. All further dilutions were prepared freshly by diluting adequate aliquots of the 1,000 mg C L^{-1} stock solution in 0.06 M HCl. The model solutions of all other compounds were prepared in the same manner and initial weights are presented in **Table 27**.

Table 27: *Weight of the organic model compounds (cysteine, methionine, urea, thiourea, glutathione, Na₂EDTA) for preparation of a 1,000 mg L^{-1} stock solution.*

Organic compound	Mass [mg] in 100 mL UPW	Total molar mass [g mol^{-1}]	Carbon molar mass [g mol^{-1}]	Carbon stock solution [mg L^{-1}]
Cysteine	336.25	121.16	36.03	1,000
Methionine	248.46	149.21	60.06	1,000
Urea	500.04	60.06	12.01	1,000
Thiourea	633.75	76.12	12.01	1,000
Glutathione	255.87	307.32	120.11	1,000
Na₂EDTA	309.92	372.24	120.11	1,000

6.4. Sampling of real water samples

Real water sampling carried out within this study was performed according to clean working procedures. The suitability of the sampling material was checked in previous studies by the working group of *Prof. Dr. Kerstin Leopold*. All water samples were taken in 125, 250 or 500 mL polyethylene terephthalate (PET; Corning, New York, USA) bottles with a high-density polyethylene (HDPE) screw cap. The sample bottles were single used and checked for their Hg blank contribution prior to sampling. PET bottles with a total volume of 250 mL were also sent to *Lars-Eric Heimbürger* (*Mediterranean Institute of Oceanography*, *Aix Marseilles Université*) who sampled a Black Sea water depth profile.

River water samples were collected in October 2011 in Munich and Ulm in South Germany. Three water samples were taken from the river Isar (Munich) and three samples were taken from the river Danube (Ulm). The sampling sites for each river were selected before, in, and behind the respective city. The locations before and behind Munich were Dürnstein and Garching, the locations before and behind Ulm were Wiblingen and Böfingen. River water was collected in a distance of approx. 1 m from the riverbank in a depth of 20-30 cm beneath the water surface. The new PET sampling

bottle was rinsed with the respective sample three times before the bottle was completely filled underwater. The cap was screwed down under the water surface. Shortly after sampling the water samples were filtered through 0.45-µm polycarbonate filters (Merck, Darmstadt, Germany) and acidified with 0.06 M HCl. Each membrane was conditioned with approx. 20 mL of the sample prior to collecting the filtered water sample in another PET bottle. The samples were then stored in the dark at 4-7°C until analysis.

Three water samples were collected in June 2012 at a wastewater treatment plant (WWTP, *Klärwerk Steinhäule*) near Ulm. Water was collected at the inlet of the WWTP, after physical and after biological treatment. The water samples were collected on the edge of the clarification tanks of the WWTP with the help of a ladle. The PET bottles were rinsed with the respective water samples three times before the bottle was filled approx. 50 cm below the water surface and closed underwater. Filtration was carried out at the same day in the ultratrace clean laboratory. The water samples were first passed through 0.7-µm glass microfiber filters (Whatman[©], Sigma-Aldrich, St. Louis, USA). Afterwards the samples were filtered through a 0.45-µm polyethersulfone (Pall Corporation, Ann Arbor, USA) membrane. Each filter was rinsed with approx. 500 mL UPW and conditioned with approx. 20 mL of the respective water sample prior to filtration. Another set of PET bottles were rinsed with the sample before the filtrate was collected. After sample preparation, the bottles were stored in the dark at 4-7°C until analysis.

6.5. Preparation of nanogold-assisted adsorbents

Within this work various adsorbing materials were developed and applied to dissolved Hg accumulation from standard and model solutions as well as from real water samples. The reagents and materials used for the preparation of the adsorbents are given in the following section.

6.5.1. Gold nanoparticle-coated silica particles

Gold nanoparticles were deposited on silica as a supporting media *via* wet chemical reduction from a gold solution according to *Leopold et al.*[22]. Here, silica particles with two different particle size ranges were used: 63-200 μm (silica gel 60 for column chromatography; Merck, Darmstadt, Germany) and 200-500 μm (silica gel 60 for column chromatography; Merck, Darmstadt, Germany). Furthermore chloroauric acid as a gold source was purchased from two different manufacturers: $HAuCl_4$ in 2 M HCl (1,000 mg Au L^{-1}) from Sigma Aldrich (St. Louis, USA) and $HAuCl_4$ (1,000 mg Au L^{-1}) from Merck (Darmstadt, Germany). 500 mg SiO_2 were suspended in 4 mL gold solution in a precleaned 1 L *Schott* flask with screw cap. The pH value was adjusted to 7 with approx. 13 mL of a 7 M sodium hydroxide (NaOH, p.a.; Merck, Darmstadt, Germany) solution. Next, 10 mL of a 0.22 M $NH_2OH \cdot HCl$ solution (≤ 0.000001 mg L^{-1} Hg, p.a. ASC, ISO; Merck, Darmstadt, Germany) were added and the suspension immediately became dark brown and cloudy. The glass flask was closed and placed on an orbital shaker at 260 rpm for 90 min. The resulting suspension was kept untreated over night to settle down the silica particles. Then, the supernatant was poured off and the particles were additionally rinsed 3 to 5 times with UPW. Each batch was transferred to an evaporating dish for subsequent drying at 250°C for 2 h. The AuNP coated silica particles appeared purple after drying (see **Figure 57**). Gold flakes were separated while washing with UPW and/or sorted out after drying using a glass pipette. The AuNP-
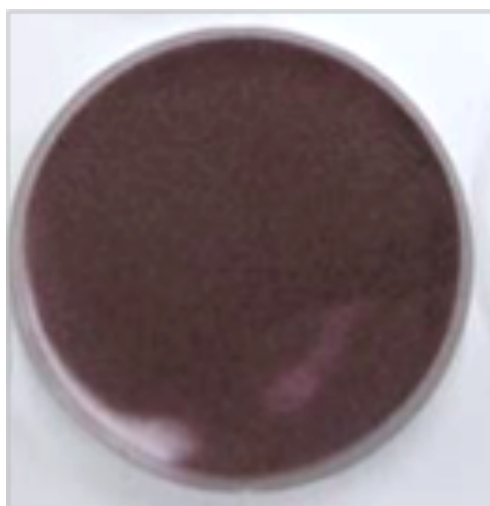
Figure 57: *Photograph of freshly prepared, dried gold nanoparticle-coated silica.*

coated silica particles were stored at room temperature in glass bottles with snap-on caps and were usually heated again to 250°C before introduced to the flow injection analysis system.

6.5.2. Gold nanoparticle-coated quartz glass tubes

The following section describes *in situ* formation and immobilization of AuNPs onto the outer surface of a quartz glass tube *via* a wet chemical synthesis route. The quartz glass tubes (L: 40 mm, ID: 3 mm, AD: 5 mm) were rinsed with acetone and UPW before they were closed with blind stoppers at both ends by means of silicone tubing (see **Figure 58**). Afterwards, the quartz glass tube was placed in a polypropylene (PP) container and
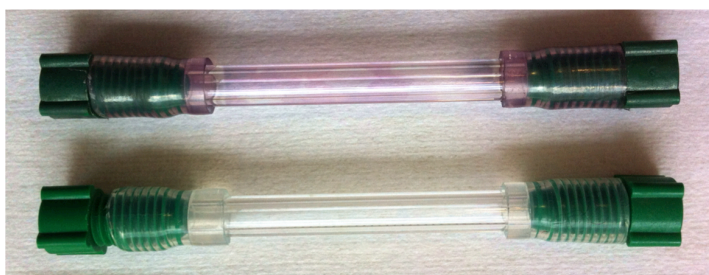
Figure 58: Photograph of quartz glass tube after immobilization of gold nanoparticles at outer surface (top), photograph of quartz glass tube after activation with stannous chloride (below); both capped with blind stoppers.

filled with 30 mL of a 0.014 M $SnCl_2 \cdot 2H_2O$ solution to completely cover the tube. The container was closed and placed on an orbital shaker for 24 hours at 120 rpm under room temperature. Afterwards, the tube was rinsed thoroughly with UPW and subsequently put in a glass flask with snap-on cap. The tube was then covered with 30 mL of a 1.02 mM gold standard solution ($HAuCl_4$ in 2 M HCl; 1,000 mg Au L^{-1}, Sigma-Aldrich, St. Louis, USA), which was adjusted to a pH of 6.5-7 using 7 M NaOH (p.a., Merck, Darmstadt, Germany). Then, 10 mL of a 0.022 M $NH_2OH \cdot HCl$ (≤ 0.000001 mg L^{-1} Hg, p.a. ASC, ISO, Merck, Darmstadt, Germany) was pipetted to each vessel. The solution was finally mixed for 10 min at 120 rpm. The quartz glass tube was rinsed with UPW and heated at 450°C for 1 hour. The freshly prepared AuNP-coated quartz glass tubes (AuNP@qt) were placed in a box, which was kept in the

ultratrace clean laboratory. In addition, a bag filled with active carbon was placed inside the box to minimize atmospheric Hg deposition onto the AuNP@qt.

6.5.3. Gold nanoparticle-coated silica monoliths

In this work, two types of silica monoliths were applied as substrate for gold nanoparticles deposition. Different reactants and silica source materials were used during synthesis. The first attempt of silica monolith preparation was performed within this thesis, the second approach was conducted by means of a collaboration project with the *Institute of Inorganic Chemistry II* (*Ulm University*). *In situ* deposition of gold nanoparticles onto the silica monolith was performed in a similar manner for both types of silica substrate and is described in the following section.

Silica monoliths from acid-base reaction as substrate for gold nanoparticle immobilization

The triblock copolymer Pluronic® P-123 (Sigma-Aldrich, St. Louis, USA) was used as the backbone to prepare a mesoporous silica monolith according to the literature [223]. First, 716 mg P-123 was dissolved in 8 mL 0.01 M acetic acid (Merck, Darmstadt, Germany). After stirring the solution for approx. 5 min the solution was cooled and stirred in an ice-bath for another 5 min. Afterwards, 500 mg urea (Sigma-Aldrich, St. Louis, USA) and 5 µL of Au(III) standard solution (1,000 mg L^{-1}) were added to the clear solution under stirring. Then, 1.25 mL tetramethoxysilane (TMOS, $\geq 98\%$, Sigma-Aldrich, St. Louis, USA) was added under stirring. The resulting solution was filled into a PP vessel with screw cap and kept at about 60°C inside a water bath. After approx. 40 min the solution became turbid and cloudy. Afterwards, the vessel was kept at 60°C for five days (ageing of the gel). The silica monoliths were removed from their respective forms, rinsed with UPW and stored in 15 mL UPW overnight. The washing solution was disposed and another washing step with ethanol/water mixture (1:1) was

154

performed overnight. The wet monoliths were dried at room temperature for five days. Afterwards, calcination took place at 800°C with a heating rate of 1°C min⁻¹. The temperature was kept constant for 5 h. During the calcination step Pluronic® P-123 is decomposed and removed from the silica framework. The resulting silica monoliths were immersed in 500 µL $HAuCl_4$ (pH 12) and reduction to Au(0) took immediately place when adding 125 µL of a 0.22 M $NH_2OH·HCl$ solution under stirring. In wet condition the freshly prepared AuNP-coated silica monoliths (AuNP@SiO_2) appeared dark pink to purple as can be seen in **Figure 59**. After washing the monolith with UPW and drying at 80°C for 10 min, the color of AuNP@SiO_2 changed to light pink.

Figure 59*: Photograph of silica monoliths in wet condition after immobilization of gold nanoparticles.*

Mesoporous-macroporous silica monolith as substrate for gold nanoparticle immobilization

The *Institute of Inorganic Chemistry II* (*Ulm University*) provided mesoporous-macroporous silica monoliths for subsequent AuNPs immobilization. The monolith was prepared by IC II according to a slight modification of the method published by *Smått et al.*[231] and is described in detail in a recent publication by *Huber et al.*[102]. The monolith fragments varied in size between 5 to 15 mm in length and width. Deposition of AuNPs onto the surface of the SiO_2 monolith fragment was conducted in a similar manner as was described for the silica monoliths from an acid-base reaction using tetramethoxysilane as a silica source (see above). AuNP formation was achieved by *in situ* reduction of Au(III) from chloroauric acid ($HAuCl_4$ in 2 M HCl; 1,000 mg Au L⁻¹,

Sigma-Aldrich, St. Louis, USA) to Au(0). First, the pH of the gold solution was adjusted to 12-13 by adding 7 M NaOH (Merck, Darmstadt, Germany). The blank SiO_2 monolith was immersed in 10 mL of $4 \cdot 10^{-3}$ M alkaline gold solution. Then, 2.5 mL of a 0.22 M hydroxylamine hydrochloride ($NH_2OH \cdot HCl$, Merck, Darmstadt, Germany) solution was added as a mild reducing agent. The vessel was closed and placed on a shaker at 150 rpm for 15 min. The reduction of Au(III) to Au(0) is clearly visible as the light yellow alkaline gold solution turns immediately to a cloudy, purple solution upon addition of $NH_2OH \cdot HCl$. At the same time the formation of AuNPs aggregates, which settled to the bottom of the vessel after shaking, was observed. After the reduction step AuNPs seem to adhere to the SiO_2 monolith surface, as they appear dark purple after preparation in wet condition (see **Figure 60A**). The AuNP-coated silica monoliths (AuNP@SiO_2) were then thoroughly rinsed with UPW to remove the reaction solution. AuNP@SiO_2 was calcined in ambient air at 500°C with a heating rate of $1°C\ min^{-1}$. The maximum temperature of 500°C was hold for 2 h. The intensity of the color was reduced upon calcination, thus dry AuNP@SiO_2 exhibit a light pink color (see **Figure 60B**).
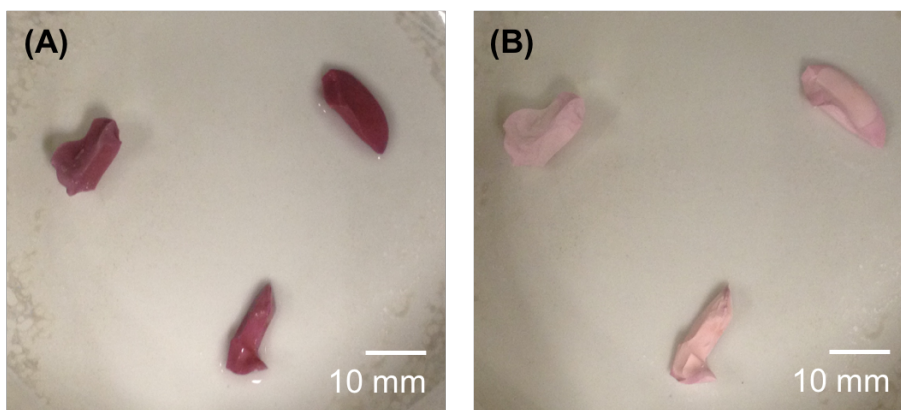
Figure 60: *Photograph of mesoporous-macroporous silica monoliths after immobilization of gold nanoparticles. (A) Dark purple appearance in wet condition after preparation and (B) after heating at 550°C.*

156

6.6. Cold vapor atomic fluorescence spectrometry

In this work, mercury detection by atomic fluorescence spectrometry was performed with a *Mercur* instrument (Analytik Jena AG, Jena, Germany). The fluorescence signal was measured at 253.7 nm and a detector voltage of 391 V. The device combines AFS with the cold vapor technique. Therefore, the spectrometer is equipped with a 1-channel and a 4-channel peristaltic pump, a reactor for the release of atomic mercury, a gas-liquid-separator, a built-in bulk gold collector for Hg(0) preconcentration and a low-pressure mercury lamp for fluorescence excitation. Depending on the number of samples the sample containers were exchanged manually or by an autosampler that is optionally connected to the *Mercur*. The instrument was applied for Hg determination according to the U.S. EPA method 1631, which is explained in more detail in the following section. For direct preconcentration of dissolved Hg onto nanogold-coated silica particles or novel nanogold-based dipsticks the optimized flow injection system (FIS) was connected to the *Mercur* for Hg detection.

6.6.1. Standard method U.S. EPA method 1631

CV-AFS was applied as a reference method for Hg ultratrace determination in this study. This technique is recommended by the U.S. EPA and by the European Union in terms of method 1631 and EN ISO 17852: 2006, respectively.[97,98] All detailed information on the instrumental set-up and the procedural steps for CV-AFS are described in the following section.

Procedure

The term *total mercury* is defined by the sum of all dissolved Hg species present in water without filtration. Hence, *total mercury* includes among others all Hg species bound to particulate matter. In this work, all real water samples were passed through 0.45-µm filters shortly after sampling. Hence, the *total dissolved mercury* concentration

was determined. According to the U.S. EPA method 1631 either 0.5% (v/v) 12 M hydrochloric acid or 0.5% (v/v) saturated bromine chloride (BrCl) solution is added to the sample for stabilization and minimization of analyte loss. Since in this work hydrochloric acid was used for preservation, BrCl was just added to the sample as oxidizing agent in a next step. Depending on the water matrix different volumes of BrCl were used. For clear water 0.5% (v/v) BrCl was added to the sample, 1% (v/v) or more was needed for brown and turbid water. The digestion of organic matter within real water samples takes at least 12 h at room temperature. In case of high concentrations of organic matter, *e.g.* wastewater, up to 5% (v/v) BrCl, higher temperatures and longer oxidation times are recommended to completely decompose the organic substances and release Hg in its "reducible" form Hg^{2+}. In this work, the amount of BrCl was increased stepwise until a constant yellow color of the samples occurred which referred to an excess of BrCl and thus to total oxidation of humic matter. Still, for some real water samples a visual differentiation between excess amount of BrCl and remaining dissolved organic matter, which is brownish to yellowish in color, was almost impossible. Before starting the measurement, excess halogens and interhalogens were decomposed by adding 0.2-0.25% (v/v) hydroxylammonium hydrochloride ($NH_2OH·HCl$) as a pre-reductant. If organic matter was completely decomposed by BrCl in the previous step, the yellow color disappears shortly after adding $NH_2OH·HCl$ and carefully shaking the sample. After this batch sample pretreatment, the following analytical steps were performed automated within the *Mercur* AFS. **Figure 61** shows the schematic set-up of the herein used *Mercur* AFS. During the first measurement of a statistical set of N repeating cycles the tubing between sample inlet and the 2-magnetic valve group (V2) was filled with the respective sample by a 1-channel peristaltic pump (P_M-1). This *pre-loading* step was omitted for the following measurements of the same sample. For the next step (*reaction*), P_M-1 continued to run and V2 was switched in a way that the sample entered the reactor (R). At the same time P_M-4 transported the carrier solution (0.5 M HCl) towards V2 where it was mixed with the sample and transferred to R. The reductant (0.105 M $SnCl_2·2H_2O$ solution in 1.008 M HCl) also entered R at an angle of 120°. Reduction of Hg(II) to volatile Hg(0) took place inside R. Elemental Hg(0) was then carried by an Ar stream (99.996%, MTI Industriegase AG, Neu-Ulm) towards the gas-liquid-separator (GLS), where the analyte was separated from the solution. Before

158

preconcentration of Hg(0) onto an built-in gold collector (Au1; Au/Pt alloy, fine-meshed net) the Hg(0)/Ar stream passed a water-permeable drying membrane (DM, Nafion®). Here, a second Ar stream flowed around the outer wall of the DM in a counterflow arrangement to remove remaining moisture. At the same time liquid was drained off from the GLS by means of P_M-4. A bubble sensor (BS) set behind the GLS automatically stopped the analysis in case of liquid flooding the GLS.
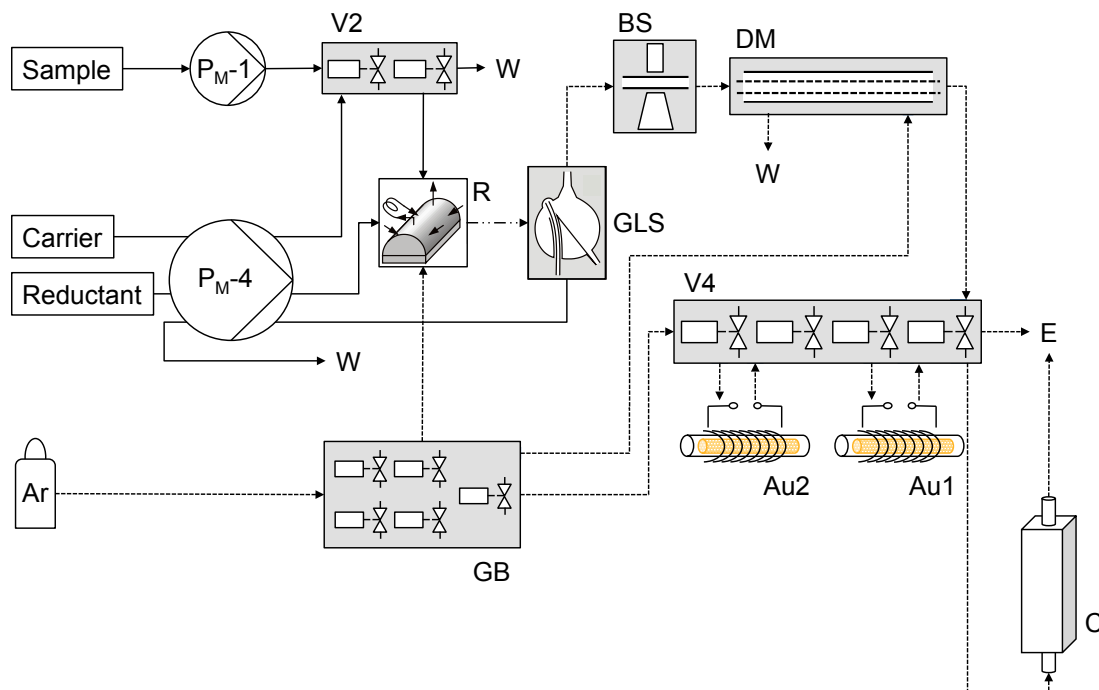
Figure 61: *Schematic set-up of CV-AFS system Mercur, solid line: liquid flow, dashed line: gas flow, dashed-dotted line: gas-liquid flow (Abbreviations: Ar argon, PM-1 1-channel peristaltic pump, PM-4 4-channel peristaltic pump, V2 magnetic valve group, V4 magnetic valve group, GB gas box, R reactor, GLS gas-liquid-separator, W waste, E exhaust, Au1 gold collector 1, Au2 gold collector 2, C cuvette, BS bubble sensor, DM drying membrane; modified and reprinted with permission from Analytik Jena AG[232], copyright 2014 by Analytik Jena AG).*

The sample volume was controlled by the reaction time and the pump speed of P_M-1. During the next step (*rinse 1*) P_M-4 continued running and transported the carrier (through V2) and the reductant towards R and the GLS. This set-up ensured that remaining sample solution was removed from the tubing and that the tubing and the reactor were rinsed. During an *auto-zero* step, precleaned Ar was passed over Au1 towards the quartz glass cuvette (C) to generate constant conditions during subsequent scattering measurement. *Heating* of Au1, *rinse 2* and *measurement* started

simultaneously after the *auto-zero* step. Release of Hg(0) from Au1 was initiated by the electric resistance heating. The temperature of the heating coil was regulated to approx. 630°C by an infrared sensor. The carrier gas transported thermally desorbed Hg(0) towards the quartz glass cuvette (inner dimension: 10 mm x 10 mm x 32 mm) that was adjusted in 90° position to the Hg vapor lamp for excitation. Subsequent *cooling* of Au1 by an axial fan adjusted the adsorbing material and the holding device to room temperature. The second built-in Au collector (Au2) was not used in this work. At the same time (*rinse 3*) precleaned Ar flushed the Au1 and the cuvette so that the fluorescence signal dropped down to a baseline level. *WinAAS* software (Analytik Jena AG, Jena, Germany) was used to control the instrument, signal acquisition and evaluation. In this work, a program recommended by Analytik Jena AG for total Hg determination *via* CV-AFS was applied. The program steps of a complete analysis cycle as well as detailed information on liquid and gas streams is given in **Table 28**.

Table 28: *WinAAS program „Enrichment/0... 1 µg L^{-1} (abbreviations: S sample, C carrier, Red reductant, Ar argon).*

No.	Program step	Duration [sec]	Flow rate [mL min^{-1}]
1	Loading (1st cycle only)	10	S: 8 [a]
2	Reaction	10	S: 8 [a], C/Red: 2 [b], Ar: 167
3	Rinse 1	30	C/Red: 2 [b], Ar: 167
4	Auto-zero	10	Ar: 83
5	Heating Au1	20	
	Rinse 2	15	Ar: 167
	Measurement	dng	
6	Cooling Au1	50	Ar: 167
	Rinse 3	25	
	Total	130	na

[a] Pharmed® tubing with inner diameter of 1.42 mm, [b] Pharmed® tubing with inner diameter of 0.89 mm for carrier (C) and reductant (Red) and 2.06 mm for waste; dng data not given: *measurement* begins with *heating Au1* and *rinse 2*, duration of measurement is not given in the *Mercur* manual, na not applicable.

Calibration

For external calibration of the system the fluorescence peak height was assigned to the respective Hg concentration of the standard solution. Quantification of unknown Hg concentrations in model solutions and real water samples was performed *via* two different strategies: A) Hg(II) standard solutions of at least three different final Hg concentrations were prepared from a 1 µg L^{-1} Hg stock solution. The standard solutions were pretreated with reagents (BrCl, NH$_2$OH·HCl) and the reaction time and analysis conditions were followed in the same way as for the sample measurement. Consequently, no blank correction was considered for data evaluation. B) Hg(II) standard solutions were prepared from a stock solution and were then directly reduced with SnCl$_2$·2H$_2$O within the automated CV-AFS. However, the Hg blank contribution resulting from BrCl and NH$_2$OH·HCl added to the sample was determined separately and considered for data evaluation.

6.7. Nanogold-assisted flow injection analysis system coupled to atomic fluorescence spectrometry

The following section describes the set-up of the in-house made FIAS, the applied materials and components as well as the analytical program steps for dissolved Hg determination in the ultratrace range. In addition, modifications of the set-up by means of integrated UV digestion and photocatalytic digestion are described.

Instrumental set-up and materials

Mercury detection was performed at 253.7 nm by AFS with a *Mercur* AFS (Analytik Jena AG, Jena, Germany), which was explained in more detail in the previous chapter. Here, *Mercur* AFS was merely used as detection technique rather than for Hg separation and preconcentration as it was used within CV-AFS (*e.g.* U.S. EPA method 1631). Thus,

all tubings that were used for the transport of the sample, the carrier and the reductant were disconnected. The two peristaltic pumps (P_M-1, P_M-4) that are mounted at the front side of the *Mercur* AFS were used for different liquid transports within the developed FIAS program. The Ar stream was also controlled by the *Mercur* AFS and allowed to feed distances within the FIAS as well as distances within the *Mercur* AFS itself during measurement. The in-house made FIAS consists of two peristaltic pumps (1-channel and 3-channel, modified HS60, Analytik Jena AG, Jena, Germany), six 2-way magnetic valves, a T-piece, a sample loop, a non-return valve, a heatable nanogold collector, a commercial fan, and a Peltier cooling device. *Mercur* AFS and the in-house made FIAS were interfaced to a personal computer controlled by *WinAAS* and *Hg-Speciation* software (Analytik Jena AG, Jena, Germany), respectively. In addition, a signal transducer (trigger) interlinked the two systems, which allowed a simultaneous start of the two programs. The in-house made FIAS was connected to the *Mercur* AFS *via* a gas-liquid-separator, thus providing a fully closed system. **Figure 62** shows a schematic set-up of the combined FIAS-AFS. For a better understanding the blue line highlights the components, which correspond to the *Mercur* AFS.

All magnetic valves, a holding device for the nanogold collector including a heating coil (Al-Fe-Cr alloy) and an infrared sensor were adjusted to a supporting plate (see **Figure 9** in chapter 4.1). This construction was coupled to a modified HS60 pump and linked to a personal computer. HS60 consists of a 1-channel (P_{Ex}-1) and a 4-channel peristaltic pump (P_{Ex}-4). The 2-way magnetic valves were used to direct the liquid streams and the Ar gas stream. A T-piece was used for the same manner, but it was indirectly controlled by a magnetic valve arranged behind. A non-return valve (NRV) was installed in front of the nanogold collector in the case of compensation of excess pressure during thermal desorption. A Peltier cooling was set behind the nanogold collector. The temperature set point varied between 4-15°C. The position of the magnetic valves, the pump speed, the temperature of the heating wire, the fan, the trigger signal and all respective durations were controlled by *Hg-Speciation* software. Pharmed® tubing (ID = 1.42 mm) was used for the transportation of all solutions with peristaltic pumps. All other tubing for gas and liquid flow consisted of methoxyfluoroalkyl (MFA, ID = 1 mm). The sample loop was made of MFA and varied in length depending on the required sample volume.
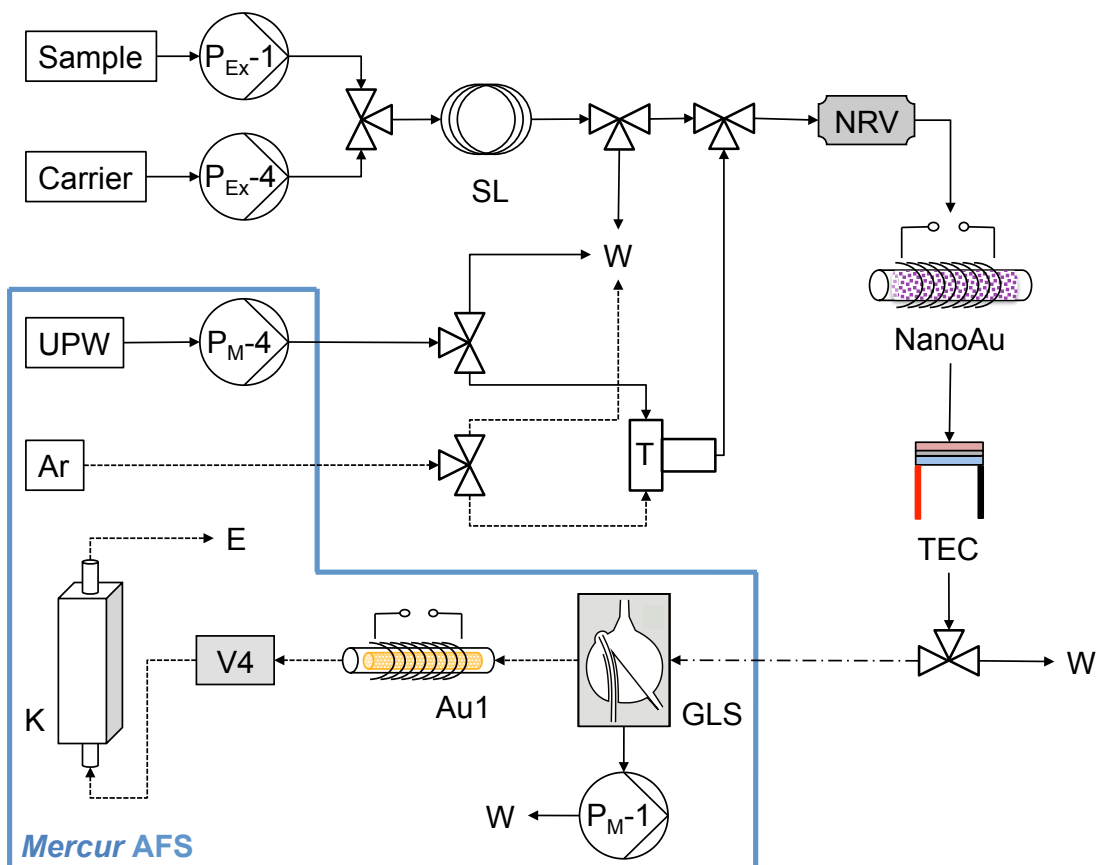
Figure 62: *Schematic set-up of the optimized FIAS-AFS, solid line: liquid flow, dashed line: gas flow, dashed-dotted line: gas-liquid flow (Abbreviations: Ar argon, PM-1 1-channel peristaltic pump, PM-4 4-channel peristaltic pump, V2 magnetic valve group, V4 magnetic valve group, GB gas box, R reactor, GLS gas-liquid-separator, W waste, E exhaust, Au1 gold collector 1, Au2 gold collector 2, C cuvette, BS bubble sensor, DM drying membrane; modified and reprinted with permission from Analytik Jena AG [232], copyright 2014 by Analytik Jena AG).*

Procedure

In a first step the sample loop was rinsed and filled with the sample. Then, the carrier solution (0.06 M HCl) passed the sample over the nanogold collector for preconcentration and subsequent rinsing. During these first steps, UPW and argon were directed to the liquid waste and the exhaust respectively, as the streams cannot be controlled manually. Instead, *WinAAS* program was set to *rinse 1* until cooling of the nanogold collector with UPW was completed (see also **Figure 62**). That means P_M-4

was continuously running and provided UPW to the FIAS. In addition, a constant argon stream from the gas box was directed to a magnetic valve of the FIAS. If UPW was needed for a program step the respective magnetic valve was switched in a way that UPW passed the T-piece and the nanogold collector subsequently. The argon carrier stream was controlled in an analogous manner. After Hg preconcentration the tubing and the nanogold collector were thoroughly rinsed with UPW to remove the carrier solution (0.06 M HCl). In a next step, argon passed the nanogold collector and removed water towards the liquid waste. During thermal desorption up to 700°C Hg(0) was released from the adsorbent and carried by Ar towards the built-in gold collector (Au1) of the *Mercur*. At the same time, the remaining water was evaporated inside the collector tube, which was subsequently condensed by a Peltier cooling device and separated from the analyte stream by a GLS. The liquid inside the GLS was drained off with a peristaltic pump (P_M-1) towards the liquid waste. The duration for sample loading, preconcentration and rinsing varied depending on the sample volume and kind of sample. Hence, **Figure 63** summarizes the procedure steps, time periods and flow rates for one analytical cycle using a sample volume of 7 mL as an example.

Procedural step FIAS	Flow rate S/C/A [ml min^{-1}]	Procedural step *Mercur*	Flow rate W/U/A [ml min^{-1}]
Sample load	S: 13.8	Reaction	W: 4.6
Sample transport & preconcentration	C: 4.7	Rinse 1	U: 4.6
Rinse (HCl)	C: 8.8		
Rinse (UPW)	U: 8.8		
Drying	A: 250		
Heating collector	A: 250		
Cooling (Ar)	A: 250		
Cooling (UPW)	U: 8.8		
Stand by	na	Auto-zero	A: 250
		Heating Au1/Rinse 2/ Measurement	A: 250
		Cooling Au1 Rinse 3	A: 250

Duration [sec]

(Time axis: 50, 100, 150, 200, 250, 300, 350, 400, 450)

Figure 63*: Optimized procedural steps for Hg determination by the flow injection analysis system coupled to Mercur AFS applying a sample volume of 7 mL. (abbreviations: S Sample, C Carrier, A Argon, U Ultrapure water, W Waste, na not applicable).*

Calibration

Aqueous standard solutions were prepared freshly from a 1 µg L^{-1} Hg(II) stock solution in 0.06 M HCl. The concentration range varied between the experiments and is given in detail in the respective chapters.

6.7.1. Nanogold-assisted flow injection analysis system with integrated UV digestion

The optimized FIAS-AFS for sensitive dissolved Hg detection from aqueous samples was further modified for online UV digestion of aqueous samples. The modification of the FIAS-AFS, the applied components and analytical steps are described within the following chapter.

Instrumental set-up for online UV modification of FIAS-AFS

The FIAS-AFS (see section 6.7) was modified for the online UV digestion of model solutions and real water samples. The schematic set-up of this modification with an integrated UV unit set before the nanogold collector is shown in **Figure 64**. The UV unit consists of a UV bulb (Narva UVU 11, 11 W, GLE mbH, Berlin, Germany) surrounded by an in-house made meander-formed quartz glass reaction tube (in-house; V = 9.12 mL, ID = 2.4 mm, OD = 4.0 mm, L = 201.7 cm) for online UV treatment of the solution. The applied UV bulb emits a single maximum at 253.7 nm, whereas higher-energy radiation (λ = 189 nm) is shielded by the lamp housing. A polypropylene (PP) tube covered with aluminum foil was used to protect the UV unit and to focus the radiation towards the sample inside the reaction tube (see **Figure 65**). Subsequent Hg preconcentration onto the nanogold-collector, thermal release of Hg(0) and AFS detection was conducted in the same manner as explained in section 6.7. The set-up of the FIAS-AFS and the procedural steps allowed that two sample replicates were processed at the same time. This caused a minimum residence time of the sample inside the reaction tube of 6 min. The UV bulb was manually switched on after the sample was completely transported to the reaction tube. For longer digestion times the FIA system was set idle, which prolongs at the same time the duration of the analysis. Here, for a higher sample throughput two additional T-pieces were used. This allowed simultaneous processing of the first replicate within the FIAS and AFS measurement of the second replicate. This means that while the first replicate was preconcentrated onto the nanogold collector,

followed by thermal desorption and AFS measurement, the second replicate was loaded into the sample loop, transported to the reaction tube and irradiated by the UV bulb.
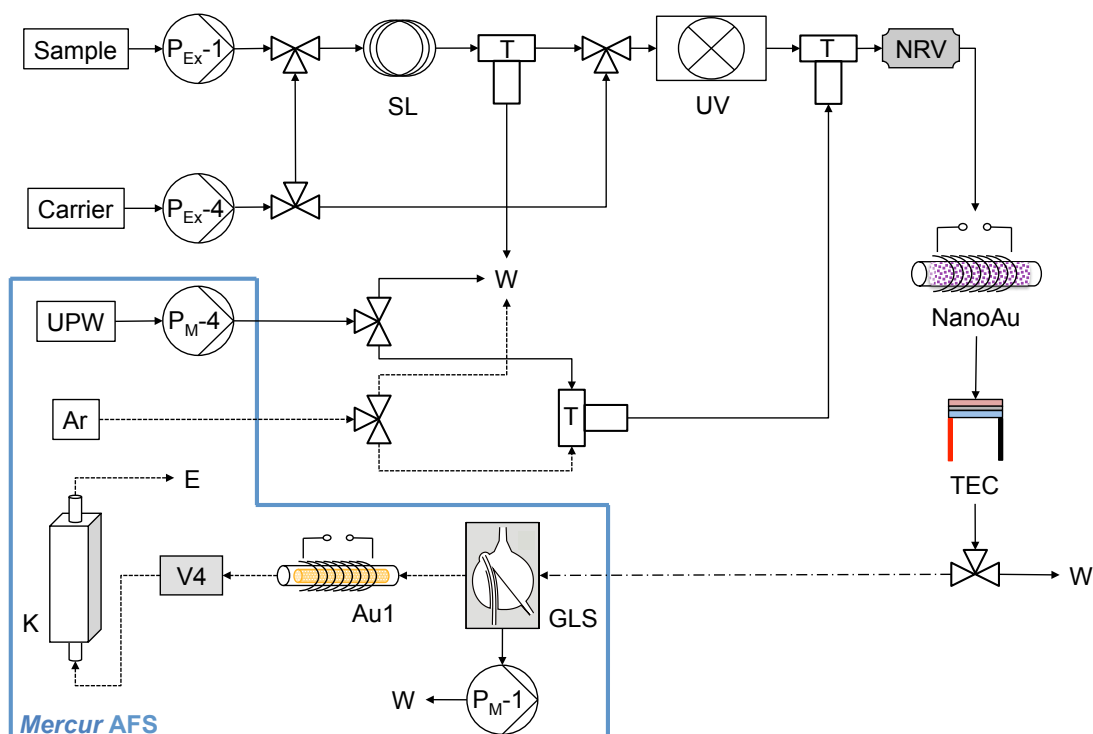
Figure 64: *Modification of the flow injection analysis system with integrated online UV digestion unit, solid line: liquid flow, dashed line: gas flow, dashed-dotted line: gas-liquid flow (abbreviations: Ar argon, P_M-1 1-channel peristaltic pump, P_M-4 4-channel peristaltic pump, GLS gas-liquid-separator, W waste, E exhaust, Au1 gold collector 1, C cuvette, P_{Ex}-1 1-channel peristaltic pump, P_{Ex}-4 4-cannel peristaltic pump, SL sample loop, T T-piece, UV UV digestion unit, NRV non-return valve, NanoAu nanogold collector, TEC thermo electric couple; modified and reprinted with permission from Analytik Jena AG[232], copyright 2014 by Analytik Jena AG).*
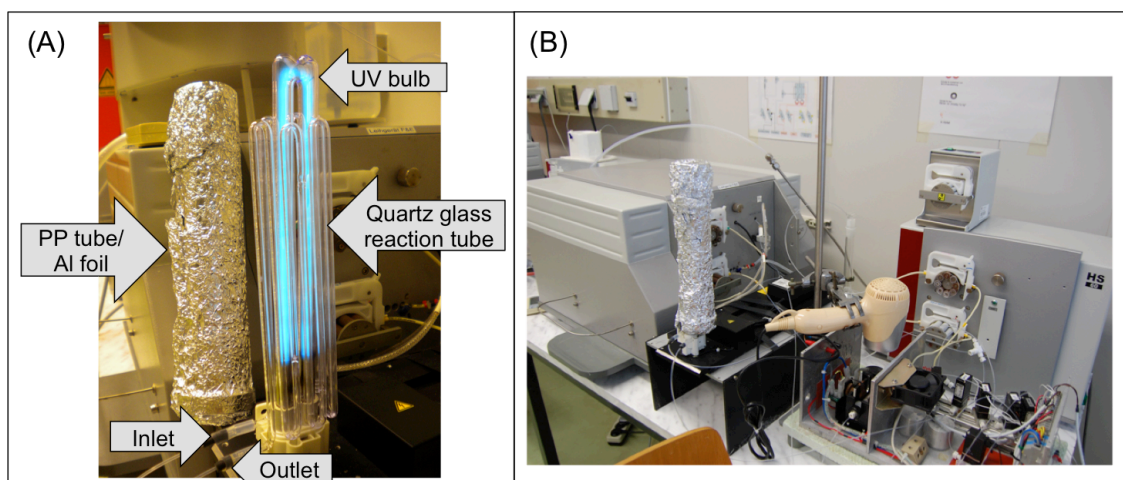
Figure 65: *Photograph of the online UV digestion unit (A) and photograph of the complete set-up of the FIAS-AFS with integrated UV bulb (B).*

Procedure for online UV modification of FIAS-AFS

To better understand the simultaneous processing of two sample replicates the analytical steps of the FIAS and for AFS measurement are separately displayed in **Figure 66**. In addition, the duration of each step and the corresponding liquid and gas flow rates are shown. As mentioned earlier in section 6.7, UPW and Ar gas were supplied by *Mercur* AFS. Thus, the AFS program was set to *rinse 1* after the AFS measurement was finished. The UPW flow and Ar carrier stream were controlled *via* magnetic valves and were thus either directed to the waste or towards the nanogold collector for cooling and drying of the material.

AFS program	Replicate 1	Rinse 1				Trapping of mercury on in-built collector		AFS Measure-ment
FIAS program	Replicate 1	Preconcentration of Hg onto nano-gold collector (UV pretreated sample)	-	Rinsing of nano-gold collector with UPW	Dry-ing with Ar	Heating of nano-gold collector to 700°C and release of Hg^0	Purging and transport of Hg^0 to AFS in-built collector	Rinsing and cooling with UPW
	Replicate 2	Load of sample	-	Transport of sample into UV reaction tube and UV irradiation				
Ar		-	-	-	-	250	250	250	-
S/C/UPW [mL min^{-1}]		S: 8.7; C: 4.7	C: 4.7	C: 6.1	UPW: 6.4	-	-	-	UPW: 6.4

time in s: 0   100   200   300   400   500

Figure 66: Time line of the flow injection program for online UV irradiation, mercury preconcentration onto nanogold collector, and atomic fluorescence spectrometric measurement (reprinted with permission from Leopold et al.[42], copyright 2012 by Springer-Verlag).

6.7.2. Nanogold-assisted flow injection analysis system with integrated photocatalytic digestion

A further modification of the optimized FIAS-AFS for Hg determination from aqueous samples was based on online photocatalytic sample digestion. The modification of the FIAS-AFS, the applied components and analytical steps are described.

168

Instrumental set-up for photocatalytic online UV digestion

For the photocatalytic online digestion of model solutions the FIAS-AFS was modified in a similar manner as compared to the UV (only) modification (see section 6.7.2). The UV unit was slightly adapted; a straight quartz glass tube that was coated with TiO_2 at the inner surface exchanged the meander-formed reaction tube. In addition, a high-energy UV bulb (10 W, Peschl UV-consulting, Mainz, Germany) was used as excitation source. In order to focus the UV irradiation towards the sample the UV bulb and the TiO_2 coated reaction tube were covered with aluminum foil.

TiO$_2$ coating of quartz glass surface from a suspension

The inner wall of a quartz glass tube (ID: 4 mm, AD: 6 mm, L: 140 mm, V = 1.76 mL) was coated with TiO_2 from a suspension. First, the quartz glass tube was cleaned with acetone in an ultrasonic bath. A suspension of 100 mg TiO_2 particles (titanium(IV) dioxide, ReagentPlus®, Sigma-Aldrich, St. Louis, USA) in 20 mL UPW was sonicated for 10 min. The cloudy suspension was subsequently pumped through the quartz glass tube to completely cover the inner surface of the reaction tube. After approx. 10 min the tube was emptied and repeatedly filled with TiO_2 suspension. After heating the tube at 180°C for 1 h a homogenous white layer was observed at the inner surface. For calcination the coated quartz glass tube was heated up to 550°C with a heating rate of 1°C min^{-1}. The temperature was kept for 2 h.

TiO$_2$ coating of quartz glass surface via sol-gel process

4.37 mL of titanium (IV) isopropoxide (TIP, 97+%, Alfa Aesar, Ward Hill, U.S.A.) was added dropwise to 25 mL ethanol (p.a., Merck, Darmstadt, Germany). The clear solution was pipetted into a precleaned quartz glass reaction tube (ID: 4 mm, AD: 6 mm, L: 140 mm, V=1.76 mL), which was sealed by parafilm at one end. The tube was emptied after approx. 5 min and the procedure was repeated 2 times. The tube was then

dried at room temperature overnight in a fume hood. For calcination the coated quartz glass tube was heated up to 550°C with a heating rate of 1°C min^{-1} and hold for 2 h at 550°C. As a result the inner wall of the tube was covered with a homogenous, stable, granular, white coating.

6.8. Procedure for mercury preconcentration onto nanogold-decorated adsorbents

The following chapter describes the procedure for direct Hg accumulation from aqueous solution onto AuNP-based adsorbents and subsequent thermal desorption and detection of Hg(0). Preliminary experiments focused on quartz glass tubes as substrate for AuNPs immobilization (AuNP@qt). Further investigations were conducted using AuNP-coated silica monoliths (AuNP@SiO$_2$) for Hg preconcentration. Hg accumulation was carried out by dipping the different adsorbents into the sample solution. Thermal desorption and detection of Hg(0) from the adsorbents were performed with an automated flow injection system coupled to an atomic fluorescence spectrometer.

Hg accumulation onto AuNP@qt

The preparation of nanogold-coated quartz glass tubes as a novel adsorbent for Hg preconcentration from a sample solution was described in section 6.5.2. AuNP@qt was exposed to 20 mL of a sample solution using a batch procedure at room temperature. The solution was filled into a precleaned glass vessel with snap-on cap. Accumulation times of 1, 5, 10, 30, 60, 140 and 190 min were examined. During the development and optimization of the procedure Hg(II) standard solution in 0.06 M HCl ([Hg] = 10, 50, 100 ng L^{-1}) were used. Hence, 0.06 M HCl was prepared as a blank solution. Furthermore, a real water sample was investigated by the same procedure (see section 5.1.5). Hg quantification was carried out by means of the standard addition method.

Therefore, the natural water was spiked with Hg(II) standard solution to a final Hg concentration of 10, 50 and 100 ng L^{-1}.

In addition, an in-house made sample holder with a total volume of 150 mL was tested during method development. This set-up allows simultaneous Hg accumulation onto maximum 6 AuNP@qt under the same conditions. The device consists of a beaker with 6 shorted glass pipettes that were fixed at the bottom. The AuNP@qt were thus put vertically onto the narrowed tip of the pipette (see **Figure 67**) and the vessel was filled with 150 mL sample solution and placed on a shaker. AuNP@qt were exposed to Hg(II) standard solutions ([Hg] = 0.1, 1, 3, 5, 10, 30, 50, 70 ng L^{-1}) for 10 min under turbulent conditions (150 rpm).
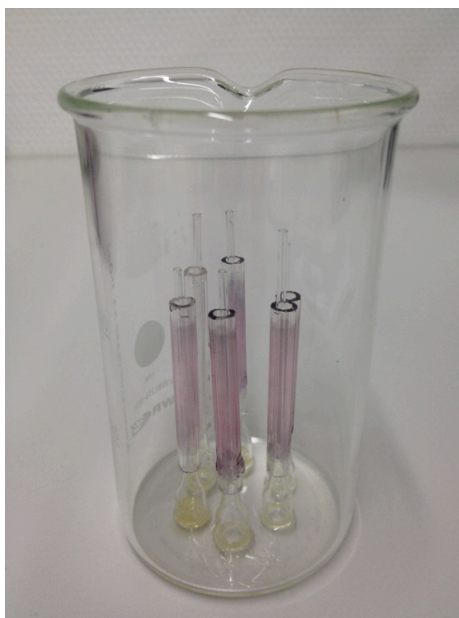
Figure 67: *Photograph of the in-house made sample holder for accumulation of dissolved Hg onto six gold nanoparticle-coated quartz glass tubes.*

Hg accumulation onto AuNP@SiO$_2$

The synthesis of silica monoliths and subsequent immobilization of AuNPs was depicted in section 6.5.3. AuNP@SiO$_2$ was exposed to 4, 5 and 4000 mL of a sample solution, using a batch procedure at room temperature. Accumulation times of 1, 3, 5, 7, 10, 30, 60, 1125, and 1135 min were investigated within this study. During the development

process Hg(II) standard solution in 0.06 M HCl were used as a sample solution similar to the approach described above. Spiked and non-spiked real water samples were treated similarly to Hg(II) standard solution. All experiments conducted with a total sample volume of 4 and 5 mL were performed using a precleaned glass vessel with snap-on cap. Some of the experiments were conducted under turbulent conditions. Therefore, the AuNP@SiO$_2$ was immersed in solution and the vessel was placed on a shaker at 150 rpm. For the simulation of an infinite water body a 4 L round-bottom flask was filled with the sample solution. A stirring bar was placed at the bottom of the flask for turbulent conditions. In order to keep the AuNP@SiO$_2$ in the center of the water body during accumulation an in-house made sampling device was constructed. It consists of a PTFE net carrier bag that is attached to a glass pipette with a nylon thread. A silicone stopper was attached below the carrier bag to prevent the AuNP@SiO$_2$ from floating on the surface of the solution. The holding device was linked to a glass stopper fitting the 4 L round-bottom flask. A scheme of this set-up is shown in **Figure 68**.
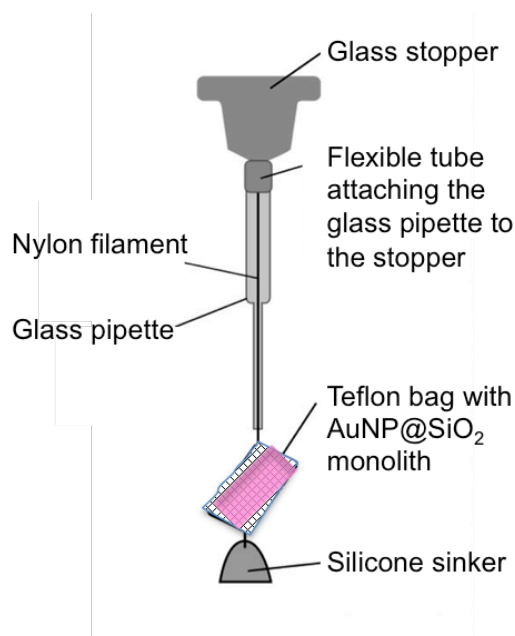
Figure 68: *Schematic illustration of the sampling device used for accumulation experiments in 4 L sample volume (reprinted with permission from Huber et al.[102], copyright 2015 by American Chemical Society).*

Thermal desorption and quantification of preconcentrated Hg

A general procedure was developed for the release and detection of Hg(0) after accumulation onto the novel AuNP-based adsorbents. AuNP@qt and AuNP@SiO$_2$ were removed carefully from the solution using tweezers and were rinsed thoroughly with UPW to remove residual sample solution. For thermal desorption of Hg(0) the adsorbent was placed in a quartz glass tube that was implemented to the heating cell of the FIAS-AFS. A scheme of this computer-controlled system is shown in **Figure 69**. The heating cell consists of a quartz glass tube (L: 75 mm; ID: 8.5 mm; AD: 10.5 mm) that is surrounded by a heating coil (Cr/Al/Fe; L: approx. 150 cm). Removable silicone plugs provide a sealed connection to the FIS *via* tubing (modified fluoralkoxy, MFA, ID: 1 mm) and allow introduction of the adsorbent. During thermal desorption Hg(0)
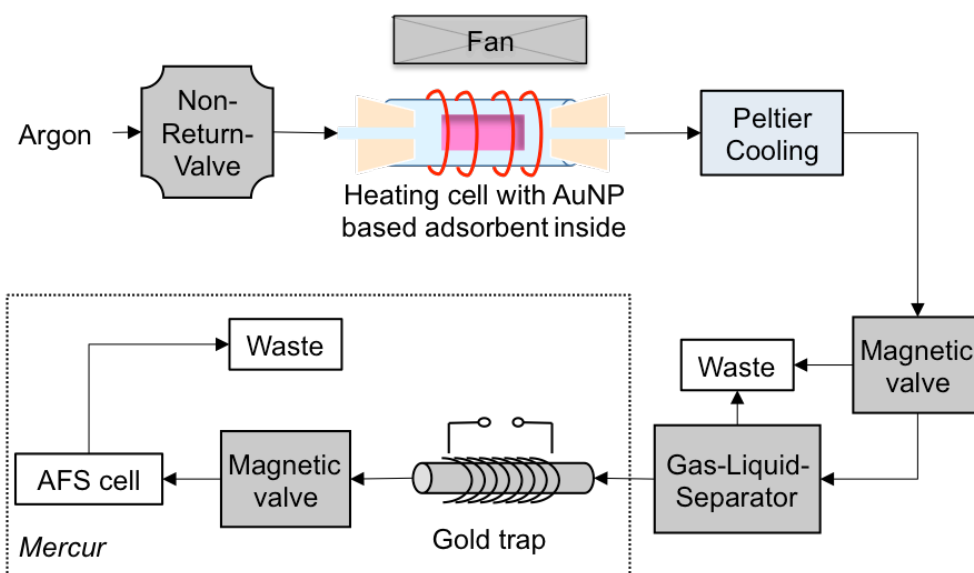
Figure 69: *Flow injection analysis system for thermal desorption of Hg(0) from nanogold-based adsorbent and detection by atomic fluorescence spectrometry. (reprinted with permission from Huber et al.[102], copyright 2015 by American Chemical Society).*

was transported towards the AFS measurement cuvette by an inert argon carrier stream (p = 4 bar). The temperature of the heating coil was controlled by *Hg-Speciation* software (Analytik Jena AG, Jena, Germany) and varied between 400-700°C. The temperature at the inner wall of the quartz glass tube was measured and controlled by a thermocouple. The optimized temperature program applied for gentle evaporating of remaining water and subsequent release of Hg(0) from the adsorbent is depicted in

Table 29. The water volume that is evaporated during the heating process is condensed inside a Peltier cooling device (Analytik Jena AG, Jena, Germany) and separated from the analyte by a GLS. The magnetic valves allow automated control of the gas flow within

Table 29: Temperature program for drying and thermal desorption of Hg(0) from nanogold-based adsorbent in the heating cell of the flow injection system (reprinted with permission from Huber et al.[102], copyright 2015 by American Chemical Society).

Time [sec]	Temperature [°C] [a]
10	20
30	82
50	178
70	606
90	614
110	614

[a] As measured at inner quartz glass tube wall.

the FIAS-AFS. Prior to each accumulation experiment Hg contamination from the heating cell and the adsorbent was removed to minimize blank contribution and to lower systematic errors. Therefore, the adsorbent was placed in the heating cell and Hg(0) was removed by successive thermal desorption until a constant fluorescence signal (FI < 0.0008) was obtained.

Calibration for Hg quantification

In order to quantify Hg mass that binds to the immobilized AuNPs (AuNP@qt, AuNP@SiO$_2$) under different experimental conditions, the optimized FIAS-AFS was calibrated using a packed column collector filled with AuNP-coated silica particles and Hg(II) standard solutions. The resulting fluorescence signals were assigned to the absolute mass of Hg as the preconcentration of dissolved Hg onto AuNP-coated silica proceeds quantitative from a defined sample volume (see chapter 4). The external calibration covers a linear working range from 3 to 235 pg when applying 2.8 to 4.7 mL

sample volume. However, it was shown earlier in chapter 4 that the linear range continues up to 2,400 pg Hg. The fluorescence signal derived from a non-spiked 0.06 M HCl was used for blank correction. An exemplary calibration function using Hg(II) standard solutions with a concentration of 5, 25 and 50 ng L^{-1} and a sample loop of 4.7 mL is presented in **Figure 70**. The analytical figures of merit for the respective calibration are listed in **Table 30**. For recovery experiments in a real water sample the AuNP@SiO$_2$ was first calibrated using Hg(II) standard solutions ([Hg] = 2, 5, 10,
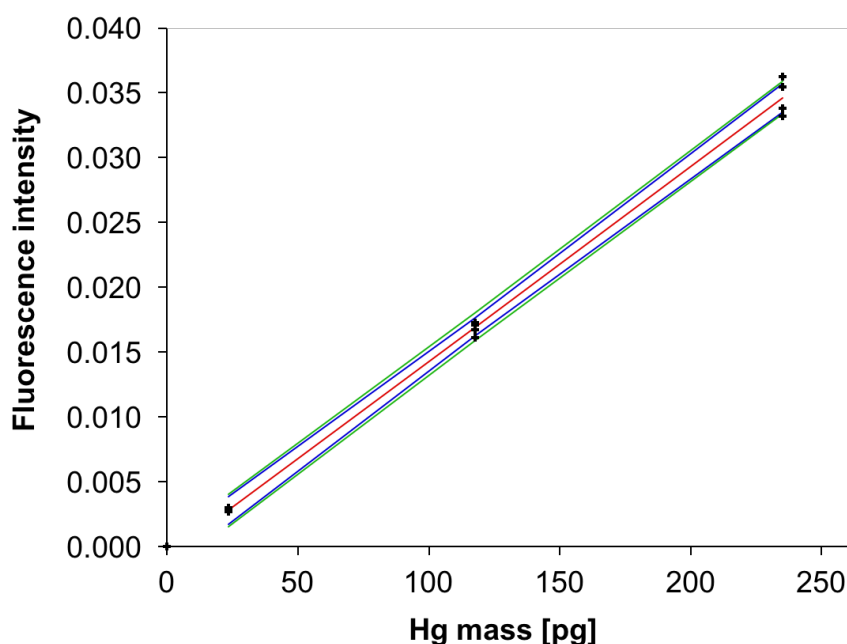
Figure 70: *Linear calibration function derived from packed column collector for quantification of Hg mass accumulated onto the dipstick (sample volume 4.7 mL; (+) calibration data, red: linear trend,* $FI = 0.0002 \cdot m(Hg) - 0.00078, R^2 = 0.9966$ *, n_c = 12, blue: confidence interval with P = 95%, green: prognosis interval).*

15 ng L^{-1}) in 0.06 M HCl. The adsorbent was exposed to 4 mL of the respective standard solution for 1 min under stirring (150 rpm). The fluorescence intensities were corrected by the average fluorescence intensity resulting from exposure of the adsorbent to solely a blank solution (0.06 M HCl) under the same conditions. As a next step, the seawater sample was spiked with Hg(II) standard solution to a final concentration of 2, 5, 10 and 15 ng L^{-1}. The adsorbent was exposed to 4 mL of Hg(II) spiked seawater in a similar manner as described above. For direct Hg determination of a freshwater sample, calibration experiments with AuNP@SiO$_2$ was performed in analog manner. The calibration function was $FI = 0.0002 \cdot c(Hg) + 0.0001$ with $R^2 = 0.9763$.

***Table 30**: Analytical figures of merit of the mass calibration with [Hg] = 5-50 ng L^{-1} (n_c = 12, sample volume 4.7 mL).*

Parameters	Achieved values
Linear working range	24 – 235 pg
Slope of the calibration function	$1.51 \cdot 10^{-4} \pm 6.16 \cdot 10^{-6}$ pg^{-1}
Intercept of the calibration function	$-7.79 \cdot 10^{-4} \pm 9.38 \cdot 10^{-4}$
Limit of detection	8.53 pg
Limit of quantification	17.07 pg
Regression coefficient (R^2)	0.9966
Method standard deviation	4.39%
Relative standard deviations (precision)	
For absolute Hg = 23.5 pg, n_s = 4	3.08%
For absolute Hg = 117.5 pg, n_s = 4	2.83%
For absolute Hg = 235.0 pg, n_s = 4	3.85%

6.9. UV-Vis absorption spectroscopy

The absorbance of humic acid in the spectral range from 190 to 1100 nm was measured using a double-beam spectrophotometer (*SPEKOL® 2000*, Analytik Jena AG, Jena, Germany) and polystyrene cuvettes (semi-micro; VWR International GmbH, Darmstadt, Germany). A HA stock solution of 500 mg C L^{-1} was prepared by dissolving 144.7 mg HA in 100 mL UPW. Subsequent dilutions (10, 25, 40, 50, 75, 100 mg C L^{-1}) were prepared freshly from this stock solution in UPW before absorption measurement. UPW was analyzed as a reference solution. As there is no distinct absorbance maximum visible in the spectra, the absorbance values at three fixed wavelengths - 400, 450 and 500 nm - were evaluated for calibration.

A HA solution with a DOC concentration of 25 mg C L^{-1} was irradiated by two different UV bulbs for 1, 3, 5 and 10 minutes and the absorbance was measured after irradiation. Two different UV bulbs served as radiation source. A UV lamp purchased from Narva GLE mbH (UVU 11, 11 W; Berlin, Germany) exhibits an emission maximum at

$\lambda = 254$ nm. Another UV lamp by Peschl UV-consulting (10 W; Mainz, Germany) exhibits two emission maxima at $\lambda = 254$ nm and $\lambda = 189$ nm. Thereby, a quartz glass lamp housing allows the transmission of the high energy UV radiation at 189 nm. The unknown DOC concentration of the UV-treated HA model solution was calculated as the average value derived from three calibration curves at 400, 450 and 500 nm.

6.10. TXRF measurements

The TXRF measurements were performed with a *S2 Picofox* (Bruker AXS GmbH, Karlsruhe, Germany) equipped with a molybdenum radiation source and a high efficiency silicon drift detector (SDD). Vanadium was added to the sample as an internal standard. Measurements were performed with *S2 Picofox* using a lifetime of 1,000 s, a generator voltage of 50 kV and a current of 600 µA. Gallium (Ga) was used for the gain correction before measurement. A volume of 10 µL of the homogenized sample was pipetted on a precleaned, siliconized quartz glass carrier. The solution was evaporated at 60 °C on a heating plate. The results were calculated using the *Spectra* software (Version: 7.2.5.0) of the *S2 Picofox* after a manual element assignment and the use of the *Profile Bayes* (optimized fit) option.

Gold loading of silica particles

The total gold load of nanogold-coated SiO_2 was determined by dissolving immobilized AuNPs in *aqua regia*. Therefore, 20-30 mg of the AuNP-coated silica particles were filled in a 10 mL volumetric flask. The exact amount was taken into account for calculation of the gold load in mg Au per g SiO_2. The particles were immersed in 300 µL HCl and 100 µL HNO_3 and were gently shaken at 80 rpm for 72 h on an orbital shaker. The glass stopper was fixed with parafilm due to the development of nitrous vapors during gold extraction. After complete dissolution the flasks were filled up to 10 mL with UPW. The samples were homogenized and 1 mL of the solution was

transferred to a 1.5-mL PP Eppendorf tube. Then, 10 µL were discarded and 10 µL of a vanadium standard solution (NH_4VO_3 in 0.5 M HCl, 1,000 mg L^{-1}; Merck, Darmstadt, Germany) was added for internal calibration. Thus, a vanadium concentration of 10 mg L^{-1} was obtained. The vessel was closed and the solution was thoroughly mixed using a vortex mixer (VWR International GmbH, Darmstadt, Germany) for approximately 20 sec. 10 µL of the homogenized sample was pipetted on a precleaned, siliconized quartz glass carrier and the solvent was evaporated on a heating plate before measurement.

Gold loading of silica monoliths

The gold amount on AuNP@SiO$_2$ was determined by TXRF after total dissolution in *aqua regia* similar to the procedure described above. The adsorbents were immersed in *aqua regia* over night and the solution was then diluted with UPW and spiked with 1 mg L^{-1} vanadium standard solution. After thoroughly mixing the solution, 10 µL of the homogenized sample was pipetted on a precleaned, siliconized quartz glass carrier and the solvent was evaporated on a heating plate before measurement.

6.11. SEM measurements

The imaging studies of the prepared nanogold-coated silica particles and monoliths were performed on a *Hitachi S-5200* cold field emission scanning electron microscope (Hitachi, Tokyo, Japan). The loose particles and the monoliths were attached to a stainless steel sample holder and the surface of the sample was covered with a few nm thick conductive layer of carbon (2,400 V, 90 mA). This film was deposited to overcome charging effects during the measurement. The instrument parameters during imaging were set to an acceleration voltage of 10 kV and an emission current of 10 µA. The morphology of the samples was visualized by detection of secondary and backscattered electrons.

6.12. Dissolved organic carbon analysis

The dissolved organic carbon concentration in filtered real water samples was measured by *Stephanie West* (*Siedlungswasserwirtschaft*, *Technical University of Munich*, Munich, Germany) with a total organic carbon analyzer (*High TOC II*, Elementar Analysensysteme GmbH, Hanau, Germany). Measurements were performed according to EN 1484 DEV H3 method. The detection limit of this method, as derived from 3σ criterion, is 1.0 mg L^{-1} and a relative standard deviation lower than 10% is obtained. Another set of real water samples was analyzed by Analytik Jena AG (Jena, Germany) with a *multi N/C 2100 S*. The limit of detection was determined as 181.5 µg L^{-1}.

6.13. Elemental analysis

The elemental composition (C, H, N, S, O) of humic and fulvic acids was performed by *Margit Lang* at the *Service Center Elemental Analysis* (*Institute of Analytical and Bioanalytical Chemistry*, *Ulm University*, Ulm, Germany). For a twofold measurement approx. 5 mg of the sample were weighed in an aluminum carrier. A *vario MICRO cube* (Elementar Analysensysteme GmbH, Hanau, Germany) equipped with an autosampler was used for analysis.

7. Applied statistics

In the following chapter the equations used for a statistical evaluation of the measurement results are illustrated and briefly explained.

7.1. Mean and standard deviation

Analytical results have constant and proportional systematical errors. They influence the trueness of an analytical method and thus have to be identified and minimized. Constant systematical errors can arise from the sample matrix and are independent on the analyte concentration. Proportional systematical errors result from the analytical procedure (*e.g.* sample digestion, adsorption to vessel wall) or from matrix components and are dependent on the analyte concentration. Furthermore, unavoidable statistical errors occur within an analytical procedure. They influence the precision of an analytical result and have to be calculated from a n-fold measurement.

Each analyte concentration is measured n times with y_i as the value of an individual measurement. The mean value $\bar{y}$ is then calculated from equation 7.1.

Equation 7.1: Mean value

$$\bar{y} = \frac{1}{n} \sum_{i=1}^{n} y_i$$

The standard deviation is a measure for the deviation of the individual values from the mean value and obtained from equation 7.2.

Equation 7.2: Standard deviation

$$s = \sqrt{\frac{\sum_{i=1}^{n} (y_i - \bar{y})^2}{n-1}}$$

7.2. Calibration

A calibration experiment was performed with the optimized flow injection analysis system coupled to atomic fluorescence spectrometry using aqueous standard solutions. A linear regression ($\hat{y}_i = bx_i + a$) with the slope b and the ordinate intercept a is then calculated by the minimum squares method. Solving the calibration function for x and applying the mean measurement value results in the concentration of an unknown sample. The analytical figures of merit are presented in the following section.

Equation 7.3: Slope of the linear regression

$$b = \frac{\sum_{i=1}^{N}[(x_i - \bar{x}) \cdot (y_i - \bar{y})]}{\sum_{i=1}^{N}(x_i - \bar{x})^2}$$

The ordinate intercept is then calculated by using equation 7.4.

Equation 7.4: Ordinate intercept

$$a = \bar{y} - b\bar{x}$$

$$\bar{x} = \frac{1}{N}\sum_{i=1}^{N} x_i$$

$$\bar{y} = \frac{1}{N}\sum_{i=1}^{N} y_i$$

The deviation of the individual results y_i of the ith measurement with respect to the linear regression is defined by the residual standard deviation s_y calculated by equation 7.5. Here, $\hat{y}_i$ is the ith calculated measurement value of the linear regression function. N_c is the total number of calibration measurements.

Equation 7.5: Residual standard deviation

$$s_y = \sqrt{\frac{\sum_{i=1}^{N}(y_i - \hat{y}_i)^2}{N - 2}}$$

The standard deviation of the procedure describes the performance of an analytical method and was calculated form equation 7.6.

Equation 7.6: Standard deviation of the procedure

$$s_{x0} = \frac{s_y}{b}$$

The coefficient of variation of the procedure V_{x0} was calculated from equation 7.7, where $\bar{x}$ is the mean of all standard concentrations x_i.

Equation 7.7: Coefficient of variation of the procedure

$$V_{x0} = \frac{s_{x0}}{\bar{x}} \cdot 100(\%)$$

The confidence interval (CI) and the prognosis interval (PI) of the linear regression were calculated from equation 7.8 and 7.9. F is the table value of the F-test with the statistical safety P ($f_1 = 2$ and $f_2 = N-2$), The student-t-factor t with statistical safety P and variance f (N_c-2) is applied to calculate the prognosis interval. The number of future measurements of a sample is expressed as N_m and y_m is the mean value of the future measurements.

Equation7. 8: Confidence interval

$$CI = \sqrt{2 \cdot F(P, f_1, f_2)} \cdot s_y \cdot \sqrt{\frac{1}{N_c} + \frac{(x_i - \bar{x})^2}{\sum_{i=1}^{N}(x_i - \bar{x})^2}}$$

Equation 7.9: Prognosis interval

182

$$PI = t(P,f) \cdot \frac{s_y}{b} \cdot \sqrt{\frac{1}{N_m} + \frac{1}{N_c} + \frac{(\bar{y}_m - \bar{y})^2}{b^2 \sum_{i=1}^{N}(x_i - \bar{x})^2}}$$

The uncertainty of the slope Δb and the ordinate intercept Δa of the linear regression are derived from equation 7.10 and 7.11.

Equation 7.10: Uncertainty of the slope

$$\Delta b = t(P,f) \cdot s_y \cdot \sqrt{\frac{1}{\sum_{i=1}^{N_c}(x_i - \bar{x})^2}}$$

Equation 7.11: Uncertainty of the intercept

$$\Delta a = t(P,f) \cdot s_y \cdot \sqrt{\frac{1}{N_c} + \frac{\bar{x}^2}{\sum_{i=1}^{N_c}(x_i - \bar{x})^2}}$$

The limit of detection (LOD) and the limit of quantification (LOQ) were derived from equation 7.12 and 7.13 with the help of the auxiliary value y_c. The value is derived from the ordinate intercept at the upper confidence interval ($x = 0$) and was calculated by equation 7.11:

Equation 7.11: Auxiliary value y_c

$$y_c = a + t(P,f) \cdot s_y \cdot \sqrt{\frac{1}{N_m} + \frac{1}{N_c} + \frac{\bar{x}^2}{\sum_{i=1}^{N}(x_i - \bar{x})^2}}$$

Equation 7.12: Limit of detection

$$LOD = t(P,f) \cdot \frac{s_y}{b} \cdot \sqrt{\frac{1}{N_m} + \frac{1}{N_c} + \frac{(y_c - \bar{y})^2}{b^2 \sum_{i=1}^{N}(x_i - \bar{x})^2}}$$

Equation 7.13: Limit of quantification

$$LOQ = 2 \cdot LOD$$

7.3. Expanded uncertainties

For the evaluation of the accuracy of an analytical method measurement values can be compared with values derived from a standard method performed in the same laboratory or from an external laboratory (intercalibration exercise). On the other hand, the method performance can be investigated by the measurement of a certified reference material. To proof if there is a significant difference between the measured value and the certified value, the absolute difference Δ_m between the measured c_m and the certified value c_{crm} is calculated by equation 14. In addition, the combined uncertainty u_Δ is calculated from the sum of the uncertainties (see equation 7.15).

Equation 7.14: Absolute difference

$$\Delta_m = |c_m - c_{crm}|$$

Equation 7.15: Combined uncertainty

$$u_\Delta = \sqrt{u_m^2 + u_{crm}^2}$$

The extended uncertainty (U_Δ) is derived from the coverage factor k as $U_\Delta = k \cdot u_\Delta$. For the case that $\Delta_m \leq U_\Delta$ there is no significant difference between the measured value and the certified value, meaning the validation was successful. A significant difference between the values is observed if $\Delta_m > U_\Delta$.

Bibliography

[1]   UNEP, *Global Mercury Assessment 2013: Sources, Emissions, Releases and Environmental Transport*, Geneva, **2013**.

[2]   N. Pirrone, S. Cinnirella, X. Feng, R. B. Finkelman, H. R. Friedli, J. Leaner, R. Mason, A. B. Mukherjee, G. B. Stracher, D. G. Streets, et al., *Atmospheric Chem. Phys.* **2010**, *10*, 5951–5964.

[3]   *Regulation (EC) No 1102/2008 of the European Parliament and the Council of 22 October 2008 on the Banning of Exports of Metallic Mercury and Certain Mercury Compounds and Mixtures and the Safe Storage of Metallic Mercury*, **2008**.

[4]   *Mercury Export Ban (US)*, **2008**.

[5]   US EPA, "Minamata Convention on Mercury," can be found under https://www.epa.gov/international-Cooperation/minamata-Convention-Mercury, **2017**.

[6]   E. G. Pacyna, J. M. Pacyna, F. Steenhuisen, S. Wilson, *Atmos. Environ.* **2006**, *40*, 4048–4063.

[7]   R. P. Mason, A. L. Choi, W. F. Fitzgerald, C. R. Hammerschmidt, C. H. Lamborg, A. L. Soerensen, E. M. Sunderland, *Environ. Res.* **2012**, *119*, 101–117.

[8]   N. E. Selin, D. J. Jacob, R. J. Park, R. M. Yantosca, S. Strode, L. Jaeglé, D. Jaffe, *J. Geophys. Res.* **2007**, *112*, 1–14.

[9]   D. P. Krabbenhoft, C. L. Barbiaz, *Water Resour. Res.* **1992**, *28*, 3119–3128.

[10]   C. T. Driscoll, Y. Cheng, C. L. Schofield, R. Munson, J. Holsapple, *Environ. Sci. Technol.* **1994**, *28*, 136A–143A.

[11]   C. H. Lamborg, C. R. Hammerschmidt, K. L. Bowman, G. J. Swarr, K. M. Munson, D. C. Ohnemus, P. J. Lam, L.-E. Heimbürger, M. J. A. Rijkenberg, M. A. Saito, *Nature* **2014**, *512*, 65–68.

[12]   C. H. Lamborg, C. R. Hammerschmidt, G. A. Gill, R. P. Mason, S. Gichuki, *Limnol. Oceanogr. Methods* **2012**, *10*, 90–100.

[13]   R. P. Mason, K. R. Rolfhus, W. F. Fitzgerald, *Water. Air. Soil Pollut.* **1995**, *80*, 665–677.

[14]   N. Bloom, *Can. J. Fish. Aquat. Sci.* **1989**, *46*, 1131–1140.

[15]   C. C. Gilmour, E. A. Henry, *Environ. Pollut.* **1991**, *71*, 131–169.

[16]   M. Harada, *Crit. Rev. Toxicol.* **1995**, *25*, 1–24.

[17]   *Verordnung (EG) Nr. 1881/2006 Der Kommission Vom 19. Dezember 2006 Zur Festsetzung Der Höchstgehalte Für Bestimmte Kontaminanten in Lebensmitteln*, **2006**.

[18]   *World Health Organization. Guidelines for Drinking-Water Quality, FIRST ADDENDUM TO THIRD EDITION, Volume 1, Recommendations.*, **2006**.

[19]   US EPA, "National Primary Drinking Water Regulations," can be found under https://www.epa.gov/ground-Water-and-Drinking-Water/national-Primary-Drinking-Water-Regulations, **2017**.

[20]   K. Leopold, M. Foulkes, P. Worsfold, *Anal. Chim. Acta* **2010**, *663*, 127–138.

[21]   J. Huber, K. Leopold, *TrAC Trends Anal. Chem.* **2016**, *80*, 280–292.

[22]   K. Leopold, M. Foulkes, P. J. Worsfold, *Anal. Chem.* **2009**, *81*, 3421–3428.

[23]   A. Zierhut, K. Leopold, L. Harwardt, P. Worsfold, M. Schuster, *J. Anal. At. Spectrom.* **2009**, *24*, 767–774.

[24]   A. Zierhut, K. Leopold, L. Harwardt, M. Schuster, *Talanta* **2010**, *81*, 1529–1535.

[25]   N. Wiberg, *Lehrbuch der Anorganischen Chemie*, De Gruyter, Berlin, Boston, **2008**.

[26]   "2015-11-30_phasing_out_table_for_website.pdf," can be found under http://www.eurochlor.org/media/100675/2015-11-30_phasing_out_table_for_website.pdf, **n.d.**

[27]   C. D. Holmes, D. Jacob, X. Yang, *Geophys. Res. Lett.* **2006**, *33*, 1–4.

[28]   W. F. Fitzgerald, D. R. Engstrom, R. P. Mason, E. A. Nater, *Environ. Sci. Technol.* **1998**, *32*, 1–7.

[29]   J. Sommar, K. Garfeldt, D. Strömberg, X. Feng, *Atmos. Environ.* **2001**, *35*, 3049–3054.

[30]   J. J. S. Tokos, B. Hall, J. A. Calhoun, E. M. Prestbo, *Atmos. Environ.* **1998**, *32*, 823–827.

[31]   J. Munthe, *Atmos. Environ.* **1992**, *26A*, 1461–1468.

[32]   A. Iverfeldt, O. Lindqvist, *Atmos. Environ.* **1986**, *20*, 1567–1573.

[33]   R. P. Mason, W. F. Fitzgerald, F. M. M. Morel, *Geochim. Cosmochim. Acta* **1994**, *58*, 3191–3198.

[34]   H. M. Amos, D. J. Jacob, D. Kocman, H. M. Horowitz, Y. Zhang, S. Dutkiewicz, M. Horvat, E. S. Corbitt, D. P. Krabbenhoft, E. M. Sunderland, *Environ. Sci. Technol.* **2014**, *48*, 9514–9522.

[35]   R. P. Mason, K. R. Rolfhus, W. F. Fitzgerald, *Mar. Chem.* **1998**, *61*, 37–53.

[36]   R. P. Mason, W. F. and Fitzgerald, *Water. Air. Soil Pollut.* **1991**, *56*, 779–789.

[37]   R. P. Mason, K. A. Sullivan, *Deep Sea Res. Part II Top. Stud. Oceanogr.* **1999**, *46*, 937–956.

[38]   G. A. Gill, W. F. Fitzgerald, *Geochim. Cosmochim. Acta* **1988**, *52*, 1719–1728.

[39]   Y.-H. Lee, A. Iverfeldt, *Water. Air. Soil Pollut.* **1991**, *56*, 309–321.

[40]   R. J. Kieber, N. E. Parler, S. A. Skrabal, J. D. Willey, *J. Atmospheric Chem.* **2008**, *60*, 153–168.

[41]   G. A. Gill, K. W. Bruland, *Environ. Sci. Technol.* **1990**, *24*, 1392–1400.

[42]   K. Leopold, A. Zierhut, J. Huber, *Anal. Bioanal. Chem.* **2012**, *403*, 2419–2428.

[43]   R. P. Mason, K. A. Sullivan, *Environ. Sci. Technol.* **1997**, *31*, 942–947.

[44]   J. Kotnik, M. Horvat, V. Fajon, M. Logar, *Water. Air. Soil Pollut.* **2002**, *134*, 317–337.

[45]   J. K. Schäfer, J. Letowski, T. Barkay, *Geomicrobiol. J.* **2002**, *19*, 87–102.

[46]   W. Stumm, J. J. Morgan, *Aquatic Chemistry. Chemical Equilibria Rates in Natural Waters*, Wiley - Interscience, **1996**.

[47]   F. M. Morel, A. M. Kraepiel, M. Amyot, *Annu. Rev. Ecol. Syst.* **1998**, 543–566.

[48]   "mercuryexposure_fluorescentbulbs_factsheet.pdf," can be found under https://www.osha.gov/Publications/mercuryexposure_fluorescentbulbs_factsheet.pdf, **2016**

[49]   Bundesanstalt für Arbeitsschutz und Arbeitsmedizin, *Technische Regel Für Gefahrstoffe 900 - Arbeitsplatzgrenzwerte*, **2006**.

[50]   G. Drasch, S. Böse-O'Reilly, C. Beinhoff, G. Roider, S. Maydl, *Sci. Total Environ.* **2001**, *267*, 151–168.

[51]   T. W. Clarkson, L. Magos, *Crit. Rev. Toxicol.* **2006**, *36*, 609–662.

[52]   T. Tomiyasu, A. Matsuyama, T. Eguchi, Y. Fuchigami, K. Oki, M. Horvat, R. Rajar, H. Akagi, *Sci. Total Environ.* **2006**, *368*, 283–290.

[53]   L. Guo, P. H. Santschi, *Mar. Chem.* **1996**, *55*, 113–127.

[54]   G. Copin-Montégut, B. Avril, *Deep-Sea Res. I* **1993**, *40*, 1963–1972.

[55]   C. R. Hammerschmidt, K. L. Bowman, M. D. Tabatchnick, C. H. Lamborg, *Limnol. Oceanogr. Methods* **2011**, *9*, 426–431.

[56]   E. R. M. Druffel, P. M. Williams, J. E. Bauer, J. R. Ertel, *J. Geophys. Res.* **1992**, *97*, 15639.

[57]   J. A. Leenheer, *Environmental Chemistry of Lakes and Reservoirs*, American Chemical Society, **1994**.

[58]   S. Boggs, D. G. Livermore, M. G. Seitz, *J. Macromol. Sci. Part C* **1985**, *25*, 599–657.

[59]   J. A. Leenheer, *Environ. Sci. Technol.* **1981**, *15*, 578–587.

[60]   E. M. Thurman, R. L. Malcolm, *Environ. Sci. Technol.* **1981**, *15*, 463–466.

[61]   G. M. Day, R. Beckett, B. T. Hart, I. D. McKelvie, *Aust. J. Mar. Freshw. Res.* **1991**, *42*, 675–687.

[62]   P. J. Curtis, H. E. Adams, *Biogeochemistry* **1995**, *30*, 59–76.

[63]   N. Bano, M. A. Moran, R. E. Hodson, *Aquat. Microb. Ecol.* **1997**, *12*, 233–238.

[64]   T. Mattsson, P. Kortelainen, M. B. David, *Environ. Int.* **1998**, *24*, 521–525.

[65]   *Aquatic Humic Substances - Ecology and Biogeochemistry | Dag Hessen | Springer*, **n.d.**

[66]   G. R. Harvey, D. A. Boran, L. A. Chesal, J. M. Tokar, *Mar. Chem.* **1983**, *12*, 119–132.

[67] Y.-P. Chin, G. Aiken, E. O'Loughlin, *Environ. Sci. Technol.* **1994**, *28*, 1853–1858.

[68] M. Schnitzer, *Dev. Soil Sci.* **1978**, *8*, 1–64.

[69] C. Steinberg, *Ecology of Humic Substances in Freshwaters*, Springer, **2003**.

[70] R. L. Malcolm, *Anal Chim Acta* **1990**, *232*, 19–30.

[71] E. M. Pena-Mendez, J. Havel, J. Patocka, *J. Appl. Biomed.* **2005**, *3*, 13–24.

[72] N. T. Loux, *Chem. Speciat. Bioavailab.* **1998**, *10*, 127–136.

[73] R. K. Kolka, D. F. Grigal, E. S. Verry, E. A. Nater, *J. Environ. Qual.* **1999**, *28*, 766–775.

[74] J. B. Shanley, P. F. Schuster, M. M. Reddy, D. A. Roth, H. E. Taylor, G. R. Aiken, *Eos Trans. Am. Geophys. Union* **2002**, *83*, 45–48.

[75] T. M. Grieb, C. T. Driscoll, S. P. Gloss, C. L. Schofield, G. L. Bowie, D. B. Porcella, *Env. Toxicol Chem* **1990**, *9*, 919–930.

[76] T. A. Haines, V. T. Komov, V. E. Matey, C. H. Jagoe, *Water. Air. Soil Pollut.* **1995**, *85*, 823–828.

[77] G. Mierle, R. Ingram, *Water. Air. Soil Pollut.* **1991**, *56*, 349–357.

[78] C. T. Driscoll, V. Blette, C. Yan, C. L. Schofield, R. Munson, J. Holsapple, *Water. Air. Soil Pollut.* **1995**, *80*, 499–508.

[79] K. Xia, U. L. Skyllberg, W. F. Bleam, P. R. Bloom, E. A. Nater, P. A. Helmke, *Environ. Sci. Technol.* **1999**, *33*, 257–261.

[80] K. Xia, F. Weesner, W. F. Bleam, P. R. Bloom, U. L. Skyllberg, P. A. Helmke, *Soil Sci Soc Am J* **1998**, *62*, 1240–1246.

[81] M. Ravichandran, G. R. Aiken, M. M. Reddy, J. N. Ryan, *Environ. Sci. Technol.* **1998**, *32*, 3305–3311.

[82] M. Ravichandran, G. R. Aiken, J. N. Ryan, M. M. Reddy, *Env. Sci Technol* **1999**, *33*, 1418–1423.

[83] M. Ravichandran, *Chemosphere* **2004**, *55*, 319–331.

[84] J. M. Benoit, R. P. Mason, C. C. Gilmour, G. R. Aiken, *Geochim. Cosmochim. Acta* **2001**, *65*, 4445–4451.

[85] R. T. Drexel, M. Haitzer, J. N. Ryan, G. R. Aiken, K. L. Nagy, *Environ. Sci. Technol.* **2002**, *36*, 4058–4064.

[86] H. Hsu, D. Sedlak, *Environ. Sci. Technol.* **2003**, *37*, 2743–2749.

[87] C. H. Lamborg, C.-M. Tseng, W. F. Fitzgerald, P. H. Balcom, C. R. Hammerschmidt, *Environ. Sci. Technol.* **2003**, *37*, 3316–3322.

[88] B. M. Miskimmin, *Bull. Environ. Contam. Toxicol.* **1991**, *47*, 743–750.

[89] J. P. Hurley, J. M. Benoit, C. L. Babiarz, M. M. Shafer, A. W. Andren, J. R. Sullivan, R. Hammond, D. A. Webb, *Environ. Sci. Technol.* **1995**, *29*, 1867–1875.

[90]   H. Hintelmann, P. M. Welbourn, R. D. Evans, *Water. Air. Soil Pollut.* **1995**, *80*, 1031–1034.

[91]   N. Ferrúa, S. Cerutti, J. A. Salonia, R. A. Olsina, L. D. Martinez, *J. Hazard. Mater.* **2007**, *141*, 693–699.

[92]   M. K. Rofouei, A. Sabouri, A. Ahmadalinezhad, H. Ferdowsi, *J. Hazard. Mater.* **2011**, *192*, 1358–1363.

[93]   N. Bloom, W. F. Fitzgerald, *Anal. Chim. Acta* **1988**, *208*, 151–161.

[94]   H. Pyhtilä, P. Perämäki, J. Piispanen, M. Niemelä, T. Suoranta, M. Starr, T. Nieminen, M. Kantola, L. Ukonmaanaho, *Microchem. J.* **2012**, *103*, 165–169.

[95]   W. R. L. Cairns, M. Ranaldo, R. Hennebelle, C. Turetta, G. Capodaglio, C. F. Ferrari, A. Dommergue, P. Cescon, C. Barbante, *Anal. Chim. Acta* **2008**, *622*, 62–69.

[96]   I. N. Aretaki, P. Koulouridakis, N. Kallithrakas-Kontos, *Anal. Chim. Acta* **2006**, *562*, 252–257.

[97]   W. A. Telliard, *Federal Register, EPA-821-R-02-019 Method 1631 Revision E*, **2002**.

[98]   Deutsches Institut für Normung, *ISO 17852:2006, Water Quality, Determination of Mercury, Method Using Atomic Fluorescence Spectrometry*, **2006**.

[99]   B. Hu, M. He, B. Chen, *Anal. Bioanal. Chem.* **2015**, *407*, 2685–2710.

[100] M.-L. Riekkola, *J. Chromatogr. A* **2011**, *1218*, 619.

[101] L. He, C.-S. Toh, *Anal. Chim. Acta* **2006**, *556*, 1–15.

[102] J. Huber, L.-E. Heimbürger, J. E. Sonke, S. Ziller, M. Lindén, K. Leopold, *Anal. Chem.* **2015**, *87*, 11122–11129.

[103] G.-W. Wu, S.-B. He, H.-P. Peng, H.-H. Deng, A.-L. Liu, X.-H. Lin, X.-H. Xia, W. Chen, *Anal. Chem.* **2014**, *86*, 10955–10960.

[104] Y. Cui, S. Liu, K. Wei, Y. Liu, Z. Hu, *Microchim. Acta* **2015**, *182*, 1337–1344.

[105] B. Parodi, A. Londonio, G. Polla, M. Savio, P. Smichowski, *J. Anal. At. Spectrom.* **2014**, *29*, 880–885.

[106] N. Panichev, M. M. Kalumba, K. L. Mandiwana, *Anal. Chim. Acta* **2014**, *813*, 56–62.

[107] W. Zhang, C. Sun, X. Yang, *Anal. Methods* **2014**, *6*, 2876–2882.

[108] T. Yordanova, P. Vasileva, I. Karadjova, D. Nihtianova, *The Analyst* **2014**, *139*, 1532–1540.

[109] G. Aragay, J. Pons, A. Merkoçi, *Chem. Rev.* **2011**, *111*, 3433–3458.

[110] M. Li, H. Gou, I. Al-Ogaidi, N. Wu, *ACS Sustain. Chem. Eng.* **2013**, *1*, 713–723.

[111] Z. Chen, C. Zhang, H. Ma, T. Zhou, B. Jiang, M. Chen, X. Chen, *Talanta* **2015**, *134*, 603–606.

[112] H. Tan, B. Liu, Y. Chen, *Plasmonics* **2013**, *8*, 705–713.

[113] L. Chen, X. Fu, W. Lu, L. Chen, *ACS Appl. Mater. Interfaces* **2013**, *5*, 284–290.

[114] Y. Zhou, H. Dong, L. Liu, M. Li, K. Xiao, M. Xu, *Sens. Actuators B Chem.* **2014**, *196*, 106–111.

[115] H. R. Rajabi, M. Shamsipur, M. M. Zahedi, M. Roushani, *Chem. Eng. J.* **2015**, *259*, 330–337.

[116] C. Li, P. Dai, X. Rao, L. Shao, G. Cheng, P. He, Y. Fang, *Talanta* **2015**, *132*, 463–468.

[117] R. Liu, H. Li, W. Kong, J. Liu, Y. Liu, C. Tong, X. Zhang, Z. Kang, *Mater. Res. Bull.* **2013**, *48*, 2529–2534.

[118] D. Liu, S. Wang, M. Swierczewska, X. Huang, A. A. Bhirde, J. Sun, Z. Wang, M. Yang, X. Jiang, X. Chen, *ACS Nano* **2012**, *6*, 10999–11008.

[119] C.-I. Wang, C.-C. Huang, Y.-W. Lin, W.-T. Chen, H.-T. Chang, *Anal. Chim. Acta* **2012**, *745*, 124–130.

[120] D. Wu, X. Huang, X. Deng, K. Wang, Q. Liu, *Anal. Methods* **2013**, *5*, 3023–3027.

[121] C. Gao, X.-J. Huang, *TrAC Trends Anal. Chem.* **2013**, *51*, 1–12.

[122] D. Martin-Yerga, B. G.-G. Maria, C.-G. Agustin, *Talanta* **2013**, *116*, 1091–1104.

[123] Y. Du, R. Liu, B. Liu, S. Wang, M.-Y. Han, Z. Zhang, *Anal. Chem.* **2013**, *85*, 3160–3165.

[124] L. Zhang, H. Chang, A. Hirata, H. Wu, Q.-K. Xue, M. Chen, *ACS Nano* **2013**, *7*, 4595–4600.

[125] B. Sun, X. Jiang, H. Wang, B. Song, Y. Zhu, H. Wang, Y. Su, Y. He, *Anal. Chem.* **2015**, *87*, 1250–1256.

[126] Y. Cai, *Encyclopedia of Analytical Chemistry*, John Wiley & Sons Ltd., **2000**.

[127] H. Haken, H. C. Wolf, *The Physics of Atoms and Quanta*, Springer, **2005**.

[128] H. Morita, H. Tanaka, S. Shimomura, *Spectrochim. Acta* **1995**, *50B*, 69–84.

[129] V. I. Muscat, T. J. Vickers, **1971**, *57*, 23–30.

[130] J. D. Winefordner, T. J. Vickers, *Anal. Chem.* **1964**, *36*, 161–165.

[131] J. D. Winefordner, R. C. Elser, *Anal Chem* **1971**, *43*, 24A–42a.

[132] R. F. Browner, R. M. Dagnall, T. S. West, *Talanta* **1969**, *16*, 75–81.

[133] B. Welz, *Atomic Absorption Spectrometry*, VCH, Weinheim, **1985**.

[134] W. R. Hatch, W. L. Ott, *Anal. Chem.* **1968**, *40*, 2085–2087.

[135] R. G. Godden, P. B. Stockwell, *J. Anal. At. Spectrom.* **1989**, *4*, 301–303.

[136] P. B. Stockwell, W. T. Corns, *Analyst* **1994**, *119*, 1641–1645.

[137] O. Szakacs, A. Lasztity, Z. S. Horvath, *Anal. Chim. Acta* **1980**, *121*, 219–224.

[138] E. Temmerman, C. Vandecasteele, G. Vermeir, R. Leyman, R. Dams, *Anal. Chim. Acta* **1990**, *236*, 371–376.

[139] C. C. Y. Chan, R. S. Sadana, *Anal. Chim. Acta* **1993**, *282*, 109–115.

[140] V. I. Muscat, T. J. Vickers, A. Andren, *Anal. Chem.* **1972**, *44*, 218–221.

[141] M. J. Fishman, *Anal. Chem.* **1970**, *42*, 1462–1463.

[142] R. S. Braman, D. L. Johnson, *Environ. Sci. Technol.* **1974**, *8*, 996–1003.

[143] W. F. Fitzgerald, G. A. Gill, *Anal. Chem.* **1979**, *51*, 1714–1720.

[144] J. Ruzicka, E. H. Hansen, *Anal. Chim. Acta* **1975**, *78*, 145–157.

[145] K. K. Stewart, G. R. Beecher, P. E. Hare, *Anal. Biochem.* **1976**, *70*, 167–173.

[146] L. T. Skeggs, *Amer J Cin Pathol* **1957**, *28*, 311–322.

[147] D. A. Skoog, J. J. Leary, *Instrumentelle Analytik*, Springer-Verlag, **1996**.

[148] J. C. De Andrade, C. Pasquini, N. Baccan, *Spectrochim. Acta Part B* **1983**, *38*, 1 329–1338.

[149] H. Morita, M. Sugimoto, S. Shimomura, *Anal. Sci.* **1990**, *6*, 91–95.

[150] K. Leopold, L. Harwardt, M. Schuster, G. Schlemmer, *Talanta* **2008**, *76*, 382–388.

[151] R. Kellner, J.-M. Mermet, M. Otto, M. Valcárcel, H. M. Widmer, *Analytical Chemistry - A Modern Approach to Analytical Science*, Wiley-VCH Verlag GmbH & Co. KGaA, **2004**.

[152] F. Rouessac, A. Rouessac, *Chemical Analysis - Modern Instrumentation Methods and Techniques*, Wiley, **2004**.

[153] R. Klockenkämper, *Total-Reflection X-Ray Fluorescence Analysis*, John Wiley & Sons, **1997**.

[154] C. Vandecasteele, C. B. Block, *Modern Methods for Trace Element Determination*, John Wiley & Sons, **1997**.

[155] J. Knoth, H. Schwenke, *Fresenius Z. Für Anal. Chem.* **1978**, *291*, 200–204.

[156] J. Knoth, H. Schwenke, *Fresenius J. Anal. Chem.* **1980**, *301*, 7–9.

[157] M. Levlin, E. Ikävalko, T. Laitinen, *Fresenius J. Anal. Chem.* **1999**, *365*, 577–586.

[158] M. Fiałkowski, P. Grzeszczak, R. Nowakowski, R. Hołyst, *J. Phys. Chem. B* **2004**, *108*, 5026–5030.

[159] G. Rosenfeld, K. Morgenstern, M. Esser, G. Comsa, *Appl. Phys. A* **1999**, *69*, 489–496.

[160] W. Funk, V. Dammann, G. Donnevert, *Qualitätssicherung in Der Analytischen Chemie*, Wiley-VCH Verlag GmbH & Co. KGaA, **2005**.

[161] J. Kotnik, M. Horvat, N. Ogrinc, V. Fajon, D. Žagar, D. Cossa, F. Sprovieri, N. Pirrone, *Mar. Pollut. Bull.* **2015**, *96*, 136–148.

[162] C. H. Lamborg, O. Yiğiterhan, W. F. Fitzgerald, P. H. Balcom, C. R. Hammerschmidt, J. Murray, *Mar. Chem.* **2008**, *111*, 77–89.

[163] O. Lindqvist, K. Johansson, L. Bringmark, B. Timm, M. Aastrup, A. Andersson, G. Hovsenius, L. Hakanson, A. Iverfeldt, M. Meili, *Water. Air. Soil Pollut.* **1991**, *55*, xi–261.

[164] US EPA Method 245.1 Revision 3.0, *Determniation of Mercury in Water by Cold Vapor Atomic Absorption Spectrometry*, **1994**.

[165] US EPA Method 7472, *Mercury in Aqueous Samples and Extracts by Anodic Stripping Voltammetry*, **1996**.

[166] E. Marguí, P. Kregsamer, M. Hidalgo, J. Tapias, I. Queralt, C. Streli, *Talanta* **2010**, *82*, 821–827.

[167] M. Horvat, J. Kotnik, M. Logar, V. Fajon, T. Zvonarić, N. Pirrone, *Atmos. Environ.* **2003**, *37*, 93–108.

[168] D. C. Baxter, W. Frech, *Anal. Chim. Acta* **1990**, *236*, 377–384.

[169] C. H. Lamborg, W. F. Fitzgerald, A. Skoog, P. T. Visscher, *Mar. Chem.* **2004**, *90*, 151–163.

[170] R. Frank, H. Rau, *Ecotoxicol. Environ. Saf.* **1990**, *19*, 55–63.

[171] Z. Ezzeddine, I. Batonneau-Gener, Y. Pouilloux, H. Hamad, Z. Saad, V. Kazpard, *Microporous Mesoporous Mater.* **2015**, *212*, 125–136.

[172] S. Loyaux-Lawniczak, J. Douch, P. Behra, *Fresenius J. Anal. Chem.* **1999**, *364*, 727–731.

[173] M. Sillanpää, J. Sorvari, M.-L. Sihvonen, *Chromatographia* **1996**, *42*, 578–582.

[174] Hessisches Landesamt für Umwelt und Geologie, **2015**.

[175] N. M. Price, P. J. Harrison, *Mar. Biol.* **1987**, *94*, 307–317.

[176] J. Rethmeier, G. Neumann, C. Stumpf, A. Rabenstein, C. Vogt, *J. Chromatogr. A* **2001**, *934*, 129–134.

[177] V. Liem-Nguyen, S. Bouchet, E. Björn, *Anal. Chem.* **2015**, *87*, 1089–1096.

[178] A.-C. Le Gall, C. M. G. van den Berg, *Analyst* **1993**, *118*, 1411–1415.

[179] "CRC Handbook of Chemistry and Physics, 91th Edition - dissociation constants of organic acids and bases.pdf," can be found under http://sites.chem.colostate.edu/diverdi/all_courses/CRC%20reference%20data/dissociation%20constants%20of%20organic%20acids%20and%20bases.pdf, **2016**.

[180] S. Bräse, J. Bülle, A. Hüttermann, *Organische Und Bioorganische Chemie: Das Basiswissen Für Master- Und Diplomprüfungen*, Wiley-VCH, **2008**.

[181] A. E. Martell, R. M. Smith, R. J. Motekaitis, *NIST Critically Selected Stability Constants of Metal Complexes Data Base, NIST Std. Ref. Database # 46, Department of Commerce, Gaithersburg, MD.*, **1998**.

[182] S. McDonald, A. G. Bishop, P. D. Prenzler, K. Robards, *Anal. Chim. Acta* **2004**, *527*, 105–124.

[183] D. A. Hansell, *Mar. Chem.* **1993**, *41*, 195–202.

[184] C. Santinelli, L. Nannicini, A. Seritti, *Deep Sea Res. Part II Top. Stud. Oceanogr.* **2010**, *57*, 1446–1459.

[185] J. A. Rice, P. MacCarthy, *Org. Geochem.* **1991**, *17*, 635–648.

[186] S. A. Visser, *Environ. Sci. Technol.* **1983**, *17*, 412–417.

[187] M. Haitzer, G. R. Aiken, J. N. Ryan, *Environ. Sci. Technol.* **2002**, *36*, 3564–3570.

[188] B. P. Chaplin, E. Roundy, K. A. Guy, J. R. Shapley, C. J. Werth, *Environ. Sci. Technol.* **2006**, *40*, 3075–3081.

[189] B. J. Farey, L. A. Nelson, M. G. Rolph, *Analyst* **1978**, *103*, 656–660.

[190] W. F. Fitzgerald, C. H. Lamborg, C. R. Hammerschmidt, *Chem. Rev.* **2007**, *107*, 641–662.

[191] Available online: *http://www.humicsubstances.org/sources.html*, [Accessed: 13.02.**2016**].

[192] Available online: *http://www.humicsubstances.org/elements.html*, [Accessed: 13.02.**2016**].

[193] E. P. Achterberg, C. M. G. van den Berg, *Anal. Chim. Acta* **1994**, *284*, 463–471.

[194] D. L. Tsalev Welz, Bernhard, Michael, Sperling, *Anal. Chim. Acta* **1992**, *261*, 91–103.

[195] D. L. Tsalev, M. Sperling, B. Welz, *Analyst* **1992**, *117*, 1729–1733.

[196] H. Kautsky, *Trans. Faraday Soc.* **1939**, *35*, 216–219.

[197] P. B. Merkel, D. A. Kearns, *J Am Chem Soc* **1972**, *94*, 7244–7253.

[198] E. P. Achterberg, C. M. G. V. D. Berg, *Science* **1994**, *2670*, 213–232.

[199] K. Golimowski, *Anal. Chim. Acta* **1996**, *325*, 111–133.

[200] C. J. Hochanadel, *Radiat. Res.* **1962**, *17*, 286.

[201] O. Legrini, E. Oliveros, A. M. Braun, *Chem. Rev.* **1993**, *93*, 671–698.

[202] D. G. Hager, *Hazard Waste Treat Technol Ser* **1990**, *2*, 143–153.

[203] T. Linsinger, *Comparison of a Measurement Results with the Certified Value, Application Note 1*, European Reference Materials, **2010**.

[204] R. W. Matthews, *J. Phys. Chem.* **1987**, *91*, 3328–3333.

[205] R. W. Matthews, *J. Catal.* **1988**, *111*, 264–272.

[206] J. E. Birdwell, A. S. Engel, *Org. Geochem.* **2010**, *41*, 270–280.

[207] P. Kowalczuk, J. Stoń-Egiert, W. J. Cooper, R. F. Whitehead, M. J. Durako, *Mar. Chem.* **2005**, *96*, 273–292.

[208] C. A. Stedmon, S. Markager, H. Kaas, *Estuar. Coast. Shelf Sci.* **2000**, *51*, 267–278.

[209] M. Bideau, B. Claudel, C. Dubien, L. Faure, H. Kazouan, *J. Photochem. Photobiol. Chem.* **1995**, *91*, 137–144.

[210] H. Al-Ekabi, N. Serpone, *J. Phys. Chem.* **1988**, *92*, 5726–5731.

[211] Y. M. Wang, S. W. Liu, Z. Xiu, X. B. Jiao, X. P. Cui, J. Pan, *Mater. Lett.* **2006**, *60*, 974–978.

[212] *Wikipedia* **2015**.

[213] L.-E. Heimbürger, J. E. Sonke, D. Cossa, D. Point, C. Lagane, L. Laffont, B. T. Galfond, M. Nicolaus, B. Rabe, M. R. van der Loeff, *Sci. Rep.* **2015**, *5*, 10318.

[214] K. Leopold, M. Foulkes, P. J. Worsfold, *TrAC Trends Anal. Chem.* **2009**, *28*, 426–435.

[215] M. H. Bothner, D. E. Robertson, *Anal. Chem.* **1975**, *47*, 592–5.

[216] M. Schlathauer, **2012**.

[217] X. Xu, M. Stevens, M. B. Cortie, *Chem. Mater.* **2004**, *16*, 2259–2266.

[218] R. M. Heck, S. Gulati, R. J. Farrauto, *Chem. Eng. J.* **2001**, *82*, 149–156.

[219] A. Ghanem, T. Ikegami, *J. Sep. Sci.* **2011**, 1945–1957.

[220] N. Tanaka, H. Nagayama, H. Kobayashi, T. Ikegami, K. Hosoya, N. Ishizuka, H. Minakuchi, K. Nakanishi, K. Cabrera, D. Lubda, *J. High Resolut. Chromatogr.* **2000**, *23*, 111–116.

[221] K. Nakanishi, *J. Porous Mater.* **1997**, *4*, 67–112.

[222] K. Nakanishi, N. Soga, *J. Am. Ceram. Soc.* **1991**, *74*, 2518–2530.

[223] Y. Zhu, K. Morisato, W. Li, K. Kanamori, K. Nakanishi, *ACS Appl. Mater. Interfaces* **2013**, *5*, 2118–2125.

[224] K. L. Kelly, E. Coronado, L. L. Zhao, G. C. Schatz, *J. Phys. Chem. B* **2003**, *107*, 668–677.

[225] E. Kowalska, O. O. P. Mahaney, R. Abe, B. Ohtani, *Phys. Chem. Chem. Phys.* **2010**, *12*, 2344–2355.

[226] B. Vrana, I. J. Allan, R. Greenwood, G. A. Mills, E. Dominiak, K. Svensson, J. Knutsson, G. Morrison, *TrAC Trends Anal. Chem.* **2005**, *24*, 845–868.

[227] Y. Gao, E. De Canck, M. Leermakers, W. Baeyens, P. Van Der Voort, *Talanta* **2011**, *87*, 262–267.

[228] H. Docekalova, P. Divis, *Talanta* **2005**, *65*, 1174–1178.

[229] P. Diviš, M. Leermakers, H. Dočekalová, Y. Gao, *Anal. Bioanal. Chem.* **2005**, *382*, 1715–1719.

[230] Y. Zhou, T. Stotesbury, B. Dimock, A. Vreugdenhil, H. Hintelmann, *Chemosphere* **2013**, *90*, 323–328.

[231] J. Smått, S. Schunk, M. Linde, *Chem Mater* **2003**, *15*, 2354–2361.

[232] Analytik Jena AG, *Mercur Quecksilber-Analysator, Betriebsanleitung*, **2014**.

Appendix

a. Additional information on real water samples

Table A1: *Additional information on Great Whale River water samples concerning DOC concentration and sampling strategy.*

Sample No.	DOC [mg L^{-1}]
1	4.90
2	2.78
3	3.47
4	4.47
5	4.99
6	5.70
7	5.14
8	4.39
9	3.94
10	18.0
12	5.64
14	5.47
15	5.22
16	5.25
17	5.57
18	6.50
19	6.84
21	7.10

Sampling strategy

Sampling bottles	500 mL PTFE bottles
Sample preparation	filtration (0.7-μm GF/F grade), acidification (0.1% (v/v) double-distilled HCl)

Table A2: *Additional information on Isar and Danube river water samples concerning temperature, pH value, DOC concentration and sampling strategy.*

Origin	Temperature [°C]	pH value	DOC [mg L^{-1}] [a]
Isar (before Munich, Dürnstein)	11.4	5.5	2.56 ± 0.26
Isar (in Munich)	10.7	5.5	2.62 ± 0.26
Isar (behind Munich, Garching)	dng	dng	2.66 ± 0.27
Donau (before Ulm, Wiblingen)	12.0	6.0	2.85 ± 0.29
Donau (in Ulm)	11.0	6.5	3.93 ± 0.39
Donau (behind Ulm, Böfingen)	11.3	6.5	3.02 ± 0.30
Sampling strategy			
Sampling bottles	500 mL PET bottles		
Sample preparation	On-site filtration (0.45-µm), on-site acidification (0.06 M HCl)		

[a] Determined by *S. West*, *Technical University of Munich*, using High TOC II (Elementar Analysensysteme *GmbH*, Hanau, Germany) with a limit of detection of 1 mg L^{-1}, uncertainty for DOC measurement expressed as 10% of the measured value; dng data not given.

Table A3: *Additional information on Black Sea water samples concerning depth, temperature, salinity, oxygen concentration, hydrogen sulfide (HS) concentration and sampling strategy.*

Sample No.	Depth [m]	Temperature [°C]	Salinity [g L^{-1}]	Oxygen [µM]	HS [µM]
5-1-1	2039.77	9.11	22.33	2.19	418.70
5-1-2	1988.88	9.11	22.33	2.19	421.00
5-1-3	1750.92	9.08	22.33	2.16	408.60
5-1-5	1250.31	9.00	22.31	1.97	380.40
5-1-9	399.71	8.87	21.96	1.82	138.50
5-1-11	250.16	8.81	21.71	1.81	64.40
5-1-13	175.10	8.70	21.42	1.80	26.40
5-1-15	145.08	8.64	21.25	1.77	14.70
5-1-17	110.44	8.55	20.93	1.75	0.00
5-1-19	84.33	8.38	20.29	15.58	0.00
5-1-20	69.34	8.06	19.69	62.54	0.00
5-1-21	54.34	7.66	18.88	217.88	0.00
5-1-22	40.47	8.41	18.33	373.83	0.00
5-1-23	28.61	9.29	18.24	396.75	0.00
5-1-24	10.10	22.31	18.13	326.41	0.00

Sampling strategy

Sampling bottles	250 mL PET and PFA Teflon bottles (Savillex Purillex™)
Sample preparation	filtration (0.7-µm GF/F grade), acidification (0.1% (v/v) double-distilled HCl)

Table A4: *Additional information on intercomparison sample (Black Sea water) concerning sampling depth and sampling strategy.*

Sampling depth: 45 m	
Sampling strategy	
Sampling bottles	1,000 mL FEP Teflon bottle
Sample preparation	Filtration (0.2-µm, Sartobran 300), acidification (0.4% (v/v) double-distilled HCl)

Table A5: *Additional information on wastewater and treated water samples from a wastewater treatment plant (WWTP) concerning origin, temperature, pH value, conductivity, DOC concentration and sampling strategy.*

Origin	Temperature [°C] [a]	pH value [a]	Conductivity [µS] [a]	DOC [mg L^{-1}] [a]
Input (WWTP)	18.5	7.2	591	36.5
After physical treatment (WWTP)	dng	dng	dng	dng
Output (WWTP), after biological treatment	17.2	7.0	872	5.2
Sampling strategy				
Sampling bottles	500 mL PET bottle			
Sample preparation	Filtration (0.7-µm glass-fiber filter, 0.45-µm polyethersulfone filter), acidification (0.06 M HCl)			

[a] Data obtained from the laboratory *Klärwerk Steinhäule*, July 2012, no data available for uncertainty for DOC measurement; dng data not given.

b. Evaluation of method performance

Dissolved Hg concentration in model solutions and real water samples was determined applying the novel approaches described in this thesis. For the validation of the measurement procedures reference measurements were carried out either by collaborative partners or as a part of this work. Therefore, different established methods for dissolved Hg analysis in natural water were applied. The found value derived by the novel method was compared with the reference measurements and their respective uncertainties.[203] Based on the formulae described in chapter 7.3. **Table A6** summarizes the relevant parameters.

Table A6: *Comparison of measurement results with results obtained by a reference method according to Linsinger.[203]*

Sample	Nanogold-based method vs reference method	Reference to section	Absolute difference Δm	Expanded uncertainty U_Δ	Significant difference [Y/N]
HA model solution: 5 mg C L^{-1}	Optimized FIAS-AFS with AuNP-coated	4.3.2	1.13	2.66	N
HA model solution: 10 mg C L^{-1}	silica particles vs U.S. EPA method 1631		0.72	3.74	N
HA model solution: 15 mg C L^{-1}			0.19	5.36	N
River Isar before Munich	FIAS-AFS integrated	4.4.1	0.03	0.39	N
River Isar in Munich	reagent-assisted UV digestion		0.12	0.39	N

River Isar behind Munich	(AuNP-coated silica particles) vs U.S. EPA		0.07	0.33	N
River Danube before Ulm	method 1631		0.00	0.25	N
River Danube in Ulm			0.06	0.17	N
River Danube behind Ulm			0.01	0.11	N
Great Whale River	AuNP@qt vs CV-AFS	5.1.5	0.96	0.82	Y
Submarine groundwater discharge	AuNP@SiO$_2$ vs modified U.S. EPA method 1631	5.2.6	1.46	3.17	N

c. List of Figures

d. List of Tables

e. List of publications, lectures and poster presentations

Publications

Jessica Huber, Kerstin Leopold; Nanomaterials-based strategies for enhanced mercury trace analysis in environmental and drinking waters, Trends in Analytical Chemistry (2016), 80, 280-292.

Jessica, Huber, Lars-Eric, Heimbürger, Jeroen Sonke, Sebastian, Ziller, Mika Lindén, Kerstin Leopold; Nanogold-decorated silica monoliths as highly efficient solid-phase adsorbent for ultra-trace mercury analysis in natural water, Analytical Chemistry (2015), 87, 11122-11129.

Jessica Huber, Kerstin Leopold; Umweltmonitoring von Quecksilber in Gewässern, GIT Labor-Fachzeitschrift (2013), 5, 2-4.

Kerstin Leopold, Anja Zierhut, Jessica Huber; Ultra-trace determination of mercury in river waters after online UV digestion of humic matter, Anal Bioanal Chem (2012), 403, 2419-2428.

Lectures

Jessica Huber, Thomas Labatzke, Kerstin Leopold; Ultratrace determination of mercury in natural water; 37th International Symposium on Environmental Analytical Chemistry, Antwerpen, Belgium, 22.-25. May 2012.

Jessica Huber, Maria Schlathauer, Kerstin Leopold; Development of a new method for on-site mercury extraction from waters based on gold nanoparticle adsorbers; 38th International Symposium on Environmental Analytical Chemistry, Lausanne, Schwitzerland, 17.-20. June, 2014.

Jessica Huber, Kerstin Leopold, Lars-Eric Heimbürger; Nanogold-assisted direct and reagent-free ultra-trace determination of dissolved Hg in pristine waters; 12th International Conference on Mercury as a Global Pollutant, Jéju, Korea, 14.-19. June, 2015.

Poster presentations

Jessica Huber, Kerstin Leopold; Reagent-free determination of dissolved mercury in humic-rich natural water; ANAKON 2013, Essen, Germany, 4.-7. March, 2013.

Jessica Huber, Kerstin Leopold; Reagent-free determination of dissolved mercury in humic-rich natural water; CANAS 2013, Freiberg, Germany, 17.-19. March, 2013.

Jessica Huber, Kerstin Leopold; Development of an online UV digestion unit for subsequent reagent-free mercury analysis in waters; 11th International Conference on Mercury as a Global Pollutant, Edinburgh, Scotland, 28. September-2. August, 2013.

f. Danksagung

g. Curriculum vitae

The curriculum vitae was removed for reasons of data protection.

Der Lebenslauf wurde aus Gründen des Datenschutzes entfernt.

h. Eidesstattliche Erklärung

Hiermit erkläre ich, dass ich die vorliegende Dissertation selbstständig erarbeitet habe und keine anderen als die in der Arbeit aufgeführten Hilfsmittel verwendet habe.

München, _____   _____

(Jessica Huber)